Homeostatic Regulation of Intrinsic Excitability in Hippocampal Neurons

Timothy Sean O'Leary (MMath, MRes)

A thesis submitted for the degree of Doctor of Philosophy at the University of Edinburgh

December 2008

Neuroinformatics and Computational Neuroscience
Doctoral Training Centre,
School of Informatics,
University of Edinburgh.

Supervisors: Dr Mark CW van Rossum,
Dr David JA Wyllie

Declaration

I hereby certify that this thesis and its composition are entirely my own work. No part of the work contained in this thesis has been submitted for any other degree or professional qualification.

Signed …… (canditate) Date …….

Abstract

The proper functioning of nervous systems requires electrical activity to be tightly regulated. Perturbations in the intrinsic properties of neurons, and in excitatory input, are imposed throughout nervous system development as cell morphology and network activity evolve. In mature nervous systems these changes continue as a result of synaptic plasticity and external stimuli. It is therefore likely that homeostatic mechanisms exist to regulate membrane conductances that determine the excitability of individual neurons, and several mechanisms have been characterised to date. This thesis characterises a novel in vitro model for homeostatic control of intrinsic excitability. The principal finding is that cultured hippocampal neurons respond to chronic depolarisation over a period of days by attenuating their response to injected current. This effect was found to depend on the level of depolarisation and the length of treatment, and is accompanied by changes in both active and passive membrane conductances. In addition, the effect is reversible and dependent on L-type calcium channel activity. Using experimental data to parameterise a conductance-based computer model suggests that the changes in conductance properties account for the observed differences in excitability.

Contents

List of figures

Abbreviations

4-AP	4-aminopyridine
AHP	after-hyperpolarisation
AMPA(R)	α-amino-3-hydroxy-5-methyl-isoxazole propionic acid (receptor)
AP	action potential
APV	(D-)2-amino-5-phosphopentanoic acid
CNQX	6-cyano-7-nitroquinoxaline-2,3-dione
CPA	CNQX (5 µM), picrotoxin (50 µM) and APV (50 µM) in solution
DIV	days in-vitro
DMSO	dimethyl sulfoxide
EDTA	ethylenediaminetetraacetic acid
EGTA	ethylene glycol tetraacetic acid
EMF	electromotive force
(E)PSC	(excitatory) postsynaptic current
GABA(R)	γ-aminobutyric acid
GHK	Goldman-Hodgkin-Katz
HEPES	4-(2-hydroxyethyl)-1-piperazineethanesulfonic acid
mEPSC	miniature excitatory postsynaptic current, 'mini'.
NMDA(R)	N-methyl-D-aspartate
PTX	picrotoxin
ROI	region of interest
TEA	tetraethylammonium (chloride)
TTX	tetrodotoxin

Acknowledgements

Three years ago I managed to persuade my supervisors, David Wyllie and Mark van Rossum, to allow me to embark on a project studying spike timing-dependent plasticity. In itself, this request sounds unremarkable, but the circumstances meant that agreeing to such a proposition involved a substantial risk. Firstly, the project was experimental and as a mathematician-turned-cook-turned-neuroscience student, who had already quit one PhD, I was less than a safe bet. Secondly, the project proposal in its initial form, in hindsight, was pretty ambitious – probably impossible, in fact. I have no doubt that, as the experimental mentor, David had to exert an enormous amount of restraint when attempting to temper my naïve and over-confident projections about how the project would go (though he was less subtle about his objections to wearing sandals in the lab and mouth-pipetting Ringer's solution). It is testament to both David and Mark's open-mindedness and willingness to risk their own reputations – not to mention a combined faith in the power of enthusiasm when ability is not necessarily a given – that I was allowed to embark on the project. When things went bad, which they inevitably did, both Mark and David maintained perspective and helped me to find a way out (with invaluable help from Phil Larkman during some of the more 'tense' meetings). I am indebted to both of my supervisors for the time and energy they devoted to me during this project.

One of the pleasures of working in physiology, which is especially evident as a newcomer, is the extent to which it demands collaborative work. Although this was essentially a solo project, the informal, but absolutely essential training that enabled me to complete it was provided through many hours of talking, watching and often harassing people who were already adept at a particular technique, or simply willing to listen and offer suggestions. Those who helped directly and indirectly in this way, with advice and support on the scientific aspects of this work, and to whom I owe sincere thanks, are: Philip Larkman, Philip Chen, Marc-Andre Martel, Guo-Qiang Bi, Paul Skehel, Frederic Leveille, Sofia Papadia, David Nauen, Richard Gerkin, Niraj Desai, Christos Gkogkas, Emma Perkins, Tom Wishart, Giles Hardingham, Jary Delagado, Matt Nolan, Melanie White, Francesc Soriano, Cathy Vickers, Mike Shipston, David Steratt and David Willshaw. Also, a project of this kind is more or less impossible without the help of the administrative and support staff, two of whom I owe particular thanks: to Pat Ferguson for putting up with me, to Darren Downing for always being around to fix things at a moment's notice.

It is more than a mere platitude to say that a PhD project is a way of life, one with high points and low points. Without doubt, the high points would have been considerably scarcer without the unconditional love and support of my close friends and family. My sanity and happiness was especially dependent on Aoife, who managed to keep a brave face through all my rants, and on the friends I have made over the past few years: John – for taking care of the philosophy for the rest of us, Finlay – even though he's an anarcho-capitalist, 'extreme' Jan – for being 'extreme', Anisha – for being a star, Joy – for the craic, to all the DTC and everyone at 'the Hugh Robson', thank you.

Chapter 1. Introduction

1.1. Background

All nervous systems rely on the excitable nature of their constituent cells in order to function. Among the cell types present in species that possess a nervous system, neurons above all are the most strikingly adapted to exploit the phenomenon of excitability, and they do so in order to transmit and process information. The very act of reading the words on this page recruits the coordinated activity of many millions of individual cells, from the receptor cells in the retina that convert light energy into graded electric potentials, to the cells forming intricate synaptic connections which successively relay visual information via the thalamus to the cortex. With every saccadic movement of the eye, this information is encoded into brief surges of electrical activity that are transmitted from each cell to its neighbour on a timescale of milliseconds. The cellular mechanisms underlying this process ultimately give rise our capacity to read, understand and remember throughout the course of our lives (Kandel *et al.* 2000).

These remarkable properties come at a price. Not only do the biochemical processes that give rise to excitability place a severe metabolic demand on organisms with a central nervous system (Rolfe and Brown 1997), but the very nature of neuronal excitability means that it can have disastrous effects if it is not properly regulated. For example, genetic mutations that directly, or indirectly, affect neuronal excitability are a major cause of mortality and disability in humans as a result of epilepsy (Meisler *et al.* 2001; Mulley *et al.* 2003). Even in cases where there is no genetic predisposition toward such pathology, environmental factors and acute physiological insults such as hypoxia and mechanical trauma can result in lasting, aberrant changes in excitability that carry equally onerous consequences.

This thesis examines one aspect of how neurons regulate their excitability in response to imposed changes in their environment. In the decades since the advent of modern electrophysiology in the 1950s and in the last three decades in particular, much has been learned about neuronal excitability and how it is determined. Far

from having fixed electrical behaviour, neurons and, indeed, non-neuronal cells are capable of modifying their biophysical properties in a dynamic fashion. One of the central results of this thesis is a carefully controlled quantification of this dynamical behaviour in neurons.

1.1.1. Organisation of the thesis

This chapter introduces the important concepts that will be assumed throughout the rest of the thesis, the central concept being that of intrinsic excitability in nervous tissue. A historical perspective has been chosen for this account, as it introduces the material in a logical progression. The latter sections of this chapter review the relevant current literature on regulation of intrinsic excitability, and discusses key experiments and the central hypothesis that motivates this work.

Chapter 2 describes the experimental techniques, materials and analysis methods that are used in the experimental work in this thesis.

Chapter 3 provides a basic electrophysiological characterisation of hippocampal cultures, which are the model systems studied in this work.

Chapter 4 comprises a brief, but important catalogue of observations made during initial experiments. Contained within it is a basic characterisation of the effects of chronic depolarisation on the intrinsic properties of cultured neurons and some experiments examining synaptic plasticity.

Chapters 5, 6 and 7 are the main results chapters. Each provides a brief introduction and motivation for the work, presents the results and offers a discussion. The interpretation of the results and suggestions for further work are included in each chapter individually. Chapter 5 deals with phenomenological aspects, characterising excitability and its regulation in response to chronic depolarisation in terms of spiking behaviour. Chapter 6 and 7, respectively, examine the underlying membrane conductances that accompany chronic depolarisation, and explore the extent to which these changes account for the altered spiking behaviour using a conductance-based model.

1.2. What is excitability?

For hundreds of years it has been known that nervous tissue is electrically excitable (for a historical account tracing this knowledge as far back as classical civilization, see Walker 1937). Experiments conducted by Luigi Galvani (1737 – 1798) and Alessandro Volta (1745 – 1827) in the sixteenth and seventeenth centuries established that muscle contraction in frogs could be provoked in recently living animal specimens with direct application of electric current (reviewed in Piccolino 1997).

Volta wrongly suspected that the spasms produced in the frog muscle preparations bore no relation to the normal physiology of the animal; that they were merely a reaction to exogenous stimuli. Galvani, on the other hand, believed that this phenomenon offered insight into the principle of muscle contraction as it occurs in intact, living creatures (Piccolino 1997). In pursuit of this underlying principle he demonstrated that spasms could be induced by placing metallic conductors between distal regions of excised muscle tissue. The indication that an animal could both 'generate' and 'use' electricity seemed to be more than mere coincidence. He proposed that this endogenously derived 'animal electricity' was the motive force behind muscle contraction in the living specimen, and raised the question as to how electrical energy might be generated in an organism:

> '…in the animal there is a particular machine capable of generating such disequilibrium, and it will be convenient to refer to this form of electricity as to animal electricity to denote, not a type of electricity whatsoever, but a particular one referred to a particular machine' – *L. Galvani, 1794* (taken from Piccolino 1998)

Thus Galvani anticipated the discovery of a feature that we now know is common to all cellular life – that the accumulation and conversion of electrochemical energy is an essential part of cellular biochemistry, in particular, muscle contraction.

A detailed, quantitative understanding of the phenomena described by Galvani and his contemporaries had to wait until substantial scientific progress had been made, not only in biology, but also in chemistry and physics. Indeed, it was not until the

mid twentieth century that modern electrophysiology emerged as a field and the phenomena underlying the muscle spasms observed by Galvani, namely action potentials and synaptic transmission, were understood. However, important contributions toward the modern understanding emerged in the intervening years, beginning with the work of Emile du Bois-Raymond (1818 – 1896), Hermann von Helmholtz (1821 – 1894) and Julius Bernstein (1839 – 1917) (reviewed in Piccolino 1998; Nilius 2003; Seyfarth 2006; Verkhratsky *et al.* 2006).

Using an excised frog muscle preparation and a galvanometer, du Bois-Raymond established the presence of a 'negative current' (inward current) occurring during muscle contraction. This was the first evidence of the action current, and it provided the mechanistic link between physiology and electricity anticipated by Galvani and Volta.

Building on this work, von Helmholtz succeeded in measuring the speed of propagation of nerve stimulation using relatively crude mechanical apparatus. The results of this experiment surprised the contemporary scientific community because they suggested that nerve impulses spread through tissue at a speed of several tens of metres per second. At the time, this was believed to conflict with the notion that muscle contraction is electrogenic in nature, because the speed of propagation of the electric field was known to be close to the speed of light. Compelling evidence that the action current and the motive force for muscle contraction are one and the same required the time-course of action currents propagation to be measured accurately. This presented a formidable technical challenge because modern apparatus such as oscilloscopes were not available. Bernstein surmounted this obstacle with the ingenious use of a mechanical galvanometer and repeated measures of the extracellular membrane current in a nerve bundle at precise time intervals after stimulation (Figure 1.1). Not only did this experiment demonstrate that the electrical signal propagated at the slow rate predicted from von Helmholtz's work, but it offered the first quantitative picture of the time-course of an action potential in terms of action current.

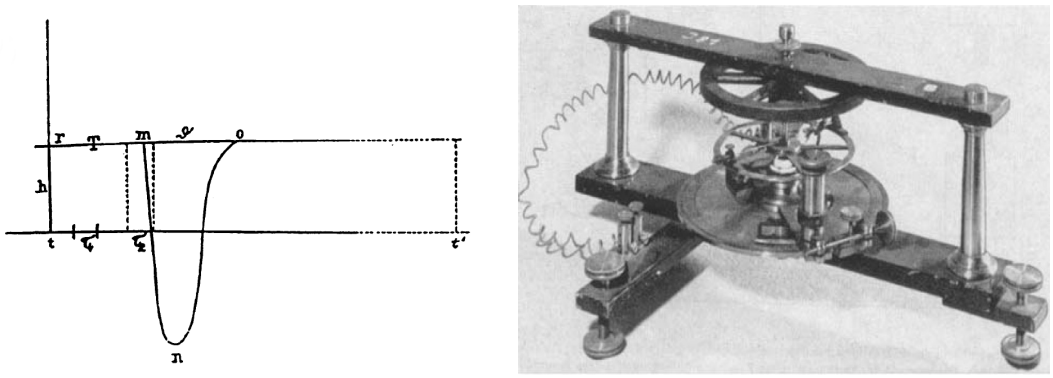

Figure 1.1: Early recordings of the action current

(Left) Bernstein's plot of the action current in a muscle fibre. Reproduced from (Seyfarth 2006) **(Right)** A photograph of the mechanical galvanometer Bernstein used to plot the action current. Reproduced from (Nilius 2003).

During the course of this work, Bernstein put forward a theory of how nerve impulses are generated. His contention was that an electric potential exists between the intracellular compartment and the extracellular fluid. The mechanism responsible for allowing current to flow during an impulse was assumed to be a transient 'breakdown' of membrane integrity which resulted in a loss of its insulating properties. This theory predicted that the action current should reverse at a membrane potential of zero. Bernstein did not consider the possibility that the reversal potential of the current flowing during stimulation might be substantially different from zero – though he did note that the potential difference achieved during the peak of the action current exceeded that produced in severed nerves, indirect evidence of the action potential 'overshoot'. The presence and importance of action potential overshoot was recognised much later, in the seminal work of Alan Hodgkin and Andrew Huxley (recounted in Huxley 2002).

Despite his failure to identify selective ion permeability as the key mechanism underlying nerve excitability (which was largely due to limitations of the experimental preparation and equipment), Bernstein did succeed in recognising selective permeability as the source of the resting membrane potential. Via an insightful application of the theory developed by Walther Nernst (1864 – 1941)

concerning ionic diffusion (Nernst 1888), Bernstein correctly suggested that the trans-membrane potential he had assumed to exist could, in principle, be generated as the result of a difference in ionic concentration on either side of the cell membrane combined with selective permeability of the membrane to particular ions such as potassium (Piccolino 1998). Indeed, an important series of experiments conducted by Sidney Ringer in the late nineteenth century offered support of the ionic selectivity hypothesis by demonstrating that the continued beating of excised heart muscle depends on the relative concentrations of sodium and potassium ions in the external solution (Ringer and Buxton 1885; 1887). However, the confirmation of a negative resting membrane potential and its ionic basis had to wait until experimental techniques permitted intracellular recordings. It is therefore to Bernstein's credit that he was able to predict this result and propose an appropriate mechanism long before any direct evidence was available.

1.2.1. The electrochemical basis of the membrane potential

The principles of the Nernst-Bernstein theory will be explained here, as they are an essential component to understanding the work in this thesis. The exposition that will be presented benefits from what is now known about the ionic basis of electrical activity in cells, and attention will be focussed on neuronal cells. However, most cells have an electrically polarised membrane, and the underlying principles are quite general (Hille 2001).

The cytosol in neurons is usually negative with respect to the extracellular medium; typical values of the electric potential across the membrane are in the range −90 to −40 mV. This potential difference, or membrane potential, is the result of two things:

1. There is a concentration difference in ionic species between the intracellular and extracellular space. Typically, potassium is more concentrated inside the cell than outside, while sodium is less concentrated inside than outside.

2. The membrane is selectively permeable to ions. At rest, neuronal membranes are more permeable to potassium than sodium.

Facts (1) and (2) together explain the negative resting potential: the selective

permeability of the membrane to potassium means that it can diffuse down its concentration gradient, leaving the cell. The resulting charge imbalance generates a potential difference across the membrane which continues to grow until it becomes thermodynamically unfavourable for any more potassium ions to move against the accumulating potential. Nernst derived a quantitative relationship to describe this process by balancing the thermal energy distribution of the ions (given by the Boltzmann distribution) with the electric potential energy stored across the membrane (Hille 2001). This is known as the *Nernst equation*:

$$E_{Ion} = \frac{RT}{zF} \ln\left(\frac{[Ion]_o}{[Ion]_i}\right)$$

where R is the gas constant, T is absolute temperature, F is Faraday's constant and z is the ionic valence of the ion in question. Intracellular and extracellular concentrations are denoted by 'i' and 'o' subscripts, respectively.

1.2.2. Toward the action potential

In the years following Bernstein's work, several additional, important facts were established concerning the nature of action potential generation. In the early twentieth century, Keith Lucas provided the first compelling evidence that the action potential is an 'all-or-nothing' event. Lucas showed that contraction intensity in muscle innervated by multiple nerve fibres increased in discrete steps as stimulus intensity was elevated. He reasoned that each step represented the recruitment of an additional nerve fibre and the contribution of an additional all-or-nothing output upon stimulation (Lucas 1905).

Lucas died as a soldier during the First World War, leaving the all-or-nothing character of the action potential to be unequivocally demonstrated by his student, Edgar Adrian. By measuring activity in individual proprioceptive nerve fibres of the sterno-cutaneus muscle in frogs, Adrian and his collaborator Yngve Zotterman were able to uncover a fixed stimulation threshold for firing by stretching the innervated muscle incrementally (Adrian and Zotterman 1926).

By the 1930s, experimental techniques had progressed to the point where intracellular recordings were practical. This was aided in part by the discovery of suitable animal preparations that could be easily manipulated and maintained, in particular, the giant axon of the squid *Loligo pealli*. Over the course of two decades, the ionic basis of the resting potential and action potential were definitively established using this preparation.

Until this time, Bernstein's membrane-breakdown theory of the action current had awaited experimental vindication. A major step toward testing this hypothesis was provided by Kenneth Cole and Howard Curtis in 1939. If the action current is indeed caused by a change in permeability, a simultaneous change in membrane impedance should occur. This was indeed detected (Cole and Curtis 1939) in an elegant experiment which measured the impedance of squid giant axons during action potentials using oscillating current. A photographed trace of the recording published by Cole and Curtis is shown in Figure 1.2, left.

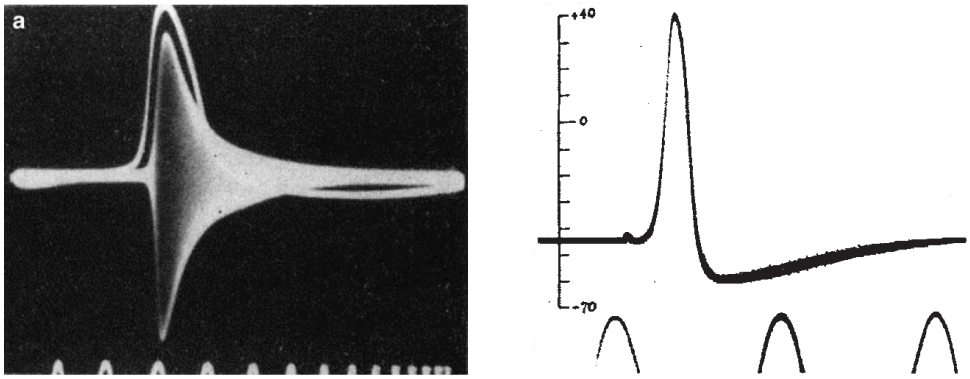

Figure 1.2 Action potential recordings by Cole, Curtis, Hodgkin and Huxley

(Left) A photograph of an oscilloscope recording during an action potential, showing the change in impedance due to increases in sodium and potassium conductances. Taken from (Cole and Curtis 1939). **(Right)** The first intracellular recording of the action potential. Taken from (Hodgkin and Huxley 1939).

1.2.3. The contributions of Hodgkin, Huxley and Katz

The first intracellular recording of an action potential was published by Hodgkin and Huxley in 1939 (Hodgkin and Huxley 1939). This was achieved using a fine, glass intracellular micropipette containing a silver chloride electrode, which were lowered together into the open end of the giant axon. The recordings of evoked action potentials in this preparation showed an 'overshoot', whereby the peak of membrane current during the action potential exceeded 0 mV (Figure 1.2, right), contradicting Bernstein's theory of membrane breakdown.

Hodgkin, Huxley and their collaborator, Bernard Katz, hypothesised that the overshoot of the action potential is a result of selective permeability of the axon membrane to sodium ions during the upward phase. A crucial experiment by Hodgkin & Katz (Hodgkin and Katz 1949) showed that the magnitude of action potentials in the giant axon were dependent on the concentration of sodium ions in the extracellular solution, corroborating their 'sodium current' hypothesis.

During this period, the voltage-clamp technique was developed, allowing membrane current-voltage relationships to be isolated for the first time. This permitted the ionic current that underlies the action potential to be dissected. A quantitative description of the ionic conductances that underlie the currents was finally achieved in 1952 (Hodgkin and Huxley 1952c; 1952b; 1952a; Hodgkin *et al.* 1952). Described in detail by Hodgkin and Huxley in this series of investigations, for which they won a Nobel Prize in 1963, the fast neuronal action potential can be understood in terms of several key points:

1. Ionic reversal potentials for potassium and sodium, determined by their relative concentrations inside and outside the cell in accordance with Nernst's relation, are substantially different in value. For sodium, current is inward at resting potential (about −60 mV) and reverses at approximately +60 mV. Potassium current is outward at −60 mV, reversing at a more negative potential still.

2. In its resting state, the membrane is permeable mainly to potassium. Sodium permeability is low.

3. Sodium conductance increases at elevated membrane potentials, leading to inward, depolarising current.

4. As the membrane potential approaches the sodium reversal potential, two things occur: voltage-gated sodium conductance begins to inactivate and diminish, and the voltage-gated potassium conductance, which take longer to activate, increases.

5. After the peak of the action potential, sodium conductance decreases further and potassium conductance begins to dominate, leading to a rapid repolarisation of the membrane due to the outward potassium current.

6. Voltage-gated potassium conductances remain active for a period after the action potential spike, causing a transient hyper-polarisation of the membrane potential.

Figure 1.3 illustrates the action potential waveform with the sodium and potassium conductances overlaid so that their relative contribution at various stages during the timecourse of the event can be appreciated.

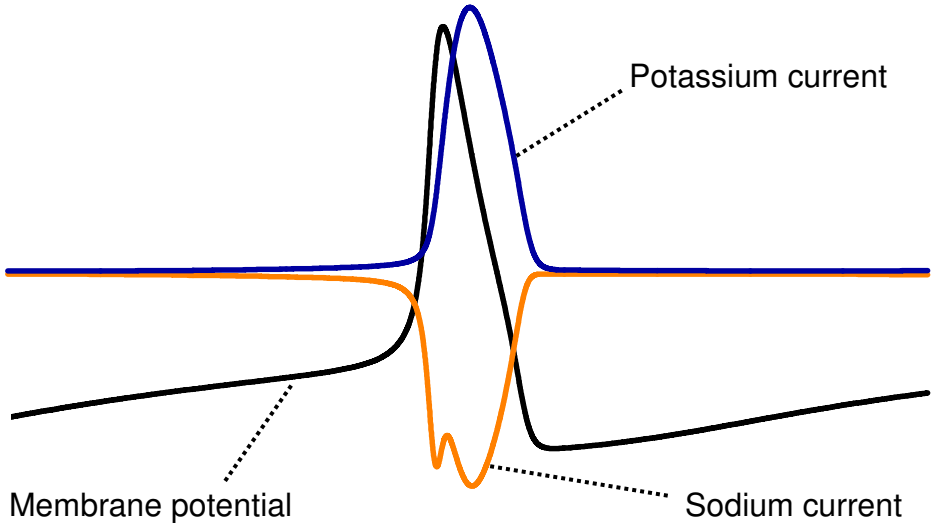

Figure 1.3: Sodium and potassium current underlying the action potential

The membrane potential and membrane current during an action potential, calculated for the Hodgkin-Huxley model using NEURON (Hines and Carnevale 1997).

Perhaps the most remarkable achievement of Hodgkin and Huxley was their capturing of the dynamics of voltage-gated membrane conductances in a system of differential equations. By systematically measuring current waveforms due to sodium and potassium, they were able to derive a quantitative, dynamical model of the current-voltage relation in the axon membrane. The differential equations themselves, which are used later in this thesis, in Chapter 7, represent first-order reactions of so-called 'gating particles'. These gating particles were tentatively hypothesised to correspond to molecular gates which had to assume a particular configuration in order to allow ions to pass through the membrane, and whose conformational state depends on membrane potential. Using the rudimentary computing equipment available at the time, Hodgkin and Huxley demonstrated that these relationships, derived from voltage-clamp data, predict the action potential waveform.

Their success in this task represents a phenomenal achievement and is an example of a theory that produces very accurate predictions from quantitative, reductionist reasoning. Situations in which such an approach is as successful are seldom encountered in biology. In the context of this discussion it is important to notice, however, that their motivation was not aimed toward predicting anything new. Action potentials in giant axon of the squid did not require prediction, they were routinely observed. However, Hodgkin and Huxley realised that in order to make their theory compelling, they needed to quantify their observations of membrane conductances, and reproduce, mathematically, the phenomenon they were trying to explain.

It was appreciated at the time that the Hodgkin-Huxley model of action potential generation as it applies in the squid giant axon is not universally applicable. In experiments using isolated axons of the crab, *Carcinus maenas*, Hodgkin observed that nerve fibres are capable of firing at low frequencies, with no obvious minimum firing rate (Hodgkin 1948). In contrast, the studies in the giant axon of the squid showed that firing frequency had a minimum that is substantially above zero. Both types of firing were observed in the crab preparation and classified by Hodgkin, which he labelled 'Type I' and 'Type II', respectively. Later work established the

presence of additional voltage-gated conductances, such as voltage-gated calcium currents that are essential for synaptic transmission and underlie slower, sodium-independent action potential-like events (Fatt and Katz 1953).

The discussion so far has circumscribed the question of how ionic concentration gradients are established and maintained across the cell membrane. Passive diffusion alone cannot explain the gradient; rather, work needs to be done within the system to drive it away from the equilibrium that would quickly become established if ions could diffuse freely. This work is done by ion pumps that drive specific ions against their concentration gradient using the chemical energy released by the hydrolysis of ATP molecules. The historical account of how this process came to be understood is as intricate and interesting as that of the progress toward the modern understanding of excitability, indeed, progress in both fields occurred synergistically. This is illustrated with reference to the sodium-potassium co-transporter in Glynn (2002).

1.2.4. What is excitability? A quantitative answer

The quantitative aspect of Hodgkin and Huxley's work is important for defining what is meant by excitability in a rigorous way. Excitability is an emergent property of the relationship between membrane potential and membrane conductance. As Hodgkin and Huxley demonstrated, the key property of the voltage dependence, kinetics and reversal potentials of the sodium and potassium conductances that leads to the abrupt change in membrane potential during an action potential is an intrinsic instability in the equations that describe these conductances. An excitable membrane is therefore one that has voltage-dependent conductance properties that make the membrane potential unstable in a particular range; the prototypical example of such an instability is the fast sodium-dependent neuronal action potential.

Insight into the nature of this instability was offered by Richard Fitzhugh (FitzHugh 1955). Interestingly, Fitzhugh's analysis showed that the Hodgkin-Huxley equations do not have a well-defined threshold for action potential initiation (FitzHugh 1955; Fitzhugh 1960) and can, in principle, exhibit voltage oscillations of arbitrary magnitude beneath that of the full-blown event. In the strictest sense, this contradicts the 'all-or-nothing' nature of the action potential. However, the parameters of the

Hodgkin-Huxley model in its original form indicate that this phenomenon is unlikely to be observed experimentally. This lack of a well-defined threshold for an all-or-none event is, in fact, true of all Type II excitable cells, and is a property which further distinguishes them from Type I cells. The details of the mathematical analysis that characterises these differences is presented in a thorough exposition by Rinzel and Ermentrout (in Koch and Segev 1998) and Izhikevich (2000). This kind of mathematical analysis, and the empirically-derived models it is applied to, are important because they gives a precise description of how excitable behaviour can be qualitatively different (Type I vs Type II) firing, and it shows that neurons do not simply behave as threshold devices that integrate synaptic input and fire at a given threshold.

Another insight provided by analysing the Hodgkin-Huxley equations is that the initiation of action potentials depends on the form of the applied stimulus. In particular, long, steady depolarising current applied to the membrane causes it to spike at a lower membrane potential than short current pulses. This fact is expounded in an elegant paper by Bennet, Hille and Obara (1970) where it is illustrated using a plot of intrinsic membrane current as a function of membrane potential for the Hodgkin-Huxley equations, reproduced in Figure 1.4.

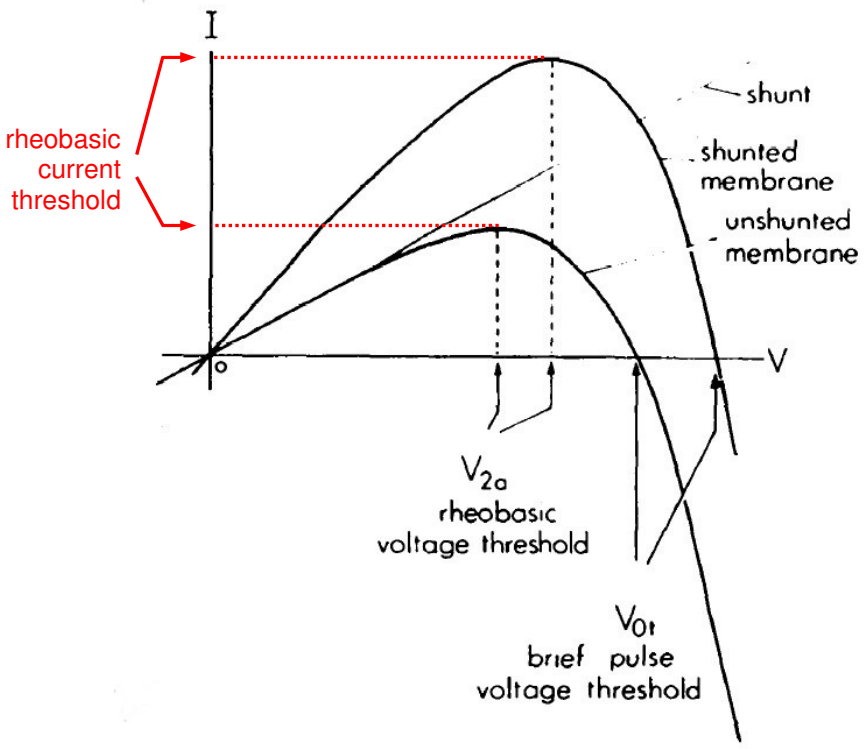

Figure 1.4: Threshold behaviour in an active membrane

Membrane current, I, plotted against membrane potential, V, for the Hodgkin-Huxley model. Voltage thresholds are shown, corresponding to the membrane potential thresholds for short and long current pulse stimuli, respectively. Taken from (Bennett *et al.* 1970) and adapted to show rheobasic current threshold (red).

In the figure, a standard convention is adopted in which inward (depolarising) current resides on the negative scale of the vertical axis, while outward (hyperpolarising) current is positive. Membrane potential is represented on the horizontal axis, such that the rightward direction is depolarising[1] with respect to the resting potential, which is at the origin. Two current-voltage curves (IV curves) are depicted, one with membrane current 'shunted', and the other 'unshunted'. Considering the former curve by itself to begin with, the voltage threshold for initiating spikes is seen to occur at a potential where the curve intersects the voltage axis and intrinsic membrane current becomes depolarising. Instantaneous excursions in voltage would

[1] 'Depolarising' is being used in the conventional physiological sense here, which indicates a shift in membrane potential toward zero, relative to the extracellular space. This does not correspond to zero on the membrane potential axis in this example because resting potential has been subtracted from the abscissa.

need to reach this value, the 'voltage threshold' in order to initiate an action potential. Thus *short, depolarising stimuli* initiate action potentials beyond this threshold.

Steady, depolarising current injection, on the other hand, would serve to translate the curve downward. If the magnitude of this current injection is large enough, a situation is reached in which the maximum point of the IV curve crosses the *x*-axis and intrinsic membrane current becomes purely depolarising. In this case, the membrane potential is unstable and action potentials are elicited.

The latter type of threshold is known as the current threshold, or 'rheobase', and the corresponding movement of the current-voltage maximum point across the voltage axis is an example of a 'bifurcation' in the dynamics of the system. From the diagram it is clear that the rheobasic voltage threshold occurs at a lower membrane potential than the 'brief pulse' voltage threshold. Consequently, depolarising current that is applied over long durations evokes action potentials at a lower membrane potential and with less current compared to short pulses. This difference is further exaggerated in the dynamic case due to membrane capacitance – an aspect of the dynamics that is not captured in the figure. The 'shunted' curve represents the effect of increasing the membrane conductance, which raises both the current and voltage thresholds. This simple diagram is clearly important for understanding the physiological behaviour of neurons, and gives a concise and rigorous meaning to excitability in terms of instability in the intrinsic current-voltage relationships of the membrane.

1.2.5. Beyond Hodgkin and Huxley: conductances become channels

In the years that followed Hodgkin and Huxley's work, advances were made in the technology available for electrophysiology, in particular in amplification equipment and microelectrodes for conducting recordings using small cells such as neurons in the CNS. In addition, a variety of new preparations became established as favourite model systems for studying excitability.

In a series of papers published in 1971 John Connor and Charles Stevens offered several insights into excitable behaviour, including the identification of a new type of

voltage-gated potassium current, the 'A' current (Connor and Stevens 1971c; 1971b; 1971a). Taking advantage of the recently-developed whole-cell two-electrode voltage-clamp recording method, Connor and Stevens characterised the membrane conductance behaviour of single, dissociated neurons isolated from molluscan ganglia. As part of this work, they applied the Hodgkin-Huxley formalism to model the repetitive spiking behaviour of a single neuron expressing the A-current.

Although it did not refer to the earlier work of Hodgkin (1948), Connor and Stevens' paper on the A-current established its involvement in Type I excitability (Connor and Stevens 1971b). Indeed, their careful analysis using a computer model shows that A-current dominates in the inter-spike interval during repetitive firing, and provides shunting current to delay the onset of action potentials at low stimulus intensities.

Deeper insight into the nature of voltage-gated membrane conductances, and confirmation, to a certain extent, of the gating particle theory of Hodgkin and Huxley, was provided with the first observation of 'gating current' (Armstrong and Bezanilla 1973; Schneider and Chandler 1973). In this work, the small current flow associated with the movement of charged regions, or 'voltage sensors' in putative membrane channels was detected in muscle preparations. At the time, the pore theory of membrane conductance was widely accepted[2], to the degree that conductances were already termed 'channels', even though no direct evidence for their existence had been established.

The first electrophysiological recording of single ion channel currents, which provided strong evidence of the existence of ion channels was published by Erwin Neher and Bert Sakmann in 1976 (Neher and Sakmann 1976). This achievement is a milestone in the modern era in electrophysiology and it stimulated research into the identification of genes responsible for ion channels. It is interesting to note that the pore theory of membrane conductance remained controversial throughout this time, until the molecular structure of individual ion channels was finally uncovered (for a lively account of the controversy and its eventual resolution, see Hille *et al.* 1999).

[2] The origin of the idea of membrane channels is attributed (Hille 2001) to Ernst Bruke (1819 – 1892), a contemporary of du Bois Raymond and von Helmholtz, who postulated their existence while investigating osmosis using pigs' bladders.

This had to wait for more than twenty years, when, in 1998, the first crystallographic structure of the pore-forming protein subunits of the *streptomyces* K^+ channel were published (Doyle *et al.* 1998).

It would be difficult to dispute the contention that advances in understanding electrical excitability throughout the intervening years are dominated by the discovery and classification of ion channels. In the early 1980s the first ion channel gene sequences were identified, which permitted cloning of individual channel subunits. The first channels to be identified and cloned in this way were voltage-gated sodium channels and nicotinic acetylcholine receptors (Noda *et al.* 1982; Mishina *et al.* 1984; Noda *et al.* 1984; Noda *et al.* 1986). These channels were heterologously expressed in *Xenopus laevis* oocytes, a process that exploits the translation machinery of the cells to make protein from injected mRNA. Cloning and heterologous expression of the first calcium channels followed a few years later (Tanabe *et al.* 1987; Mikami *et al.* 1989).

One particularly interesting account of channel identification and cloning is that of the *Shaker* potassium channel gene in the fly species *Drosophila melanogaster*. These channels were identified by isolating cDNA from a strain of flies that had been observed to shake uncontrollably when anaesthetised with ether. A defect in A-type potassium current was later found to be the electrophysiological correlate of this phenotype (Salkoff and Wyman 1981). Subsequent cloning and expression of the gene responsible for this phenotype established that is was, indeed, a gene for a potassium channel with properties that were characteristically A-type (Papazian *et al.* 1987; Tempel *et al.* 1987; Iverson *et al.* 1988).

The identification and cloning of ion channel genes is important for many reasons, four will be provided here. Firstly it permits structure-function relationships of individual ion channel subtypes to be explored, including the mechanism of action of pharmacological agents on the channels and the structural features that determine gating and ion selectivity (Armstrong and Hille 1998).

Secondly, it enables the study of expression level and localisation within tissue. For example, ion channel protein can be used to raise antibodies for examining regional

expression of ion channels in the brain, and even the distribution over the membrane of single cells (Harlow and Lane 1999). In addition, the expression profiles of ionic conductances can be examined from the levels of mRNA expressed in cells using in-situ hybridisation with short, complementary RNA probes labelled with radioactive markers (Darby and Hewitson 2006).

Thirdly, knowledge of ion channel genes, in tandem with the availability of methods to manipulate gene expression in transgenic animals (Picciotto and Wickman 1998), allows precise manipulation of the electrophysiologcal characteristics of cells in living animals. Not only does this permit study of the physiological function of ion channels, but it enables the etiology of diseases associated with ion channel mutations to be studied using animal models (Meisler *et al.* 1997). Work of this kind bridges the gap between ion channel biophysics, electrophysiology on the single-cell level and behavioural phenotypes manifested in the organism as a whole.

Fourthly, and most importantly from a philosophical viewpoint, gene sequences for ion channels enable the process of evolution to be understood on a molecular level. Many structural features of ion channels are conserved across species. This is particularly evident in sequence domains that code for important regions of the protein such as the pore region (for examples related to potassium channel evolution, see Jan and Jan 1997).

Comparisons of ion channel subtype structure and expression between species, and between cell types for a given species, helps to account for the diverse ways in which ionic currents and excitability contribute to physiology. Indeed, part of the power and flexibility of the nervous system as a whole is attributable to the fact that it comprises neurons with many different electrophysiological behaviours. The next section will discuss this diversity, its origin, and its functional significance.

1.2.6. Diversity in excitable properties of neurons and factors that contribute to this diversity.

As neurons differentiate and develop in the cortex, their ion channel expression profiles change and they acquire a characteristic membrane conductance profile, which can differ systematically across brain regions and cell types (Spitzer 1991). Accordingly, diverse types of firing patterns are found across cell types (Llinas 1988; Connors and Gutnick 1990).

For instance, inhibitory neurons, or interneurons, in the cortex and hippocampus, often have distinct type II firing properties that distinguishes them from excitatory cells such as pyramidal cells (McBain and Fisahn 2001). This difference can often be explained by differential ion channel expression in the two broad cell types. To give an example, fast spiking interneurons in the cortex express Kv3.X channel subunits, whereas expression of this gene is low in pyramidal cells, which do not possess the fast-spiking phenotype (Martina *et al.* 1998). Indeed, morphological features that distinguish these cells are often correlated with either Type I or Type II firing (Kawaguchi 1993; 1995; Tateno *et al.* 2004).

Another distinct physiological phenotype that is expressed through excitability is the phenomenon of *resonance*. A passive electrical membrane acts as a low-pass filter, responding to prolonged changes in membrane potential but filtering, or 'averaging out' more transient signals. The sub-threshold behaviour of many cells approximates this kind of behaviour (exemplified in hippocampal pyramidal cells in Spruston and Johnston 1992). However, certain membrane conductances that are active at sub-threshold potentials, particularly the hyperpolarisation-activated mixed-cation current, I_h, endow the membrane with a resonant frequency response (Dickson *et al.* 2000). This property means that cells are selectively tuned to fire action potentials in response to input at a given frequency. Interestingly, a physiological role for sub-threshold resonance in the entorhinal cortex has been hypothesised recently (Burgess *et al.* 2007), suggesting that interference patterns in the activity of coupled stellate cells give rise to the 'grid cell' phenomenon – a promising candidate for the physiological substrate of spatial navigation in rats (Hafting *et al.* 2005; Witter and Moser 2006).

Cells with a particular electrophysiological phenotype can often be identified by their morphology as well as the region of the nervous system they inhabit. Indeed, cell morphology itself has a significant impact on electrical behaviour (Rall 1962; Koch *et al.* 1983; Koch 1999; van Ooyen *et al.* 2002). The extensive dendritic processes in a typical neuron serve to shunt current and filter electrical signals, and can often display regional variations in ion channel distribution. In addition, dendrites often express active, voltage-gated ion channels which further contribute to the complexity of their electrical behaviour (Johnston *et al.* 1996).

Morphology, by itself, can have surprising effects on the qualitative nature of excitability as well as determining passive characteristics and constraining the distribution of ion channels. The propensity of cells to fire either tonically, or in bursts, can, in fact, be dictated by cell morphology alone for certain distributions of active membrane conductances. This has been demonstrated in computer modelling work which explores the effect of varying the coupling strength between dendritic compartments and the soma, and axon (van Ooyen *et al.* 2002).

Interestingly, a systematic study of the relationship between intrinsic properties and morphology in a single subtype of neurons of the deep cerebellar nuclei showed that gross morphology was independent of intrinsic properties across this population (Aizenman *et al.* 2003b). The same study also reported a high degree of variability in intrinsic properties of the same cells, which may suggest that membrane conductances are regulated in a way that compensates for the effects of morphology.

The interplay between morphology and ion channel expression, and their impact on excitability is therefore complex, and there is considerable redundancy in the factors that determine the electrophysiological phenotypes of neurons. As a consequence, it is difficult to establish a causal link between morphology and ion channel expression because both are heavily dependent on endogenous and exogenous regulatory processes. For example, during growth, ion channel expression changes, as does cell morphology – but it is hard to say whether changes in ion channel expression occur as the result of a compensatory response to morphological changes, and this would be difficult to test experimentally. These matters will be returned to in the next section, which discusses how intrinsic conductances are dynamically regulated to

achieve stable firing properties.

While distinct firing patterns are often associated with distinct cell types, it is possible for individual cell types to exhibit more than one firing mode. In fact, individual cells can switch firing modes depending on their physiological state. A classic example of this dual behaviour is given by thalamic relay cells, which can fire in burst-mode or tonic-mode (Llinas and Jahnsen 1982). These two modes are thought to correspond to distinct modes of information transfer, and the physiological basis for the change in firing pattern is the modulation of a T-type voltage-gated calcium conductance (Coulter *et al.* 1989; McCormick and Huguenard 1992; Sherman 2001).

A change in firing pattern within a given cell type can also be associated with pathological states. Part of the etiology of Parkinson's disease is thought to be linked to a change in the properties of glutamatergic neurons in the sub-thalamic nucleus. These cells change their firing pattern from single spikes to bursts when Parkinsonism is induced in animal models. This change is due, also, to modulation of voltage-gated calcium conductances (Beurrier *et al.* 1999).

1.2.7. Changes in excitability associated with learning and memory – *plasticity* of intrinsic excitability

One of the over-arching goals of physiology in neuroscience is to understand the cellular basis of learning and memory (Thompson 1986; Kandel *et al.* 2000). Until relatively recently, this research has been dominated by work on synaptic plasticity and its relation to Hebbian learning, a principle in which correlated activity between synaptically coupled cells leads to stable changes in the strength of the synaptic connection. This process and its underlying biochemistry have been characterised in many species and preparations from *Aplysia* to rabbits (Kandel 1989; Malenka and Bear 2004). One of the most well-characterised mammalian models of synaptic plasticity is long-term potentiation in the hippocampal slice preparation (Bliss and Collingridge 1993). In this model, brief trains of high-frequency stimulation are observed to cause lasting changes in the synaptic strength between excitatory synapses.

While conducting experiments to study this phenomenon at Schaffer collateral/commissural fibre-CA1 synapses in the rat, a stable decrease in the amount of current required to elicit action potentials was observed in the postsynaptic cells (Chavez-Noriega *et al.* 1990). This provoked interest in examining activity-dependent plasticity in the intrinsic excitability of neurons, as this provided a potential mechanism for the cellular basis of learning and memory that is distinct from synaptic plasticity.

Later studies established that acute Hebbian-like enhancement of neuronal excitability can be reliably induced in a variety of preparations in response to direct stimulation. (Armano *et al.* 2000; Ganguly *et al.* 2000; Daoudal *et al.* 2002; Cudmore and Turrigiano 2004; Li *et al.* 2004; Xu *et al.* 2005). Due to the way in which these changes are induced, which typically involves high frequency stimulation of individual cells, the collective phenomenon has been dubbed 'long-term potentiation of intrinsic excitability' (LTP-IE) by some authors (Cudmore and Turrigiano 2004; Xu *et al.* 2005). While most studies induce these changes using artificial stimulation, similar changes have been reported to occur in response to purely synaptic input (Aizenman and Linden 2000; for a review, see Zhang and Linden 2003).

Such 'intrinsic plasticity' has been directly linked to behaviour and is a candidate mechanism for learning and memory, and physiological processes that facilitate learning and memory such as attentional modulation (Zhang and Linden 2003). One of the most remarkable examples of this role for intrinsic excitability comes from studies of the trace-eyeblink conditioning protocol in rabbits. This protocol isolates a hippocampus-dependent component[3] of conditioned learning, in which a conditioned response (eyeblink) is learned by associating an air-puff (unconditioned stimulus) onto the eye with a brief, audible tone (conditioned stimulus) (Solomon *et al.* 1986). Hippocampal slices obtained from animals that are trained to respond to the conditioned stimulus showed an increase in excitability in the CA1 pyramidal cell population, moreover, this increase was not observed in animals that did not respond to conditioning (Moyer *et al.* 1996). This study establishes a link between intrinsic

[3] This form of learning is not exclusively dependent on the hippocampus; in particular, it also has a cerebellar component.

plasticity and learning and memory analogous to the evidence for synaptic mechanisms such as LTP.

1.3. Excitability in context: the need for regulation.

The purpose of this thesis is to study how excitability is regulated in response to chronically-induced membrane potential depolarisation. The motivation for this work comes, in part, from a popular hypothesis concerning the regulation of intrinsic excitability. This hypothesis, its motivation and the evidence in support of it will be outlined here.

1.3.1. The homeostatic hypothesis of intrinsic excitability regulation

As pointed out in Marder (2006) a typical neuron in the human CNS lives for decades. During this time, numerous perturbations in its mean activity will be imposed as a result of the normal function of the nervous system: synapses form, synapses are eliminated and synapses alter in strength; afferent input and endogenous activity vary constantly as a result of external stimuli and attentional modulation. Consequently, individual cells will be exposed to periods of quiescence and periods of very high activity. In order to retain stable function, it is hypothesised that cells possess homeostatic mechanisms which track their mean activity and alter membrane channel expression in such a way as to counter long-term perturbations.

To summarise, three motivating reasons are postulated for homeostasis of intrinsic excitability:

1. To compensate for changes in the mean levels of activity that occur in a cell or network of cells as a result of activity-dependent plasticity.

   Changes in excitatory synapse efficacy are known to occur as a result of elevated activity (Malenka and Nicoll 1999). This is thought to underlie certain types of learning and memory in the mammalian hippocampus (Bliss and Collingridge 1993). Runaway excitation might occur if there were no regulatory mechanisms in place to control mean activity levels in the presence of this kind of synaptic plasticity (Abbott and Nelson 2000). Moreover, the acute activity-dependent changes in intrinsic excitability that

are analogous to synaptic (LTP-IE) contribute to such instability. Homeostatic regulation of intrinsic excitability is posited as one of the ways the nervous system can achieve this balance (Davis and Bezprozvanny 2001; Desai 2003; Turrigiano 2007).

2. To counter the effect of changes in cell morphology and afferent input that occur during development, and changes in mean activity due to external stimuli.

   As the nervous system develops and matures neurons are exposed to drastic changes in the mean excitatory drive, for example, during synaptogenesis (Turrigiano 1999). By modulating the complement of ion channels expressed in the cell membrane, neurons are able to compensate for these changes, and changes that are imposed post-developmentally, in order to remain electrically active within an optimal range (Zhang and Poo 2001; Turrigiano and Nelson 2004).

3. As a means of robustly and efficiently defining electrical properties of individual cell types.

   Different cell types exhibit different electrical properties. These properties can, however, be achieved using a variety of combinations of membrane conductances (Golowasch *et al.* 2002; Prinz *et al.* 2004; Swensen and Bean 2005). Such redundancy in the mapping between electrophysiological phenotype and ion channel expression suggests that general parameters that determine an individual cell's firing properties are determined when the cell terminally differentiates, but the precise expression levels within that cell are determined dynamically (Golowasch *et al.* 1999b; Goldman *et al.* 2001; Marder and Goaillard 2006). This means that cells are robust to changes in mean levels of activity, and that the amount of 'genetic information' required to specify the electrophysiological phenotype of different cell types is minimised.

The homeostatic hypothesis does not place constraints on the precise mechanisms by

which mean activity is controlled. Indeed, homeostatic control of mean network activity has been observed to occur in other ways, often in the form of distributed changes in synaptic strength, a phenomenon termed 'synaptic scaling' (Turrigiano 1999). Synaptic scaling involves upregulation of excitatory synaptic strength and downregulation of inhibitory synaptic strength in response to activity deprivation (Turrigiano *et al.* 1998; Kilman *et al.* 2002). Opposite changes occur in response to elevated activity, or sustained depolarisation (Leslie *et al.* 2001). This thesis is principally concerned with homeostasis of intrinsic properties, for which there is corresponding experimental evidence, discussed next.

1.3.2. Evidence for regulation of intrinsic excitability

By the 1990s cell culture technology had progressed to a point which allowed neurons to be isolated from many different sources, including mammalian species, and maintained for extended periods in well-defined culture conditions. Accordingly, a great deal of progress was made in the intervening years toward understanding how conditions in the extracellular environment impinge on the properties of neurons over time.

Early evidence for regulation of intrinsic conductances was provided in a study of chronically depolarised hippocampal neurons (Franklin *et al.* 1992). Elevated extracellular potassium (25 mM) was found to down-regulate the expression of voltage-gated calcium currents over a period of several days in culture. Importantly, this alteration in expression is transcription and translation-dependent – a feature that was demonstrated by blocking these processes with actinomycin and cycloheximide. This suggests that neurons are capable of countering the effects of perturbations in their level of depolarisation by altering the expression of genes responsible for voltage-gated ion channels. Moreover, the study in question reported that blockade of L-type calcium channels with dihydropyridines during the depolarisation period prevented the change in expression of L-type current, but did not appear to prevent a change in other calcium channel subtypes. This suggests that the regulation mechanism is specific to particular channels, and is capable of detecting channel activity independently of ion flux within the cell.

Such channel-specific regulation should be anticipated given the potentially drastic effect that changes in particular conductances can have on the electrical properties of cells, especially neurons. In order to maintain these properties in spite of extraneous changes that occur naturally in the nervous system, some kind of homeostasis must exist in the expression levels of channel proteins. This idea fuelled speculation that neurons possess a characteristic signature in their spiking behaviour and they strive to maintain this by modulating their electrical properties when necessary (LeMasson *et al.* 1993). Such a hypothesis is conceptually straightforward to test experimentally: find a neuron subtype with well-defined firing properties and perturb its environment in a way that alters these properties. According to the homeostatic hypothesis, the cell should alter its conductances in such a way as to counter the imposed changes and re-establish its original firing properties.

1.3.3. A crucial experiment

The first concrete and convincing experimental test of this hypothesis was provided by Eve Marder and Gina Turrigiano (Turrigiano *et al.* 1994). Using primary cultures of crustacean central neurons, Turrigiano examined how the intrinsic electrical properties of the cells alters in response to long-term changes in spiking activity.

The stomatogastric ganglion (STG) of the lobster *Panulirus interruptus* contains a reciprocal excitatory-inhibitory network of neurons which acts as a pattern-generating network for controlling muscle contraction during feeding (Weimann *et al.* 1991). This network can be excised from the animal and maintained in vitro, where the stereotyped bursting activity pattern of the cells can be recorded. If the cells are pharmacologically isolated in this preparation using blockers of synaptic transmission, the bursting activity ceases and the cells respond to injected current by firing tonically (Figure 1.5B).

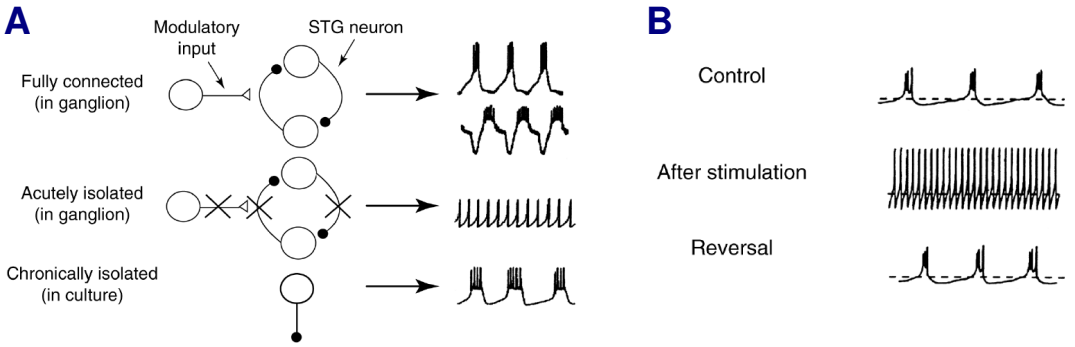

Figure 1.5: Homeostatic regulation of intrinsic excitability in STG neurons

(A) STG neurons fire rhythmically in the intact STG network as a result of synaptic and modulatory input. When pharmacologically isolated from this input in an acute manner, they fire tonically. Chronic isolation, however, induces a gradual change in intrinsic properties of STG neurons and they regain their rhythmic firing phenotype despite being deprived of synaptic and modulatory drive. **(B)** Chronically isolated cells return to tonic firing if artificially stimulated in a way that mimics the rhythmic bursting activity seen in an intact network. This effect reverses hours after stimulation is withdrawn. All figures reproduced from (Turrigiano 1999)

As an alternative to using antagonists of synaptic transmission, physical isolation of STG cells from each other imposes a permanent elimination of the synaptic network which should also abolish the rhythmic firing pattern. Indeed, when the ganglion cells are dissociated and maintained in culture for 1-2 days, bursting ceases and the electrophysiological behaviour of the cells is found to be similar to that of the pharmacologically isolated cells. However, after several additional days in culture, the cells reacquire their bursting behaviour, even though the synaptic connectivity pattern is absent (Turrigiano and Marder 1993). Remarkably, this transition can be reversed if the cells are artificially stimulated in a rhythmic fashion, as though they are once again part of an intact ganglion network (Figure 1.5).

A series of publications associated with this work established that alterations in the expression of active membrane conductances, in particular, voltage-gated calcium channels, underlie this particular example of excitability homeostasis (Golowasch *et al.* 1992; Marder *et al.* 1993; Golowasch *et al.* 1999b; Richards *et al.* 2003; Marder and Bucher 2007).

The favoured interpretation of this result is that the stomatogastric ganglion cells somehow 'want' to fire in a bursting pattern and will adjust their intrinsic conductances in order to achieve this goal (Marder and Goaillard 2006; Marder and Bucher 2007). Presumably, this cell-autonomous determinant of electrical properties is a result of a stable genetic programme that is invoked when the cell differentiates – a programme that is perhaps analogous to the processes that give rise to distinctive cell morphologies and the type of neurotransmitter they release.

1.3.4. Related work

The seminal work of Turrigiano and Marder has been extended in other studies of intrinsic homeostasis. One particularly important publication that is closely related to the work in this thesis is a study by Desai *et al.* (1999b) that examines how intrinsic excitability is modulated by a sustained reduction in mean activity. The study in question reports that activity deprivation by TTX over the course of days induces a lasting increase in the intrinsic excitability of cultured cortical neurons. This change is accompanied by corresponding changes in the active membrane conductances of the affected cells; in particular, the amplitude of evoked voltage-gated sodium currents is increased relative to control values, while the amplitude of delayed-rectifying voltage-gated potassium current is reduced. Similar observations were, in fact, made nearly a decade earlier by Ramakers *et al.* (1990), who reported increases in mean network activity after TTX-induced activity deprivation.

Other work has demonstrated the involvement of the mixed cation, hyperpolarisation-activated current, I_h, in homeostasis. Artificially induced barrages of excitatory input using direct glutamate application and latrotoxin-induced synaptic release has been shown by van Wellie et al. (2004) to lower the intrinsic excitability of affected cells by selectively enhancing I_h. A further study showed a rapid downregulation of voltage-gated potassium conductances in response to activity blockade, establishing that homeostatic regulation of conductances can occur on a timescale of minutes (van Welie *et al.* 2006).

What biochemical signalling pathways are responsible for activity-dependent ion channel expression? Both theoretical and experimental work have provided some

insights. Intracellular calcium is often posited as the 'activity sensor' in neurons which triggers the homeostatic response, and has been shown to produce realistic behaviour in computer models of homeostasis which use intracellular calcium as the state variable that governs ion channel regulation (LeMasson *et al.* 1993; Siegel *et al.* 1994; Liu *et al.* 1998). This hypothesis is attractive for two reasons. Firstly, intracellular calcium concentration is dependent on membrane depolarisation through the action of voltage-gated calcium channels. Secondly, calcium is a ubiquitous intracellular second messenger, on which numerous enzymatic pathways depend, including ion channel gene expression (Barish 1998). However, there is little direct evidence that calcium influx, *per se*, is the trigger for homeostatic responses. One of the results of this thesis is a demonstration of this dependence for one particular type of homeostasis.

Other work has uncovered several distinct regulatory mechanisms involved in controlling ion channel expression in an activity-dependent way. Prolonged seizure-like excitation in organotypic hippocampal slices is know to induce compensatory changes in synaptic strength and intrinsic properties. In one study (Seeburg and Sheng 2008) this was found to depend on the activity of a polo-like kinase. Interestingly, these kinases are important in regulating the cell-cycle and are implicated in pathological states such as tumour growth in non-neuronal cells. This suggests that ion channel regulation involves fundamental biochemical pathways that are common to many cell types.

In similar experimental models, direct phosphorylation of Kv2.1 channels is observed in response to elevated, seizure-like activity in systematic studies in the hippocampi of rats *in-vivo* and *in-vitro* (Misonou *et al.* 2004; Misonou *et al.* 2006). This initial response is accompanied by corresponding changes in membrane conductance density and in the surface expression pattern of subunits, revealed by whole-cell recordings and immunocytochemistry. In Drosophila, direct regulation of sodium channel subunit mRNA translation via the action of a translational repressor, *pumillo*, has been demonstrated to both enhance and reduce excitability when excitatory synaptic transmission is, respectively, blocked and facilitated (Mee *et al.* 2004).

The latter studies also show direct evidence of homeostatic excitability regulation in intact nervous systems. More subtle manipulations, in vivo, can also induce excitability homeostasis. For example, long-term modifications in $GABA_A$ receptor-mediated tonic inhibition in mice have been shown to provoke a compensatory response in the intrinsic properties of neurons in the cerebellum. Interestingly, this is conferred by changes in leak conductances, but not voltage-gated conductances (Brickley *et al.* 2001). Finally, a remarkable recent study provides direct experimental evidence that homeostasis is employed to maintain optimal function in the nervous system. In this work, Aizenman *et al.* (2003a) show that visual stimulation of tadpoles simultaneously modulates the intrinsic excitability and synaptic efficacy of neurons in the optic tectum, in a way that optimises stimulus detection along the visual pathway. This work contributes to the mounting evidence of the synergy between alterations in synaptic transmission and afferent input, and intrinsic homeostasis.

1.3.5. Recapitulation and final thoughts

Excitability, defined in terms of the firing properties of a neuron, is a function of the passive and active electrical properties of the cell membrane. Membrane properties differ widely between cells, as does electrical behaviour. In many cases the electrical behaviour of a neuron is tailored to a particular task in the nervous system. As Bertil Hille puts it, “Like the stops on an organ, the diversity of available channels is used to give timbre to the functions played by excitable cells.” (pp 131, Hille 2001). An important question emerges from these observations: how do cells regulate their membrane properties to achieve and maintain their characteristic properties? This question defines the agenda of a substantial body of current research, and the answer to it is likely to be very complicated indeed. What is known presently, is that, in response to perturbations the input they receive, neurons appear to homeostatically regulate their membrane conductances to achieve a target level of activity, and even a particular pattern of activity. In addition, a considerable diversity exists in the preparations in which this is observed, and in the types of underlying membrane conductances that are involved.

The specific conductance profile for a given target activity is not well-defined,

however. For example, active conductances in particular can exhibit a dramatic variability in their relative expression levels, even across a population with stereotyped excitable behaviour (Swensen and Bean 2005). From the point of view of understanding ion channel regulation, this impasse is as frustrating as it is interesting: if a given behaviour can be achieved with numerous combinations of conductances, how does a cell 'choose' which channel subtypes to regulate?

Put another way, the mapping from the parameter space of conductance distributions to firing properties is many-to-one. If we accept that firing properties are regulated to achieve proper functioning of neural circuits, as a weight of evidence suggests (Marder and Goaillard 2006), then the underlying regulatory mechanisms must somehow find an inverse to this mapping – even though a global inverse does not exist.

Presumably each cell finds a local inverse to this mapping, perhaps due to some predisposition for expressing a given channel subunit over another. Why, then, do cells not converge on the same expression profile for a particular target behaviour? The answers to the questions posed here will only emerge through further research into the relationships between perturbations in activity and ion channel regulation, and the relationships between ion channel expression and intrinsic excitability.

The remaining chapters of this thesis will describe work that makes a small contribution toward answering the wider questions posed here. Specifically, the long-term response of neurons to sustained depolarisation will be characterised, along with the changes in membrane conductances that underlie the response.

Chapter 2. Methods

2.1. Introduction

This chapter describes the methods, equipment and regents that are used throughout the experimental work. For certain experiments and methods, it is more appropriate to discuss methodological details in the corresponding results section, for example, the concentration of a particular drug being used. Therefore, the methods described here are those that are general in nature, or those which require a particularly detailed exposition. Supplier and manufacturer details are provided for reagents and equipment where appropriate[4].

2.2. Cell cultures

The protocol for primary hippocampal cultures is derived from that of Banker & Goslin (1998) with modifications implemented through direct consultation with investigators in three labs: Dr Guo Qiang Bi (University of Pittsburgh), Dr Giles Hardingham (University of Edinburgh) and Dr Paul Skehel (University of Edinburgh).

One of the most important tasks in this work is to obtain healthy cultures at a low plating density. Low density cultures permit identification of cell morphology and processes. This facilitates the identification of synaptically coupled excitatory cells for STDP experiments (Bi and Poo 1998).

Cells are grown on 15 mm glass coverslips for up to 18 days in a humidified incubator at 37ºC, 5% CO_2. The coverslips are transferred directly to the recording chamber for electrophysiology after incubating them in external recording solution for several minutes at room temperature. Cell health is monitored and recorded according to the observations made during experiments, or by visual examination of the cultures using a phase-contrast microscope at various stages after plating.

[4] For example, patch amplifier models are listed, but the NaCl supplier is not. The convention that determines this distinction is that the former item might exhibit peculiarities that affect the experimental results, whereas the latter is quite generic

2.2.1. Materials and equipment

Reagents, equipment and consumables that are used specifically for cell culture are listed below.

Reagents	**Details;** *supplier*
70% Ethanol	Diluted from 100% with dH_20; *Fisher*
Halothane	*Sigma*
Dissection buffer: sterile, Ca^{2+}- and Mg^{2+}-free HBS (HEPES-buffered saline)	pH 7.3, contains phenol red; *Invitrogen*
Complete media	Neurobasal media supplemented with: 100% B-27, 1% foetal bovine serum, 100 µM l-glutamine, 100% penicillin-streptomycin solution; *all supplied by Invitrogen*
Poly-D-lysine hydrobromide (molecular weight 150,000+)	10% (w/v) solution in dH_20; *Sigma*
Trypan blue solution	*Sigma*
Trypsin-EDTA solution	*Invitrogen*
Chicken egg white trypsin inhibitor	Stock: 10 mg/ml in dH_20, −20ºC; *Sigma*
DNAse	Stock: 1 mg/ml in dH_20, −20ºC; *Sigma*
Cytosine arabinoside	Stock: 30 mM in HBS, −20ºC; *Sigma*

Equipment	**Comments**
Cell culture:	
Sterile flow-hood	
Water bath	Set to 37 ºC
Dissection microscope	Top-lit
Humidified CO_2 incubator	
Haemocytometer	
Inverted phase microscope with 20X objective	For cell counting
Gilson pipettes: P1000, P200	Sterilised with ethanol
Dissection:	
Rodent guillotine	
Round-nosed surgical scissors (10 cm)	
Vanass spring scissors (14 mm)	
Vanass spring scissors (10 mm)	
Iris scissors	
Curved Dumont #7 forceps	
Dumont #5 forceps (×2)	
Spatula (5 mm width)	
Pasteur pipette	Cut at taper (2-3 mm hole), fire-polished and autoclaved

Consumables:	
Paper tissue	
Sterile latex gloves	
90 mm vented cell culture dishes	Sterile
35 mm vented cell culture dishes	Sterile
15 mm gauge-1 glass coverslips	Ethanol-washed, autoclaved
15 ml centrifuge tubes	Sterile
5 ml sample tubes	
dH_20 in squirt-bottle	
70% Ethanol in spray-bottle	
Re-usable ice pack	
Pipette tips: 1 ml and 250 µl	Autoclaved
Pasteur pipettes	Autoclaved

2.2.2. Preparation of coverslips

At least one day before culturing cells, sterilised 15 mm glass coverslips are placed in threes in 35 mm cell culture dishes. 1 ml poly-D-lysine solution that has been equilibriated at 37ºC is then added to each dish. After ensuring the slips are completely submerged, the 35 mm dishes are placed inside 90 mm dishes (three in each) and transferred to the incubator. A total of nine 35 mm dishes are usually prepared for each culture.

2.2.3. Primary hippocampal culture protocol

All dissection equipment and preparation surfaces are cleaned with 70% ethanol before proceeding. Sterile latex gloves are used throughout and changed between each procedure. Dissection tools are quickly rinsed with dH_20 when no longer needed. Care is taken to complete each procedure as quickly as possible; the typical time from termination of the animals to cell plating is one hour. Excluding dissection and cell counting, all procedures are performed in a sterile flow-hood. The protocol is described in steps as follows:

Step 1. Caesarean section

Sprague-Dawley rat pups aged E17 to E19 are obtained by caesarean section. The mother is terminally anaesthetised using halothane, decapitated to confirm death, then placed on a sterile bench area covered with 70% ethanol-soaked tissue. A serrated forceps is used to extrude the skin at the midpoint between the genitals and

the base of the ribcage and a v-shaped cut is made into the skin using round-nosed surgical scissors. The cut is extended up the midline approximately 3–4 cm, and laterally, if necessary, to expose the muscle tissue above the gut. Any loose fur is cleaned from the carcass and tools at this point, and the tools are sprayed with 70% ethanol once more. The muscle tissue is extruded in the same way as the skin, and in approximately the same place. Again, a v-shaped cut is made and extended along two lines in the direction of each forelimb for 3–4 cm. The abdominal cavity is now exposed, revealing the uterus which is gently teased from the abdomen using the serrated forceps. The uterus is then entirely removed by cutting the connective tissue along it, and severing it at the base, close to the cervix. A sterilised, lidded glass petri dish is used to receive the uterus.

Step 2. Cranial excision

Using a curved Dumont forceps and a 13 mm Vanass spring scissors, the pups are removed first from the uterus and then from their amniotic sacs by carefully piercing the membrane and dragging the pup out. The heads are cut off in one, clean cut with an iris scissors and placed in ice-cold dissection buffer in 5 mm sample tubes.

Once enough pups have been harvested, the heads are removed one by one from the dissection buffer to excise the brains. This is done under a dissection microscope in a 35 mm culture dish lid. The head is placed under the objective, scalp upward and secured at the nose with a curved Dumont forceps. A 10 mm Vanass scissors is used to make an incision at the back of the skull, just beneath the cerebellum. This incision is then extended around the base to the eyes on both sides.

Next, the scalp is peeled away from the brain using the curved forceps with the Vanass scissors holding the base of the skull at the back. The brain is then scooped out of the skull in one motion with a fine spatula and submerged in ice-cold dissection buffer in a 35 mm dish, which is placed on an ice-pack to maintain the temperature of the dish. This is continued until a sufficient number of intact brains have been obtained.

Step 3. Hippocampal dissection

Brains are transferred one at a time to a 35 mm culture dish containing fresh ice-cold dissection buffer for hippocampal isolation. Using a pair of Dumont #5 forceps, the meninges are removed first. Next, each hemisphere is teased away from the thalamus and cut free by pinching the connecting tissue. The hippocampi are isolated by using the tip of the forceps to cut along the entorhinal axis with small pinching motions. Once separated from the rest of the hemisphere, a Pasteur pipette is used to transfer the hippocampus to a 15 mm centrifuge tube containing 4 ml cold dissection buffer and placed on ice. This is continued until sufficient hippocampi have been obtained (six hippocampi are enough for a least nine 35 mm dishes).

Step 5. Dissociation

The tube containing the hippocampi is transferred to the 37ºC water bath for one minute. Pre-warmed trypsin-EDTA solution (6 ml) is then added to 4 ml volume of dissection buffer containing the hippocampi to obtain a 60% dilution. The tube is incubated at 37ºC for 15 minutes in the water bath, gently shaking every few minutes.

During the incubation with trypsin, the coverslips are removed from the incubator and rinsed in warm dissection buffer, then returned to the incubator after ensuring that the slips are arranged side-by side in the 35 mm dishes, with none of them overlapping.

One minute before the end of the 15-minute incubation period, aliquots (50 µl) of trypsin inhibitor and DNAse solution are defrosted in the water bath. At the end of the 15 minute incubation, the tube containing the hippocampi is transferred to the sterile flow hood and 8 ml of the trypsin solution aspirated, leaving 2 ml. Trypsin inhibitor solution (50 µl) is added to the tube and gently mixed using a pipette. The tube is returned to the water bath for a further 2 minutes. During this period, two sterile Pasteur pipettes are prepared and fire-polished, one to a fine tip and the other such that the hole remains similar in diameter to the thin shaft.

Next, the hippocampi are washed three times in warmed dissection buffer and placed in a fresh 15 mm centrifuge tube containing 5 ml warmed (37ºC) dissection buffer. 50 µl DNAse solution is added to the buffer and the hippocampi are gently triturated with the wide fire-polished Pasteur pipette for 1 minute, then with the fine pipette for a further minute, or until no lumps of tissue remain visible. The cell suspension is allowed to settle for one minute, then the supernatant carefully removed to a fresh 15 ml tube with a sterile pipette, leaving behind the surface fraction and the bottom 500 µl-fraction.

Step 6. Cell counting and plating

100 µl cell suspension is mixed with an equal volume of trypan blue solution in 1.5 ml centrifuge tube. A drop is placed on the haemocytometer and the glass slip replaced gently. The cells are then counted under an inverted phase-contrast microscope by taking the average cell density from the four counting grids on the haemocytometer. Cells that are filled blue are omitted from the count.

Next, the cell suspension is diluted to a final plating density of 50,000 cells/ml by adding an appropriate quantity to warm complete media, such that 14 ml final volume is obtained. The coverslips are removed from the incubator and 1.5 ml diluted cell suspension is added to each 35 mm dish. The dishes are returned to the incubator after ensuring the coverslips are settled at the bottom of each dish and are not overlapping.

Step 7. Feeding

One day after plating, the cultures are removed from the incubator and 1 ml media replaced with fresh media, or media supplemented with KCl, as appropriate. After 4 days in vitro (DIV) the cells are fed again by replacing 500 µl media. At 7 DIV, 50 µl ara-C solution is added to the cultures to inhibit growth of non-terminally differentiated cells. The cells are fed once more at 14 DIV if they are required, again by replacing 500 µl of the media.

2.3. Electrophysiology

2.3.1. Materials and equipment

The materials and equipment used for electrophysiology are listed as follows.

Item	Comments
Electrophysiology equipment:	*Manufacturer/supplier*
Upright phase-contrast microscope with 40× water-immersion objective	*Zeiss*
Axopatch 200B amplifier with headstage	*Axon instruments*
Axoclamp 700B amplifier with headstage	*Axon instruments*
Micromanipulator (×2)	*Sutter, Scientifica*
8-pole analogue low-pass Bessel filter	*UCL*
Digital oscilloscope	*Tektronix*
PCI analogue/digital board with external BNC module	*National instruments*
Pentium 4 PC running Windows XP and LabVIEW 8.2, LCD monitor	*Dell*
Rotary pump, perfusion system	
Drugs and reagents:	Stock solution; *supplier*
TTX (*Tetrodotoxin citrate*)	1 mM in dH_20; *Tocris*
CNQX (*6-cyano-7-nitroquinoxaline-2,3-dione*)	5 mM in dH_20; *Tocris*
PTX (*picrotoxin*)	5 mM in dH_20; *Tocris*
D-APV (*D-2-amino-5-phosphonopentanoate*)	50 mM in equimolar NaOH; *Tocris*
Nifedipine (*dimethyl2,6-dimethyl-4-(2-nitrophenyl)- 1,4-dihydropyridine-3,5-dicarboxylate*)	5 mM in DMSO; *Tocris*
Baclofen (*4-amino-3-(4-chlorophenyl)-butanoic acid*)	50 mM in equimolar NaOH; *Tocris*
Consumables:	Comments
Thick-walled borosillicate glass capillaries	
Thin-walled borosillicate glass capillaries	No filament, for perforated patch recording
35 mm vented cell culture dishes	Used for transferring coverslips from the incubator to the recording chamber
dH_20 in squirt-bottle	

2.3.2. Recording solutions

The external recording solution used in all experiments is a HEPES-buffered saline solution containing the following (in mM): NaCl (150), KCl (3), HEPES (10), Glucose (10), $CaCl_2$ (3), $MgCl_2$ (2), Glycine (0.05); pH adjusted to 7.3 using NaOH, osmolarity in the range 310-320 mOsm. This solution is made fresh for each experiment from a 10× stock solution that is free of $CaCl_2$, $MgCl_2$ and glycine. Pharmacological agents are dissolved in this solution at the working concentration in 50 ml aliquots.

Internal solutions are prepared and frozen at −20ºC in 1 ml aliquots that are defrosted immediately before use. The composition of each of the internal solutions used in this work is as follows.

Internal recording solutions

	Standard whole-cell	Caesium-based whole-cell	Perforated-patch whole cell
	Concentrations in mM		
K-gluconate	130	-	136.5
KCl	10	-	17.5
Cs-gluconate	-	130	-
CsCl	-	10	-
HEPES	10	10	10
EGTA	0.1	0.1	0.2
Glucose	10	10	-
NaCl	-	-	9
$MgCl_2$	-	-	1
Na-phosphocreatine*	10	10	-
Mg-ATP*	4	4	-
Mg-GTP*	0.5	0.5	-

Regents marked with an asterisk (*) are added to the internal solution separately and stored at −20ºC for no longer than one month before use. The pH of all internal solutions is adjusted to 7.3 using KOH (4M) or CsOH (2M) where appropriate; osmolarity is 290-300 mOsm.

Amphoteracin B (Sigma) is prepared at a concentration of 21 mg/ml in anhydrous DMSO and dissolved using a vortex mixer. Stock solution is stored in 10 µl aliquots

at −20ºC and protected from light.

2.3.3. Ionic reversal potentials and liquid junction potential

The Nernst equation (Section 1.2.1) is used to calculate the ionic reversal potential for chloride, potassium and sodium ions based on the concentrations of these ions in the internal and external recording solutions. For the standard whole-cell solution, the values (at 20ºC) are as follows: E_{Cl} = −69.2 mV, E_K = −97.1 mV, E_{Na} = +68.4 mV. The liquid junction potential was measured to be −12.3 mV for the bath and whole-cell recording solution (Neher 1992). Reported membrane potential measurements are uncorrected.

2.3.4. Recording

The reference text used for electrophysiological methods and analysis in this work is *The Plymouth Workshop Handbook* (Ogden 1994). Whole-cell recordings are performed on cultures that are at least one week old at room temperature (18 – 22 °C) using an upright microscope. Up to two cells can be patched simultaneously using the equipment available. Recording signals are low-pass filtered at a cut-off frequency of 5 kHz using an 8-pole Bessel filter. Tip, seal and access resistance are measured in real-time using a −5 mV, 5 ms square pulse at 100 Hz. Two distinct protocols are used in this work: standard whole-cell and perforated patch whole-cell.

External recording solution is continually perfused through the recording chamber at a rate of approximately 1 ml per minute using a gravity-fed perfusion line. Drugs are applied by switching the perfusion source between each of the five available 60 ml syringe reservoirs.

The criteria for including a recording at the analysis stage for voltage-clamp experiments are: stable access resistance, defined as a deviation of no more than 20% and with a value less than 30 MΩ; stable holding current (maximum 20% deviation), with a maximum value of 150 pA at a holding potential of −70 mV. From Ohm's law, the maximum error in the clamp potential with these criteria is 4.5 mV. For current-clamp experiments the criteria are the same, apart from allowing a higher maximum access resistance of 40 MΩ and defining stable resting potential as a

deviation of less than 5 mV. Cells with a resting potential more positive than −45 mV are excluded.

Series resistance introduces considerable voltage clamp errors in experiments where voltage-gated conductances are induced, especially if the magnitude of the resulting current is large. Whole-cell sodium currents, for example, which are large (several nA) and inward at the membrane potential required for initiation (about −40 mV) cause a substantial potential difference between the electrode and the cell compartment: a series resistance of 20 MΩ introduces a peak error of +20 mV per nA of current, a situation in which voltage control of the membrane is lost and an 'unclamped' current is recorded. Under such circumstances, the true IV relationship of the evoked current cannot be accurately measured and comparisons between cells can only be made provided there is no systematic difference in access resistance between recordings.

2.3.5. Standard whole-cell protocol

This recording protocol is used for most of the experiments in the thesis. Experiments which require stable recordings in excess of half an hour (STDP experiments) use the perforated-patch protocol described in the following section.

Step 1. Preparing and mounting electrodes

The method for obtaining standard whole-cell patches uses patch pipettes pulled from thick-walled glass capillaries to a tip resistance of 4−8 MΩ. After filling the electrodes with internal solution, the side of the electrode is tapped carefully to remove bubbles and then mounted on the electrode holder. The electrode itself consists of a piece of fine silver wire coated with silver chloride. Coating is replenished by electrolysis every week, or when the coating, which is black in colour, is visibly chipped or tarnished.

After mounting the electrode, slight positive air pressure is applied using the patch mouthpiece. The tip is then lowered into the recording bath under low-power magnification using a 4× bright field objective. Once the tip is in a focal plane several hundred microns above the target cell, a high-power water immersion phase-

contrast objective is used to guide the tip to the cell.

Step 2. Obtaining a gigaohm seal

To obtain a gigaohm seal, the glass electrode tip is manoeuvred to a point above the plane of the cell, at a position that corresponds to a normal orientation of the electrode when projected onto the plane of the coverslip. The tip is then slowly lowered onto the cell membrane a few microns at a time until a transient change in the tip resistance is registered in the test pulse waveform.

Positive pressure is relieved, and gentle suction applied until the seal resistance climbs above 100 MΩ. The holding potential is lowered to −40 mV at this point and suction applied as necessary to increase the seal resistance to above 1 GΩ. After a gigaohm seal is obtained, the seal resistance is monitored for several minutes. At this point, fast capacitance compensation is adjusted on the amplifier to remove the transient due to the patch pipette capacitance.

Step 3. Whole-cell configuration

If the seal remains stable, the holding potential is lowered to −60 mV and whole-cell configuration is obtained using short, gentle sucks on the patching mouthpiece until the characteristic exponential capacitive transient appears in the seal pulse current trace (Figure 2.1). The access resistance is measured directly from this trace. If necessary, additional suction is applied to obtain an access resistance less than 35 MΩ, or if the membrane spontaneously seals up. The cell is monitored for five minutes in this configuration, at which point experiments can commence.

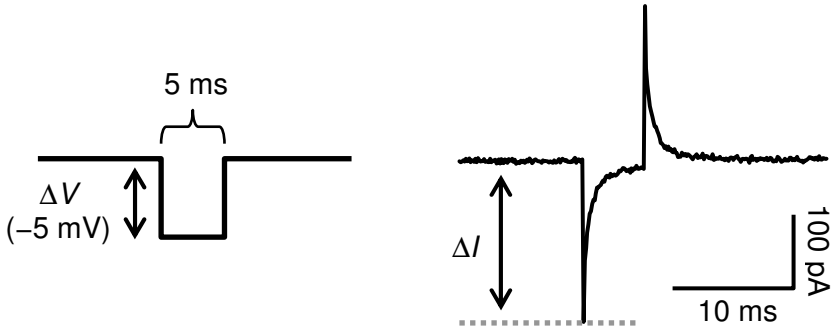

Figure 2.1: Whole-cell seal test

Access resistance is measured in voltage-clamp using 5 ms pulses with an amplitude of –5 mV (left). When whole-cell configuration is achieved, a characteristic exponential current trace appears (right). The value of the access resistance, R_a, is given by the quotient of the amplitude of the exponential transient to the amplitude of the voltage pulse: $R_a = \Delta V/\Delta I$.

2.3.6. Perforated-patch recordings.

Prior to performing perforated-patch recordings, a 10-µl aliquot of amphoteracin/DMSO stock solution is defrosted and mixed with 1.4 ml perforated patch internal solution to a final amphoteracin concentration of 150 µg/ml. The amphoteracin solution is dissolved fully by sonication for 30 s. An additional amphoteracin-free aliquot of perforated-patch internal solution is reserved for tip filling. Solution containing amphoteracin is kept away from light and replaced after three hours of use. The method for obtaining whole-cell recordings using the perforated-patch method is essentially the same as for standard whole-cell recordings, with several important differences that are described in the points that follow.

Step 1. Preparing and mounting electrodes

Patch pipettes with a wide tip diameter (> 2 µm) and a low tip resistance (2-4 MΩ) are pulled from thin walled, non-filamented borosilicate glass capillaries. Immediately before patching a cell, the pipette is tip-filled by carefully dipping the tip in amphoteracin-free internal solution for two seconds. The pipette is then back-filled with internal solution containing amphoteracin and tapped gently with a Pasteur pipette to remove air bubbles. The patch pipette is then mounted on the

manipulator, without applying positive internal pressure.

Step 2. Obtaining a seal.

Once the patch pipette is filed it is important to patch a cell before the amphoteracin diffuses as far as the tip, where it can interfere with seal formation. If a seal is not established within five minutes of filling the patch pipette, the attempt is abandoned and a fresh pipette is prepared. The method for obtaining a seal is identical to that described for standard whole-cell recordings, except no positive pressure is maintained in the pipette. It is important to use extremely gentle suction when forming a seal because the cells are prone to being sucked entirely into the wide opening at the tip.

Step 3. Whole-cell configuration

Once a giga-ohm seal is established, whole cell access develops over time as the amphoteracin concentration near the membrane patch increases. In general this takes 15-25 minutes to reach a stable value less than 30 MΩ. If this value is not achieved within half an hour, the recording is abandoned. During the waiting period, the microscope illumination is turned off to prevent degradation of the amphoteracin, and only turned on periodically to inspect the cell. As with standard whole-cell recordings, the cell is clamped at −60 mV once a seal is formed, in anticipation of whole-cell access being achieved.

2.4. Data acquisition

Data are sampled directly from the low-pass filtered output of the patch amplifiers using LabVIEW 8.2 (*National Instruments Inc.*). The sampling rate is fixed at 10 kHz with a resolution of 16 bits per sample, per channel. Both amplifiers rectify the output signal to the range ±10 V, so the error due to sample aliasing for a signed 16 bit integer is:

$$10/2^{15} = 3\times10^{-4}, \text{or } 0.3\,\text{mV}$$

Consequently, the minimum signal that can be resolved in voltage-clamp at the lowest gain of 1 mV/pA is 0.3 pA. The RMS amplitude of the noise in most recordings is at least 2 pA, so even at low gain, error due to sample aliasing is

negligible. Recordings of synaptic currents and mEPSCs are recorded at a gain of at least 10 mV/pA, so the sampling error in these recordings is no greater than 0.03 pA.

All stimulation data, including the seal test pulse and holding potential/current, are generated in LabVIEW and delivered to the external command input of each amplifier independently. The sampling rate for the signal output is set to 1 kHz.

Electrode tip resistance, seal resistance and access resistance are all monitored automatically when the seal test pulse is running. Square pulses lasting 5 ms with an amplitude of −5 mV are delivered in voltage-clamp (Figure 2.1). Tip resistance is calculated from the ratio of the amplitudes of the current to the applied voltage. Seal resistance is calculated by changing the holding potential to −40 mV after forming a seal and calculating the ratio of the steady holding current to the holding potential. Finally, access resistance is calculated from the ratio of the peak amplitude of the exponential current waveform to the applied voltage pulse. Cell capacitance is calculated at the same time as access resistance, by fitting an exponential curve to the decaying portion of the current waveform (Figure 2.1).

During extended voltage-clamp recordings, access resistance is monitored using single test pulses lasting 100 ms, delivered every 10-20 seconds. This pulse duration also allows membrane conductance to be estimated from the difference in current amplitude after the exponential phase of the waveform has decayed.

For short-duration experiments (FI curve experiments and voltage-gated current experiments) access resistance is monitored before and after the experiment using the seal test pulse. In addition, current-clamp recordings (FI curve experiments) include a 500 ms, 10 mV hyperpolarising pulse at the beginning of the recording to estimate input resistance. Experiments are repeated at least three times in each condition and the input resistance must remain within 20% of its initial value for the recording to be included in analysis.

2.5. Analysis

Analysis is performed off-line, or after the experiment has concluded. All raw data is analysed using LabVIEW, which has in-built libraries for signal manipulation and analysis, digital filtering and curve-fitting. Subsequent statistical analysis is performed in Microsoft Excel, or R (www.r-project.org). Tests for statistically significant trends or differences in means are conducted using ANOVA or Student's *t*-test (paired where appropriate, and using the Bonferroni correction for multiple comparisons). All numerically quantified results are presented as means ± standard error of the mean (SEM).

2.5.1. mEPSC analysis

Spontaneous miniature (excitatory) postsynaptic currents (mEPSCs) are analysed from recordings with a stable holding current, or baseline. Recordings with fluctuations in the baseline or a large amount of noise (greater than 4 pA RMS) are excluded. The minimum event frequency required for including a recording is 0.33 Hz (200 events in a 10-minute recording).

Recordings are analysed off-line using LabVIEW 8.2, which provides a number of in-build digital filter kernels and threshold detection subroutines. A comprehensive exposition of how digital filters are implemented in general can be found in Jackson (1989). mEPSCs are detected by setting an amplitude threshold relative to a baseline. The baseline is a obtained by filtering the signal using an exponential filter kernel with a time-constant of 2 ms. This ensures that the baseline is perturbed only by events with a characteristic duration greater than 2 ms, a value that is comparable to the rise-time of mEPSCs. An event amplitude threshold is set at 4 pA above this baseline, which is twice the typical RMS noise that is measured in these recordings. This gives a threshold function that tracks the holding current 4 pA above the mean holding current (green trace in Figure 2.2A).

Fluctuations in the original signal that exceed the moving threshold are isolated and analysed. In order to compare the original signal to this threshold, a zero-phase filter is applied to the signal over an 11-sample window. Sample windows for these filters require an odd number of samples because they integrate the signal over an equal

number of samples in each direction relative to the current sample. Owing to the fact that this process requires data 'from the past' as well as data 'from the future', such filters are described as 'non-causal' and can only be implemented off-line. The window size is chosen so that the portion of the signal over approximately one millisecond (sampling is at 10 kHz, or 10 samples per millisecond), which is the characteristic timescale of mEPSC events. A zero-phase filter with this window size does not cause appreciable attenuation of the event amplitude or, by definition, a shift the phase of the signal (Jackson 1989).

The process for analysing individual events is as follows. Event amplitudes are calculated relative to a 15 ms baseline preceding the event, risetimes are calculated as the time taken for the event to reach 90% of its maximum value after exceeding 10% of its maximum, and decay time-constants are estimated by fitting a single exponential curve to the decaying phase of the event. Each of these parameters is fitted automatically and adjusted by hand if the initial fit is unsatisfactory.

Events that are separated by an interval of less than 15 ms are excluded from the analysis; this imposes a cut-off on the maximum event frequency and inter-event-interval (IEI). Fluctuations in the current which are isolated as events but do not resemble mEPSCs are excluded from the analysis. Likewise, portions of recordings that show transient instability in the baseline are skipped and do not contribute to the IEI measurement of events at each end.

To calculate mean event traces, the individual traces are aligned to the time of the half-maximal value during the rising phase. A mean is then take over all events. In experiments where data from multiple cells are pooled, the first 200 events from each cell are included in the analysis.

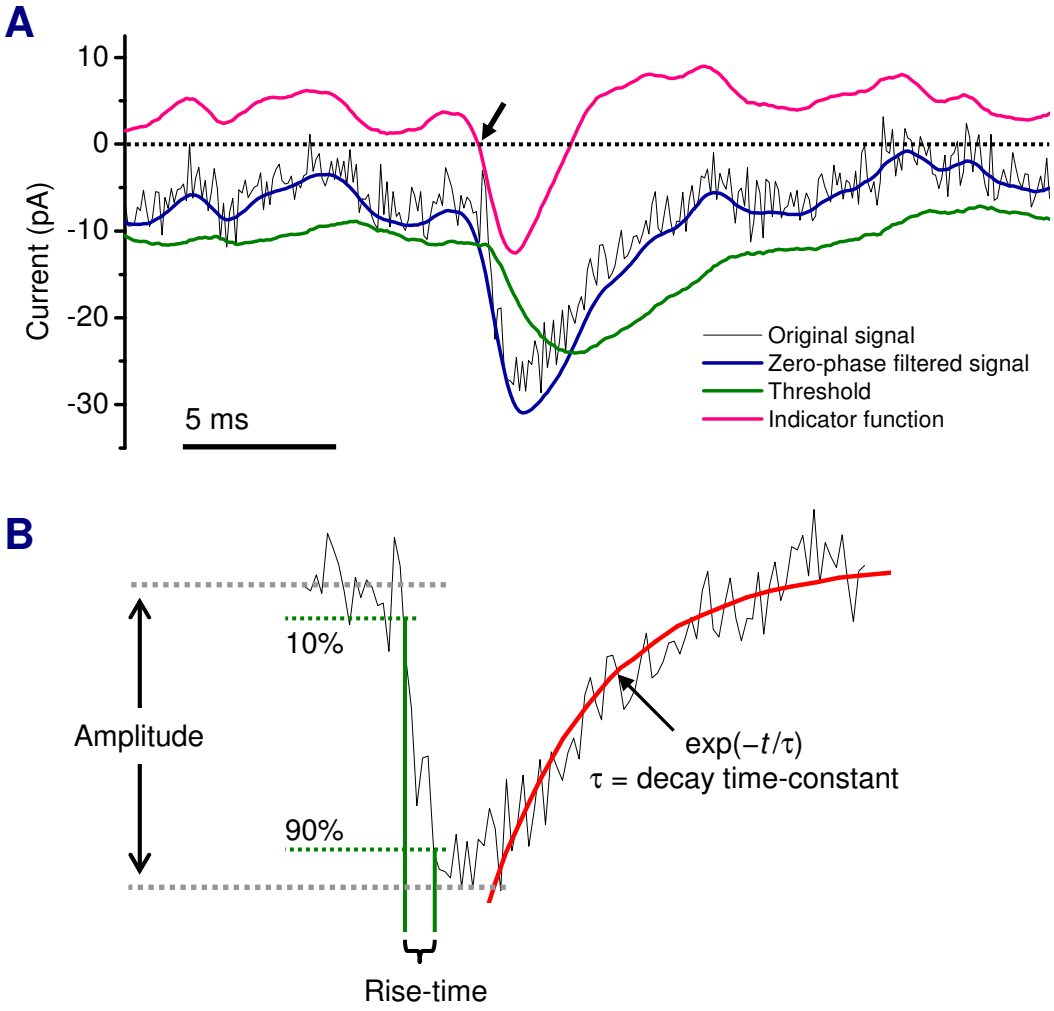

Figure 2.2: mEPSC detection and measurement

(A) mEPSCs are detected by subtracting a zero-phase filtered signal (blue trace) from a moving threshold (green trace). A zero-phase filter over 11 points (5 either size of the current point) is used because it does not attenuate the amplitude of the original signal, or, by definition, result in a time lag. The resulting 'indicator function' (pink trace) crosses zero when events exceed the threshold, as shown by the arrow. **(B)** Event amplitudes, 10-90% rise-time and exponential decay time-constants are calculated automatically, but can be hand-fitted if necessary. The exponential function is fitted to the signal using the Levenburg-Marquardt algorithm (Marquardt 1963) with an initial value of 10 ms for the time-constant, τ.

2.5.2. Voltage-gated potassium currents

It is difficult to isolate voltage-gated potassium currents pharmacologically. This is due to the diversity of the channels responsible, and due to the fact that there are many non-voltage-gated potassium channels present in the cell membrane that contribute to the linear electrical characteristics of the cell. For this reason, an estimate of the contribution of linear leak to the total current evoked during the step depolarisations used in voltage-gated potassium current experiments is subtracted from the current traces off-line.

It should be noted the IV characteristic of the leak will not be linear over large membrane potential ranges if it is selective to particular ions. Rather, it will equal the sum of the currents due to each ionic species that contribute to leak, each of which is given by the Goldman-Hodgkin-Katz (GHK) relationship (Hille 2001):

$$I_A = \frac{P_A z_A^2 V_m F^2}{RT} \left\{ \frac{[A]_i - [A]_o \exp(-z_A F V_m / RT)}{1 - \exp(-z_A F V_m / RT)} \right\}$$

Where I_A is the current carried by ion species A. P_A is the permeability of the membrane to A, z_A the multiple of the fundamental unit charge carried by A and V_m the membrane potential. All other symbols have their usual meaning.

The GHK equation accounts for the rectification that occurs in the current due to ion flux when the driving force is opposed by differences in intracellular and extracellular concentrations. For example, calcium, which is more concentrated outside the cell than inside, will show outward rectification because calcium efflux requires calcium ions to flow up a concentration gradient, which is thermodynamically unfavourable. Using the GHK relation for leak current requires knowledge of the permeability and concentrations of all ions responsible for the current. Such information is unavailable in the data here, and in any case exceedingly difficult to measure, even in the case of a single ionic species. On the other hand, attempting to fit the GHK relation over the limited range of membrane potentials for which the leak component is measured would result in substantial error due to the exponential terms and the number of free parameters in the equations. A linear leak approximation, therefore, represents a necessary compromise.

Extracting the passive current component

Two components make up the passive response function: the linear, or leak, IV characteristic and the capacitive transient. These are estimated for each cell using voltage steps in the range −75 to −45 mV. An example trace of the current due to these voltage steps is shown in Figure 2.3A.

The steady current at each voltage step, taken to be the mean current in the final 250 ms of the 500 ms pulse, is used to generate the IV data. Linear regression on these data provides estimates of the steady leak conductance, g_{leak}, and reversal potential, E_{leak}.

Next, the mean unit capacitive transient, $\bar{I}_{cap}$, is calculated by scaling the individual transients, $\bar{I}^{i}_{cap}$, to the magnitude of each applied voltage step, according to:

$$\bar{I}_{cap}(t) = \frac{1}{N}\sum_{i=1}^{N}\frac{I_{cap}(t,i)}{V_i} \qquad \text{where, } I^{i}_{cap}(t) = \frac{V_i}{R_a}e^{-t/\tau}.$$

V_i is the (signed) amplitude of the i^{th} voltage step, N the number of steps, R_a the access resistance and τ the membrane time constant[5]. The access resistance is, of course, required to be constant.

Together, the IV characteristic and the mean unit capacitive transient permits the linear response of the cell to arbitrary voltage steps to be calculated. For a given voltage step, the amplitude, V_{step}, is used to generate an estimate of the leak current for the duration of the step using the measured leak conductance, g_{leak}, and reversal potential, E_{leak},

$$I_{leak} = g_{leak}\left(V_{step} - E_{leak}\right)$$

[5] This solution for the capacitive current holds for a single compartment. In general, the exponential term is replaced by a more complex function. This function is, however, always linear in V_0 so the scaling is still appropriate.

Examples of reconstructed leak current traces are shown in Figure 2.3B (top). The mean capacitive transient is scaled by V_{step}, as depicted in Figure 2.3B (bottom).

Cell capacitance is in series with leak conductance, so the estimate of the transient capacitive current may be added directly to each leak current estimate to reconstruct the total passive current waveform. (Figure 2.3C).

Figure 2.4 shows the result of applying this procedure to a family of voltage steps recorded in a cell. When compared to the original currents in the same cell, the reconstructed currents are found to give a very close approximation, as shown by the residual current in Figure 2.4C.

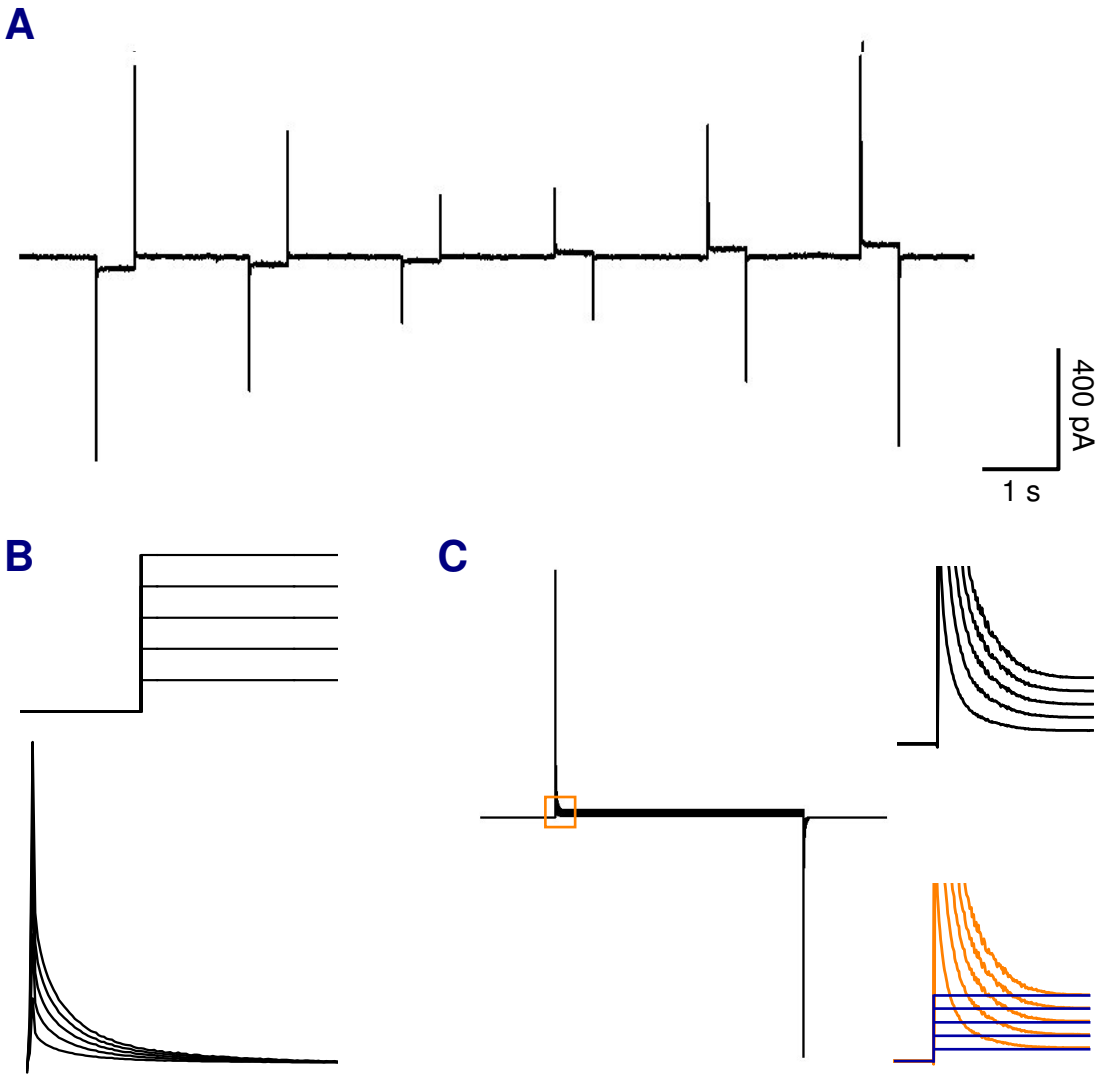

Figure 2.3: Reconstructing the passive current

(A) Example IV trace in voltage-clamp. 500 ms voltage steps in the range –75 to –45 mV are delivered in increments of 5 mV. Linear regression on the mean steady current provides estimates of the slope conductance and reversal potential of the leak current. The normalised mean capacitive transient waveform is calculated from the first 50 ms of each trace by scaling to the magnitude of the voltage step. **(B, Top)** Steady current traces calculated by applying the conductance and reversal potential estimates to positive voltage step waveforms **(Bottom)** Mean capacitive transients scaled to the magnitude of the voltage steps. **(C)** Summing the leak (inset, blue) and capacitive (inset, orange) components provides a reconstruction of the passive current waveform.

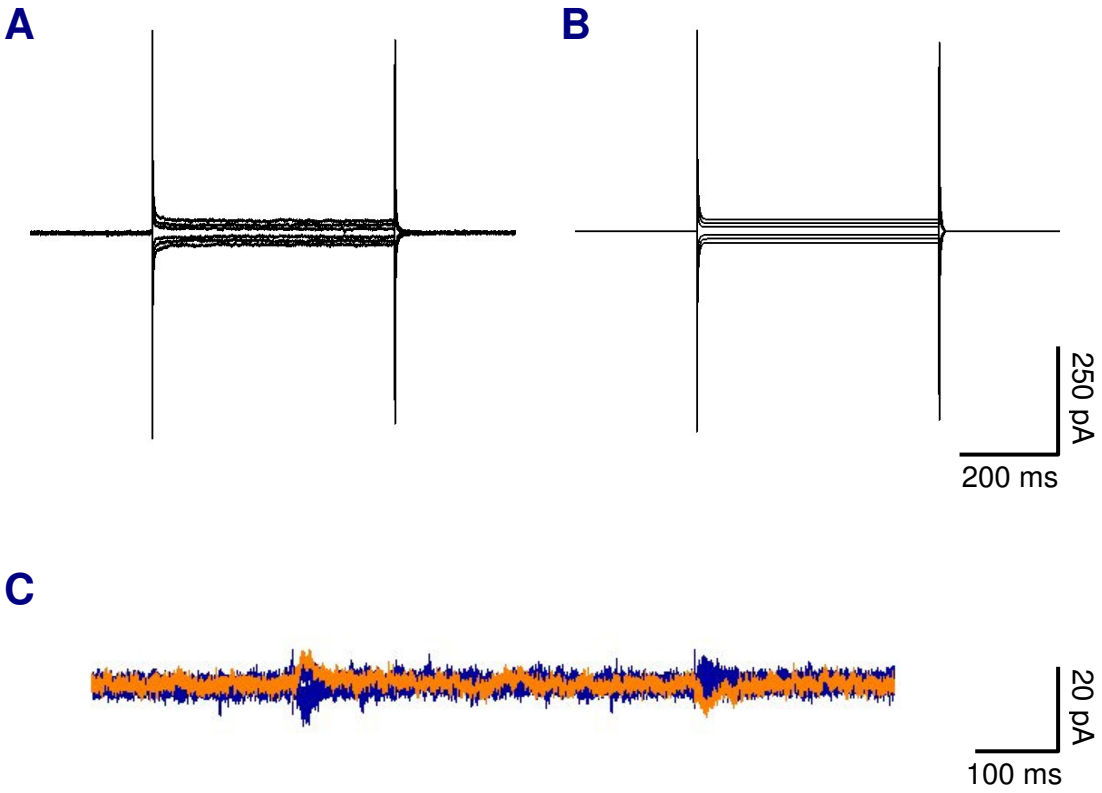

Figure 2.4: Reconstructing the passive current, validation

(A) Raw current traces from a hippocampal neuron; 500 ms voltage steps in the range –75 to –45 mV are delivered in increments of 5 mV to determine the passive characteristics of the cell. **(B)** Reconstructed current traces for the same cell. Current waveforms were calculated from voltage step waveforms using the conductance and reversal potential estimates and scaled capacitive transients, as described in Figure 2.3. **(C)** Residual, or 'deconvolved' current obtained by subtracting the reconstructed currents from the raw currents. A single trace is emphasized in orange to show the general form of the traces.

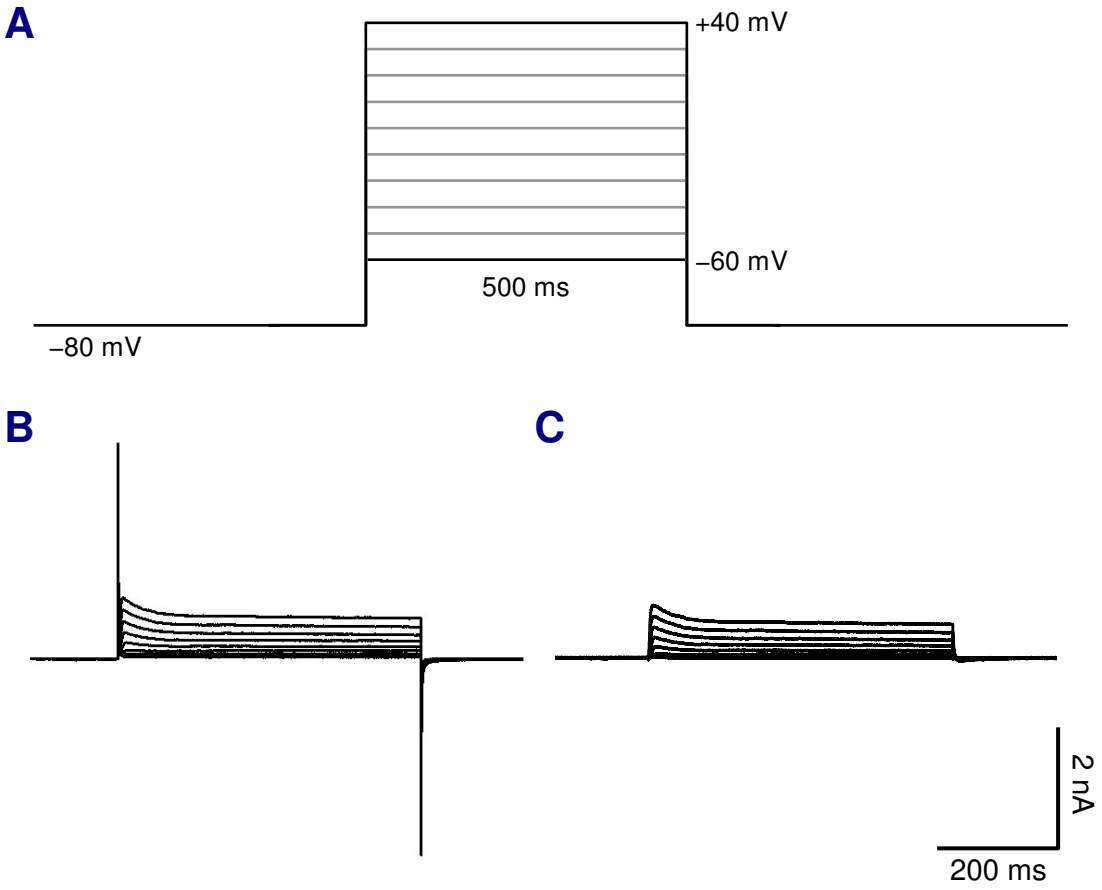

Figure 2.5: Removing the passive current

(A) Voltage-clamp stimulation waveforms for evoking voltage-gated currents. Holding potential is stepped to potentials in the range –60 to +40 mV from a holding potential of –80 mV in increments of 10 mV. Each step lasts 500 ms and consecutive steps are separated by 4 seconds. **(B)** Raw current traces resulting from the stimulation protocol in (A) applied to an 11 DIV cell in the presence of TTX (1 µM), $CdCl_2$ (200 µM) and with fast synaptic transmission blocked by CNQX (5 µM), APV (50 µM) and picrotoxin (50 µM). **(C)** Deconvolved voltage-gated potassium currents obtained via pointwise subtraction of the reconstructed passive current waveforms. These residual traces show a clear outward current with an initial transient component. The stimulation waveforms in (A) are used to reconstruct the passive current component for the cell from IV assay data, as described in Figure 2.4B.

2.5.3. Access resistance correction in current-clamp

It is possible to compensate and correct for access resistance using in-built circuitry on the patch amplifiers. This was not done in this work for several reasons. First, in the amplifiers being used, access resistance compensation is prone to becoming unstable and causing oscillations that destroy the cell. Second, correcting access resistance in this way is done 'by eye' and therefore subject to an uncontrolled degree of variability. In addition, a change in access resistance will lead to an error in the compensation. Finally, two different amplifiers were used in this work and it proved difficult to achieve qualitatively similar results using the compensation circuitry on each.

In general, the error in current-clamp recordings caused by access resistance is not important for the experimental work in this project: input resistance can be accurately measured because a low amplitude (10 pA) current step is used and action potential firing rate is not affected. Resting potential (measured by clamping at 0 pA) is also independent of access resistance because the no current flows between the electrode and the cell in this case. The only quantity that is affected is action potential threshold, because access resistance introduces a systematic error in the measured membrane potential that is proportional to the amplitude of the injected current. In cells with a high current threshold for spike initiation, this error can be substantial. For example, the maximum permitted access resistance in current-clamp is 40 MΩ. If a current pulse amplitude of 200 pA is required to initiate spiking, the error in the voltage trace, and the estimated voltage threshold, will be +8 mV.

To address this problem, access resistance is corrected off-line by subtracting the steady deflection in the voltage trace caused by the access resistance. The error is visible in uncorrected recordings as a steep vertical step at the onset of stimulation Figure 2.6. By examining the second derivative of the voltage waveform it is straightforward to detect the beginning and end of this step artefact and subtract the magnitude of the step from the remaining trace. Examples of corrected and uncorrected traces are shown in Figure 2.6B. This still leaves an error in the shape of the voltage waveform which is left uncorrected. Full correction can be achieved using a sophisticated technique recently published by Brette *et al.* (2008).

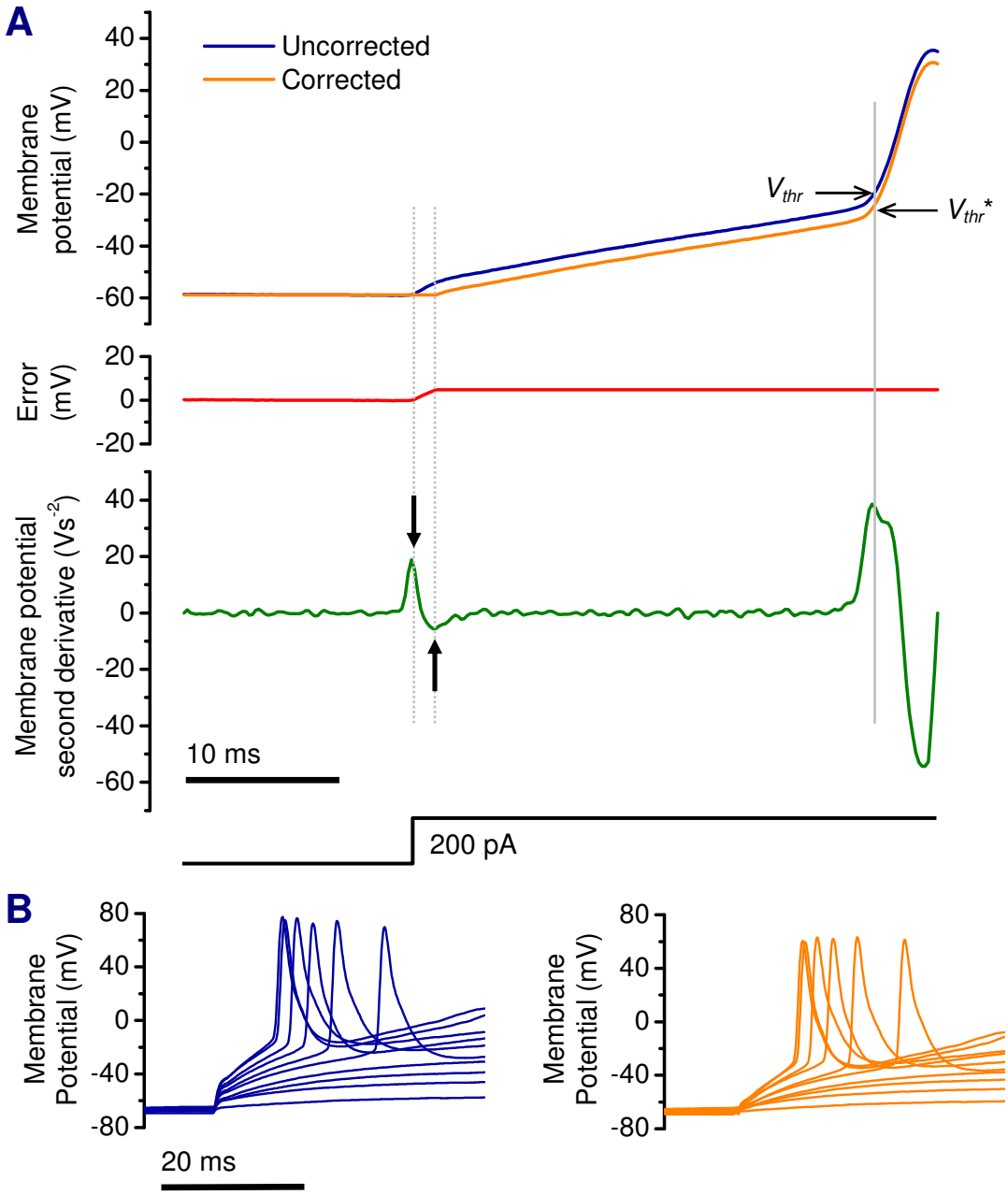

Figure 2.6: Access resistance correction

(A) Membrane potential traces in a cell subjected to a depolarising current injection (200 pA). The estimated error due to the steady current and access resistance (red trace, middle plot) is subtracted from the original trace (blue) to obtain a corrected trace (orange). The second derivative of the membrane potential, with the onset and end of the access resistance artefact indicated by black arrows, is plotted beneath (green trace). Voltage threshold is defined to be the membrane potential at which the second derivative reaches its maximum before the first spike, the uncorrected (V_{thr}) and corrected (V_{thr}*) values are indicated in the top trace. **(B)** Examples membrane potential traces resulting from a family of current injections applied (20 – 200 pA) to a cell before (left) and after (right) correction.

2.5.4. FI curves: quantifying excitability

Hippocampal cells are capable of firing regenerative action potentials in response to depolarising current. The rate of firing, and the quantity of current required to induce firing are characteristics that may be taken to define *excitability*. Here I describe briefly how the excitability of cells is quantified in this work; To eliminate synaptic activity, all experiments are conducted with fast synaptic transmission blocked by CNQX (5 μM), APV (50 μM) and picrotoxin (50 μM).

Figure 2.7A shows a current clamp recording of a cell being subjected to ten pulses of current lasting 500 ms, at equally-spaced amplitudes in the range 7.5 to 75 pA. A hyperpolarising pulse lasting 500 ms is included at the start of the recording to estimate input resistance. As can be seen in the figure, amplitudes lower than 30 pA are incapable of eliciting action potentials. Above this value, the cell fires at a rate that is roughly proportional to the amplitude of the injected current. The stimulations are presented in a random order and separated by an interval of four seconds to minimise the effect of sustained ion-channel inactivation (in particular, sodium channel inactivation) and spike frequency adapation on successive stimulations.

This stimulation assay is repeated three times and the mean number of spikes plotted against current (Figure 2.7C). The resulting FI curve captures the excitable nature of the cell: the threshold for initiating spikes is estimated by fitting a line to the non-zero data points, and the slope of this line describes how the cell responds when the applied current is elevated beyond threshold. Voltage threshold is calculated from the (corrected) membrane potential at the maximum point of its second derivative before the first spike of each stimulation (Figure 2.6); the final value is the average over all stimulations for each cell.

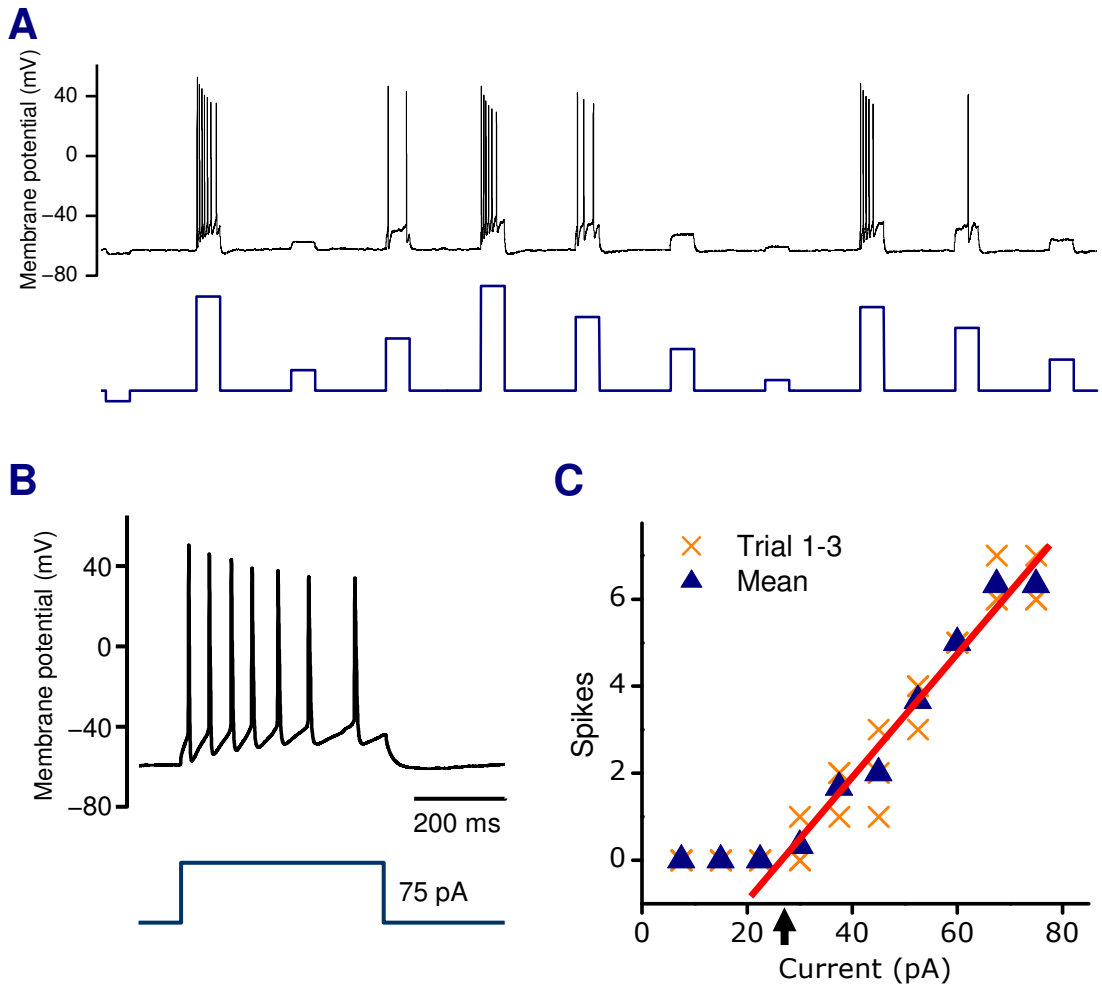

Figure 2.7: Measuring FI curves

(A) Example recording of an FI assay. (Top) Membrane potential of the cell. (Bottom) Stimulation waveform. An initial hyperpolarising pulse of 10 pA, 500 ms is applied for measuring input resistance, followed by ten 500 ms pulses in the range 7.5–75 pA delivered in a random order at 4-second intervals **(B)** Example of a single stimulation trace in the same cell **(C)** Construction of the FI curve: the data from three assays are pooled and the mean curve is calculated for the cell. A least squares linear fit (red line) is applied to the non-zero mean points to estimate the firing threshold (black arrow) of the cell and the slope of the FI curve.

2.6. Calcium imaging

2.6.1. Materials and equipment

The equipment, consumables and reagents used for calcium imaging are listed below.

	Comments; *manufacturer/supplier*
Equipment and consumables	
Integrated calcium imaging system	*Leica (AF6000)*
Imaging chamber	13 mm diameter
Rotary pump, perfusion system	
Forceps	
High-vacuum grease	
Cotton swabs	
Pasteur pipette	
Gilson pipettes: P1000, P200, P20	
Pipette tips: 1 ml and 250 µl	
35 mm culture dishes	
50 ml centrifuge tubes	
13 mm glass coverslips	Autoclaved, for cell plating.
5 ml sample tubes	
Reagents	
Fluo-3-AM calcium-sensitive fluorescent probe	Stored at −20ºC, light-sensitive; *Invitrogen*
DMSO	*Sigma*
F-127 Pluronic detergent	*Sigma*
Ionomycin	Stored at −20ºC
Manganese chloride	*Sigma*
Ethanol	
Modified external recording solution (Imaging buffer)	As in section 2.3.2, but with ionic concentrations matched to culture media: $CaCl_2$ (1.8 mM), $MgCl_2$ (812 µM), KCl (5.3 mM), (Brewer *et al.* 1993)
Nifedipine	*Tocris*

2.6.2. Solutions

Fluo-3-AM stock solution

Fluo-3-AM stock solution is prepared at a concentration of 1.2 mM in anhydrous DMSO containing 20% w/v pluronic detergent (36.5 µl DMSO/detergent added to each 50 µg aliquot). This stock solution is keep frozen at −20ºC and protected from light.

Loading solution

Loading solution is prepared fresh for each experiment by dissolving 5 µl of Fluo-3 AM stock solution 2 ml imaging buffer to achieve a working concentration of 5.5 µM.

Ionomycin solution

Stock solution of ionomycin is prepared at a concentration of 10 mM in 100% ethanol. Aliquots (10 µl) are stored at −20 ºC and protected from light. Working solution is prepared in imaging buffer, at concentration of ionomycin is 50 µM (equal to one aliquot per 2 ml imaging buffer)

Manganese chloride solution

Prepared in imaging buffer at a working concentration of 10 mM, from 1 M stock solution.

2.6.3. Method

Two 35 mm dishes are prepared, one containing 2 ml loading solution and the other containing 2 ml extracellular imaging buffer, for washing. Both dishes are placed in the incubator with the cells at 37ºC.

Fluo-3-AM is 'loaded' into the cell by placing a coverslip in loading solution for 30 minutes in the incubator. The detergent prevents aggregation of the fluorescent probe and makes the cell membranes more permeable so that the probe can enter the cell. Once inside the cell, endogenous eterases cleave the pentaacetoxymethyl (AM) ester tail from the membrane impermeable Fluo-3 probe (Kao *et al.* 1989).

Remaining procedures are all performed at room temperature (22 °C). After loading, the coverslip is washed in the other 35 mm dish and carefully mounted in the imaging chamber, ensuring continuous contact with imaging buffer and the cell-side of the coverslip. High-vacuum grease is used to seal the imaging chamber and bubbles are carefully excluded using a pipette.

Once the imaging chamber is placed on the calcium imaging microscope, imaging can begin. Image intensity is calibrated so that fluorescence measurements do not saturate by washing imaging buffer containing high KCl (15 mM). Acquisition frequency is set to no more than 0.1 Hz to prevent bleaching of the fluorophore. At the end of the experiment, the maximum and minimum fluorescence intensities are calibrated by applying, respectively, ionomycin solution and manganese chloride solution. All experiments are no more than 30 minutes in duration.

Quantification of the calcium imaging experiments can be performed in real-time or off-line using the proprietary software included with the imaging system (Leica Application Suite version 2.8.1). Regions of interest (ROI) are defined by highlighting an elliptical region of the neuronal somata in the field of view (Figure 2.8). Fluorescence intensity is automatically calculated within the analysis software by averaging the pixel intensities over each ROI.

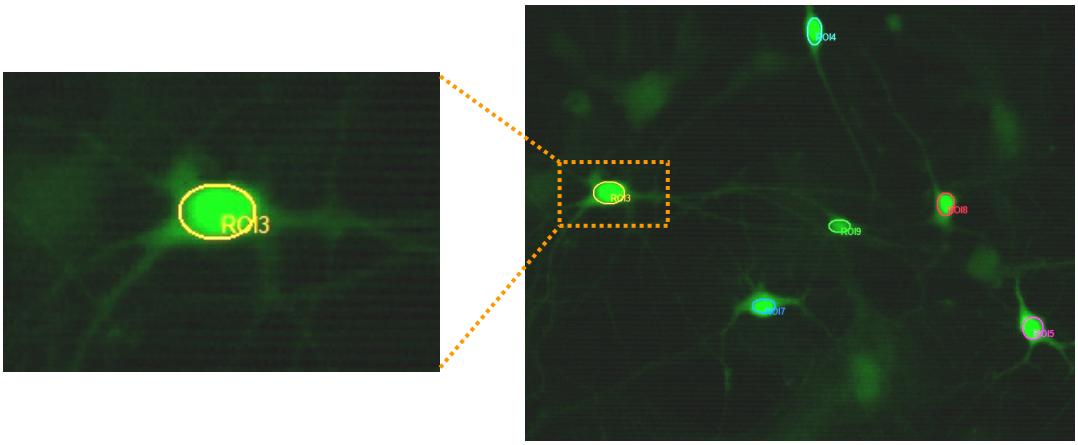

Figure 2.8: Calcium imaging

Regions of interest (ROI) are depicted by the multi-coloured ellipses in the portion of the field of view on the right. To the left is an enlarged image of one neuronal cell body with a ROI enclosing the soma.

Chapter 3. Electrophysiological Characterisation of Primary Hippocampal Cultures

3.1. Chapter summary and key findings

1. It is possible to culture and maintain embryonic hippocampal cells at a low density that allows the morphology of single neurons to be discerned. Cells with a pyramidal-like morphology are routinely observed.

2. Whole-cell recordings reveal spontaneous synaptic and spiking activity. Synaptic currents are both action potential-driven and dependent on spontaneous release, the latter being evident when action potentials are blocked.

3. Miniature synaptic currents recorded in the presence of TTX are mostly mediated by AMPA/kainate receptors. GABAR-mediated minis are also evident, but less common.

4. TTX-sensitive action potentials and action currents can be evoked in neurons by step depolarisation in current- and voltage-clamp, respectively. In dual whole-cell recordings this permits a detailed study of the nature of synaptic transmission in the cultures. In particular, connectivity is high, and synaptic currents are often amorphous, consisting of superposed components that appear to originate from multiple synapses.

5. At least three subtypes of receptors responsible for fast synaptic transmission are present: AMPA/kainate and NMDA receptors in glutamatergic synapses, and $GABA_A$ receptors.

3.2. Introduction

Primary hippocampal cultures are the subject of the experiments in this chapter, and throughout the remainder of this thesis. Despite the fact that cultures of this kind are widely used and well-characterised, it is important to establish an independent characterisation of some basic electrophysiological properties of the cultures used in this study at the outset. This is necessary in order to establish whether there are any fundamental differences with published findings.

Both the characterisation data presented here and that which is available in the literature are important for deeper reasons. In this work, as in other studies, neuronal cultures will be viewed as a model for nervous systems in general. Adopting this viewpoint is not arbitrary or whimsical; on the contrary, it is necessary. Forming hypotheses and interpreting data often requires general physiological principles to be applied to the particular system being studied. In the case of neuronal cultures, the appropriateness of these principles relies on the assumption that important features are common to both the reduced preparation and the intact animal from which the tissue originates. Evidently, the extent of this commonality is open to question because the constituent cells in a neuronal culture are stripped of the normal conditions present *in vivo*. Therefore, we need to know what the basic characteristics of this model system are, how they might differ from other systems, and what constitutes 'normal' phenomena under our experimental conditions.

Several authors have conducted investigations aimed solely toward characterising the properties of dissociated neuronal cultures. John Peacock (Peacock 1979) published the earliest electrophysiological study of hippocampal cultures, which established that cultures contained fully differentiated neurons capable of firing action potentials and forming functional synapses. As techniques and reagents advanced during the 1980s, dissociated neural cultures became widely studied. In a series of studies spanning several years Bekkers and Stevens published pioneering work on the properties of synaptic transmission in dissociated cultures (Bekkers and Stevens 1989; Bekkers *et al.* 1990; Bekkers and Stevens 1993; 1995; 1996). These papers established that functional excitatory and inhibitory connections are present and sensitive to antagonists of glutamate and GABA receptors. This work also

established important properties of cultured cells which distinguish them from neurons in acute preparations, such as their propensity for forming synapses onto themselves, termed 'autaptic connections' (Bekkers and Stevens 1991). Around the same time, the first detailed characterisation of low-density hippocampal cultures, similar to the preparation being used here, was carried out by Wilcox, Buchhalter and Dichter (Wilcox *et al.* 1994). This study provides a very thorough characterisation of the synaptic and intrinsic properties of the cultured neurons and concludes that they provide a good model system for studying synaptic transmission.

3.3. Cell morphology and general appearance

In all experiments hippocampal cells from rat embryos aged between E17 and E21 were used (see Methods). After 8 days in culture at a plating density of 120 cells mm^{-2} a network of neurons with easily recognisable cell bodies and processes is visible along with a confluent glial layer (Figure 3.1).

Various neuronal morphologies are evident in the cultures, some of which are similar to pyramidal cell types that are observed in hippocampal slices. These cells are typified as having a teardrop-shaped/tetrahedral soma and a prominent primary process resembling the apical dendrite of CA1-3 pyramidal cells. Other cell morphologies that were observed can be coarsely classified into groups: small bipolar cells, spherical multi-polar cells and large star-shaped cells.

Attention was restricted to pyramidal-like cells in all the work in this project, in an attempt to narrow the variability in results. However, even when this measure was taken, a great diversity in electrophysiological properties was observed. For example, both regular and fast-spiking cells were encountered, and in paired recordings both glutamatergic and GABAergic cells were observed via evoked synaptic responses.

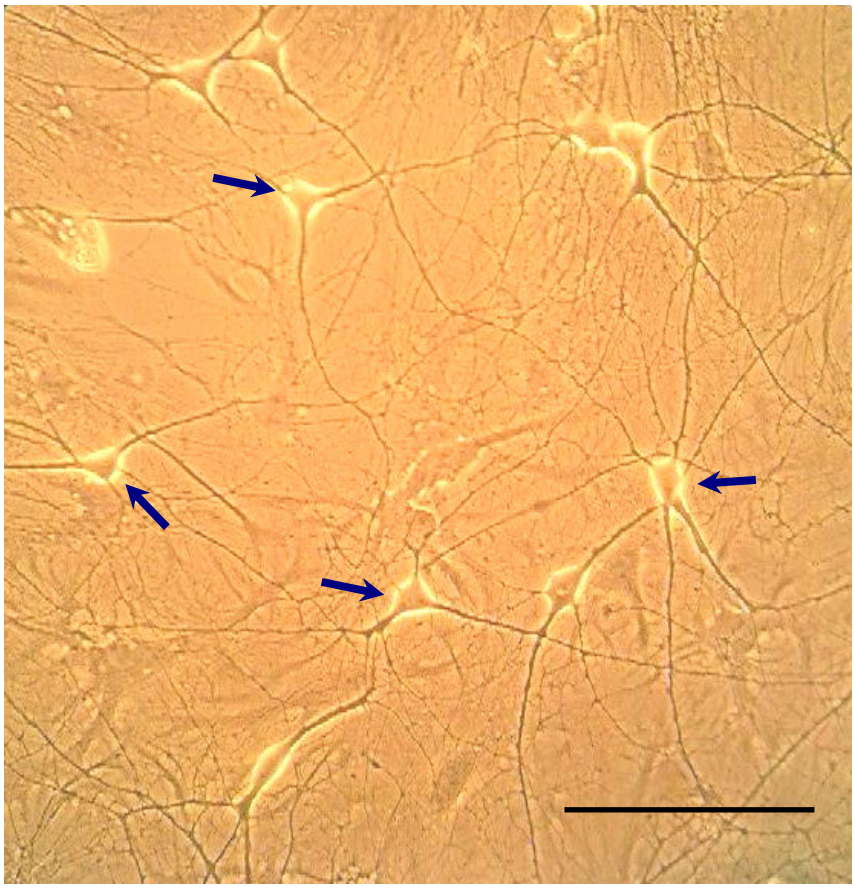

Figure 3.1: Cultured hippocampal neurons with pyramidal-like morphology

A phase-contrast image of a 10 DIV culture. Pyramidal-like cells account for the main class of neuronal morphologies in the cultures; the arrows in the figure indicate typical examples. Scale bar = 100 µM.

3.4. Spontaneous activity

Whole-cell patch recordings from cells at 8-14 DIV reveal spontaneous currents when voltage-clamped at –70 mV. Figure 3.2 shows recordings from five cells with clear inward currents, which are often organised into bursts of events interspersed with periods of relative quiescence. Figure 3.3 provides a detailed view of spontaneous currents in a cell over three orders of magnitude in time, highlighting the burst and inter-burst sections. Current-clamp recordings in the same five cells reveal spontaneous action potentials along with subthreshold membrane potential deflections that resemble EPSPs (Figure 3.4). As with the voltage-clamp recordings, bursting behaviour is evident in the timing of the action potentials and large membrane potential deflections.

Spontaneous activity in voltage-clamp is completely abolished by bath-applying antagonists of fast glutamatergic and GABAergic synaptic transmission. Figure 3.5 shows the result of applying a cocktail of three receptor-specific drugs: CNQX (5 μM), picrotoxin (50 μM), APV (50 μM). This combination will be referred to as 'CPA' and at the concentrations used, the component antagonists effectively block AMPA, $GABA_A$ and NMDA receptor-mediated currents, respectively.

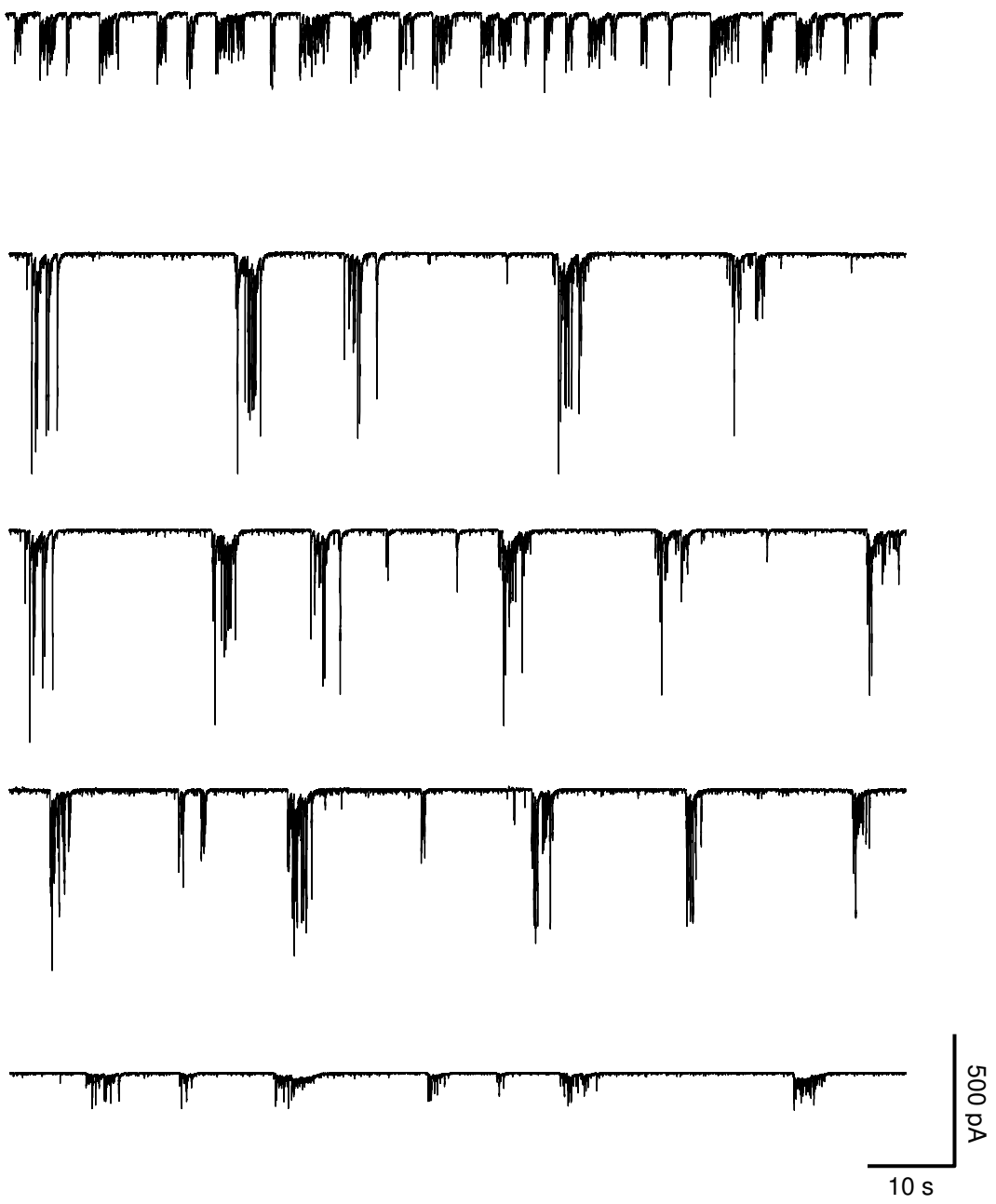

Figure 3.2: Spontaneous activity in voltage-clamp

Recordings from 5 cells held in voltage-clamp at –70mV, in normal external solution. The age range of the cells in this figure is 12-14 DIV, at which spontaneous activity is routinely observed. Large-amplitude currents are often organised into bursts of events, the periods between these are littered with small amplitude (< 20 pA) events akin to spontaneous synaptic events, or minis.

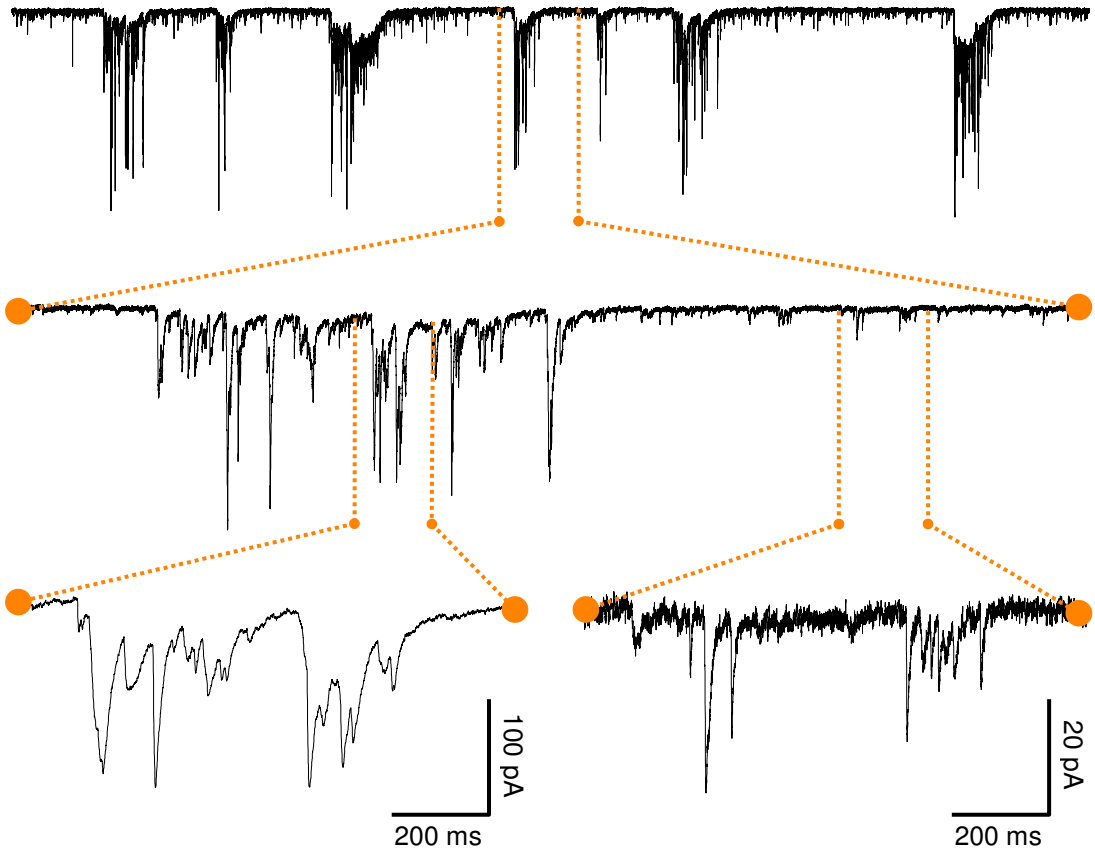

Figure 3.3: Spontaneous activity over multiple timescales

Voltage-clamp recording from a 12 DIV cell showing spontaneous synaptic currents at a holding potential of –70 mV. The timescale is expanded twice by a factor of 10 each time from the 100 s trace at the top to show the detail in the traces below, as denoted by the red dotted lines.

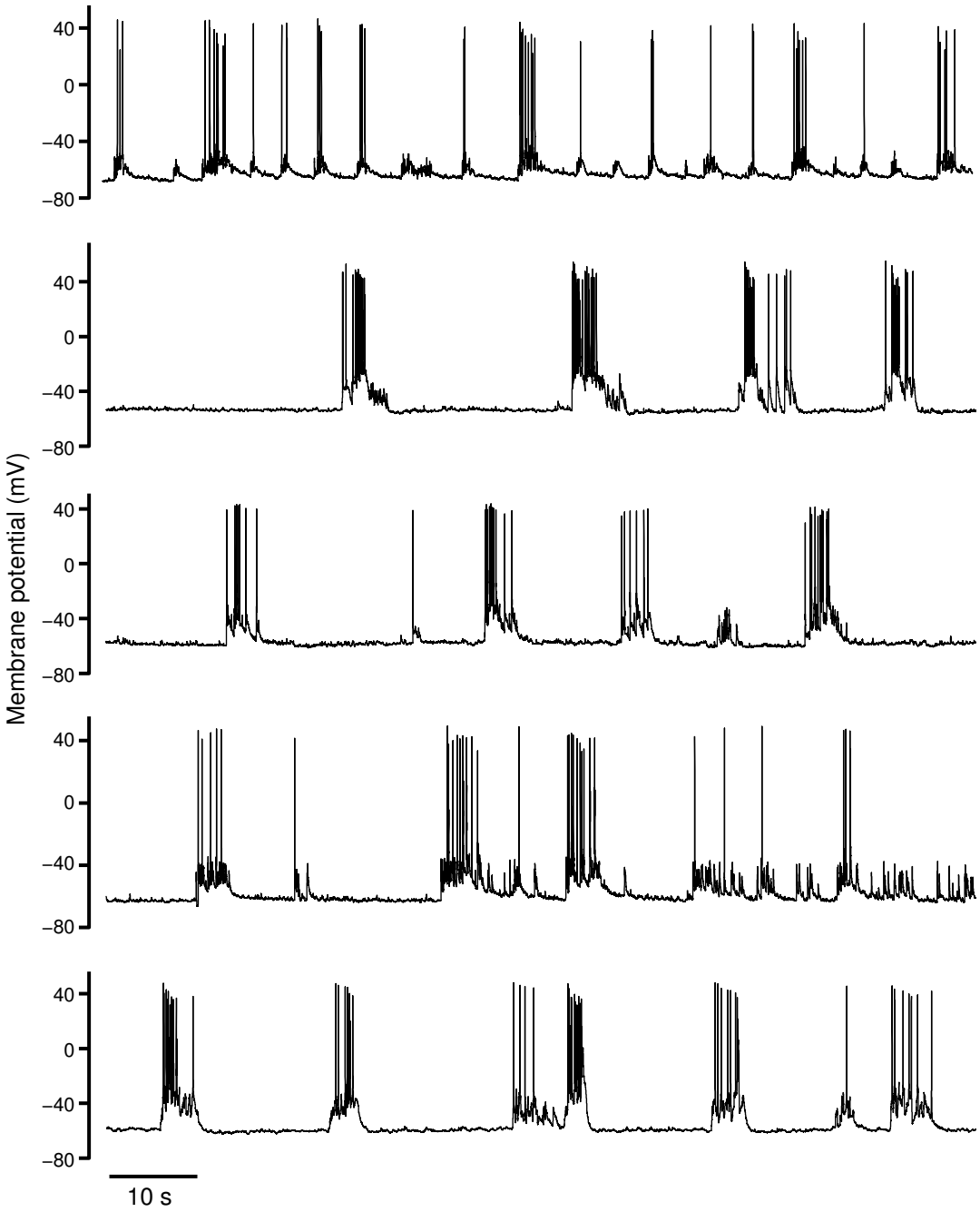

Figure 3.4: Spontaneous activity in current-clamp

Current-clamp recordings from the same 5 cells as in Figure 3.2, in normal external solution, held at 0 pA. The cells are in the age range 12-14 DIV and plated at a density of 120 cells mm^{-2}, conditions under which spontaneous action potential-driven activity is routinely observed, and is often characterised by bursts of events interspersed with periods of quiescence lasting several seconds. This type of activity is mirrored in voltage-clamp recordings, indicating that the large currents seen in such recordings are the result of bursts of action potentials.

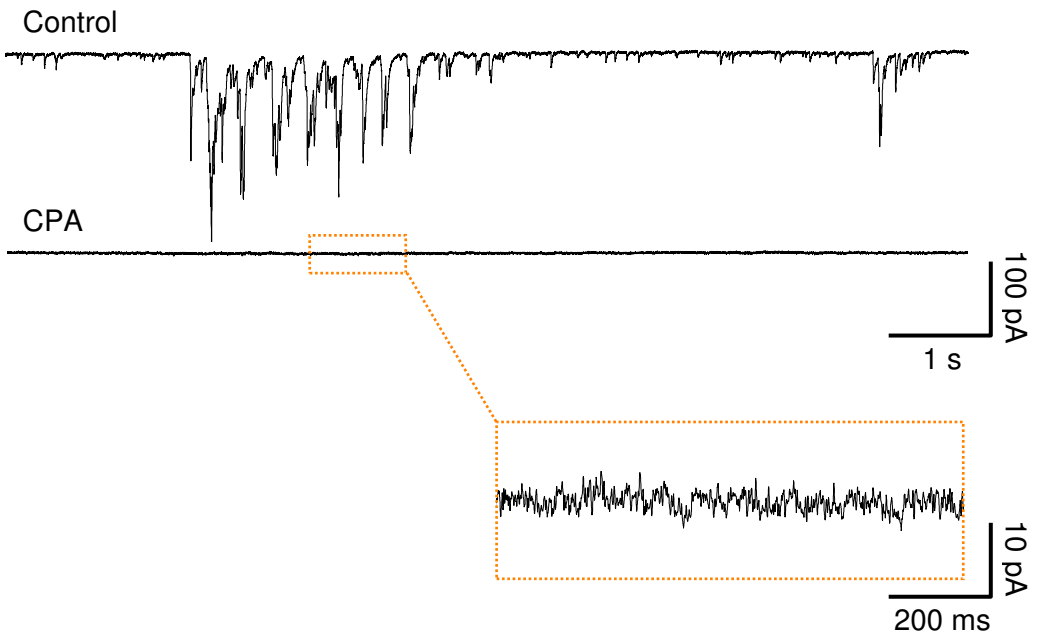

Figure 3.5: Spontaneous synaptic activity is abolished by blocking AMPA, $GABA_A$ and NMDA receptor currents

A voltage-clamp recording at a holding potential of –70 mV in a 12 DIV cell shows spontaneous currents. These currents are blocked completely by the addition of a cocktail of drugs (CPA) consisting of CNQX (5 µM), picrotoxin (50 µM) and APV (50 µM).

3.5. Spontaneous miniature postsynaptic currents

The application of TTX (1 µM) abolishes large-amplitude spontaneous currents and reveals miniature postsynaptic currents, often referred to as 'minis' (Figure 3.6). As shown in the figure, minis are effectively blocked by CNQX (5 µM), suggesting that they are largely mediated by AMPA receptors, which are excitatory in nature. Such miniature excitatory postsynaptic currents, or mEPSCs, are known to be action potential-independent, resulting instead from the spontaneous membrane fusion of presynaptic neurotransmitter vesicles and the subsequent release of a small quantity of neurotransmitter into the synaptic cleft. At a concentration of 1 µM, TTX does indeed abolish evoked action potentials in current-clamp, as exemplified in Figure 3.10A.

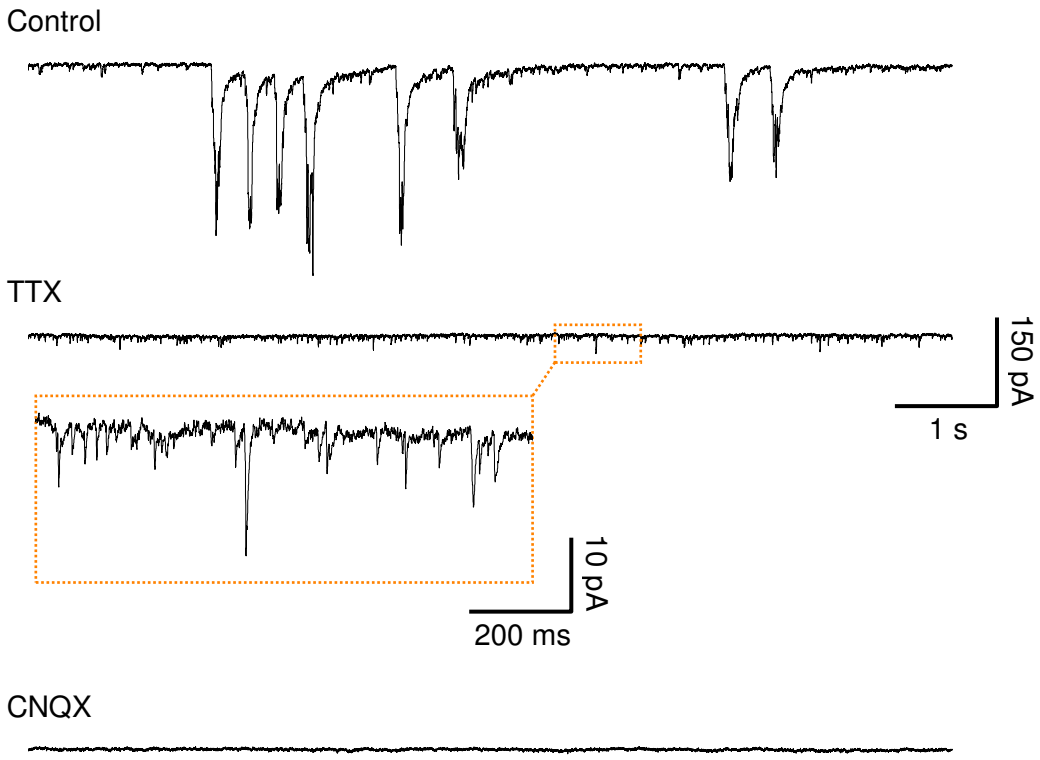

Figure 3.6: TTX reveals spontaneous miniature synaptic currents

An example voltage-clamp recording at a holding potential of −70 mV in a 14 DIV cell. The control recording (top trace) shows large spontaneous currents. Application of TTX (1 µM) abolishes the large-amplitude events (middle traces), revealing spontaneous miniature events that are sensitive to CNQX (5 µM) (bottom trace).

In order to characterise the kinetics and temporal statistics of mEPSCs, a set of recordings from nine cells at 10-14 DIV was performed in the presence of TTX (1 µM), picrotoxin (50 µM) and APV (50 µM). Events with amplitudes greater than 4 pA were analysed by measuring their peak amplitude, 10–90% rise-time and decay time-constant, as described in Methods, Section 2.5.1. For each cell, only the first 200 events were included in the analysis. Recordings with event frequencies less than 0.5 Hz, or greater than 5 Hz. Figure 3.7A shows an example recording trace and the mean mEPSC waveform obtained by horizontally aligning all the analysed events to the time of the half-maximum point of the rising phase.

Amplitude, rise-time and decay time-constant histograms for all analysed mEPSCs are shown in Figure 3.7B-D. The histograms are all unimodal and have a positive skew, resembling a gamma distribution. In terms of kinetics, mEPSCs have a distinct profile with a 10-90% rise-time of 1-2 ms and an exponential decay time constant of ~7 ms.

As indicated already, blockage of AMPA receptors alone usually abolishes minis. In the absence of any pharmacological agents other than TTX this, suggests that spontaneous release at other fast chemical synapses, in particular GABAergic synapses, is relatively rare. This indeed appears to be the case. Out of 10 cells examined, only one cell exhibited spontaneous currents in the presence of CNQX (Figure 3.9). These events were sensitive to picrotoxin and had a much slower decay time-constant ~50 ms, indicative of $GABA_A$ receptor-mediated currents.

The spontaneous nature of minis is evident in the statistics of the time intervals between adjacent events, or inter-event-intervals (IEIs). Figure 3.8 depicts the pooled IEI histogram from 9 cells. An approximately exponential distribution is evident, which would be expected if the underlying process were poissonian, that is, a process in which the probability of an event occurring is fixed within a given time window, and independent of previous occurrences (Rieke 1997). A log-linear plot of the data shows that a single exponential fit is not perfect, and that there are multiple characteristic timescales in the data corresponding to recordings with low and high event frequencies. This artefact can be remedied by appropriate normalisation. When IEI values for each cell are normalised to its mean, the pooled histogram is very well approximated by a single exponential curve Figure 3.8C, D.

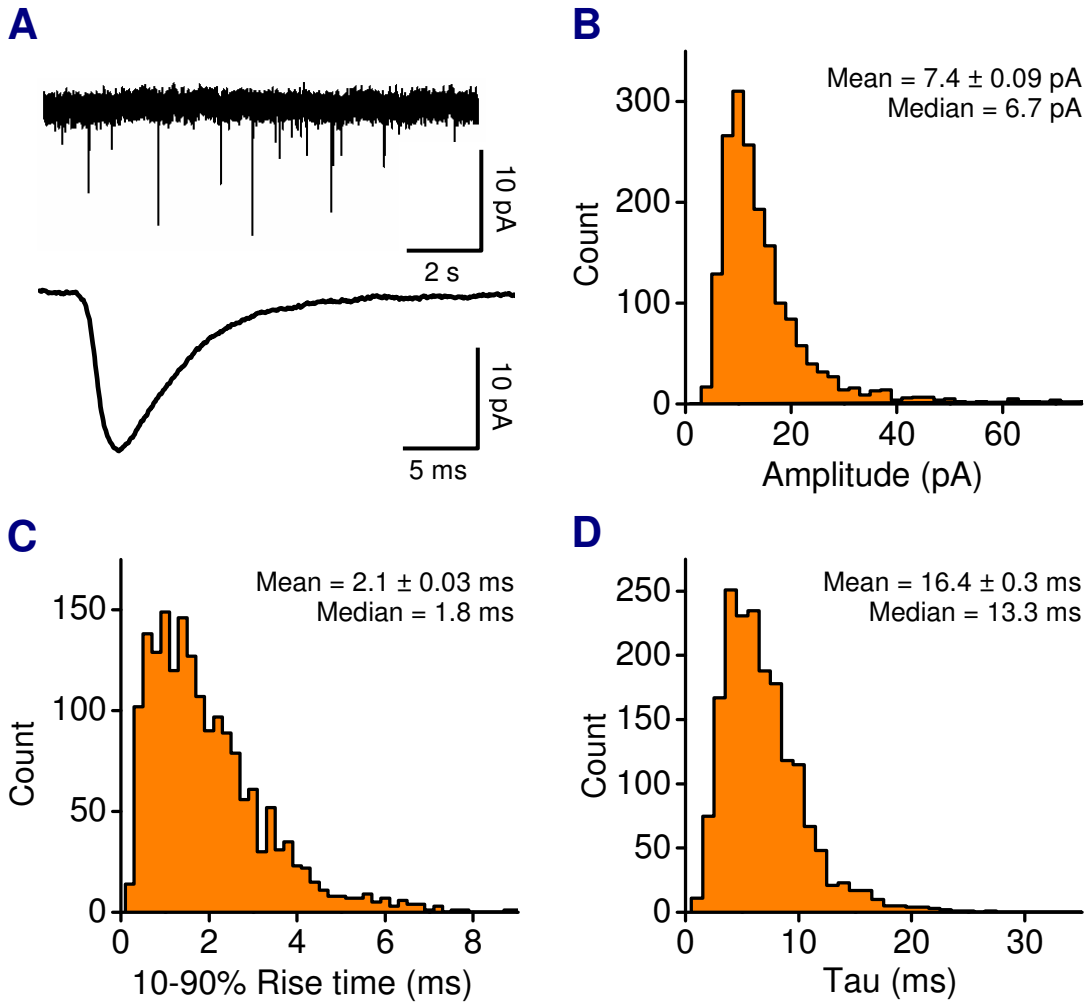

Figure 3.7: Kinetics of AMPA receptor-mediated mEPSCs

Voltage-clamp recordings at a holding potential of –70mV in the presence of TTX (1 µM) and picrotoxin (50 µM) were analysed for miniature EPSCs. **(A)** An example recording with the mean trace of 200 events beneath. **(B,C,D)** Amplitudes, 10-90% rise times and single exponential decay constants (Tau) are measured for the first 200 events exceeding an amplitude threshold of 5pA from 9 cells and pooled in each histogram. Errors for the means are expressed as ± SEM in each case. As the distributions are skewed, median values are indicated along with means.

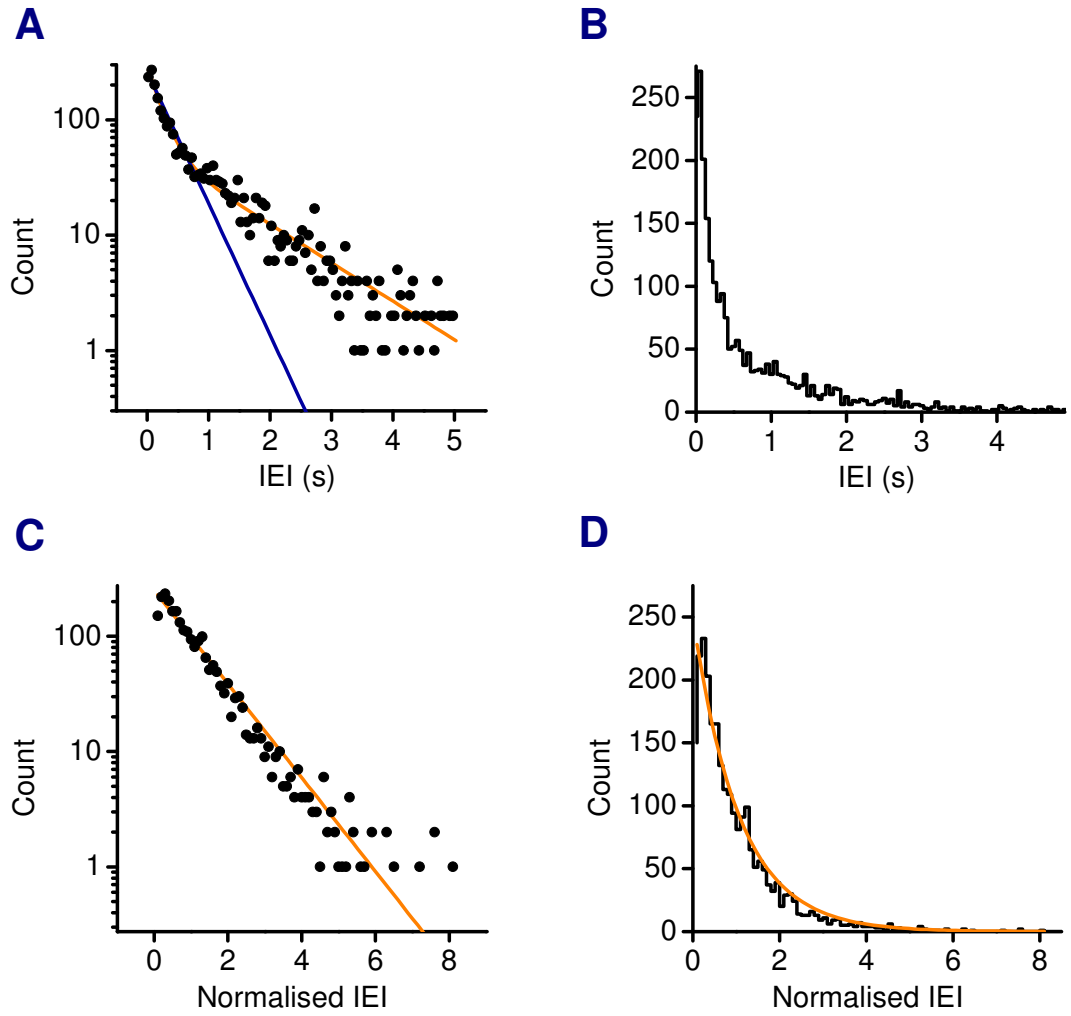

Figure 3.8: Temporal statistics of mEPSCs

(A) Log-linear fit of the inter-event interval (IEI) distribution for mEPSCs reveals an exponential distribution with at least two main components when data are pooled over all recordings (n = 9). These components correspond to populations of recordings with characteristically high (~5Hz, blue line) and low (~0.5Hz, red line) mean event frequencies. **(B)** Pooled IEI histogram. **(C, D)** When the IEIs are normalised to the mean for each cell and pooled, the IEI histogram is well-approximated by a single exponential curve (correlation coefficient, R^2 = 0.96), indicating that a single Poisson process provides a good model for event statistics.

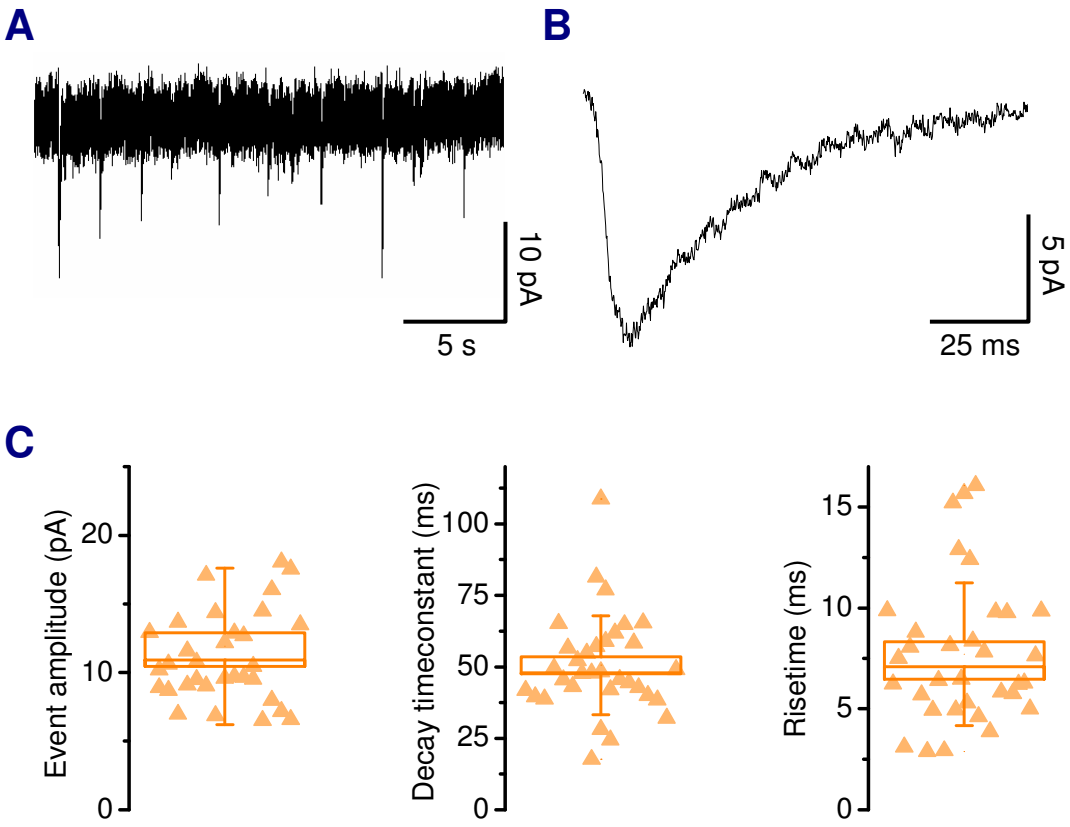

Figure 3.9: Spontaneous miniature GABAergic currents

(A) A segment of a recording in voltage-clamp at –70mV in the presence of TTX (1 µM) and CNQX (5 µM). Out of 10 cells recorded under these conditions, with holding potentials in the range –90 to –30 mV, only one cell exhibited spontaneous currents over a minimum 2 minute period. **(B)** Mean trace from all events, horizontally aligned to the half-maximum time point. **(C)** Box-plots for amplitudes, decay time-constants and rise-times for all events recorded. Box heights represent standard error, error bars represent standard deviation and the central line is the median. The mean amplitude, decay time-constant and rise-time for this recording was 11.9 ± 0.9 pA, 50 ± 3 ms and 7.7 ± 0.6 ms respectively.

3.6. Evoked synaptic currents

Dual whole-cell patch recordings make it possible to study evoked postsynaptic currents between synaptically coupled cells. Figure 3.10B shows the result of applying a brief step depolarisation of 100 mV from a holding potential of -70 mV to a cell in the absence and presence of TTX (1 μM). A fast inward current is evident between the transient passive currents. This current is reversibly blocked by TTX and is therefore a sodium current, or 'unclamped action current'. Step depolarisations of this amplitude and duration are therefore capable of eliciting action potential-like events, and can be used to elicit synaptic currents in postsynaptic targets of the stimulated cell.

Figure 3.11 shows a schematic of a dual whole-cell voltage-clamp recording with example traces of the current recorded in a pair of cells (pictured). In this example, both autaptic and reciprocal currents are present. Stronger evidence of autaptic currents can be obtained by recording from cells that are physically isolated from other neurons. On occasion, lone cells were found on an isolated patch of glia where there was no visual evidence of processes from other neurons. Such a cell is pictured in Figure 3.12, along with current- and voltage-clamp recordings showing the evoked response due to a glutamatergic, autaptic synapse.

In contrast to the stereotyped profile of the mPSCs, action current-evoked events are often messy. Postsynaptic currents vary in amplitude over nearly two orders of magnitude and frequently consist of multiple components. Figure 3.13 shows recordings of 24 putative synaptic connections in 6 paired recordings. The variability in the amplitude and shape of the synaptic currents is evident in these traces. All but one of the cells here is glutamatergic: the cell whose traces are shown in panels 1A and 1D induced a current with a time course characteristic of a GABAergic synapse in its neighbour (1B, 1C); this was later confirmed pharmacologically by its sensitivity to picrotoxin. The fast component of the current in 6D saturates the recording amplifier and is likely to be an unclamped sodium current induced by activation of a suprathreshold synapse.

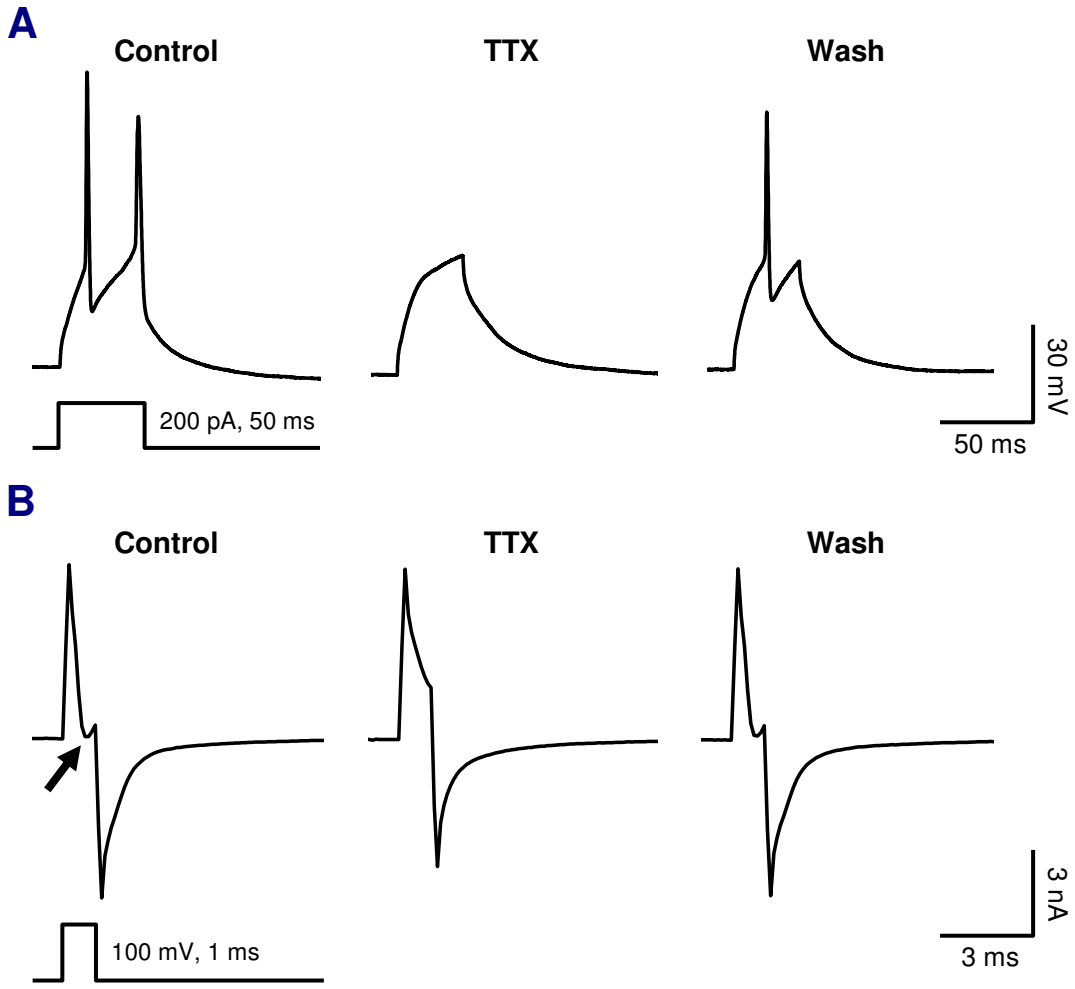

Figure 3.10: Evoked action potentials and currents

(A) Current-clamp recording of cell being delivered a 50 ms, 200 pA depolarising pulse. This is sufficient to elicit action potentials which are reversible blocked by TTX (1 µM) **(B)** Voltage-clamp recording of the same cell stimulated by a 1 ms, 100 mV pulse from a holding potential of -70 mV. The Arrow indicates the peak of the sodium action current which is reversibly blocked by TTX (1 µM).

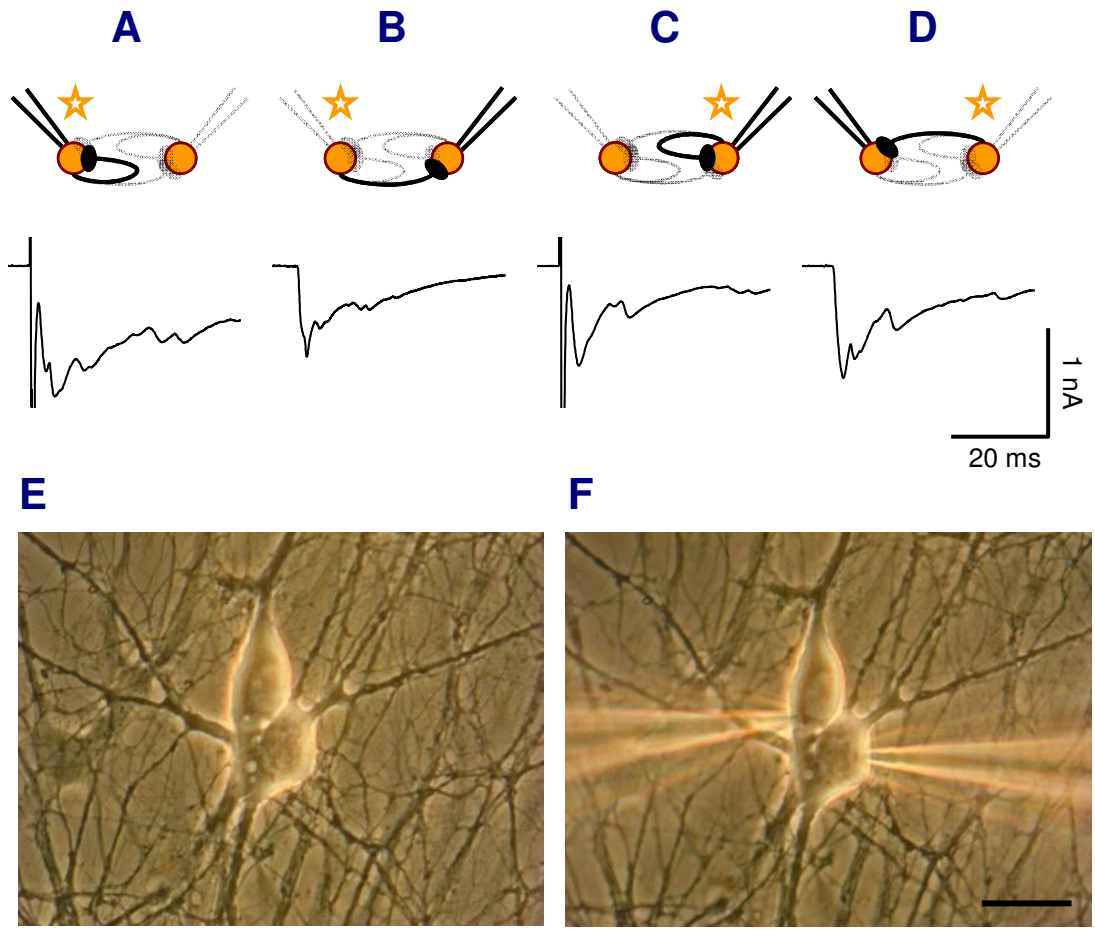

Figure 3.11: Paired whole-cell recordings

Synaptic currents in paired whole-cell recordings can be evoked in four different ways, depicted in the diagrams at the top of the figure. Emboldened recording pipettes signify the origin of the traces in each case and the star indicates the cell being stimulated. The traces in panels **A** and **C** show the current induced in the stimulated cell. The initial deflection in the trace is a combination of capacitive current and the fast sodium current induced by step-depolarising the cell. The subsequent inward currents are the result of synaptic activation caused by this action current: the earlier component occurs within 5 ms of the depolarisation onset and is therefore probably autaptic, while the later components are likely to be due to polysynaptic activation of neighbouring cells. Panels **B** and **D** depict simultaneous recordings in the unstimulated cell. The onset of the current occurs within 5 ms of stimulating each cell so there is probably a monosynaptic component to the current. **(E, F)** Phase contrast images of the two neurons from which the recordings were obtained, before and after establishing whole-cell configuration. Scale bar = 10 µm.

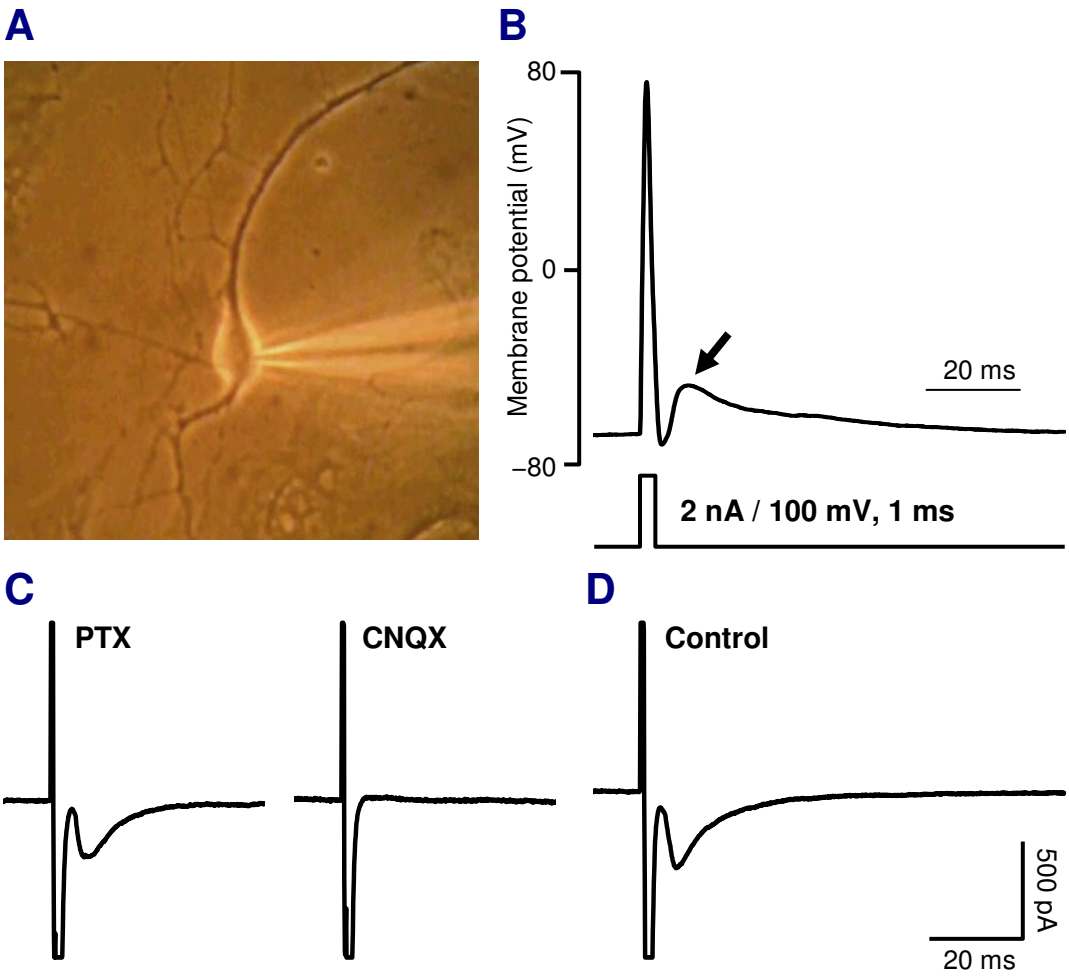

Figure 3.12: Autaptic response

(A) Phase contrast image of a patch-clamped neuron on a glial monolayer. The cell is well-isolated from other cells, minimising the likelihood of polysynaptic responses upon stimulation. **(B)** Current-clamp trace of the same cell following a 1 ms, 2 nA current pulse. A unimodal EPSP with an onset at 5 ms and peak at 7.5 ms after the stimulating pulse is evident (arrow). **(C)** Voltage-clamp recordings showing the response of the cell following a 1 ms, 100 mV step depolarisation from –70 mV in the presence of picrotoxin (PTX) (50 µM) and CNQX (5 µM) suggest that the synaptic response is glutamatergic. **(D)** A voltage-clamp recording of a stimulation in the absence of drugs and with the same timescale as B.

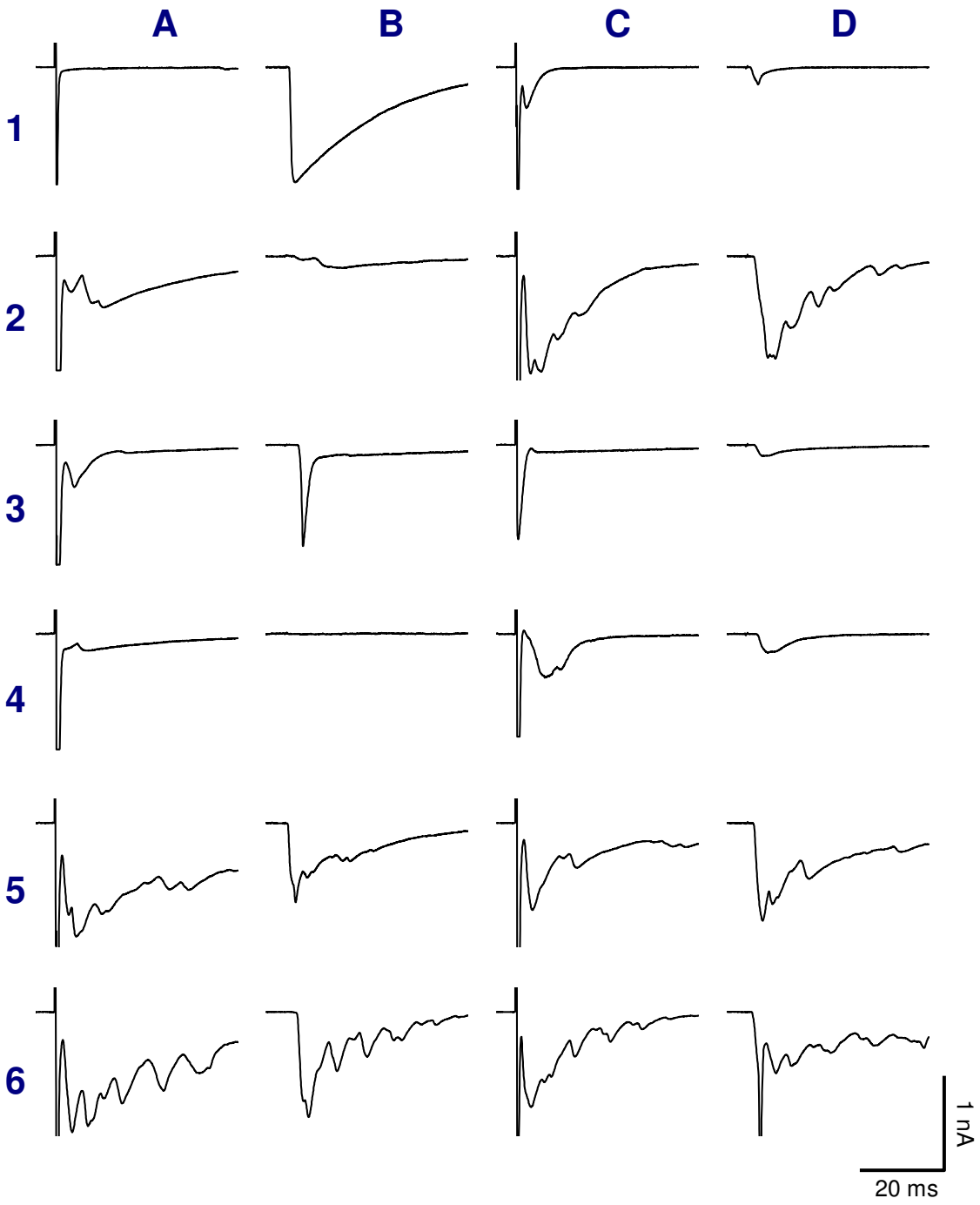

Figure 3.13: Typical evoked synaptic currents

Evoked currents from six paired recordings (top to bottom) showing autaptic and reciprocal responses. Columns **A** and **C** show currents in the stimulated cell following a 1 ms depolarising voltage step of 100 mV from a holding potential of –70 mV, while columns **B** and **D** contain current traces recorded simultaneously from the unstimulated cell (see figure Figure 3.11).

One difficulty with characterising traces that show multiple synaptic activations is that it is sometimes difficult to distinguish unclamped action potential currents from glutamatergic synaptic currents. Two possible distinguishing features are the initial onset and total magnitude of the current: sodium currents often show an inflection in the onset and are very large in magnitude (> 1 nA) compared with AMPAR-like currents (Figure 3.13, panel 6D). Distinguishing the currents pharmacologically is problematic because the use of either TTX or CNQX would abolish fast excitatory transmission, so both unclamped action currents and large glutamatergic synaptic currents would show sensitivity to these drugs. Varying the postsynaptic holding current should reveal a higher reversal potential for action currents than glutamatergic currents, which typically reverse at potentials close to 0 mV. The pharmacological behaviour and reversal potentials of evoked synaptic currents are dealt with in the next section.

3.7. Pharmacology of evoked synaptic currents

In dual recordings from cell pairs where the synaptic currents had a single component it was possible to define the type of synaptic connection pharmacologically. Figure 3.14A shows evoked postsynaptic currents due to a glutamatergic synapse. The identity of the currents is confirmed by their sensitivity to CNQX (5 μM) and insensitivity to picrotoxin (50 μM). The principle receptor subtype at glutamatergic synapses is the AMPA/kainate receptor, which is responsible for the fast, rapidly-decaying component of the current (estimated time-constant, τ_{AMPA} = 7.6 ± 1.4 ms). In the presence of millimolar concentrations of magnesium in the extracellular solution, no additional component is observable at the −70 mV holding potential.

If the recording solution is replaced with magnesium-free solution, an additional long-lasting (τ_{NMDA} = 360 ± 130 ms) component to the evoked current is visible (Figure 3.15A). This current is mediated by NMDA receptors, which are normally blocked by magnesium. The specific NMDA receptor antagonist APV (50 μM) completely blocks this component. In addition, the NMDAR current is seen to be insensitive to picrotoxin (50 μM) and CNQX (5 μM).

Corresponsingly, GABA synapses can be identified by their sensitivity to picrotoxin and insensitivity to CNQX. Figure 3.16A shows evoked synaptic currents in a paired recording in which the presynaptic cell is GABAergic. At a holding potential of −70 mV the current is strongly inward, suggesting a somewhat more positive reversal potential. In agreement with the miniature postsynaptic current data, the decay time-course of the current is conspicuously longer than that of AMPA/kainate receptor currents (τ_{GABA} = 36 ± 13 ms), but slower than NMDA receptor currents.

Having dissected the glutamate and GABA-evoked currents pharmacologically, it is possible to examine their reversal potential in voltage-clamp by holding the postsynaptic cell at a range of potentials, generating an IV-characteristic for each current type.

Figure 3.14C shows example traces of AMPAR-type currents at a range of holding potentials. When the peak current amplitude as a function of holding potential for a group of cells (n = 5) is pooled and normalised, the resulting IV plot gives a reversal potential estimate of the synaptic current. In the case of these currents the reversal potential, E_{AMPA}, was +5 ± 8 mV. The same plots for NMDA and GABA receptor-mediated currents give estimated reversal potentials E_{NMDA} = −7 ± 7 mV and E_{GABA} = −40 ± 5 mV, respectively.

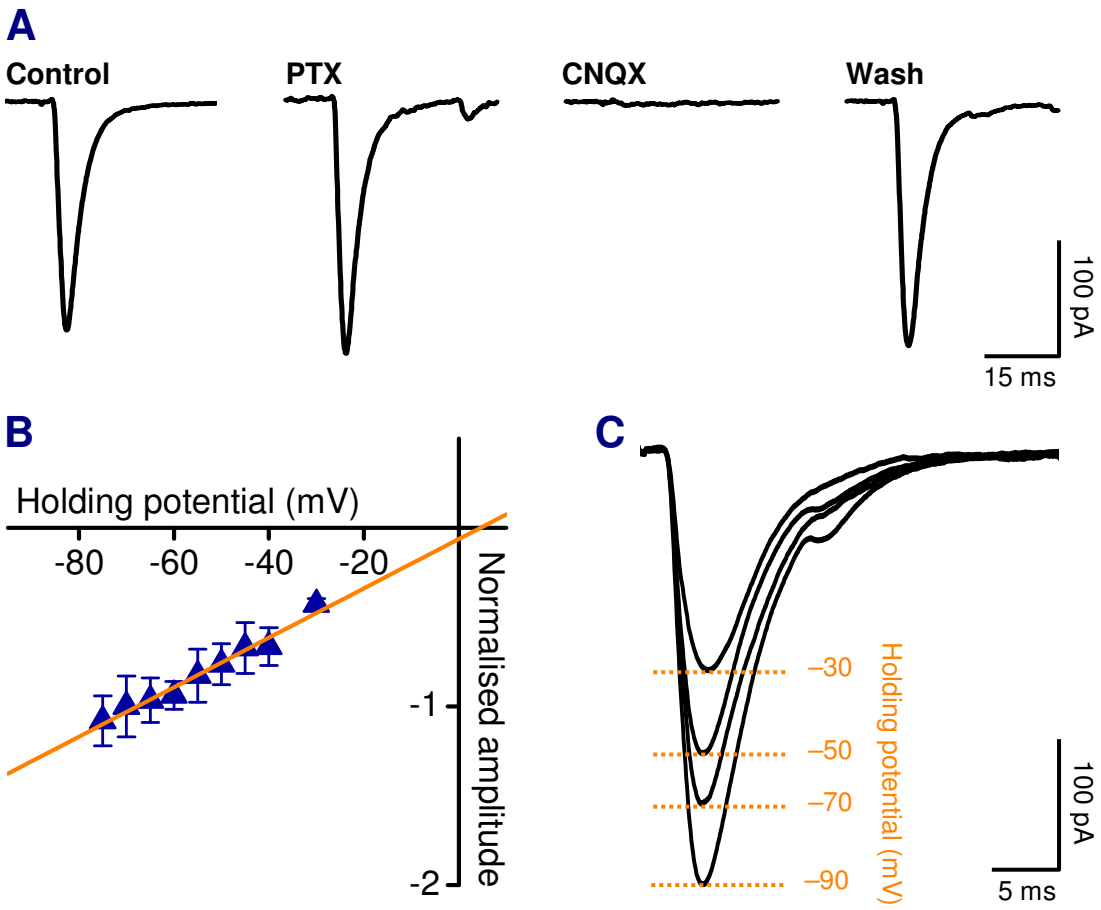

Figure 3.14: AMPAR-type synapses

(A) Pharmacological characterisation of evoked currents at an AMPAR-type glutamatergic synapse. Such synapses are insensitive to the GABA receptor antagonist picrotoxin (50 μM), and are completely and reversibly blocked by CNQX (5 μM). **(B)** IV plot of pooled responses from 6 paired recordings of cells in which the currents were pharmacologically confirmed to be glutamatergic. Both cells were held in voltage-clamp and a brief (1-5 ms) depolarising pulse to +100 mV was delivered to the presynaptic cell. The resulting current amplitudes in the postsynaptic cell were averaged over 5 trials at the holding potentials indicated, and normalised to the mean response at –70 mV. The reversal potential for these currents was 5 ± 8 mV and the decay time constant was 7.6 ± 1.4 ms. Errors and error bars represent one standard deviation. **(C)** Example traces of currents evoked at a glutamatergic synapse over a range of postsynaptic holding potentials.

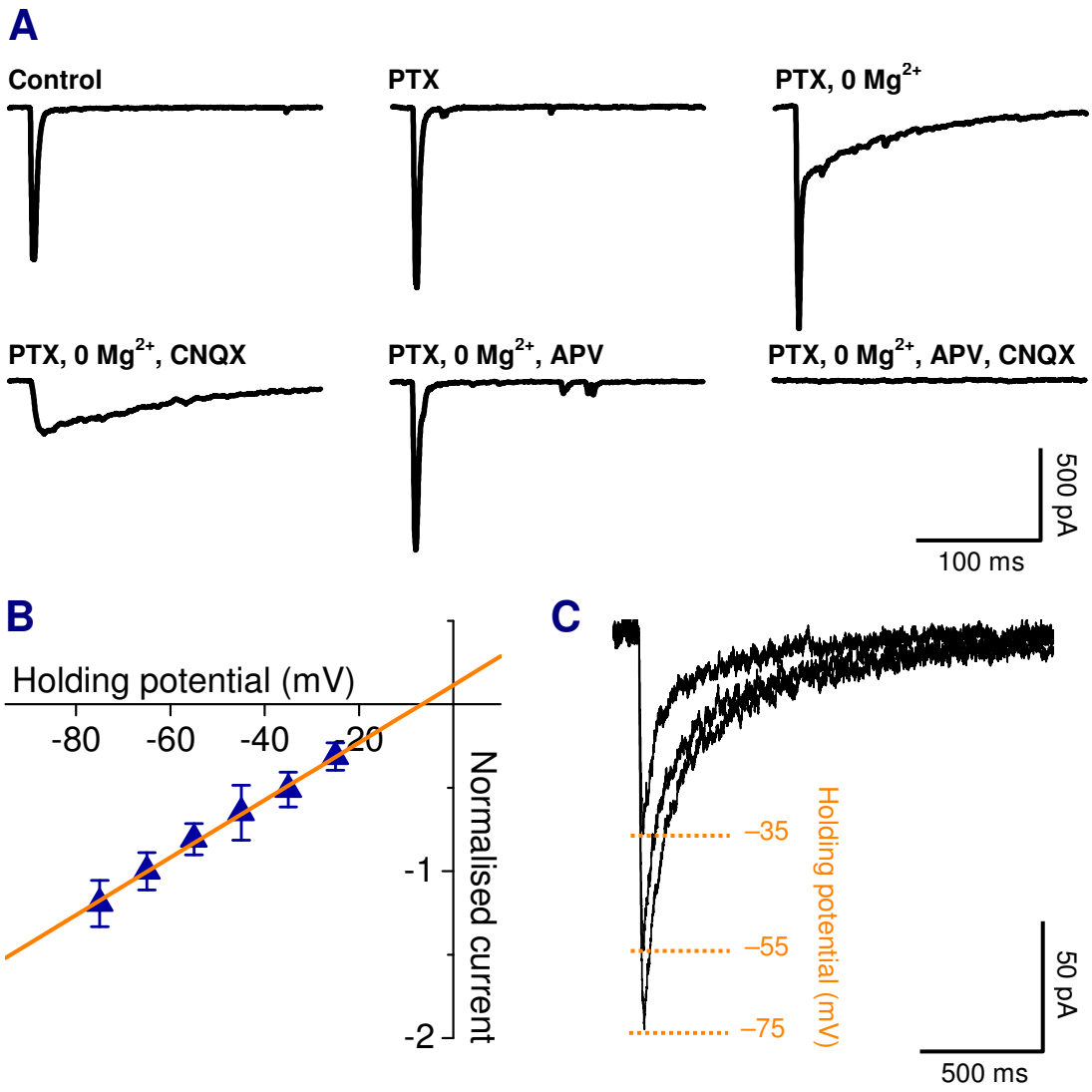

Figure 3.15: NMDAR-containing synapses

(A) Pharmacological characterisation of the NMDAR current at a glutamatergic synapse. Recording in plain external solution shows AMPAR-like currents that are insensitive to picrotoxin (50 μM). When extracellular magnesium is removed, an additional slowly-decaying current component appears. This component is insensitive to CNQX (5 μM), but completely blocked by 50 μM APV. **(B)** IV plot of pooled responses from 5 paired recordings of cells in which the currents recorded in magnesium-free solution containing picrotoxin (50 μM) and CNQX (5 μM) were pharmacologically confirmed to be mediated by NMDA receptors using APV. The amplitudes of currents evoked under these conditions were measured for a range of postsynaptic holding potentials and normalised to the mean response at –70 mV. The reversal potential was estimated to be –7 ± 7 mV and the mean decay time constant was 360 ± 134 ms. Errors and error bars represent one standard deviation. **(C)** Example traces of mean evoked NMDA currents over a range of postsynaptic holding potentials.

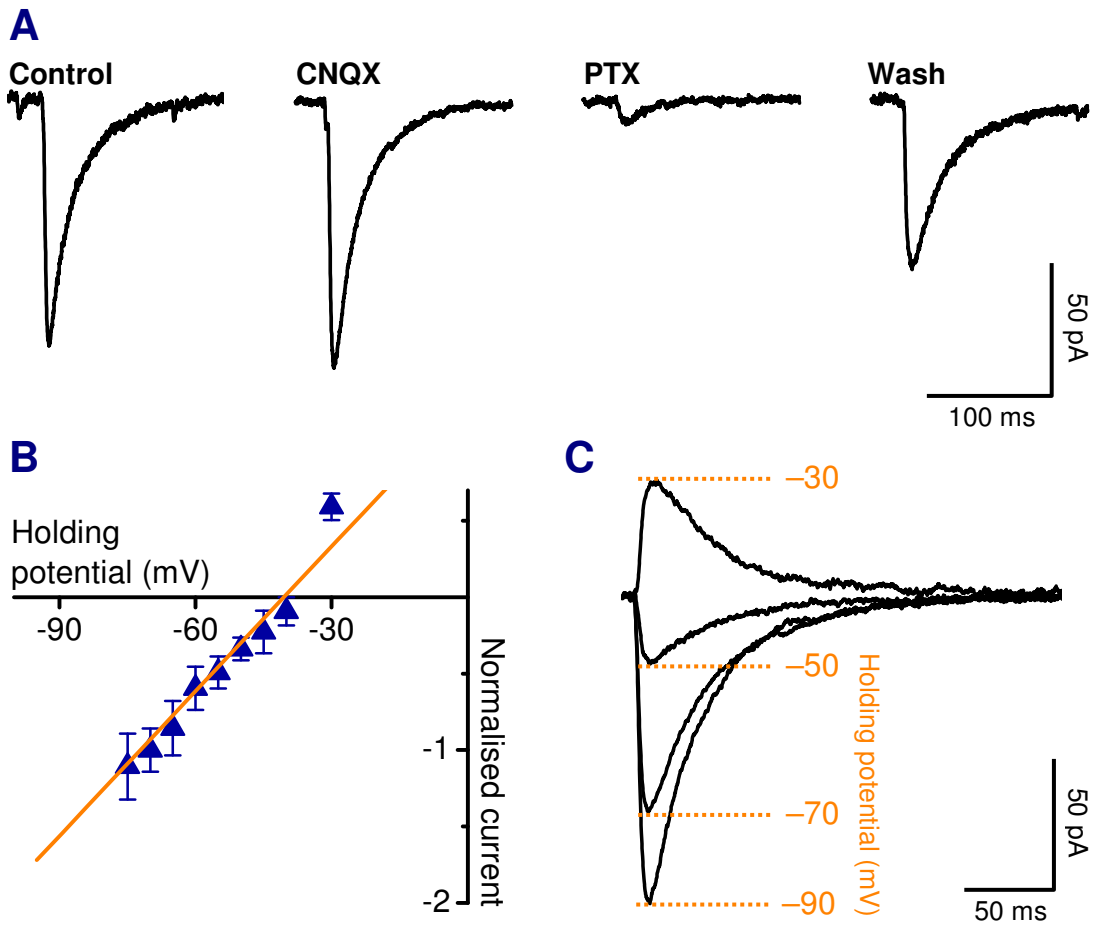

Figure 3.16: $GABA_AR$-type synapses

(A) Pharmacological characterisation of a GABA synapse. GABAergic synapses are insensitive to CNQX (5 μM) and reversibly blocked by picrotoxin (50 μM). **(B)** An IV plot of pooled responses from 6 paired recordings of cells in which the currents were pharmacologically confirmed to be GABAergic. Both cells were held in voltage-clamp and a brief (1-5 ms) depolarising pulse to +100 mV was delivered to the presynaptic cell. The resulting current amplitudes in the postsynaptic cell were averaged over 5 trials at the holding potentials indicated, and normalised to the mean response at -70 mV. The reversal potential for these currents was -40 ± 5 mV and the decay time constant was 36 ± 13 ms. Errors and error bars represent one standard deviation. **(C)** Example traces of currents evoked at a GABA synapse over a range of postsynaptic holding potentials.

3.8. Discussion

Apart from a few idiosyncrasies that will be highlighted in what follows, the electrophysiological data presented in this chapter indicates that neurons in embryonic hippocampal cultures behave in a similar way to neurons in other preparations. Morphologically, the cells have a similar appearance to hippocampal cells in slice preparations. The cytoarchitecture is, of course, totally absent in cultures. Similar conclusions have been reached in the published literature on electrophysiology of dissociated cultures (Bekkers *et al.* 1990; Bekkers and Stevens 1991; Wilcox *et al.* 1994; Bekkers and Stevens 1995).

Spontaneous activity is high. This is not commonly reported in acute slice preparations, whereas other studies using dissociated hippocampal cultures and slice cultures report similar levels of activity (Caeser *et al.* 1989; Kamioka *et al.* 1996; Beggs and Plenz 2003). In whole-cell voltage-clamp recordings the features of this activity are characteristic of normal action potential-driven and miniature synaptic currents. In current-clamp, the cells fire action potentials during spontaneous activity, and action potentials can be evoked by injecting depolarising current. In addition, the burst-like activity that has been reported elsewhere in a variety of neuronal culture systems (Kamioka *et al.* 1996; Canepari *et al.* 1997; Jimbo and Robinson 2000; Kuehl-Kovarik *et al.* 2002) was evident in the recordings, although no attempt was made to study this phenomenon in detail here.

Action potentials in these cultures are TTX-sensitive and the inclusion of TTX (1 μM) in the external solution abolishes action potentials and often reveals spontaneous miniature currents. Under such conditions, AMPA receptor-mediated mEPSCs were routinely observed. Analysis of the temporal statistics of these events revealed them to be spontaneous in nature, and well-approximated by a Poisson process. Such a process is ‘memoryless’, that is, the probability of an event occurring is independent of previous occurrences. For a large number of synapses this independence is anticipated because the mechanism of spontaneous release is dependent on conditions that are local to individual presynaptic boutons. $GABA_A$ receptor-mediated minis were appreciably less common. Since the recordings were performed at a fixed holding potential of −70 mV, one could argue that the apparent

lack of events is due to the reversal potential of $GABA_AR$ currents being close to this value and therefore undetectable. Subsequent analysis of evoked GABAergic currents in dual recordings, however, indicates that the chloride reversal potential (measured to be −45 mV) under the same recording conditions is far enough away from the standard holding potential of −70 mV to make events detectable. Furthermore, the low likelihood of detecting $GABA_A$ minis agrees with published data (Edwards *et al.* 1990; Wilcox *et al.* 1994; Nusser *et al.* 1997).

Unitary evoked synaptic currents that were pharmacologically classified as $GABA_A$, AMPA and NMDA receptor-mediated currents had kinetic properties (decay time-constants) and reversal potentials that agree with published results (Bekkers and Stevens 1991; McBain and Dingledine 1992; Nusser *et al.* 1997; Bi and Poo 1998).

The relatively depolarised chloride reversal potential observed here is typical of neonatal systems and reflects the absence of the K^+–Cl^- co-transporter KCC2 at this developmental stage (Ben-Ari *et al.* 1989; Ben-Ari 2002). One notable consequence of this is that GABAergic synapses, usually thought of as inhibitory, are not necessarily inhibitory in this system. In fact, in dual recordings where a presynaptic GABAergic cell was stimulated to initiate action potentials, excitatory synaptic potentials could be observed in the postsynaptic cell when held in current-clamp.

Perhaps the most striking feature of the cultures, made striking by its dissimilarity to more intact preparations, is the amorphous appearance of evoked synaptic currents. Readily identifiable, unitary postsynaptic currents were relatively uncommon when presynaptic cells were fired in paired recordings. More often than not, currents were messy, exhibiting multiple components which bore little resemblance to the kinetics of AMPAR or $GABA_AR$ currents despite being sensitive to specific antagonists of these receptors. This observation is not unique to the work here, for numerous other studies report complex postsynaptic currents in culture conditions (examples include, but are not limited to, Bekkers and Stevens 1991; Bi and Poo 1998; Ivenshitz and Segal 2006).

Two explanations, not mutually exclusive, are offered for this observation. The first possibility is that the presynaptic axon bifurcates and forms functional connections

with the postsynaptic cell that are some distance apart. Alternatively, the presynaptic cell forms supra-threshold synapses with neighbouring cells that also form functional connections with the postsynaptic cell. In this way evoked action currents in the presynaptic cell result in polysynaptic activity which may in some cases reverberate via reciprocal connections for extended periods.

The disorganised nature of the synapses in this preparation is not surprising, given the random nature of the connectivity that is imposed by dissociating cells and allowing them to grow in the absence of guidance cues. Whilst some studies report little differences in the form of synaptic connections in dissociated cultures (for example, Wilcox *et al.* 1994), others report similar results to those obtained here. It is not clear what underlies these differences. One possibility is that the culture conditions are capable of modulating the degree of synaptogenesis or axon growth, either because extraneous growth factors or signalling molecules are present in the culture media, or because the growth conditions and levels of activity trigger endogenous metabolic processes in the cells themselves. These questions are interesting and important in their own right, but do not constitute the focus of the remaining work in this thesis. They do, however, highlight the importance of adhering to the chosen experimental conditions in any study throughout its course, and illustrate the fact that basic results cannot always be taken for granted in any given experimental system.

Chapter 4. Synaptic plasticity and modulation of intrinsic excitability: some preliminary experiments

4.1. Chapter summary and key findings

1. Potentiating spike timing dependent plasticity (STDP) is reproduced in the current experimental system.

2. The reliability and success rate of STDP experiments is questionable. It is concluded that deeper experimental questions concerning the underlying mechanism of STDP will be impractical to answer in this project.

3. An observation concerning the effect of growing cells in elevated extracellular potassium (20 mM) is reported. Cells grown in this condition exhibit lower input resistance (270 ± 20 MΩ compared to the control value of 600 ± 60 MΩ) and lower excitability, as quantified by the amount of steady current required to elicit action potentials in current-clamp: 190 ± 20 pA (treated), 40 ± 10 pA (control).

4. mEPSCs are analysed in control and potassium-treated cells. There is a 40% enhancement in the amplitude of events in treated cells compared to control.

5. It is concluded that the remainder of the work in this project will focus on characterising the previously undocumented changes in intrinsic excitability observed in cells that are chronically depolarised with elevated extracellular potassium.

4.2. Introduction

The original goal of this project was to investigate how properties of NMDA receptors affect a type of synaptic plasticity known as spike timing-dependent plasticity (STDP). STDP leads to lasting changes in synaptic efficacy according to the relative timing of pre- and postsynaptic action potentials: potentiation is observed if an action potential arrives at the synaptic terminal a few milliseconds before the postsynaptic cell fires, and depression occurs in response to the opposite temporal order of events (Markram *et al.* 1997; Bi and Poo 1998; Sjostrom *et al.* 2001). The degree of potentiation and depression depends on the magnitude as well as the sign of pre- and postsynaptic spike timing, and, in hippocampal neurons, it is dependent on the activation of NMDA receptors (Bi and Poo 1998; Wang *et al.* 2005).

In the classical account of hippocampal long-term potentiation (LTP), calcium influx mediated by NMDA receptors activates postsynaptic signalling complexes responsible for regulating synaptic strength (Bliss and Collingridge 1993). A favoured model of how this determines the 'timing-dependent' attribute of STDP is via the relative timing of back-propagating action potentials (BPAPs) and postsynaptic depolarisation (Shouval *et al.* 2002). This model incorporates the fact that NMDA receptors are calcium-permeable and exhibit voltage-dependent block in physiological concentrations of extracellular magnesium (Ascher and Nowak 1988). Postsynaptic depolarisation caused by a BPAP arriving at the synapse relieves magnesium block of NMDARs milliseconds before presynaptic glutamate release, causing substantial calcium influx upon binding of glutamate to these receptors. On the other hand, presynaptic release prior to, or in the absence of, a BPAP would lead to diminished NMDA activity. However, NMDA activity is certainly not absent in the latter case, because depression caused by negatively-timed spike pairs is NMDA-dependent.

The kinetic properties of NMDA receptors are therefore likely to be implicated in determining the 'timing window' for STDP; the proposed goal of this project was to examine this dependence. This was to be achieved using hippocampal cultures transfected with chimaeric NMDA receptors that posses biophysical characteristics, in particular, deactivation rates, which differ from native receptors (Chen *et al.* 2004;

Erreger *et al.* 2005). An early and essential milestone in such an investigation is to reproduce the basic STDP phenomenon using a system in which it has been previously characterised, in this case using hippocampal cultures (Bi and Poo 1998).

4.2.1. A change of focus

During the pursuit of this initial result it became clear that the technical hurdles that would need to be negotiated in later stages of the project were insurmountable given the time and resources available. The decision was made to change the direction of the work some time after STDP had been reproduced. However, the results of the experiments conducted up to this point remain pertinent to the project, for they serve as further characterisation data and are interesting in their own right. As pointed out in the introduction to the previous chapter, the interpretation of later results relies heavily on assumptions about what constitutes 'normal' neuronal behaviour, and about the nature of ongoing electrophysiological activity in the cultures. The material in this chapter allows such assumptions to be substantiated with data and permits informed comparisons with other work and other systems.

In fact, it was while attempting to reproduce the STDP result using established protocols that the idea for the revised goal of the project emerged. Serendipitously, a modification of the cell culture protocol that was being used for the STDP experiments uncovered a previously uncharacterised phenomenon relating to the intrinsic properties of the cells. The culture protocol used in the work of Bi and Poo (1998) required cells to be grown in media containing elevated KCl concentration (20 mM). Supplementing the culture media with such a concentration of KCl chronically depolarises the membrane potential of the cells, an effect that has been reported to enhance neuronal viability (Gallo *et al.* 1987; Collins *et al.* 1991; Wilcox *et al.* 1994). This permitted low density cultures to be maintained in media that was not specifically optimised for embryonic hippocampal neurons (private communication, G Q Bi).

However, in this project an optimised medium was used and the high KCl condition was omitted initially because it was found to be unnecessary for maintaining healthy low-density cultures, and was considered to be 'un-physiological'. At a later stage,

after the STDP result had been reproduced, the high KCl condition was reintroduced to see if it improved the state of the cultures further. This enabled the effect of chronic depolarisation on the electrophysiological properties of the cells to be examined in a controlled manner. Notably, the intrinsic properties of the cells were found to be markedly altered in cell that were grown in 20 mM KCl-containing media, relative to control cells grown in normal culture media. As this effect had not been previously documented, a full characterisation became the focus of the project.

The organisation of the remainder of this chapter is as follows. A description of the STDP experimental protocol as it is used here will be presented, followed by some initial experimental data that characterises the stability of the recordings. Next, the results of the STDP experiments themselves are analysed. Finally, the preliminary observations concerning the effects of chronic depolarisation will be offered.

4.3. The spike timing dependent plasticity (STDP) protocol

The characterisation of STDP in hippocampal cultures by Bi and Poo (1998) provides the protocol for inducing this type of plasticity that will be followed here. One important stipulation that results from the Bi and Poo study is that pairs of synaptically coupled glutamatergic neurons are required; GABAergic cells do not exhibit STDP in hippocampal cultures. Therefore, it was decided that attention should be focussed on glutamatergic pairs in order to reproduce the basic positive result in the present work. As outlined in the previous chapter, cell type can be identified by the time-course and reversal potential of the synaptic currents, and their sensitivity to CNQX (5 μM). As a maximum of two cells can be patched simultaneously using the available equipment, cell pairs need to be either bidirectionally coupled, or unidirectionally coupled with an additional autaptic connection in the postsynaptic cell.

In addition, ‘clean’ EPSC traces are required. Synaptic connections with multiple components in the evoked current, and those that are potentially polysynaptic are to be excluded from STDP experiments. This is to ensure that precise pairing of EPSPs with postsynaptic action potentials can be achieved.

Figure 4.1 describes the standard STDP protocol that will be used. Induction requires the postsynaptic cell to be held in current-clamp during the induction period. EPSPs are then evoked by stimulating the presynaptic cell (in voltage-clamp) at a rate of 1 Hz. During the same period, single postsynaptic action potentials (APs) are induced in the postsynaptic cell at a precise time relative to the onset of the EPSP: spikes that are evoked several milliseconds after the EPSP onset are referred to as 'positively-timed' pairings (Figure 4.1A), while those that are evoked before are 'negatively-timed' (Figure 4.1B). A timing window of up to 50 ms in each direction is required to induce detectable changes in synaptic strength over the course of a 1-minute protocol, and the magnitude of the change has been found to be inversely proportional to the timing interval (Bi and Poo 1998). The distinction between the terms 'positively-timed' and 'negatively-timed' is chosen to reflect the resulting change in EPSC amplitude that has been found to be associated with these timings. Positively-timed pairings potentiate the EPSC amplitude, whereas negatively-timed pairings depress them (Markram *et al.* 1997; Bi and Poo 1998; Sjostrom *et al.* 2001).

Stable, long-lasting recordings are required for STDP experiments. In addition, it is important to disturb the intracellular composition of the cells as little as possible, as the expression of plasticity on the single-cell level is extremely sensitive to 'wash out' caused by dialysis of the cytoplasm with the intracellular recording solution. For this reason, all the experiments in this chapter are conducted using the amphoteracin perforated patch technique (Rae *et al.* 1991; Spruston and Johnston 1992).

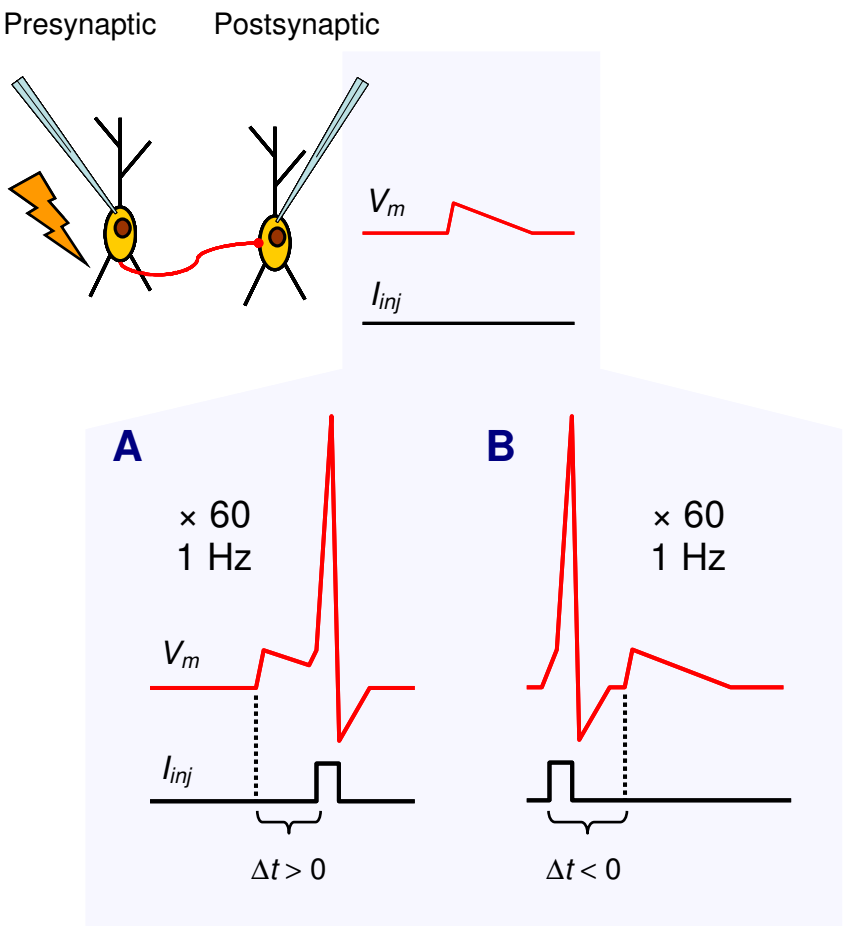

Figure 4.1: STDP protocol

A schematic diagram of a pair of glutamatergic cells with a synaptic connection (depicted by a red line joining the cells). EPSPs are elicited in the postsynaptic cell by stimulating presynaptically (**top**). To induce changes in synaptic strength, individual EPSPs are paired within 50 ms of single evoked postsynaptic action potentials for one minute at a rate of 1 Hz. The relative timing (Δt) of the EPSP onset and the action potential determines the resulting change in synaptic strength: positive timings (**A**), where the postsynaptic AP follows the EPSP, cause potentiation; negative timings (**B**) cause depression.

4.4. Stability of evoked EPSCs

Before attempting to induce a change in EPSC amplitude between synaptically coupled cells, it is important to ensure that the amplitudes of evoked EPSCs do not vary over time in the absence of a plasticity protocol.

To this end, paired recordings of glutamatergic currents in synaptically coupled cells were measured over an extended period at a rate of 0.1 to 0.05 Hz. Figure 4.2 shows an example recording of a glutamatergic cell pair. The EPSC amplitude is measured over a 50 minute period, during which time access resistance is monitored in the postsynaptic cell. As can be seen in the figure, both the amplitude of the evoked currents and the access resistance remain stable throughout the recording: the coefficient of variation (CV) throughout the recording is 0.11, and the mean EPSC amplitudes at the start and end of the recordings are 153 ± 2.3 pA and 159 ± 2.9 pA, respectively (p = 0.1, homoscedastic, paired t-test). In addition, mean EPSC waveforms exhibit a stable shape, as shown in the mean traces in Figure 4.2C.

The same experiment was repeated five times in different cells. EPSC amplitudes in all recordings remained stable for as long as the holding current and access resistance could be maintained, which was at least 30 minutes in each case. The summary data for these recordings is included in Figure 4.4, where is referred to as a control for the potentiating STDP recordings. In accordance with previous work (Bi and Poo 1998), the criterion for a stable recording in all experiments is taken to be a COV in event amplitude less than 0.3, and no more than a 10% change in amplitude over the course of the recording.

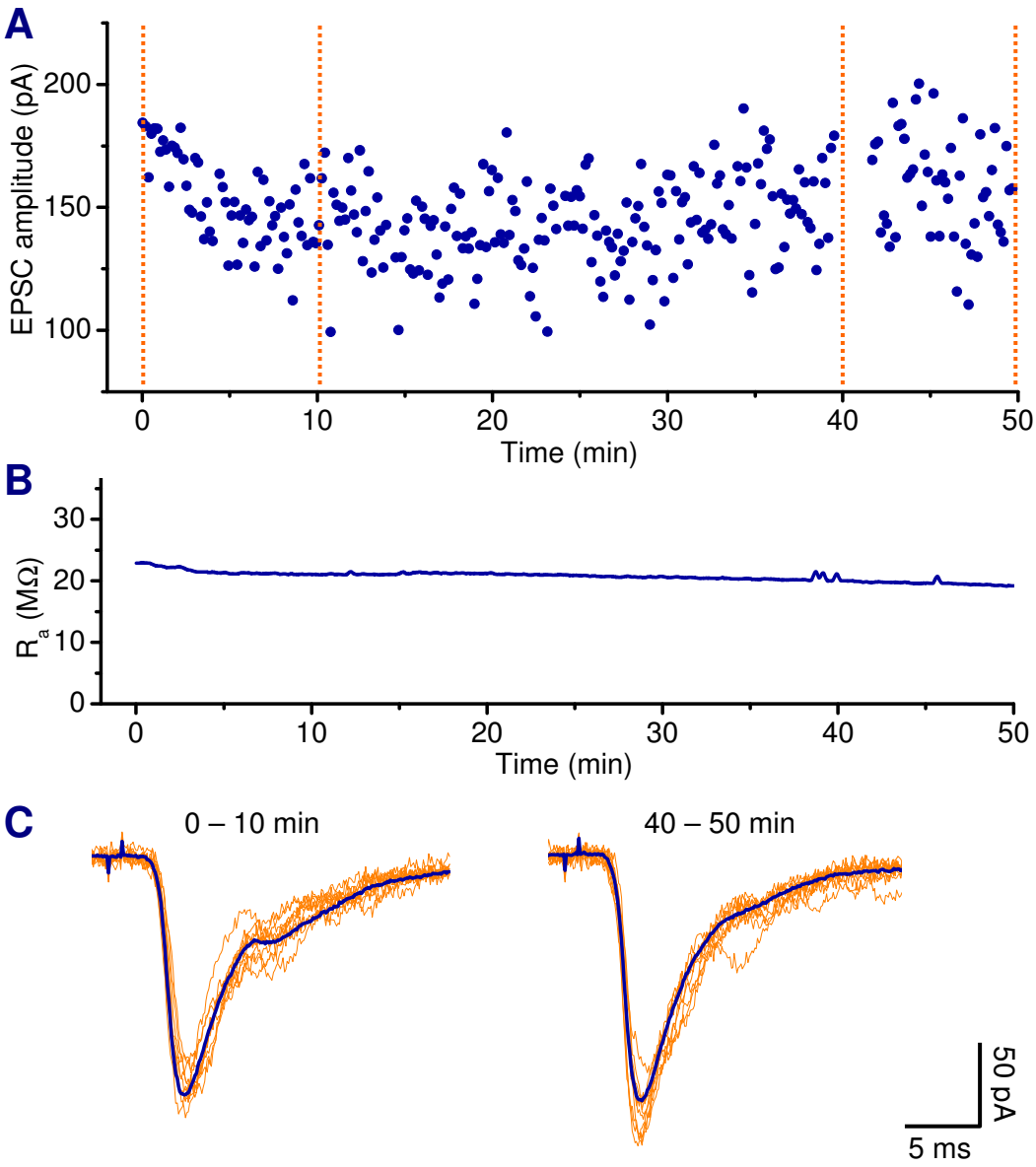

Figure 4.2 Stability of evoked EPSCs

(A) A time-series plot of EPSC amplitude **(B)** A time-series plot of the access resistance, R_a. **(C)** Mean evoked EPSC waveforms in the postsynaptic cell, estimated over a ten-minute period at the beginning and end of the full 50-minute recording.

4.5. Potentiation of EPSCs resulting from positively-timed EPSP/AP pairing

Now that the stability of paired recordings has been demonstrated over extended periods, it is possible to examine the effect of introducing a plasticity protocol. To establish individual controls for each cell, a 10-minute baseline recording of EPSC amplitudes at a rate of 0.05 Hz will be included prior to placing the postsynaptic cell in current-clamp for the induction phase. During this period, the access resistance is monitored for stability within a range of 10%, and the EPSC amplitudes must have a CV less than 0.3. Recordings that fail to meet this criterion are excluded.

Figure 4.3 shows the result of a positively-timed STDP induction protocol applied to the postsynaptic cell in a pair of glutamatergic cells, with time interval equal to 7.5 ms. A clear potentiation of the EPSC amplitude (by 22.2 ± 1.7% of baseline amplitude, $p = 1.1\times10^{-4}$, unpaired *t*-test) is evident, and remains stable for 40 minutes following induction, at which point the recording was terminated. Up until this point, the access resistance and holding current remained stable and the cells showed no visible signs of degradation.

Similar experiments were performed in a total of 5 cells using positive timing intervals between 5 and 10 ms. Summary data for all these recordings is shown in Figure 4.4, alongside the stability recordings of the previous section. The mean potentiation, as measured by the relative change between the EPSC amplitude in the 10-minute control phase and the 20-minute interval following induction, was 32 ± 9% ($p = 0.026$, paired *t*-test).

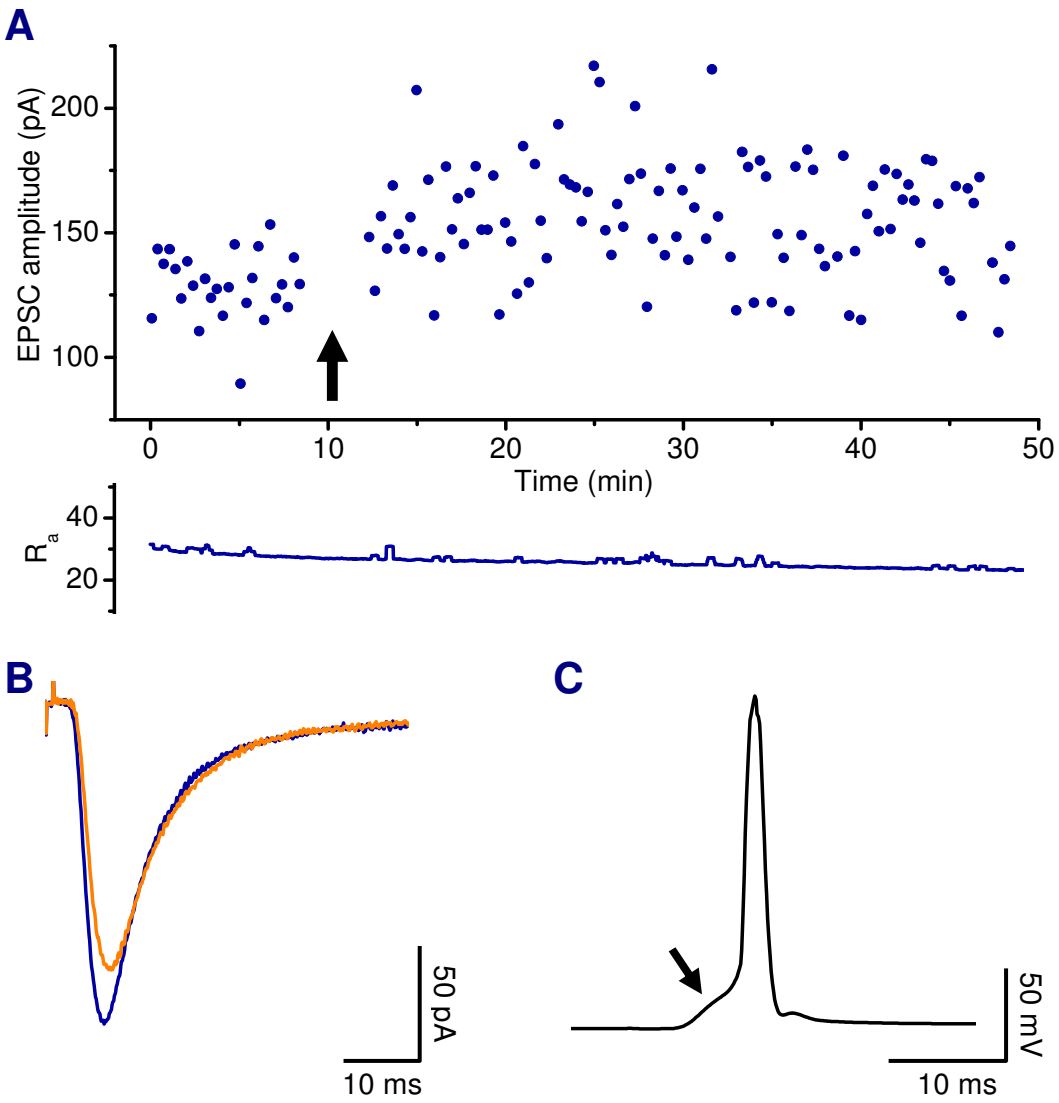

Figure 4.3 Potentiating STDP

(A) An example of spike timing-dependent potentiation of evoked excitatory synaptic currents. After a 10-minute control period, EPSC potentiation was induced by pairing postsynaptic spikes and evoked EPSPs with a positive timing delay 7.5 ms, at a rate of 1 Hz for 60s (black arrow). **(B)** Mean traces of the evoked postsynaptic cell before (orange trace) and after (dark blue trace) the pairing protocol, which resulted in a potentiation of 22.2 ± 1.7% relative to baseline values (p = 1.1×10^{-4}, two-tailed t-test.) **(C)** Mean current clamp trace of the postsynaptic cell showing the rising phase of the evoked EPSP (black arrow) and the induced action potential.

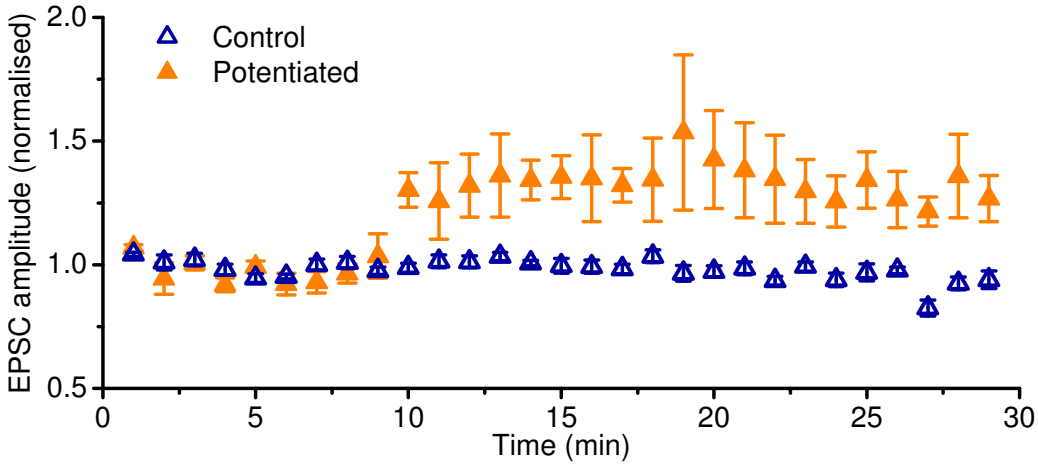

Figure 4.4: Potentiating STDP – summary

A Summary plot of control and potentiating STDP experiments (n = 5 in each case). The mean amplitude of potentiated EPSCs, normalised to control values in the same cells is 132 ± 9% (p = 0.026, paired, two-tailed t-test).

4.6. A counterexample to the basic STDP result

STDP was not found to be completely reliable in the experiments conducted here. Often, this turned out to be explainable in terms of the health of the cells or the stability of the recording during the control period. However, one example will be shown here in which two successive attempts to elicit potentiation using a positively-timed STDP protocol resulted in stable depression following the first attempt, and no change after the second attempt.

Figure 4.5 shows the example recording in question. EPSCs elicited in the baseline control period were stable, with a coefficient of variation of 0.15. The first induction phase (indicated by the leftmost arrow on the time series in Figure 4.5A) consisted of one minute of spike pairings at a timing interval of 5 ms relative to EPSP onset (Figure 4.5C). This resulted in significant depression of the EPSC amplitude (–24 ± 2%, $p = 3\times10^{-6}$, t-test) that remained stable for 15 minutes, after which time a second protocol was applied, this time with a wider timing interval of 10 ms. The second induction phase resulted in no discernable change in EPSC amplitude and the recording remained stable until it was terminated at 40 minutes.

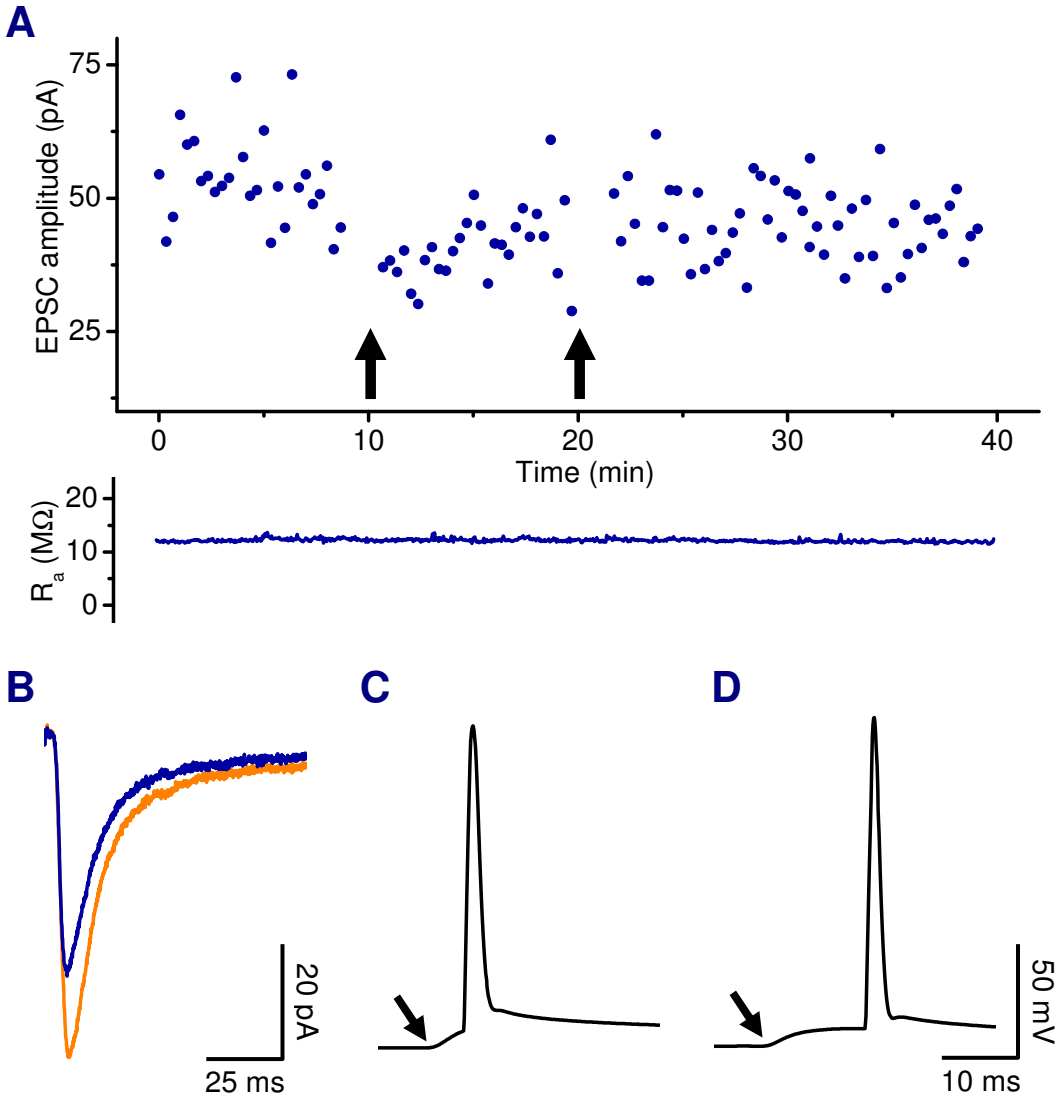

Figure 4.5: Stable depression resulting from a potentiating time window

(A) After a 10-minute control period, a nominally potentiating STDP protocol (black arrows) was applied with a positive timing delay 5 ms. This resulted in a stable depression of 23.6 ± 2.8% ($p = 3\times10^{-6}$, two-tailed *t*-test) relative to control values. The synaptic strength remained stably depressed in spite of an additional induction protocol with a timing window of 15ms, which was applied 10 minutes later. **(B)** Mean traces of the evoked postsynaptic cell before (orange trace) and after (dark blue trace) the first pairing protocol **(C)** Mean current clamp trace of the postsynaptic cell during the first and **(D)** second pairing protocol. The EPSP onset is indicated by the black arrow in each case.

4.7. An observation concerning chronic depolarisation

The original characterisation of STDP carried out by Bi and Poo (1998) used low-density cultures grown in culture media containing 20 mM KCl. In the the present study it was found that low density cultures could be maintained without supplementing the culture media with KCl, possibly because an optimised media recipe was used instead of the DMEM-based media used by Bi and Poo (see Methods). However, a number of cultures were prepared using elevated KCl with a view to finding a more reliable system for studying plasticity. Although no STDP recordings were obtained from these cultures, a number of cells were recorded from in preliminary experiment during which altered intrinsic properties were observed.

4.7.1. Intrinsic properties of chronically depolarised cells

Cells grown in 20 mM KCl tended to have lower resting membrane potentials than those grown in its absence, and when examined further in current-clamp, it appeared that a substantially higher depolarising current amplitude was required to elicit action potentials. This was systematically investigated by generating FI curves (current vs. spike rate) using 500 ms pulses of current at varying amplitudes.

Figure 4.6 shows current-clamp traces from a cell grown in normal culture media compared to a cell obtained in the same culture and grown in the same media supplemented with 20 mM KCl from 1 DIV onwards. While the control cell (grown under normal conditions) requires 15 pA of depolarising current to elecit an action potential, the cell grown in 20 mM KCl requires 180 pA. Both cells were recorded on the same day, using the same internal and external recording solutions (3 mM KCl in the external).

Cells from four separate cultures were recorded in the same way between 9 and 16 DIV. A control group, grown in normal media, was maintained alongside a 'treatment group' grown in 20 mM KCl-containing media. The pooled FI data from 38 control and 20 treated cells are shown in Figure 4.7A, with the mean resting membrane potential (in current-clamp) and input resistance in B. Current threshold was defined as the minimum amplitude of depolarising current required to elicit action potentials, averaged over three trials for each cell. Mean vales for each of these quantities were significantly different between conditions.

4.7.2. mEPSCs in chronically depolarised cells

In addition to examining the effects of KCl-induced depolarisation on intrinsic cell properties, mEPSCs were measured to see whether there were any systematic differences in synaptic properties. Example recordings and mean mEPSC waveforms for all recordings are shown in Figure 4.8, summary histograms of measured properties of mEPSCs are in Figure 4.9. A significantly higher mean mEPSC amplitude was observed in treated cells compared to control (control: 12.4 ± 1.0 pA, treated: 17.4 ± 1.2 pA; $p = 5\times10^{-3}$, *t*-test). Also, the event frequency is higher in the treated cells (control: 2.2 ± 0.3 Hz, treated: 4.4 ± 0.7 Hz; $p = 0.02$, *t*-test), and, interestingly, there is a slightly smaller decay time-constant in the treated group (control: 8.2 ± 0.8 ms, treated: 6.0 ± 0.5 ms; $p = 0.03$, *t*-test). The mean rise-time (control: 1.9 ± 0.1 ms, treated: 1.8 ± 0.1 ms; $p = 0.5$, *t*-test) of the events is not significantly different, however.

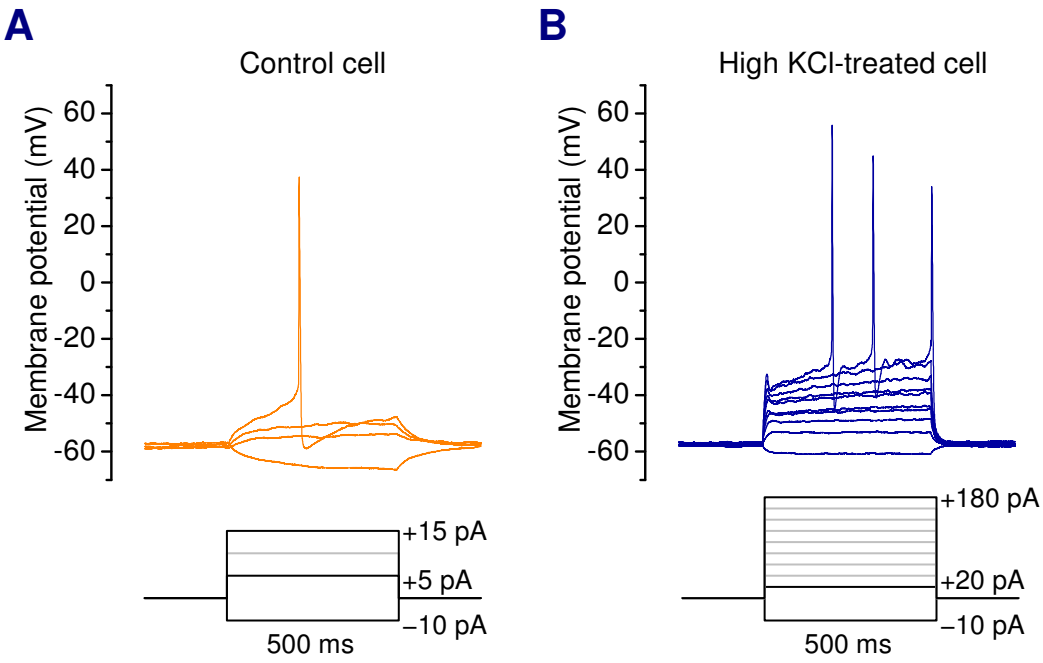

Figure 4.6: Attenuated excitability of neurons grown in media containing 20 mM KCl

(A) Example current-clamp traces from a cell grown in ordinary culture media, recorded at 14 DIV.A family of 500 ms current injection steps were delivered to the cell, starting with a 10 pA hyperpolarising step to measure input resistance, followed by depolarising steps starting at an amplitude of 5 pA and increasing in 5 pA-increments until spiking was evoked at 15 pA (B) Example current-clamp traces from a cell grown in media containing 20 mM KCl from 24 hours after plating, until recording at 14 DIV. As with the cell in (A), a 10 pA hyperpolarising step is delivered, followed by depolarising steps in increments of 20 pA. Spiking is elicited at 180 pA.

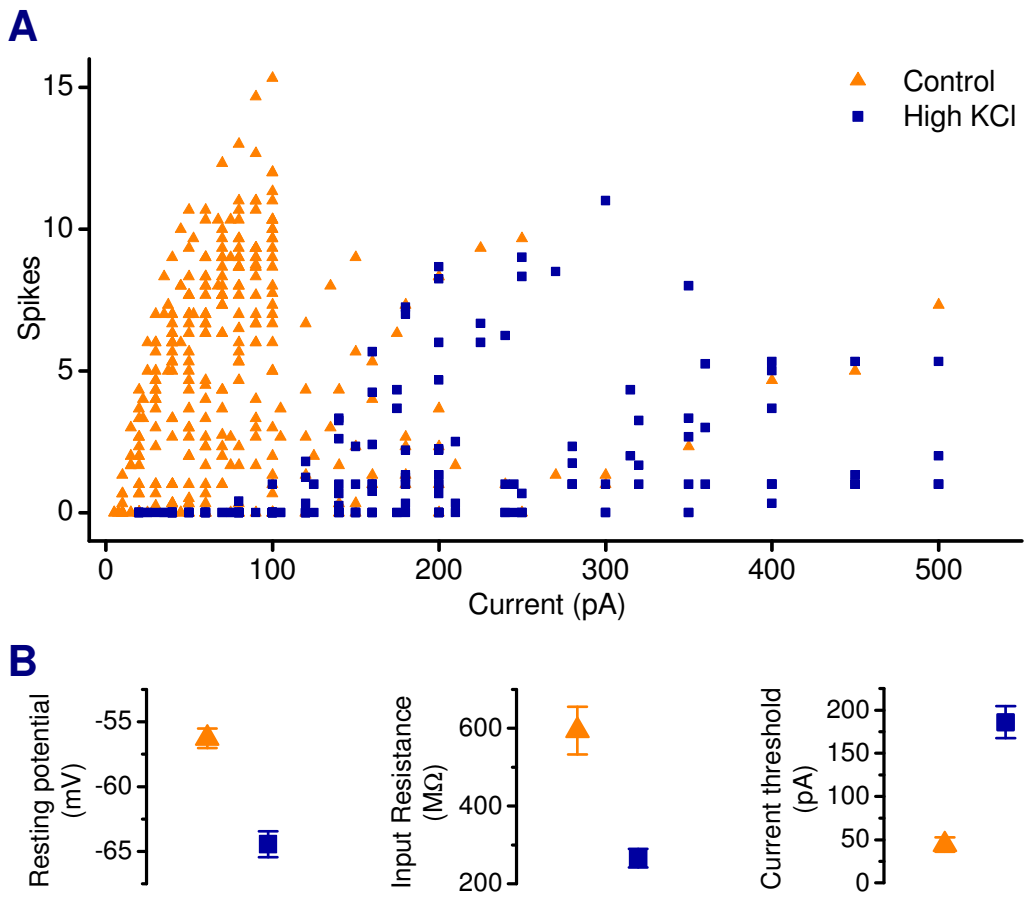

Figure 4.7: Chronic depolarisation with 20 mM KCl alters the intrinsic excitability of cultured hippocampal neurons

(A) Scatter data of FI assays applied to control cells grown in normal culture media (n = 38) and cells grown in media supplemented with KCl (20 mM final concentration, n = 20). Each data point represents the mean number of spikes evoked in a single cell by a 500 ms long current pulse, averaged over three trials.**(B)** Mean resting potential, input resistance and current threshold for all cells in each condition. Current threshold was estimated from a least-squares linear fit of the non-zero data points in each FI assay.

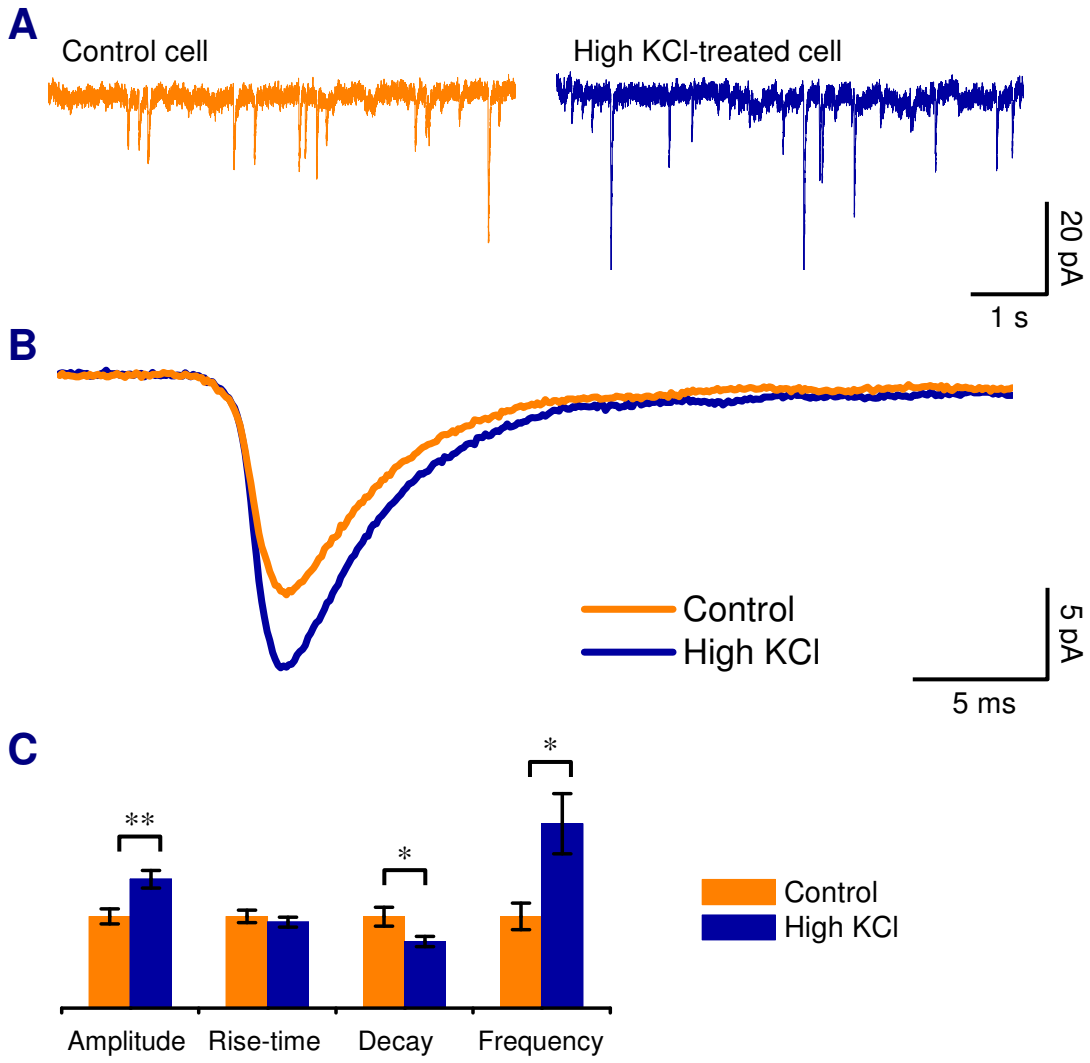

Figure 4.8: mEPSCs in control and chronically depolarised cells

(A) Example recording segments from a control cell and a cell grown in 20 mM KCl. Both cells are recorded at 14 DIV. **(B)** Mean mEPSC waveforms for control (n = 10) and treated (n = 11) cells. For each cell, 200 events are gathered and aligned to the half-maximum time; the traces shown are means taken across all events in each condition. **(C)** Quantification of mean mEPSC parameters, normalised to control values.

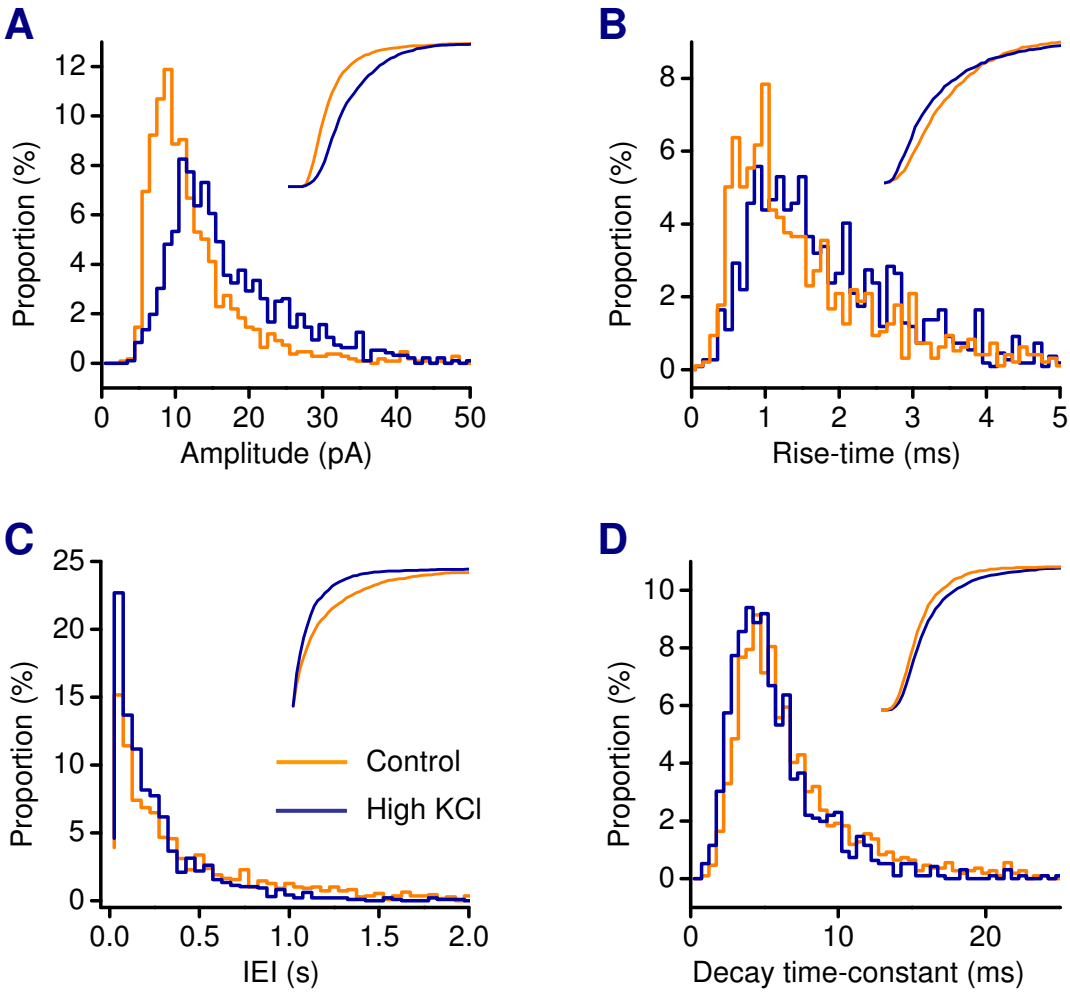

Figure 4.9: mEPSCs in control and chronically depolarised cells

Statistics for mEPSCs recorded in control cells (n = 10) and cells grown in 20 mM KCl (n = 11). All recordings were performed at 10–14 DIV in normal recoding solution. **(A-D)** Histograms with cumulative proportions (insets) for event amplitudes, rise-times, inter-event-intervals (IEIs) and decay time-constants pooled over 200 events for each cell.

4.8. Discussion

This chapter is intended to provide a brief synopsis of a number of important results that determine the goals of the remainder of the thesis. As previously mentioned, the original goal of the project was to study spike-timing dependent (synaptic) plasticity (STDP). The observed differences in intrinsic properties of neurons grown in high potassium during the pursuit of this goal are, however, the central theme for the work in what follows.

4.8.1. STDP experiments

The main result in this chapter concerning spike timing-dependent plasticity is that potentiation can be induced using positively-timed EPSP-spike pairings with a timing window of 5-10 ms (Figure 4.4). The magnitude of potentiation is comparable to that published elsewhere, given the degree of variability associated with this phenomenon (Bi and Poo 1998). However, STDP was not characterised beyond this basic reproduction of the result.

It is important to explain why the direction of the work was changed at such an advanced stage. Several obstacles presented themselves. Most importantly, STDP is a difficult phenomenon to reproduce, and unreliable even in a system where is can be demonstrated to exist (Wittenberg and Wang 2006; Carlisle *et al.* 2008). Indeed, the example recording in Figure 4.5, in which depression is induced by a positively-timed pairing protocol, shows how unreliable STDP is in the present work.

Furthermore, despite the relative ease with which stable paired recordings could be obtained, only a handful proved to be suitable for STDP experiments. This was, in part, due to technical limitations. In order to reproduce the original finding, paired glutamatergic cells are required (Bi and Poo 1998). With only two recording electrodes available, the identity of both cells could only be confirmed if connections were reciprocal, or if the postsynaptic cell also had an autaptic connection. Such a configuration is found only in a percentage of recordings, and among those cell pairs that have this pattern of connectivity, many also exhibit undesirable polysynaptic connections or lack a ‘clean’ unimodal postsynaptic response.

In order to study the effect of altered NMDA receptor kinetics in these recordings using transfected chimaeric subunits, one would have to identify cell pairs which satisfy all the requirements necessary for an STDP recording, and which, additionally, have a transfected postsynaptic cell. Even with a high-efficiency transfection protocol, the odds of success are diminished considerably by these additional constraints.

Finally, and perhaps most importantly, the scientific reasoning behind the original project is somewhat superficial. Suppose a difference was observed in the properties of STDP in transfected neurons. For the sake of the argument, suppose STDP potentiation turned out to be enhanced in cells transfected with slowly-desensitising NMDA receptors. What can we conclude? Have the transfected constructs even reached the synapses of the target cell? Is it a result of depolarisation, or enhanced calcium influx, or biochemical signalling due to the additional receptors, or merely an artefact of the transfection protocol? Each of these questions would require a detailed control experiment. The resulting catalogue of controls would likely constitute the bulk of the work and would address questions that have more to do with the peculiarities of the experiment than the phenomenon itself. Experiments that are capable of dissecting individual components of the STDP mechanism in such a way will have to wait for more precise technology and for a clearer picture of how synaptic plasticity in general operates on a biochemical level.

4.8.2. Changes in intrinsic excitability induced by prolonged depolarisation

Cells grown in media containing an elevated extracellular potassium concentration (20 mM) exhibited marked differences in their intrinsic properties when compared to control cells, which were grown in normal culture media. Significantly more current was required to elicit action potentials in the chronically-depolarised cells, and this difference is accompanied by a hyperpolarising shift in the resting membrane potential and a decrease in input resistance.

All of these observed changes are consistent, in the sense that if we assume Ohm's law gives a reasonable prediction of the sub-threshold current-voltage relation for membrane potential, then significantly more current will be required to reach a fixed

action potential threshold in cells with low input resistance and a hyperpolarised resting potential. Whether or not the voltage threshold itself is altered in the chronically depolarised cells remains to be established. Indeed, there are numerous questions that can be explored regarding the wider phenomenon. For instance: what are the temporal characteristics of this effect? Is the effect dependent on the concentration of KCl used? Can it be blocked pharmacologically? Is it reversible? These questions will be discussed and addressed in detail the next chapter, and determine the agenda of the work that follows. Judging by the results in this chapter, the effect, as quantified by the change in current threshold, is large enough to enable detailed, quantitative measurements.

4.8.3. mEPSCs in chronically-depolarised cells

Chronic depolarisation also resulted in a higher mean amplitude and event frequency of mEPSCs compared to control cells. This result contradicts results published work using cortical cultures, which shows that mEPSCs decrease in amplitude as a result of chronic depolarisation (Leslie *et al.* 2001). Several important differences between the study of Leslie *et al.* and the current work may account for this discrepancy. First, the experimental systems use neurons from two distinct brain regions, cortex and hippocampus, which differ in their physiological properties. For example, although early studies show LTP can be induced with high-frequency stimulation in both the cortex and hippocampus (Kirkwood *et al.* 1993), later work shows many aspects of synaptic plasticity are different at excitatory synapses in these two systems (Castro-Alamancos and Connors 1997; Buonomano 1999). In addition, the concentration of KCl (20 mM) and duration of depolarisation used here (8-15 days) both differ from Leslie *et al.* (2001): 3-12 mM, 48 hours.

Indeed, the elevated amplitude of mEPSCs observed here contradicts the synaptic homeostasis hypothesis (Turrigiano 2007): if depolarisation is a model for heightened activity, one would expect the homeostatic response to constitute a down-regulation of excitatory synaptic strength. This observation, coupled with the unreliable nature of STDP, raises questions concerning the consistency of synaptic phenomena in culture systems. It also places a strain on the homeostatic interpretation of the results in this context.

Chapter 5. Characterisation of the homeostatic response to chronic depolarisation

5.1. Chapter summary and key findings

1. Prolonged depolarisation with KCl over the course of 8-11 days induces changes in the intrinsic excitability of hippocampal neurons that are dependent on, and proportional to, the concentration of extracellular KCl used. Elevated KCl concentrations in the range 10-30 mM are examined.

2. The magnitude of the changes in intrinsic excitability are dependent on the duration of depolarisation. Effects can be observed after 12 hours and continue to enhance in magnitude as long as healthy cells could be maintained (17 days). The most reliable direct measure of the effect is the magnitude of steady current required to initiate action potentials, or current threshold.

3. The current threshold in cells that have been depolarised for one week returns to control levels within 60 hours of returning the cells to control conditions. This form of regulation of intrinsic excitability is therefore reversible, and homeostatic in nature.

4. Homeostatic regulation of intrinsic excitability, as it is defined here, is dependent on the depolarisation-induced influx of calcium via L-type calcium channels and is independent of NMDA receptor activation.

5.2. Introduction

The previous chapter described a basic observation: neurons that are kept in a depolarised state for several days using KCl-supplemented media respond by attenuating their excitability. Specifically, the cells require more depolarising current to elicit action potentials when compared to cells grown in ordinary media under identical recording conditions. The purpose of this chapter is a systematic characterisation of this effect. Several natural questions arise:

1. How can the effect be suitably quantified?

   Excitability is usually defined by the amount of input required to elicit a given output from a neuron. For whole-cell current clamp recordings, the level of steady current required for a cell to reach spiking threshold is a natural measure of excitability, and this can be estimated for a given cell by delivering current pulses of varying magnitudes and counting the number of spikes elicited in a fixed time window. The resulting 'FI curve' ('F' for frequency, 'I' for current) will then have a well-defined current threshold[6] above which spikes are elicited (see Methods, Section 2.5.4). There are other features of the cell's excitability that can also be quantified during such an experiment, namely, the cell's resting membrane potential, input resistance, the slope of the suprathreshold region of the FI curve and the membrane potential at which spikes are elicited, or voltage threshold.

2. Once quantified, is the magnitude of the effect dependent on the level of depolarisation or KCl concentration?

   The guiding hypothesis in this work is that the modulation of excitability brought about by chronic depolarisation is homeostatic in nature. This means that a given cell's response should oppose the change in the environment and be proportional in magnitude to the change. To offer a concrete example, if neurons insert more leak channels to compensate for an elevation in extracellular potassium, say, then the rate of insertion should parallel the

[6] The current threshold as it is defined here is sometimes called the 'rheobase' (Koch and Segev 1998).

difference in potassium concentration from normative levels.

3. What is the time-course of the effect?

   The intrinsic properties of a neuron are governed by a host of biochemical pathways; in particular, those responsible for ion channel expression and modulation. An environmentally-triggered response mediated by these pathways is likely to include gene expression, protein trafficking and other types of enzymatic activity, and may therefore exhibit multiple timescales from fractions of a second to hours and even days. From a computational viewpoint it is also natural to ask what time-course this effect has: a very fast time-course may lead to instability, a very slow time-course would impair the performance of the system in the short term. It is therefore important to quantify how rapidly the observable changes occur.

4. Is the effect reversible?

   This is related to the second question: a genuinely homeostatic phenomenon should dynamically oppose changes in the environment. If chronically depolarised cells are returned to non-depolarising conditions, any changes accrued in their intrinsic properties should reverse according to this principle.

5. Is it possible to block the effect pharmacologically?

   A change in intrinsic properties has been observed to accompany chronic depolarisation. For these changes to occur, the cells must be able to detect the imposed change in their membrane potential, for example, so that the pathways responsible for modulating intrinsic properties can be activated. These pathways are currently unknown. Pharmacological blockade of the effect would help identify them, and assist in developing a model of the mechanism governing intrinsic excitability.

We shall proceed by addressing each of these questions in turn. Subsequent chapters deal with the membrane conductances that underlie the change in excitability.

5.3. Concentration dependence of the homeostatic response to KCl-induced depolarisation

Increasing the extracellular concentration of KCl over a period of days diminishes the excitability of cultured neurons. We would like to know how big a shift in excitability occurs for a given increase in concentration above control levels, and whether the shift is proportional to the final KCl concentration. Toward this end, cultures were grown for 9-14 days in ordinary media (containing approximately 5 mM KCl – see Methods) as a control, and at the same time in media containing 10 and 15 mM KCl from DIV 1 onwards. Whole-cell recordings were performed under the same conditions for each group, using a nominally physiological extracellular KCl concentration (3 mM). Pooled FI curves and example stimulation traces for each condition are shown in Figure 5.1.

A rightward shift in the FI curve is induced by 10 mM KCl (5 mM above control levels); this shift is nearly double for 15 mM KCl (Figure 5.1A) as can be seen by comparing the current threshold values (control: 11.7 ± 3.5 pA; 10 mM KCl: 51.5 ± 6.6 pA; 15 mM KCl: 104 ± 17 pA). The slope of the pooled FI curve also decreases as the KCl concentration is increased. Chronically depolarised cells typically fire irregularly, in contrast to control cells which showed relatively evenly-spaced action potentials during the stimulating current pulses (Figure 5.1B). No attempt was made to quantify this irregularity.

Summary data for all of the cells included in this experiment are shown in Figure 5.2. In addition to the current threshold and FI slope, the input resistance, resting membrane potential and voltage threshold are included. Details of the how these parameters are measured are included in the methods chapter.

As can be seen from the tables in Figure 5.2, all of the trends in these parameters were statistically significant with respect to a 1% criterion (one way ANOVA) except the apparent increase in voltage threshold in treated cells, which was only marginally significant by comparison ($p = 0.012$).

Input resistance was lower in treated cells compared to control (control: 760 ± 100 MΩ; 10 mM KCl: 380 ± 40 MΩ; 15 mM KCl: 270 ± 30 MΩ) and the resting

membrane potential became more hyperpolarised as KCl treatment concentration increased (control: −50.6 ± 1.4 mV; 10 mM KCl: −55.6 ± 1.1 mV; 15 mM KCl: −59.7 ± 2.0 mV).

These changes in input resistance and membrane potential largely account for the shift in current threshold according to a simple linear estimate of the amount of steady current required to reach voltage threshold from resting potential using Ohm's law:

$$I_{thr} \approx \frac{(V_{thr} - V_m)}{R_{in}}$$

Where I_{thr} is the current threshold; V_{thr} the voltage threshold and R_{in} the input resistance. Figure 5.3 compares this estimate with the experimental value for each group.

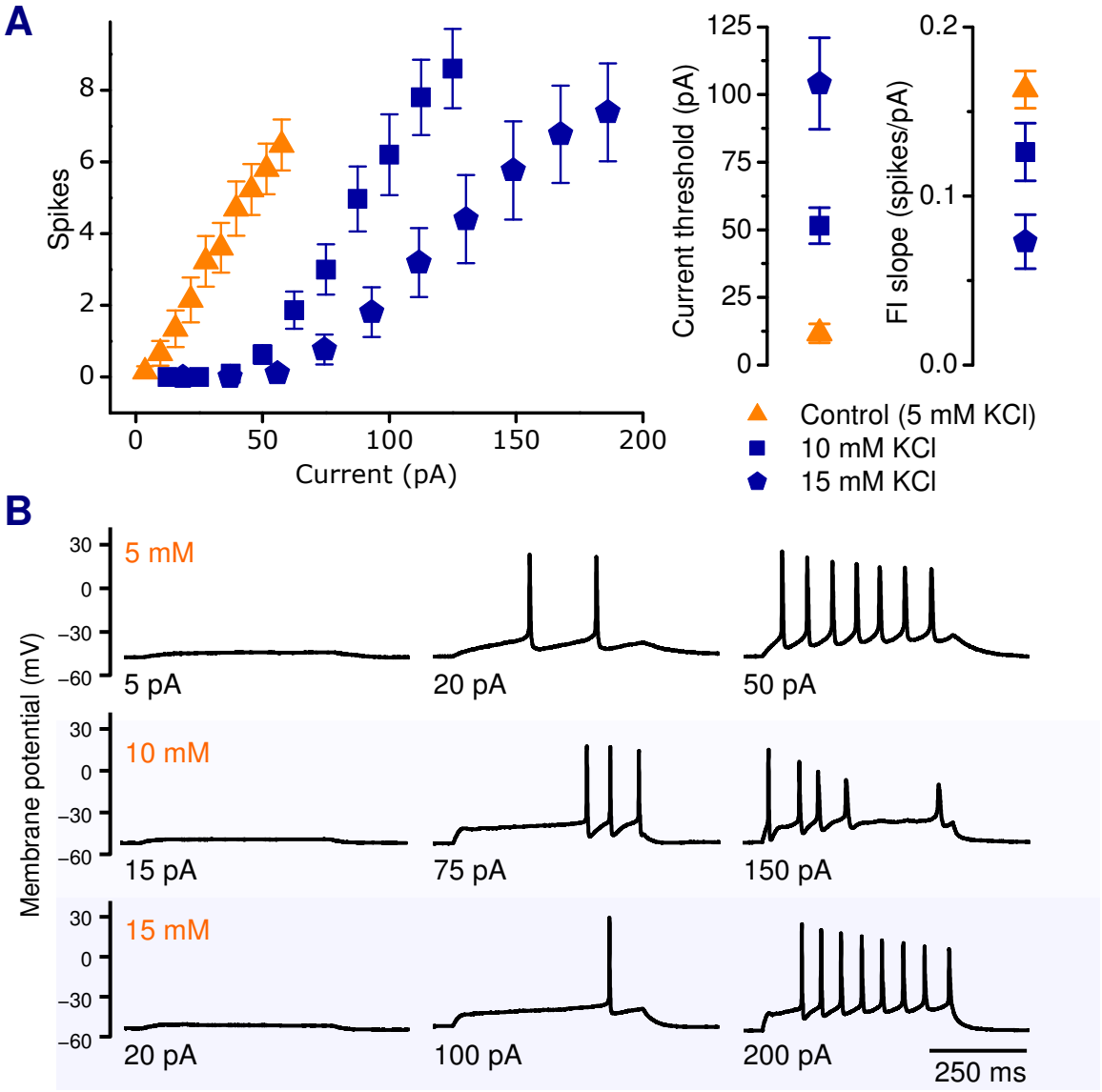

Figure 5.1: Concentration dependence of the response to chronic depolarisation

(A) Pooled FI curves for cells grown in media with 5 (control, n = 10), 10 mM (n = 10) and 15 mM (n = 9) KCl for 7-10 days. Linear regression on the non-zero data points provides estimates of the current threshold and slope of the FI curve in each condition (right). **(B)** Example current-clamp traces of three cells grown in media with 5 (control), 10 and 15 mM KCl for 10 days. A 500 ms pulse of current was delivered to the cells at the amplitudes indicated. All recordings were performed in external solution with normal (3 mM) KCl concentration.

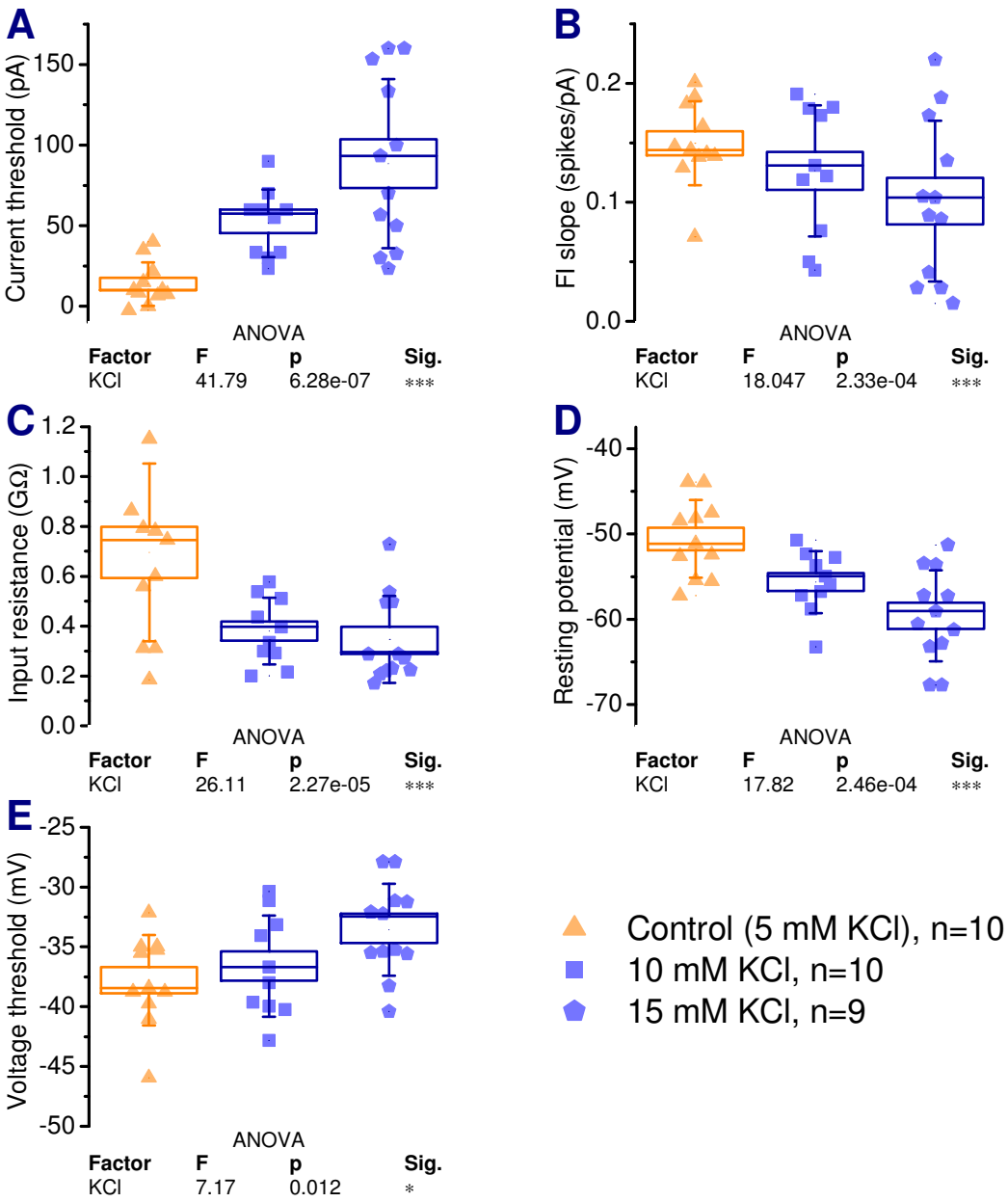

Figure 5.2: Intrinsic properties of chronically depolarised neurons

Summary data for the intrinsic properties of cells grown in 5, 10 and 15 mM KCl and recorded at 8-11 DIV. Each box plot shows the entire data set for: **(A)** current thresholds for inducing spikes, estimated from a linear fit of the FI curve of each cell; **(B)** the slopes of the linear fits; **(C)** input resistance, estimated using a 10 pA, 500 ms hyperpolarising pulse; **(D)** resting potential, taken to be the zero-current potential in current clamp; and **(E)** voltage threshold, taken to be the membrane potential induced by the maximum sub-threshold current pulse in the FI assay.

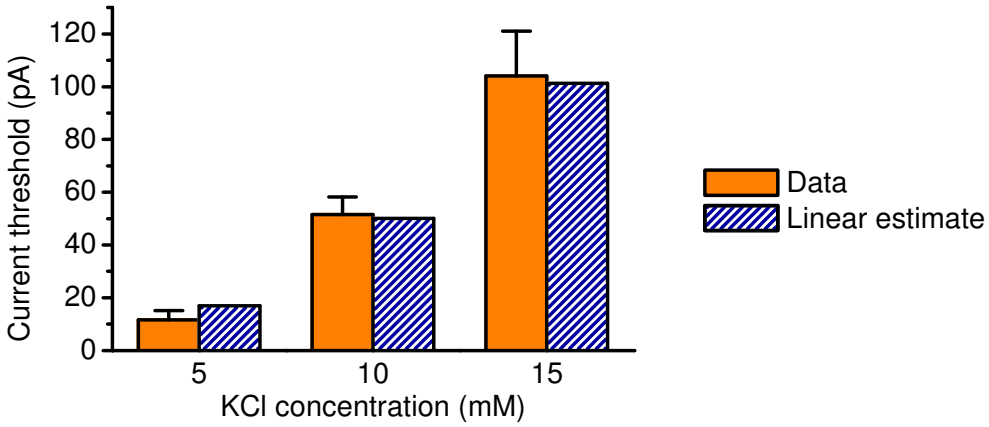

Figure 5.3: Linear estimate of current threshold

Applying Ohm's law to the measured values for resting potential, voltage threshold and input resistance provides a god estimate of the current threshold, indicating that changes these parameters are largely responsible for the observed decrease in excitability of chronically depolarised cells.

5.4. Acutely-applied KCl

Now that reliable, lasting changes in the intrinsic properties of neurons have been established to occur in response to chronic depolarisation, it is instructive to examine the effect of bath-applying KCl on the membrane potential of the cells. This experiment is important for two reasons: firstly, to quantify the magnitude of depolarisation that is induced in untreated cells. This gives some insight into the effect that prolonged KCl treatment has on membrane potential. Secondly, to see if the depolarising effect is attenuated in cells treated with elevated extracellular KCl for extended periods, as would be predicted if the cells modulate their properties homeostatically.

Prior to discussing the results, an important point need to be made regarding the first objective. The conditions during whole-cell recordings are quite different to those in the incubator: the temperature is much lower (37ºC in the incubator, 20ºC in the recording chamber) and the extracellular recording solution is different to the culture media. Unfortunately these discrepancies cannot be avoided in this work for practical reasons, so the interpretation of the data must assume these caveats.

Figure 5.4A shows example current clamp recordings of a control cell and a treated cell during 15 mM KCl application. Both cells depolarise markedly as the solution is washed in, then reach a stable plateau. Interestingly, the control cell fires rapidly during the initial phase of depolarisation, then stops – presumably due to depolarisation block. On the other hand, the treated cell begins to fire after reaching the plateau, then continues to fire spontaneously.

Figure 5.4B shows the result of repeating this experiment on (n = 6) control cells and (n = 6) cells grown in 15 mM KCl for 8-10 days. Cells from both groups were recorded in current clamp in normal external solution containing 5 mM KCl (matched to the culture media concentration of KCl, Methods) to establish a baseline membrane potential. At the time indicated in the figure, 15 mM KCl was applied. All cells show an immediate depolarisation in their resting potential; this rise in membrane potential was enough to initiate action potentials in most cells. The membrane potential of treated cells plateaus at a more negative value than that of control cells: −24.7 ± 1.6 mV (control) vs. −32.3 ± 1.7 mV (treated), (p = 0.01, two-tailed t-test, Figure 5.4B). In addition, treated cells are capable of firing action potentials with an extracellular KCl concentration of 15 mM, whereas control cells are not.

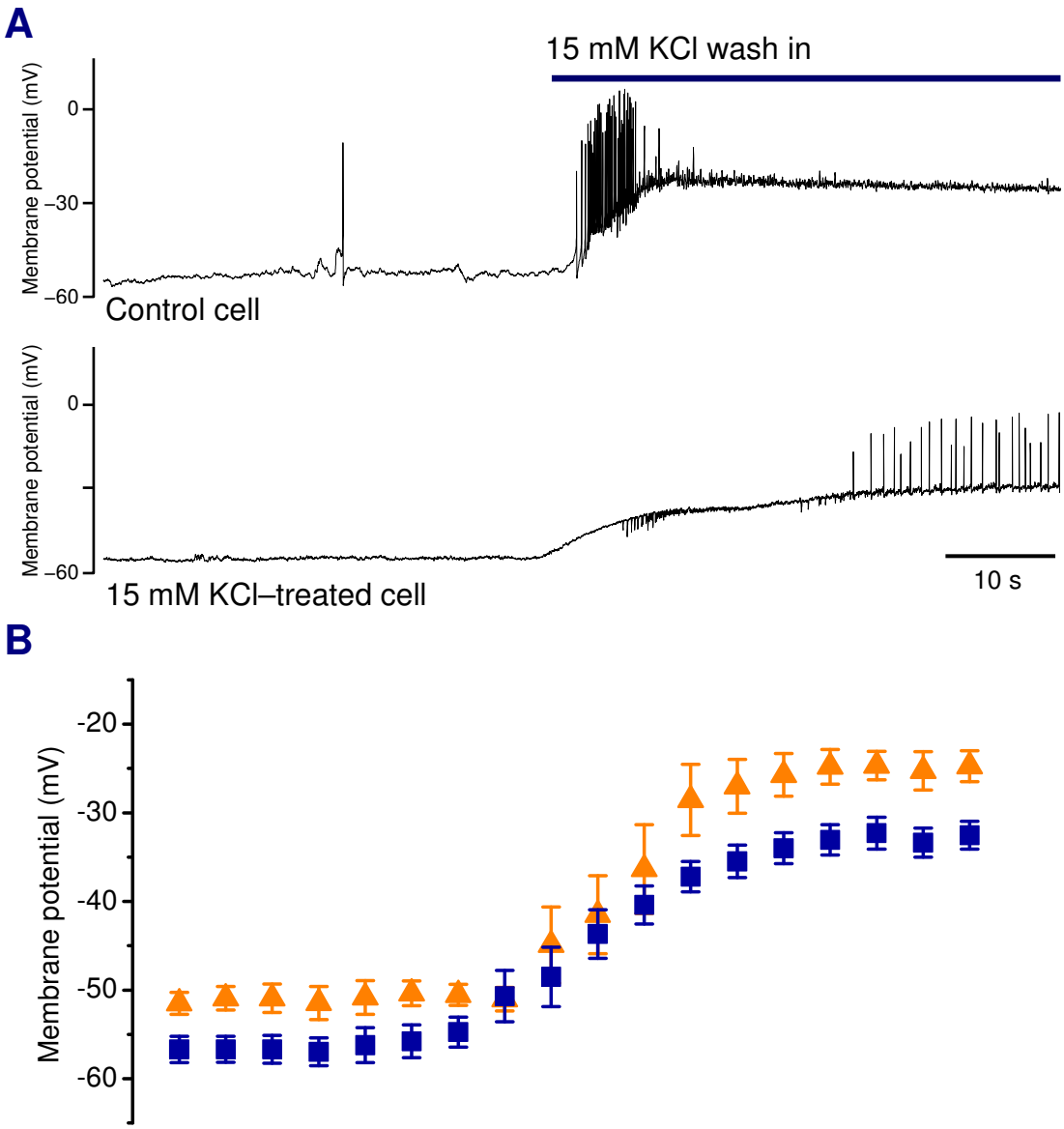

Figure 5.4: Acutely-applied KCl

(A) Example recordings of cells in current-clamp showing the effect of acute bath application of 15 mM KCl after a baseline period in external solution containing 5.4 mM KCl. These KCl concentrations are chosen to match those in the culture media during incubation. Spontaneous action potentials are evident in both cells. Both cells are recorded at 11 DIV. **(B)** Quantification of the average membrane potential of 6 cells in each condition, averaged at 5-second intervals. The final membrane potential for each group is –24.7 ± 1.6 mV (control) and –32.3 ± 1.7 mV (15 mM cells). This difference is statistically significant (p = 0.01, two-tailed paired t-test).

5.5. Co-dependence on magnitude and duration of depolarisation

The experiment in section 5.3 characterised depolarisation-induced changes in the neuronal excitability at a single time-point. It is important to examine how excitability varies with the duration of depolarisation because numerous possibilities exist for the temporal characteristics of this effect: it may be a discrete, step change which remains stable in spite of continuous depolarisation; it may continue to exacerbate over time; or it may plateau and even diminish. To ascertain which profile applies, additional data are required at different time points. As a first step in addressing this unknown, cells were grown in 15 and 30 mM KCl alongside control cells and recorded from a further week beyond the age of the 8-11 DIV cells discussed previously, at 14-17 DIV. As a comparison, cells from the same cultures were also recorded at 8-11 DIV. Thus, the following experiment has two factors and six groups: *time* (8-11 DIV and 14-17 DIV) and *KCl concentration* (control/5 mM, 15 mM and 30 mM). The higher value of 30 mM KCl was used in this experiment to ensure a large effect size.

FI curves were measured in approximately 10 cells in each group (Figure 5.5). As anticipated, the 30 mM KCl group shows a more pronounced shift in the current threshold than the 15 mM cells. This shift grows with time: at 14-17 DIV it is approximately double the effect size at 8-11 DIV at both concentrations (57 ± 6 pA vs. 117 ± 18 pA for 15 mM cells; 118 ± 14 pA vs. 176 ± 27 pA for 30 mM cells). Two-way ANOVA showed the dependence on age and KCl concentration to be significant ($p = 2.5 \times 10^{-13}$ for age, $p = 6.0 \times 10^{-4}$ for KCl concentration); there was no significant interaction between the factors ($p = 0.13$). The FI slope does not appear to vary over time, but is lower than control values in the chronically depolarised cells. Excluding voltage threshold, clear trends are evident in the other intrinsic properties of the cells. As can be seen in Figure 5.5, both the input resistance and resting membrane potential of the cells follow the same trend as in the previous experiment: input resistance decreases as the treatment concentration of KCl increases and resting potential hyperpolarises. The trend in time was not apparent for input resistance, but it is evident in resting potential, which tends to more hyperpolarised in the 14-17 DIV group than at 8-11 DIV.

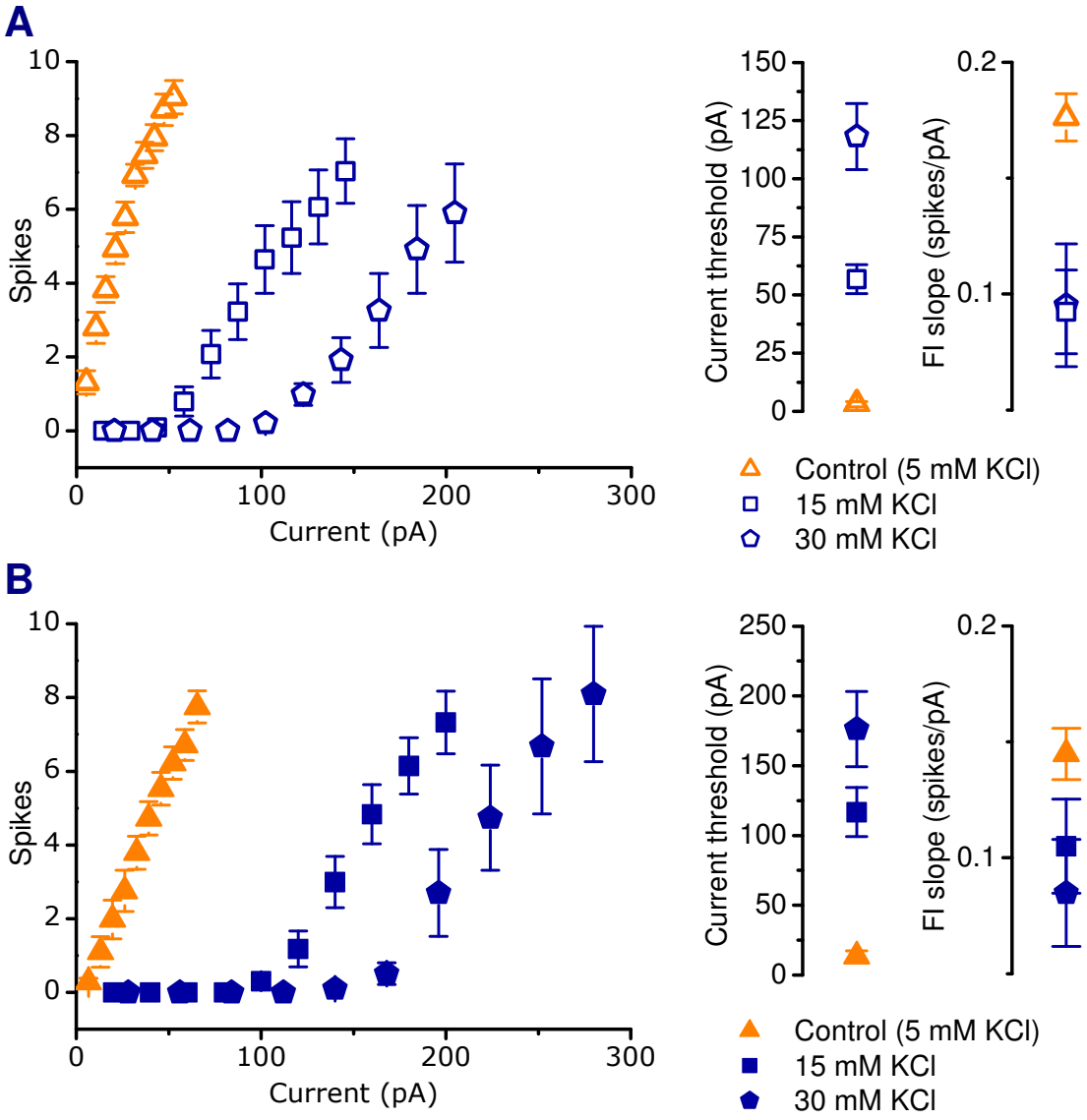

Figure 5.5: Time and concentration dependence of the effect of chronic depolarisation on intrinsic excitability

(A) Pooled FI curves for cells grown for 8-11 days in media with 5 (control, n = 11), 15 mM (n = 11) and 30 mM KCl (n = 11). (Right) Linear regression on the non-zero data points provides estimates of the current threshold and slope of the FI curve in each condition. **(B)** Pooled FI curves for cells grown for 14-17 days in media with 5 (control, n = 11), 15 mM (n = 11) and 30 mM KCl (n = 10). All recordings were performed in normal (3 mM) KCl.

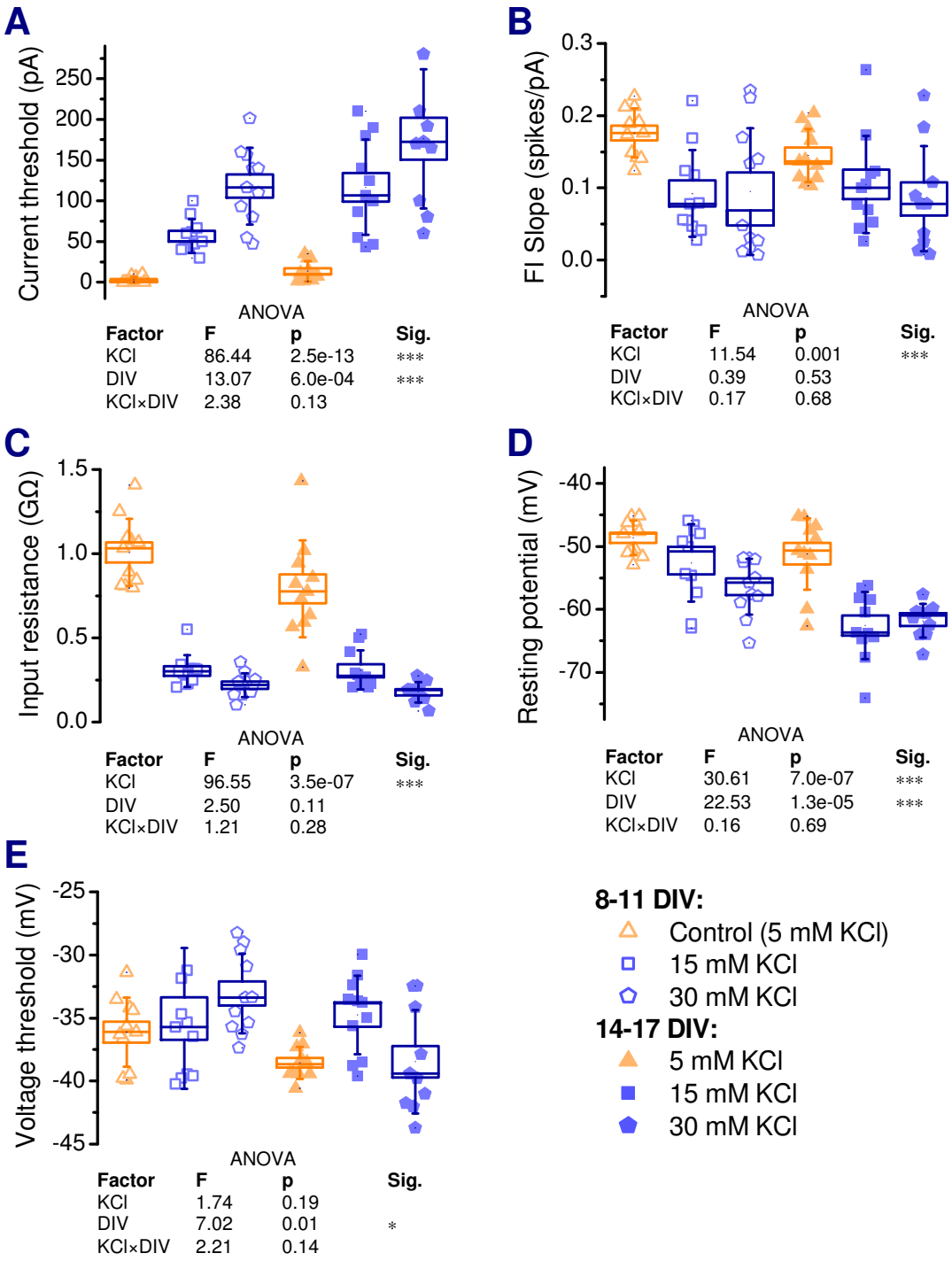

Figure 5.6: Intrinsic properties of chronically depolarised neurons

(A-E) Summary of intrinsic properties of cells recorded after 8-11 DIV and 14-17 DIV after being grown in three different extracellular KCl concentrations from 1 DIV: 5 mM (Control), 15 mM and 30 mM. Beneath each plot is the result of applying two-way ANOVA to the data, with significant trends indicated by asterisks.

5.6. Short timescales: 12-24 hours of depolarisation

One week is a long time relative to the developmental period of the rodent brain and presumably a long time relative to sustained elevations of neural activity that may occur in the brain normally, or during pathological states. If neurons modulate their intrinsic properties to achieve homeostasis in a physiological context, they should exhibit modulation on shorter timescales as well. The changes in excitability documented in this study so far are dramatic and the result of many days of continuous depolarisation. Consequently, it is necessary to characterise the effect of chronic depolarisation over briefer periods.

Figure 5.7 shows the result of depolarising cells for 12-24 hours using 15 mM KCl on the mean FI curve. An additional positive control group was included in the experiment, consisting of cells that were chronically depolarised for 7 days or more (maximum 13 days). Though smaller than in previous experiments, there is again a rightward shift in the FI curve of the cells treated for the shorter period, relative to the control group. This is quantified by a difference in the current threshold between the groups: 1.8 ± 1.3 pA (control) compared with 27.3±7.9 (depolarised cells) a two-tailed, Bonferroni-corrected *t*-test revealed statistical significance between these mean values (p = 0.02). A shift in the mean FI slope is also apparent, but not statistically significant (p = 0.6).

In addition, the control cells in this experiment were found to be hyper-excitable, and often fired spontaneously in the absence of depolarising current. In these cases, a small (< 10 pA), constant hyperpolarising current was applied whilst measuring the FI curve. The amplitude of this hyperpolarising current is subtracted from the injected current values in the FI curve assay, thus correcting the measured current threshold. The contribution of this hyper-excitability is evident in the low mean current threshold in the control group for this experiment as compared to previous experiments. Such hyper-excitability was not observed in previous experiments, and might be a result of recording from the cells soon after the media was completely replaced – a measure put in place to ensure a proper control condition for the (12-24h)-depolarised group.

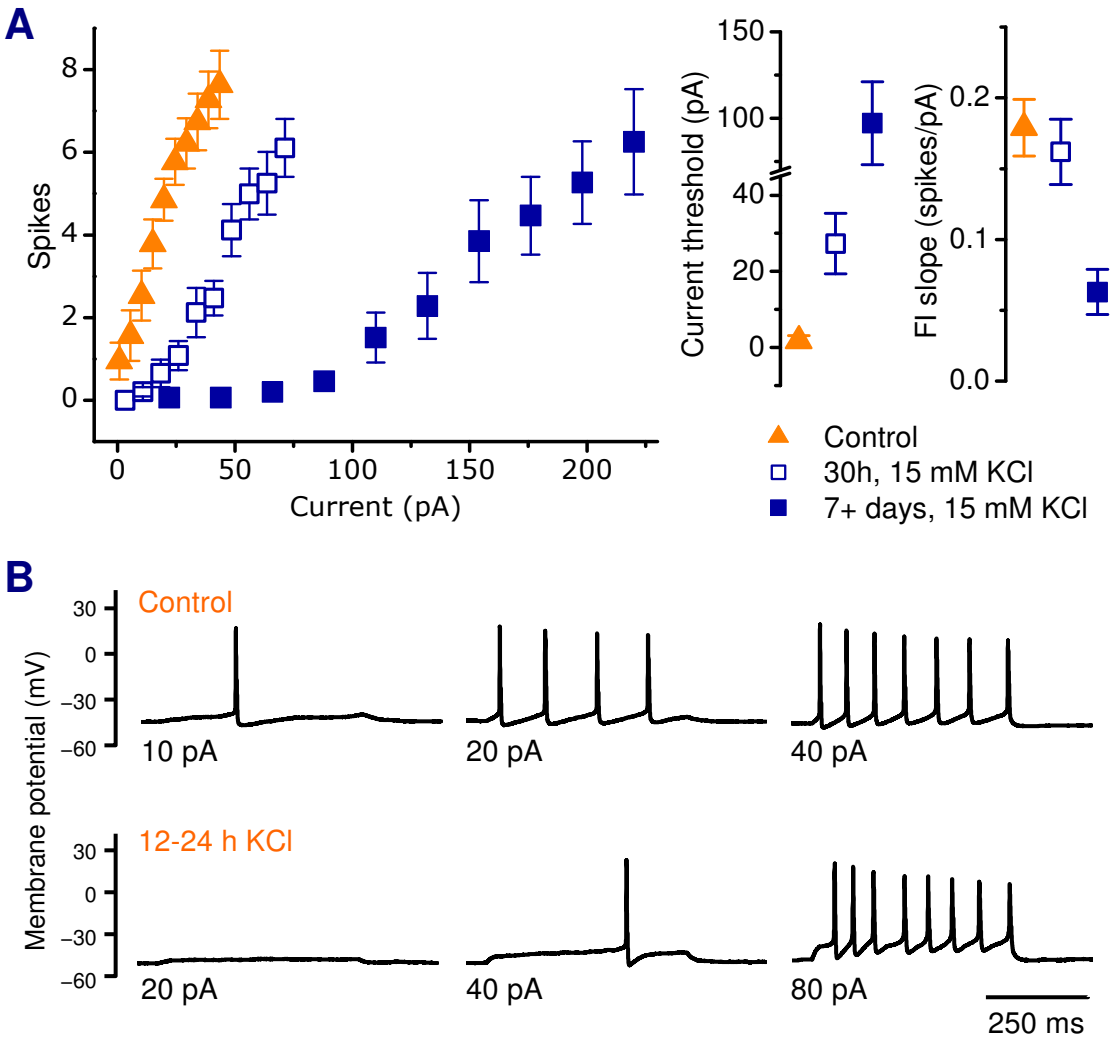

Figure 5.7: Short timescales

(A) Pooled FI cures for cells treated with 15 mM KCl for 12-24 hours after 8-9 DIV (n = 12), along with curves from cells in the same culture grown as controls in normal media (n = 10) and 15 mM KCl from 1 DIV (7+ days of depolarisation, n = 10). Current threshold was significantly different between control and 12-24 h depolarised groups (p = 0.008, two-tailed *t*-test) whereas FI slope was not (*p* = 0.6). **(B)** Example current-clamp traces from control cells and cells depolarised for 12-24 hours in 15 mM KCl.

5.7. Reversibility

According to the definition laid out in the introduction to this chapter, homeostatic phenomena must exhibit *reversibility*. In other words, a system should revert back to its original state once the triggering stimulus is removed. Here, we would expect the intrinsic excitability of the chronically depolarised cells to return toward control levels once the depolarising media is replaced with normal media. This change is unlikely to be immediate: the change is certainly stable over the course of an hour because it is observable after placing treated cells in a recording chamber with normal recording solution for such a time. Furthermore, the results of the short-timescale experiment suggest that the change itself takes many hours to express at a significant level. If we assume that the mechanisms responsible for elevating and decreasing excitability are related, it would follow that the time-courses of the changes in both directions would be similar.

Figure 5.8 shows FI curves for cells from the same cultures grown in three different conditions. The 'recovery' group was grown in media containing 15 mM KCl for 7 days from 1 DIV. The media was then completely replaced with normal culture media for a further 60 hours before recording. As a negative control, cells were grown at the same time in normal media, which was replaced at the same time prior to recording. The positive control was provided by a group grown in 15 mM KCl from 1 DIV and replaced for media containing the same KCl concentration at the same time as the other two groups.

A reversal of the effect was observed in the recovery group (n = 16), whose FI curve closely approximates the negative control (n = 13). Both the current threshold (negative control group: 13 ± 6 pA; recovery group: 11 ± 5 pA; $p = 0.59$, *t*-test) and FI slope (negative control group: 0.10 ± 0.01 spikes/pA; recovery group: 0.11 ± 0.01 spikes/pA; p = 0.36, *t*-test) are indistinguishable between these groups, whilst the positive control group (n = 13) exhibits the expected shift in current threshold (140 ± 20 pA; Bonferroni-corrected *p*-value = 0.003, *t*-test). The difference in FI slope between chronically-depolarised cells and control was not statistically significant in this experiment (FI slope: 0.06 ± 0.02 spikes/pA; $p = 0.18$, *t*-test).

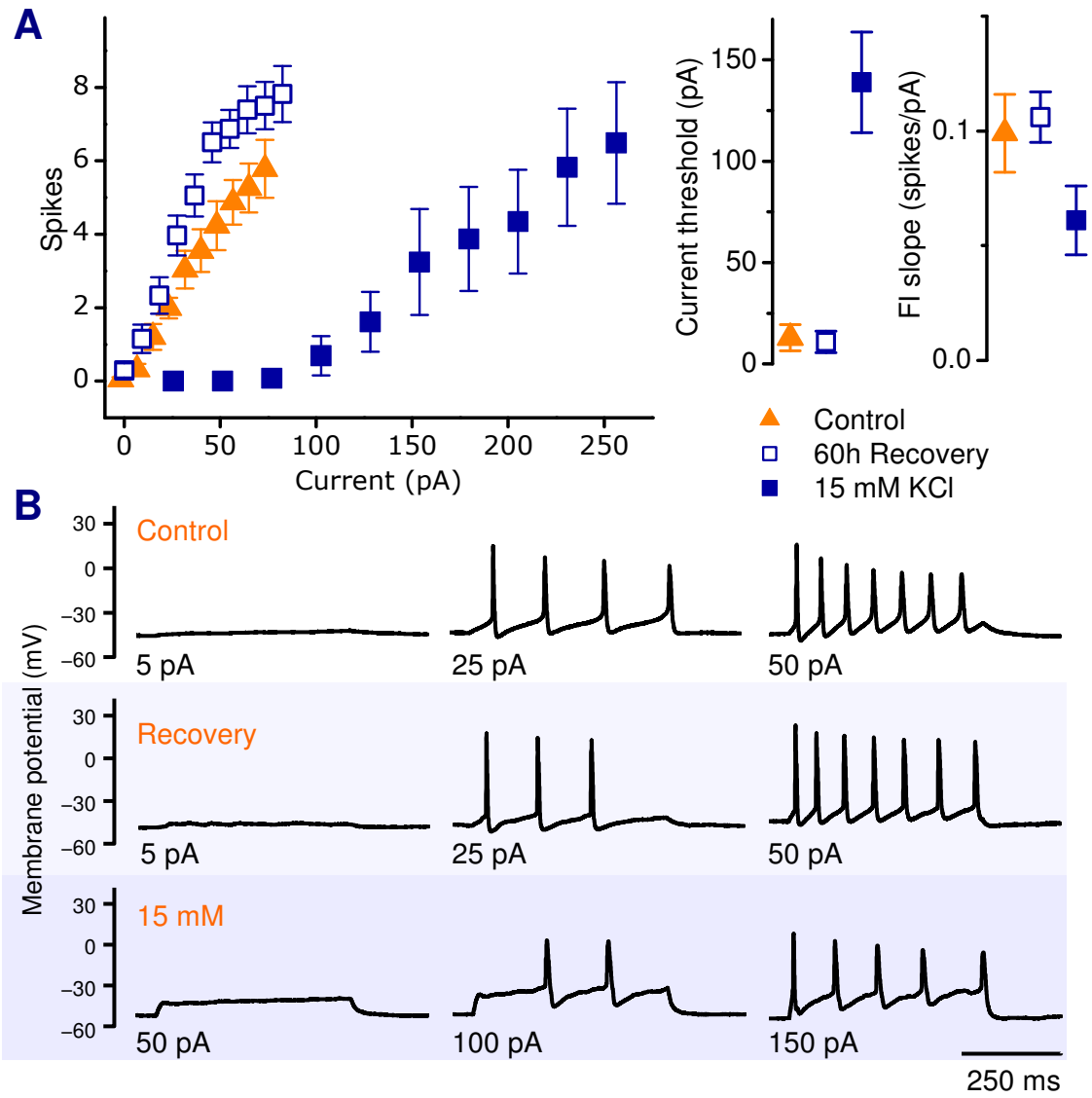

Figure 5.8: Reversibility of the response to chronic depolarisation

(A) Pooled FI curves for cells grown in normal media ('Control', n = 13) and media containing 15 mM KCl ('Recovery', n = 16; '15 mM', n = 13). At 7 DIV the media in the Control and Recovery groups was replaced with normal media and the media in the 15 mM group was replaced with media containing 15 mM KCl. Recordings were performed 60h later in 3 mM KCl each case. (Right) Linear regression on the non-zero data points provides estimates of the current threshold and slope of the FI curve in each condition. **(B)** Example current-clamp traces from a cell in each of the three conditions. Cells were stimulated with a 500 ms pulse of current at the amplitudes indicated.

5.8. Pharmacological intervention

Some mechanism for detecting chronic depolarisation must exist in neurons so that they can modify their properties in the ways we have observed so far. As this response is capable of being expressed and reliably detected on a timescale of hours, it is feasible to attempt to interfere with it pharmacologically. The most obvious way to proceed is by blocking well-defined pathways during the depolarisation period to see if this prevents changes in the FI curve, in particular, the current threshold, as this is the most reliable measure of the effect. This will help identify components of the expression mechanism, or at the very least rule out certain candidates.

Calcium influx has been identified as a likely candidate for the 'depolarisation signal' or 'activity signal' in neurons (Barish 1998; Golowasch *et al.* 1999a). Moreover, depolarisation-induced calcium influx is known to be involved in the regulation of ion channel expression through trafficking, translation and transcription (Barish 1998). Voltage-gated calcium channels, especially the L-type family, are a natural target for this experiment because calcium influx through these channels in particular is known to regulate gene expression via activation of CREB (cAMP response element binding protein) (Ghosh *et al.* 1994; Deisseroth *et al.* 1998; Mermelstein *et al.* 2000; West *et al.* 2001), a transcription factor that has been directly linked to the regulation of intrinsic excitability in a recent study (Dong *et al.* 2006).

5.8.1. The homeostatic response is influenced by L-type calcium channel activity

Prolonged depolarisation with KCl is likely to elevate the activity of L-type calcium channels. Therefore, if the mechanism responsible for regulating intrinsic excitability is indeed dependent on L-type calcium channel activation, blocking their activation during depolarisation should prevent or diminish the homeostatic response. In addition, selective and potent antagonists of L-type calcium channels – dihydropyridines such as nifedipine and nimodipine (Tsien *et al.* 1988) – are readily available.

In the present experiment, depolarisation was induced (KCl, 15 mM) over a period of 60 hours in the presence and absence of nifedipine (5 μM). Cells were placed in these conditions after being grown in control conditions, at 7 DIV.

Figure 5.9A shows the resulting FI curves measured in (n = 11) control cells compared to cells grown in 15 mM KCl (n = 12), and cells grown in both 15 mM KCl and nifedipine (n = 9) for the 60-hour period before recording. As part of the same experiment, a further control group was recorded from that consisted of cells that were grown in media containing nifedipine, but no additional KCl, over the same period (n = 11).

The cells that were subjected to depolarisation alone exhibit a rightward shift in their FI curve. Current thresholds were 0.5 ± 4.7 pA (control), 53 ± 9 pA (15 mM KCl), 14 ± 6 pA (KCl + nifedipine) and −4.6 ± 1.6 (nifedipine). As observed in the experiments using short depolarisation periods (section 5.6), the control cells were hyper-excitable in some cases, and for the cells treated with nifedipine this was observed in almost all cases. Again, this could be put down to the effect of changing the media completely and recording from the cells before they have time to recover.

In addition, the cells treated with nifedipine during depolarisation exhibited a much smaller shift in current threshold. Comparison with treated cells reveals a statistically significant difference in this threshold ($p = 0.006$, *t*-test with Bonferroni correction), indicating that nifedipine does indeed interfere with the expression of the homeostatic response. The difference in current threshold between control cells and cells treated with nifedipine alone was not significant ($p = 0.46$, *t*-test), nor was the difference in threshold between control cells and depolarised cells that were treated with nifedipine ($p = 0.06$, *t*-test).

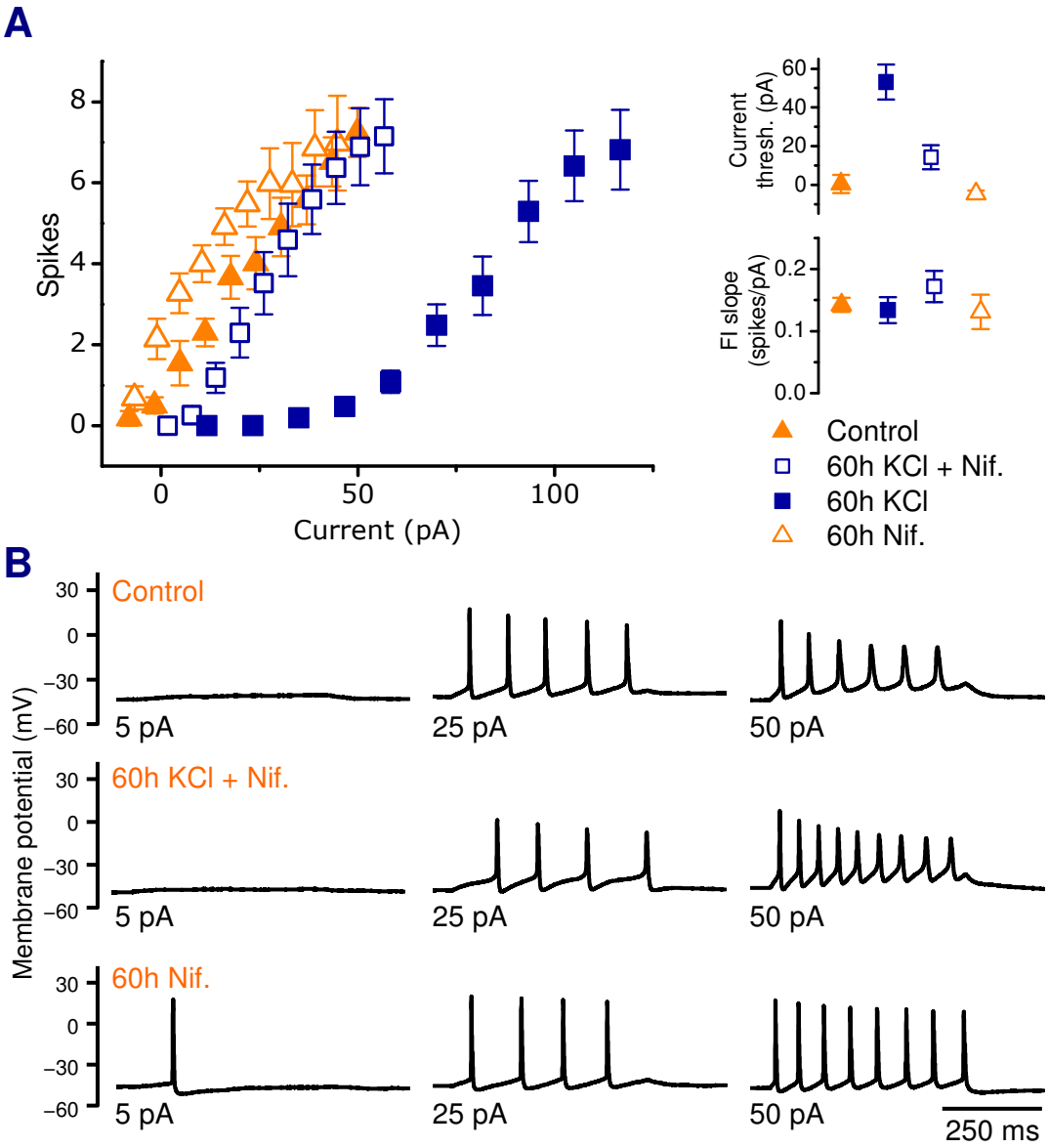

Figure 5.9: Effect of L-type calcium channel activity on regulation of intrinsic excitability

(A) Pooled FI curves for cells grown for 7-8 days in normal media, then 60 hours in fresh media (control, n = 11) or media containing 15 mM KCl (n = 12), 5 µM nifedipine (n = 11) or both (n = 9). All recordings were performed in external solution with normal (3 mM) concentrations of KCl. Linear regression on the non-zero data points provides estimates of the current threshold and slope of the FI curve in each condition (right). **(B)** Example current-clamp traces of three cells recorded at 9 DIV. A 500 ms pulse of current was delivered to the cells at the amplitudes indicated.

5.8.2. Do NMDA receptors influence excitability homeostasis?

If calcium influx does indeed provide a signal for modulating intrinsic properties within a cell, then sources other than L-type calcium channels may also be capable of initiating this response. In neurons, NMDA receptors are important conduits of calcium influx during synaptic activity (Mayer and Westbrook 1987). In addition, the elevated resting potential of the depolarised cells (−24.7 ± 1.6 mV, as measured in the recording chamber) is in the range in which magnesium-block of NMDA receptors begins to decrease: the half-maximal conductance of NMDA receptors is −20 mV for an extracellular Mg concentration of 1 mM (Jahr and Stevens 1990). The concentration of magnesium in the culture media is slightly lower than this reference value, at 812 µM (Brewer *et al.* 1993). Therefore, it is likely that a substantial amount of calcium will enter the cells through NMDA receptors as a result of spontaneous synaptic activity when the extracellular KCl concentration of the culture media is raised to 15 mM.

To see whether NMDA receptor activity influences the modulation of intrinsic excitability, an experiment similar to the previous experiment was conducted, this time using APV (50 µM) to prevent NMDA receptor activation instead of the blocking L-type calcium channels with nifedipine. In contrast to the previous result, APV was found to have no effect on the shift in current threshold caused by depolarisation (15 mM KCl for 60 h). Moreover, no alteration in intrinsic excitability was observed in cells that were incubated with APV for the same period in the absence of KCl-induced depolarisation.

Figure 5.10 shows pooled FI curves for cells subjected to 60 hours of depolarisation and control cells in the presence and absence of APV (50 µM). The mean current threshold in each group was measured to be 1.0 ± 4.7 pA (control, n = 11), 53 ± 9 pA (15 mM KCl, n = 12), 62 ± 8 pA (15 mM KCl + APV, n = 15) and 2.1 ± 3.6 pA (APV only). These values were not significantly different for depolarised groups (p = 0.4, t-test), nor were the values for non-depolarised groups (p = 0.9).

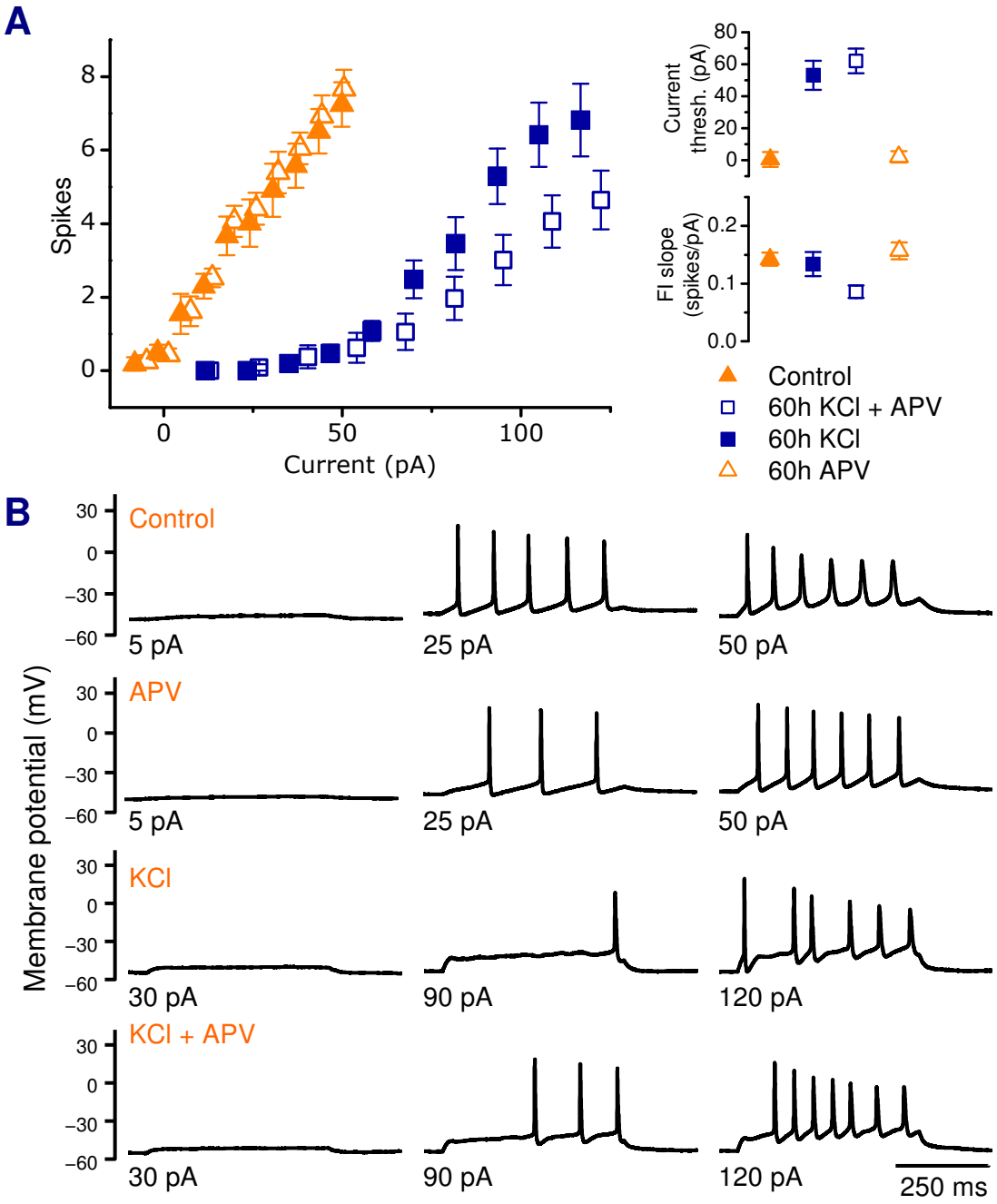

Figure 5.10: Effect of NMDA receptor activity on regulation of intrinsic excitability

(A) Pooled FI curves for cells grown for 7-8 days in normal media, then 60 hours in fresh media (control, n = 11) or media containing 15 mM KCl (n = 12), 5 µM nifedipine (n = 11) or both (n = 9). All recordings were performed in external solution with normal (3 mM) concentrations of KCl. Linear regression on the non-zero data points provides estimates of the current threshold and slope of the FI curve in each condition (RIGHT). **(B)** Example current-clamp traces of three cells recorded at 9 DIV. A 500 ms pulse of current was delivered to the cells at the amplitudes indicated.

5.8.3. Is calcium influx the 'depolarisation sensor?'

Preventing the homeostatic shift by blocking L-type calcium channel activation does not, by itself, constitute irrefutable evidence that calcium influx is part of the mechanism responsible. Two results would strengthen this position: first, establishing that elevating extracellular KCl causes significant calcium influx; second, showing that nifedipine substantially reduces this influx at the concentration used (5 μM).

I addressed this issue using calcium imaging. This technique provides quantitative measures of changes in intracellular calcium concentration at high spatial and temporal resolutions, and is relatively straightforward to perform using the cell cultures in this study.

Cells grown under normal conditions were loaded with a calcium-sensitive dye, Flura-3AM (see Methods, Section 2.6) and imaged for several minutes to establish a basal mean intracellular calcium signal with an external KCl concentration identical to the culture media (5.3 mM). Before attempting to interfere with calcium influx using nifedipine, it is important to establish the time course of the relative fluorescence change resulting from KCl application. Figure 5.11 shows a calcium imaging time-series from a preliminary experiment in which the extracellular concentration of KCl is elevated to 15 mM after a control period. A sharp rise in relative fluorescence occurs in all cells within seconds of solution exchange, this decays exponentially with a time-constant of 1.8 ± 0.4 min.

In order to assess the impact of nifedipine on the steady-state calcium levels inside depolarised cells, it is necessary to allow the calcium levels to reach a plateau before applying nifedipine. Figure 5.12 shows the effect of washing-in nifedipine (5 μM) on the steady-state intracellular calcium levels in 7 cells that are depolarised with KCl (15 mM). When quantified, nifedipine application was found to reduce the plateau to 61 ± 3% of its mean value ($p = 0.002$, Bonferroni-corrected, paired *t*-test). The mean value of the plateau itself, relative to the baseline, is 310 ± 70% ($p = 0.02$).

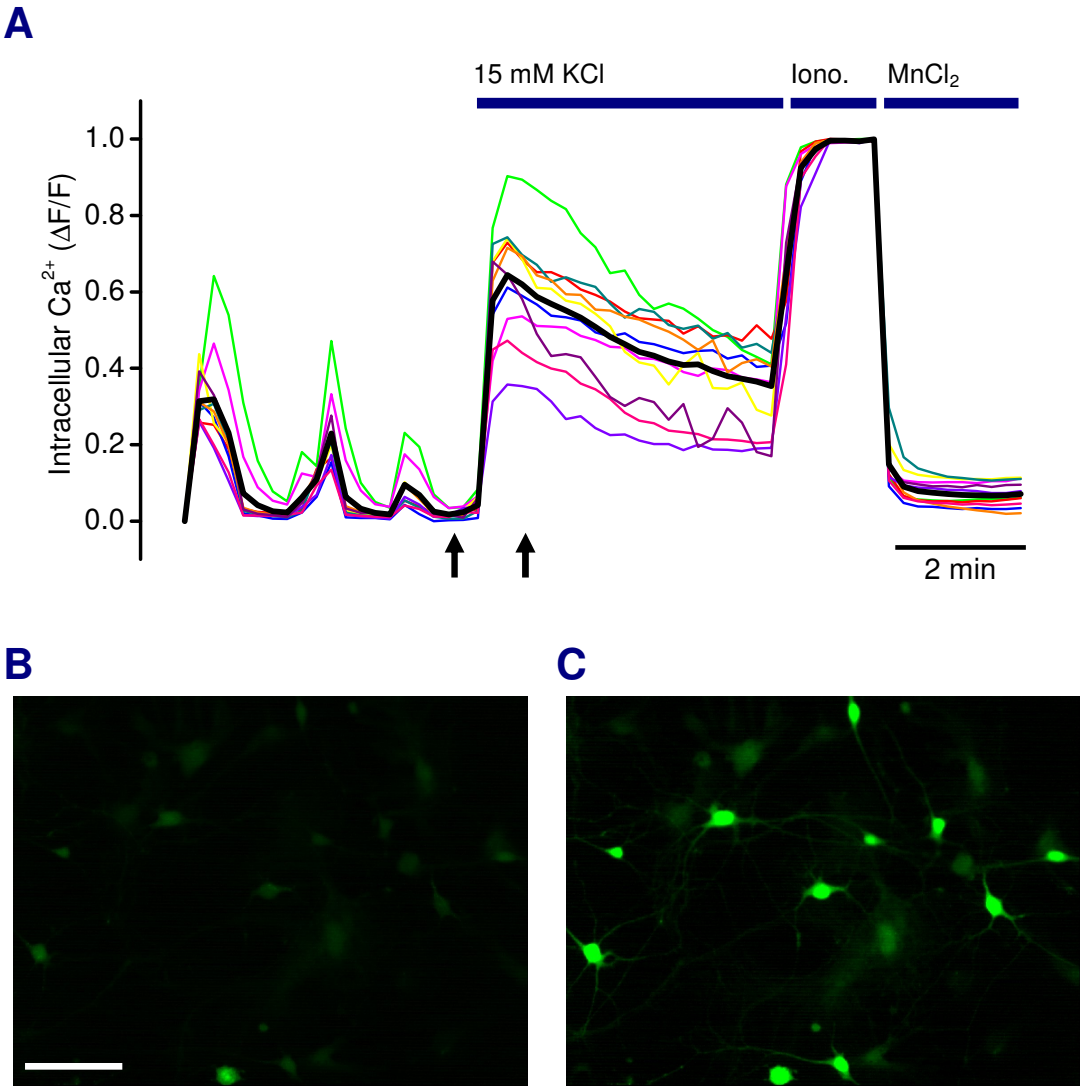

Figure 5.11: Calcium imaging – acute 15 mM KCl application

(A) A calcium imaging experiment performed on cells at 8 DIV. Spontaneous calcium transients are evident in the early part of the recording. Following application of external solution containing KCl (15 mM), the fluorescence levels rise sharply and decay until ionomycin and $MnCl_2$ are applied to ascertain the maximum and minimum fluorescence levels, respectively. Traces for each cell are normalised to the difference between maximum and minimum fluorescence; the mean is plotted with a bold black line. **(B)** Fluorescence imaging of the cells before and **(C)** during calcium influx. Images are selected from the time points in the recording indicated by the black arrows in (A). Scale bar = 100 µm.

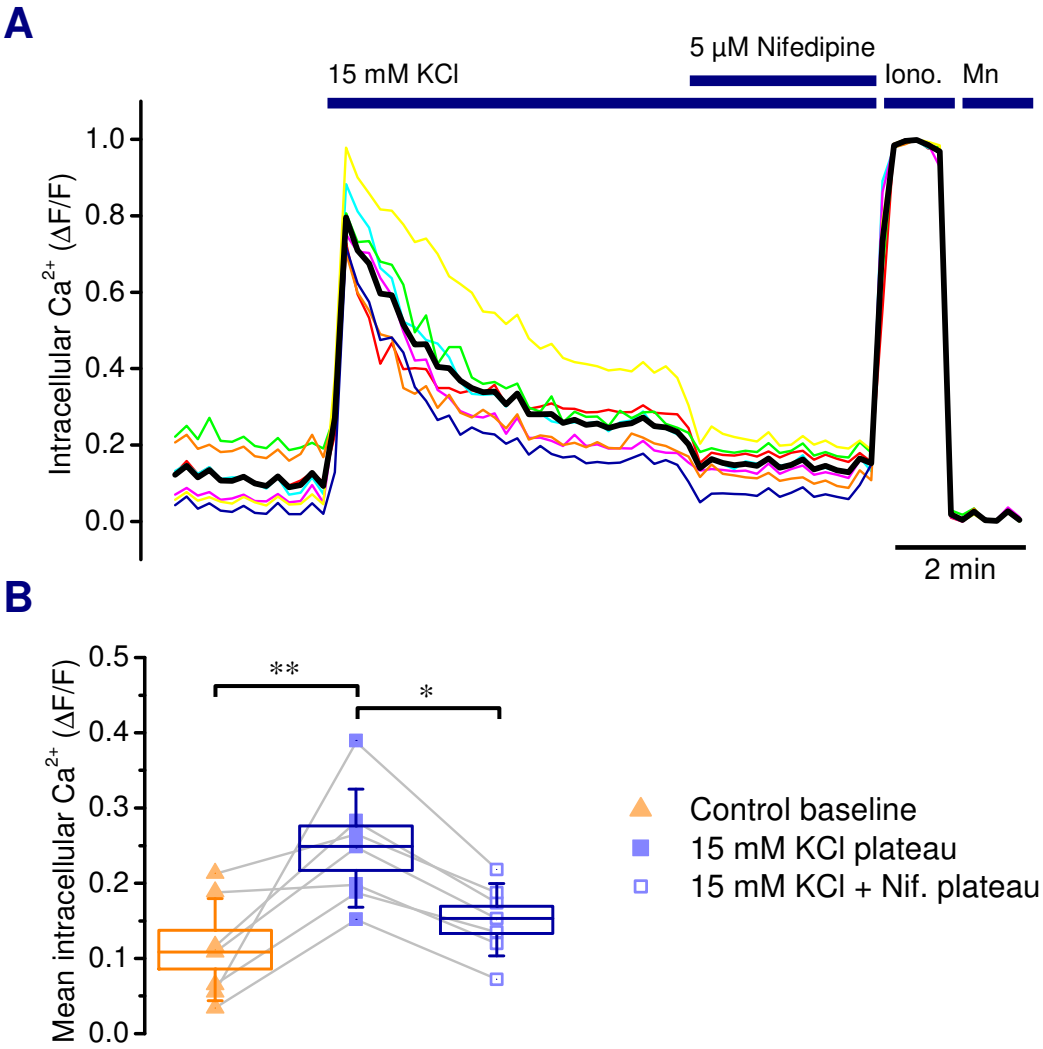

Figure 5.12: Nifedipine lowers steady-state intracellular calcium in presence of 15 mM KCl

(A) Calcium imaging traces for cells at 8 DIV. KCl (15 mM) is applied, causing a rise in intracellular calcium. Once a plateau is reached, nifedipine (5 µM) is co-applied, resulting in a reduction of the steady-state intracellular calcium levels in all 7 cells. The maximum and minimum fluorescence values used to normalise the recordings are obtained by sequentially applying ionomycin and $MnCl_2$. **(B)** Quantification of the steady-state fluorescence during the recording. The values for the control baseline, the KCl plateau and the KCl + nifedipine plateau are averaged over the 1-minute period before the application of each subsequent condition.

5.9. Discussion

The experimental results in this chapter characterise the change in the FI curve of cells that are chronically depolarised with potassium chloride. This depolarisation leads to a rise in the current threshold for eliciting action potentials, and to corresponding changes in the electrophysiological properties, such as input resistance and resting membrane potential, when compared with control cells in the same culture that are not subjected to the same depolarising conditions.

Importantly, the effect proved to be reversible, which is a key property of homeostasis that distinguishes it from *plasticity*. Plastic changes are those that remain stable over time, which is why they are assumed to underlie learning and memory – especially in the case of synaptic plasticity (Bliss and Collingridge 1993; Martin *et al.* 2000). Homeostatic processes, by contrast, are those that continually modify the properties of a system in the face of external perturbations[7]. The timescale over which this modification occurs is not necessarily immediate, indeed, in the case of the current phenomenon the changes in excitability that accompany depolarisation are slow enough to be detected when the cells are placed in non-depolarising recording solution for the purpose of measuring FI curves. Nevertheless, over a period of days the intrinsic excitability of chronically depolarised cells does indeed return to control levels (Figure 5.8)

5.9.1. Quantifying the homeostatic response

Input resistance, resting membrane potential and FI curve slope all changed in a manner consistent with diminished excitability following depolarisation. This change can be triggered by elevations in the external KCl concentration of as little as 5 mM over several days (comparing cells grown in control concentration of 5 mM to those grown in 10 mM KCl, Figure 5.1). Using higher final concentrations (15, 30 mM)

[7] The phrase 'homeostatic plasticity' is used commonly in experimental literature on this subject (for example, see Turrigiano 1999). In this context, 'plasticity' is synonymous with 'the capacity to change'. This is a redundant use of the word because homeostasis, of necessity, entails the capacity to change. Moreover, if we are to be consistent about the meaning of the word 'plasticity' as it is used context of development, and when discussing learning and memory mechanisms, then its meaning contrasts with that of 'homeostasis' in the manner described in the text above. Therefore, 'homeostatic plasticity' is either a tautology or a contradiction. Nervous systems are both plastic and homeostatic; in order to avoid confusion when discussing how homeostasis and plasticity interact, it is helpful to keep the meaning of these words separate.

led to a bigger shift (Figure 5.5), and to measurable changes over a time period less than one day (Figure 5.7).

Current threshold is the best measure of the response to depolarisation in these experiments, both in terms of effect size and consistency of results. Mean FI slope is variable within and between experiments, and suffers from the problem of being awkward to define for cells that do not fire repeatedly in response to sustained depolarising current injection. Some of the treated cells fell into this category, and their inclusion resulted in a lowering of the mean FI slope and a high variability in this value. To exclude them, however, would be arbitrary, and would introduce a bias in the result. Voltage threshold is also problematic as measure of intrinsic excitability in the current study. As described in detail in Methods (Section 2.5.3), the potential difference due to access resistance is proportional to the applied current, and is in series with the path to ground. This leads to an additive error in the measured membrane potential, which is corrected before analysis, but there may nevertheless be a residual, systematic error in this value. It is, however, reassuring that the trend in voltage threshold was weak as KCl-induced depolarisation, and consequently current threshold, were increased by elevating KCl concentration and the duration of treatment (Figure 5.6E). This may indicate that there is in fact no substantial change in this parameter associated with the homeostatic response.

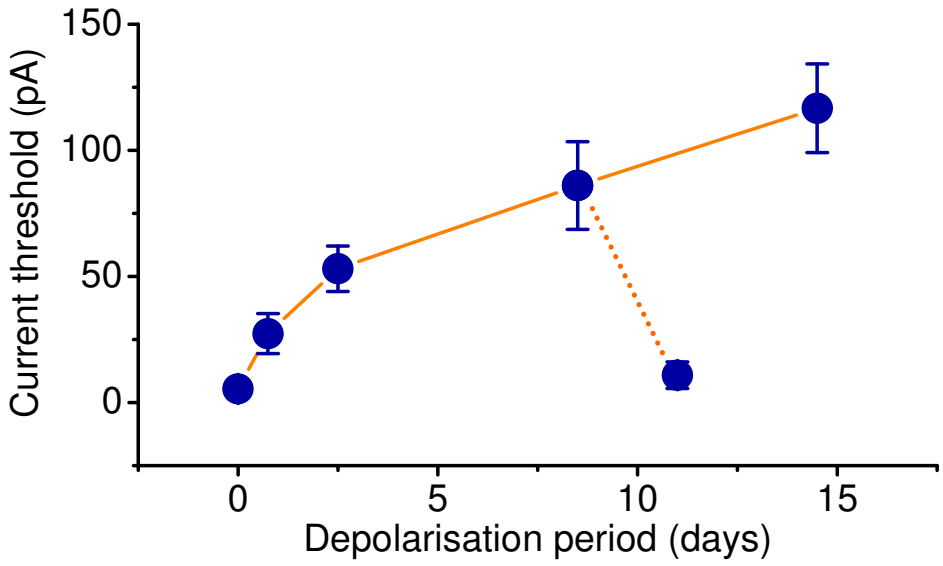

Figure 5.13: Temporal profile of the homeostatic response

Each point in the plot represents the mean current threshold after a given period of depolarisation. The abscissa represents the mean depolarisation period; for example, the data point representing groups that were depolarised for 7-10 days is plotted at 8.5 days. Day 0 corresponds to the value of the current threshold for control cells at 8-11 DIV. The dotted line and adjacent data point represents the result of the recovery experiment (section 5.7), where cells grown for one week in depolarising media were returned to control conditions and recorded from 60 hours later.

A particularly important result in this chapter is the quantification of the temporal dynamics of the homeostatic response. Chronic depolarisation was induced in cells over several different time periods from 12 hours to two weeks. By characterising the intrinsic excitability in terms of current threshold, it is possible map the temporal profile of the effect. This is done for the cells that were depolarised using 15 mM KCl in Figure 5.13. The plot shows the difference between the threshold for control cells at 8-11 DIV and treated cells at each time-point during the depolarisation period.

Timescales shorter than 12-24 hours were not investigated. Assuming that the effect remains proportional to duration of depolarisation for briefer periods, one would anticipate a still smaller shift of the FI curve in this case. Such a small shift would

require many more recordings to detect, and would be unlikely to reveal anything new about the phenomenon.

Interestingly, the profile of the effect has a high initial rate of change which reduces to a slower, steady rate after two days. Two explanations may account for this. First, suppose the cells have a pre-determined 'target' membrane potential that they achieve by modulating their intrinsic properties, and that the rate at which these properties are altered at any given time is proportional to the discrepancy between their current membrane potential and the target membrane potential. If such a process were at work, the mean membrane potential in chronically depolarised cells should become more hyperpolarised with time and the response of chronically depolarised cells to acute KCl administration, as quantified by the level of depolarisation induced, should be diminished. Both of these effects are indeed observed: resting membrane potential hyperpolarises as KCl concentration and treatment duration are increased (Figure 5.6D); similarly, the response of treated cells to acutely-applied KCl is diminished when compared to control cells (Figure 5.4). So a gradual repolarisaton of the membrane potential in the cells that are being treated with KCl may in turn reduce the rate at which the cell continues to modify its excitability, leading to a slowing in the rate of change of current threshold as observed in Figure 5.13.

A second explanation is that the decrease in rate may be a consequence of metabolic load. The cellular resources available for homeostasis might begin to saturate after two days of continuous depolarisation, resulting in a slowing of the change in magnitude of the effect. This might, for example, be due to limits in the amount of ion channel protein the cells can express, or due to additional demand placed on trafficking and regulatory mechanisms involved in ion channel expression.

It is difficult to conceive of an experiment that would distinguish between these two possibilities. Elevating the KCl concentration of chronically depolarised cells for a further period would, perhaps, offer some insight. A sustained high rate of change in response to stronger depolarisation at this stage would favour the former scenario, whilst a robust tailing-off of the rate would suggest that the cells are physically incapable of adjusting to the additional demand, favouring the second. Of course,

both explanations may be equally valid. Either way, a detailed dissection of the underlying biochemistry and gene regulation is undoubtedly a priority for any further work on this phenomenon; suggestions for future experiments are offered later on in this discussion.

Another interesting result captured in Figure 5.13 is the time taken for the cells to return to a state comparable to control. When quantified in terms of the current threshold, an almost complete recovery from the cumulative effect of one week in depolarising conditions is seen to occur in just 60 hours. This discrepancy in timescales could be explained by postulating a mechanism for expression of the effect that involves changes in the expression of leak channels in the membrane. Following prolonged depolarisation, the increase in current threshold is closely predicted by the increase in input resistance (Figure 5.3). The reduction in input resistance is likely to be caused by increased membrane conductance, which is in turn the result of higher ion channel expression in the treated cells. Presumably, expressing additional channels takes longer than the sequestration and degradation of surplus channels. Hence, treated cells are able to regain their original electrophysiological properties more quickly than they can alter them to cope with chronic depolarisation.

5.9.2. Toward a mechanism

Some clues as to the underlying biochemical signalling mechanisms responsible for the modulation of excitability are provided by the experiments where nifedipine was included in the culture medium during the depolarisation period (Figure 5.9). Evidently, nifedipine counters the homeostatic response to depolarisation in this experiment. The shift in excitability was almost entirely blocked over the 60-hour depolarisation period, suggesting that calcium influx through L-type calcium channels is an essential component of the signalling pathway. In fact, nifedipine alone was capable of enhancing neuronal excitability over this time-course. This may be due to the fact that basal L-type calcium influx is present in control conditions, so a further reduction in L-type activity induces the same type of changes in excitability, relative to control values.

KCl-induced polarisation has been known to induce calcium influx ever since calcium imaging methods emerged (Barish 1991; Barish and Mansdorf 1991; Collins *et al.* 1991). Nevertheless, it was important to verify that the level of depolarisation induced here is also capable of inducing calcium influx, and that the plateau concentration of intracellular calcium is, in fact, reduced by the application of nifedipine. This verification is provided in the calcium imaging experiments in this chapter (Figure 5.11, Figure 5.12).

As mentioned in section 5.4, it is unwise to consider the acute effect of KCl application observed in the recording chamber at room temperature to be precisely the same as what occurs under culture conditions at 37 ºC. This is also true of the calcium imaging experiments. However, for the purpose of comparing the responses between control cells and treated cells, and for verifying the effect of nifedipine on calcium influx, these experiments suffice. If appropriate equipment were available, it would be enlightening to perform these experiments under identical conditions to those in the incubator. Although a precise picture of cytosolic calcium dynamics is lacking in the present study, it is reasonable to assume that elevated extracellular potassium leads to sustained increases in intracellular calcium over the time period that the changes in intrinsic excitability are observed to occur.

In other studies, such depolarisation-induced calcium influx has been found to activate numerous biochemical pathways in neurons, leading to enhanced survival (Lasher and Zagon 1972; Gallo *et al.* 1987; Collins *et al.* 1991; Moulder *et al.* 2003) and changes in ion channel subunit expression, as evinced by alterations in mRNA and protein levels (Delorme and McGee 1986; Offord and Catterall 1989). It would be interesting to continue the present study by examining ion channel subunit expression using similar biochemical methods, as this would provide direct test of the hypothesis that changes in ion channel expression underlie the phenomena observed in this chapter. Such an approach might also be useful in determining further details of the regulatory signalling pathways underlying the homeostatic response. In particular, it would be interesting to examine whether transcription factors that control gene expression such as CREB are part of this mechanism, especially in light of the evidence that links calcium influx through L-type calcium

channels to CREB activation (Ghosh *et al.* 1994; Mermelstein *et al.* 2000), and the evidence which, in turn, links CREB activity to changes in intrinsic excitability (Dong *et al.* 2006).

5.9.3. Interpretation: the need for homeostasis

It is of fundamental importance for neurons to maintain their mean resting potential at a particular value; for mature neurons this usually in the range −70 to −50 mV. There are several reasons why sustained deviations outside this range are undesirable. Most obviously, the voltage gated conductances that endow neurons with excitable properties are tuned to operate close to this range of membrane potentials. Many subtypes of voltage-gated sodium channels, potassium channels and calcium channels begin to activate at potentials above −50 mV (Hille 2001). Channels that remain active in response to prolonged depolarisation could contribute to a deleterious imbalance in the ionic composition of the cytosol. Excessive intracellular calcium, in particular, leads to cell death over time (Schlaepfer and Bunge 1973; Choi 1988).

In fact, this need to regulate membrane potential is common to all cell types and species. Many metabolic pathways are dependent on a steady membrane potential, and deviations are often important for regulating cellular processes such as mitosis in smooth muscle (Platoshyn *et al.* 2000), nodulation in plant roots (Ehrhardt *et al.* 1992) and oocyte fertilization in sea urchins (McCulloh *et al.* 1987). So it would be anticipated that mechanisms exist to alter the biophysical properties of both neuronal and non-neuronal cells, should they need to compensate for environmentally-imposed perturbations in their membrane potential.

For example, sustained activation resulting from membrane potential depolarisation would lead to inactivation of many types of channels – most conspicuously, sodium channels. In the short term, such inactivation is part of the normal neuronal function, but longer-lasting changes that are associated with prolonged depolarisation are likely to lead to pathological conditions. Indeed, cortical spreading depression (CSD) is an example of a pathological drop in neural activity that is linked to elevations in extracellular potassium (Bures *et al.* 1984; Busch *et al.* 1996). An initial elevation in

extracellular potassium, caused, for example, by trauma or hypoxia, which depolarises neighbouring cells and induces further potassium efflux. This positive-feedback mechanism is believed to underlie the 'spreading' aspect of this condition and lead to sustained, potassium-induced depolarisation not-unlike the kind studied here. However, the mechanism of CSD in the intact nervous system is complex, an unlikely to be due to a single, simple mechanism such as ion channel inactivation (Somjen 2001).

Fortunately, such pathological phenomena are normally prevented in the in the intact, healthy CNS. For example, extracellular potassium is buffered, mainly by astrocytes (Kofuji and Newman 2004), which counteracts the fluctuations in extracellular potassium that occur during neuronal activity. It is also likely that the various intrinsic forms of homeostasis that regulate activity within neurons have evolved to promote cell health in response to the increasing complexity of the mammalian CNS, and the risk of instabilities in activity levels that such a system carries. The type of excitability regulation characterised in this chapter may therefore offer insight into the pathology of conditions like CSD, particularly if mechanisms can be identified within the cells that are crucial for controlling the homeostatic response. Perhaps impairments in these mechanisms lead to a predisposition toward, or a heightened sensitivity to, pathological states associated with intrinsic excitability.

As has been discussed in the introductory chapter, the need to regulate excitability goes beyond maintaining cell health in the case of neurons. The excitable properties of neurons are highly specialised so that their membrane potential can be used as a means of processing information. If these properties are not maintained in an appropriate regime for integrating synaptic input and generating action potentials, the nervous system as a whole would cease to function properly (Davis and Bezprozvanny 2001; Turrigiano and Nelson 2004; Marder and Goaillard 2006).

It would be surprising, therefore, if the hippocampal neurons examined here did not respond to chronic depolarisation by somehow altering their intrinsic properties. Nevertheless, until recently, relatively little research had been done on homeostatic modulation of intrinsic excitability (Davis 2006), and the particular phenomenon described here has not been previously documented.

5.9.4. Beyond the present study: further characterisation of the phenomenon of excitability homeostasis

There are many ways in which the characterisation work in this chapter could be extended as part of a further study. For example, it remains to be seen if the kind of changes induced by depolarisation with KCl can be induced with other types of stimuli. In the introduction to this thesis, several studies were mentioned which characterised responses to artificial stimulation (Golowasch *et al.* 1999a) and enhanced neurotransmitter release (van Welie *et al.* 2004). It would be interesting to carry out a comparative study with the culture system used here by elevating activity using a multi-electrode array, or similar device for inducing spiking in the cells over extended periods.

It would also be interesting to see if the type of homeostasis observed here interacts with synaptic plasticity, or intrinsic plasticity. For example, one might anticipate a change in the degree to which synaptic LTP or LTD can be induced would be affected by chronic depolarisation. A purely homeostatic hypothesis would predict diminished LTP and/or enhanced LTD in cells that have been depolarised (Turrigiano and Nelson 2000; Turrigiano 2007). Likewise, acute forms of intrinsic plasticity (such as that reported by Cudmore and Turrigiano 2004) might exhibit changes in expression when coupled with long-term, homeostatic changes in intrinsic excitability. For such work to be fruitful, experiments would require reliable protocols for inducing plasticity, and there may be problems interpreting results if the changes in intrinsic properties of depolarised cells *per se* interfere with synaptic and intrinsic plasticity mechanisms.

Computational studies that implement homeostatic mechanisms for controlling excitability, either by modulating membrane conductances (LeMasson *et al.* 1993; Stemmler and Koch 1999), or by modulating parameters that govern excitability in more abstract, rate-based models (Triesch 2005), assume quantitative relationships between the level of activity and the rate of change of parameters determining excitability. The ability to study the temporal dynamics of excitability homeostasis that is afforded in the present work could be exploited further to test the applicability of these models, or to derive empirical relationships for more biologically plausible

models. It is quite possible to use data as it is presented in Figure 5.13 for the latter purpose, but additional experiments at finer time-points would be relatively easy to conduct, and would greatly enhance the applicability of the data to computational work.

Although there are many ways in which the phenomenological aspect of excitability homeostasis can be explored, a more immediate, mechanistic issue is the question of which membrane conductances underlie the changes observed in this chapter. The next chapter deals with this question by systematically characterising several major active and passive membrane conductance types in control cells and cells that have been chronically depolarised according to the protocols used in the current chapter.

Chapter 6. Changes in membrane conductances following prolonged depolarisation

6.1. Chapter summary and key findings

1. Leak conductance is increased in chronically depolarised cells. The slope conductance in treated cells (15 mM KCl, 8-11 DIV) is two-fold steeper at reversal potential compared to control. Reversal potential of the leak conductance is hyperpolarised in trated cells relative to control: −49.1 ± 1.9 mV (control) and −56.3 ± 2.2 mV (treated).

2. Voltage-gated sodium currents are reduced in treated cells. The peak amplitude of evoked current is −3777 ± 321 pA for control and −1537 ± 190 pA for treated cells.

3. Voltage-gated potassium currents are not significantly altered by chronic depolarisation. Peak control and treated amplitudes for total evoked potassium current, and current sensitive to millimolar concentrations of 4-AP and TEA were not significantly different between groups.

4. Voltage-gated calcium currents are diminished in chronically depolarised cells. Peak amplitudes of evoked currents are 550 ± 50 pA (control) and 270 ± 45 pA (treated). FI curves recorded in the presence and absence of cadmium (200 μM) indicates that calcium currents do not affect current threshold.

5. Action potential waveform is altered in chronically depolarised cells. Mean evoked action potentials in treated cells exhibited an enhanced after-hyperpolarisation (AHP) and spike width compared to control cells. Mean AHPs are: 2.7 ± 0.2 mV (control) and 1.8 ± 0.1 mV (treated); whilst spike widths are: 2.7 ± 0.2 ms (control) and 1.8 ± 0.1 ms (treated).

6.2. Introduction

The previous chapter provided a detailed characterisation of how the intrinsic properties of neurons respond to chronic depolarisation. As it stands, this characterisation is largely phenomenological. In other words, the phenomena are described in detail, but the underlying causes remain obscure. There are, however, important clues which assist in making educated guesses as to what the underlying causes might be. Input resistance, for instance, reduced in response to depolarisation which suggests an increase in the sub-threshold membrane conductance of the cells.

This chapter characterises the membrane conductances that underlie the altered excitability of chronically depolarised cells. Exhaustively identifying and measuring all of the types of membrane conductances in the cells would present a bewilderingly difficult, if not impossible task. Several reasons account for this. Foremost among these is the diversity of ion channels that are known to be expressed in mammalian neurons, and in hippocampal neurons in particular (Magee *et al.* 1998). Secondly, pharmacological agents which allow dissection of the individual currents are only available for a subset of these channels. Third, the presence of many channels is specific to neuronal subtypes. Although care is taken to record from morphologically similar cells in this study, this measure only offers a very crude control over cell type – particularly in a system such as a dissociated culture. Finally, for the sake of pragmatism, it makes sense to look at conductances that are known to impact excitability most directly: fast voltage-gated sodium conductances, leak conductances and voltage-gated potassium conductances are ubiquitous in neurons across species, and their role in excitability is well-understood.

Therefore, the work in this chapter focuses on several key conductances, defined pharmacologically and by their voltage dependence. It should be noted, however, that membrane current due to each of these groups of conductances is probably mediated by numerous channel subtypes due to the similarity in their biophysical properties and in their sensitivity to the pharmacological compounds used, especially in the case of potassium channels (Coetzee *et al.* 1999; Hille 2001).

Several studies have characterised intrinsic excitability in ways similar to the work

presented here and examined the conductances which influence excitability at the same time (Turrigiano *et al.* 1995; Desai *et al.* 1999b; Aizenman *et al.* 2003a; van Welie *et al.* 2006); these studies serve as guides for the task ahead. Particularly relevant among these is the work of Desai *et al.* (1999b) which investigates membrane conductances in cultured cortical pyramidal cells following TTX-induced activity deprivation. The phenomenon described by Desai *et al.* (1999b) is a 'converse' to that being studied here, inasmuch as it examines the long-term effects of depriving cells of sources of depolarisation. Their approach to classifying voltage-gated conductances, including the protocols used for measuring them, is closely followed in this chapter.

Cells grown in two experimental conditions are used in all the experiments in what follows. The 'treatment group', as it will be referred to, consists of cells that are grown in 15 mM KCl-containing media from 1 DIV onwards. A control group for each experiment is provided using cells grown at the same time and from the same culture as the treated cells, using normal culture media. All recordings are performed at 8-11 DIV.

6.3. Linear sub-threshold conductance

Chronic depolarisation causes changes in input resistance which largely explain the accompanying changes in current threshold (Figure 5.3). Membrane conductances that contribute to input resistance are therefore important for understanding the effect. The linear sub-threshold conductance, or leak conductance, has a strong influence on input resistance (Rall and Rinzel 1973). This prompts the question as to whether KCl-treated cells exhibit any systematic differences in their leak conductance when compared with control cells.

To address this question, a group of control cells (n = 11), and treated cells (n = 11) were placed in voltage-clamp, and subjected to 500 ms–long step potentials in the range −80 to −40 mV. Example traces from this protocol are shown in Figure 6.1A. The mean steady holding current at each of these potentials, measured over the middle 250 ms-portion of each step, is plotted in Figure 6.1B for both groups.

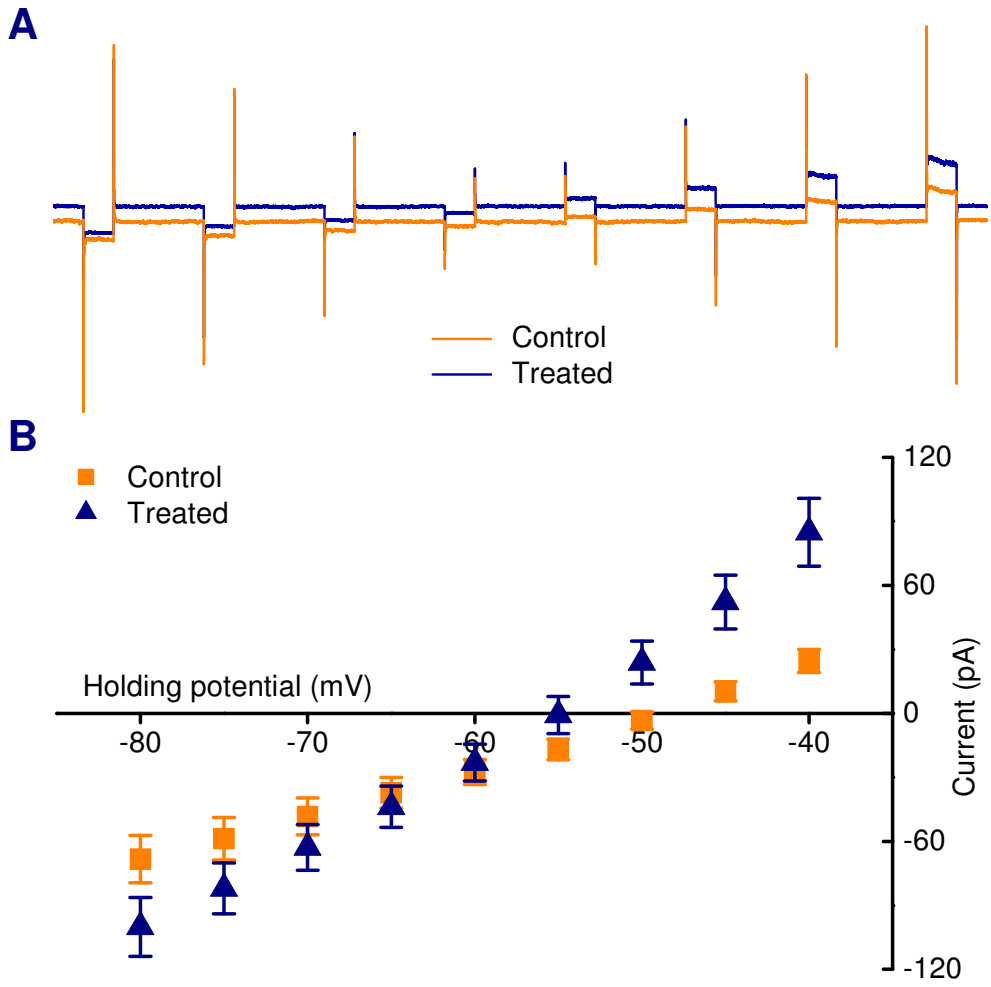

Figure 6.1: Linear IV characteristics

(A) Example current traces from control and 15 mM KCl-treated cells recorded at 10 DIV. Each cell is stimulated in voltage-clamp with 500 ms voltage steps in the range –80 to –40 mV, in 5 mV intervals. **(B)** Pooled mean IV characteristics for control (n = 11) and treated (n = 11) cells. For each cell, the steady current is averaged over the middle 250 ms of each 500 ms voltage step to exclude capacitive current. Mean access resistance values for both groups were not statistically significantly different (control: 28.4 ± 1.3 MΩ, treated: 29.3 ± 1.2 MΩ; $p = 0.6$, *t*-test).

A clear difference in slope conductance and leak reversal potential is evident between groups, both of which have an approximately linear IV characteristic over the range of holding potentials examined. When quantified using linear regression, the mean slope, or membrane conductance is 2.30 ± 0.33 nS for control (n = 11) and 4.53 ± 0.38 nS for treated cells (n = 11, $p = 1\times10^{-5}$, two-tailed *t*-test). For a fixed channel density, membrane conductance is proportional to membrane surface area. To control for possible differences in surface area between conditions, the slope conductances were normalised to cell capacitance. This did not affect the significance of the result, statistically ($p = 1\times10^{-7}$). The reversal potential of the leak is also significantly different between groups:−49.1 ± 1.9 mV (control) and −56.3 ± 2.2 mV (treated, $p = 4\times10^{-6}$, *t*-test).

Leak current is largely mediated by potassium channels (Hille 2001). A proportion of potassium leak channels are blocked by extracellular barium ions, including some members of the subfamily of two-pore domain channels, (Coetzee *et al.* 1999; Patel and Honore 2001). To isolate the barium-sensitive component of the conductance, the cells in both groups were subjected to the same voltage step protocol in extracellular solution containing 1 mM $BaCl_2$. The resulting IV plots, and the residual barium-sensitive component are shown in Figure 6.2.

As with the total leak conductance, a significant difference in the barium-sensitive current is evident between conditions over the range of membrane potentials tested. Absolute slope conductances was found to be 350 ± 70 pS and 930 ± 110 pS for control and treated cells, respectively ($p = 3\times10^{-4}$). This difference remains statistically significant when the conductance estimates are normalised to cell capacitance ($p = 7\times10^{-4}$). This result suggests that among the channels responsible for leak current, barium-sensitive channels, which are potassium channels, are upregulated in chronically depolarised neurons. Consistent with this is the depolarising shift in leak reversal potential caused by the application of $BaCl_2$: +4.0 ± 0.9 mV (control, $p = 5\times10^{-4}$) and +4.4 ± 0.4 mV (treated, $p = 6\times10^{-7}$, paired *t*-test).

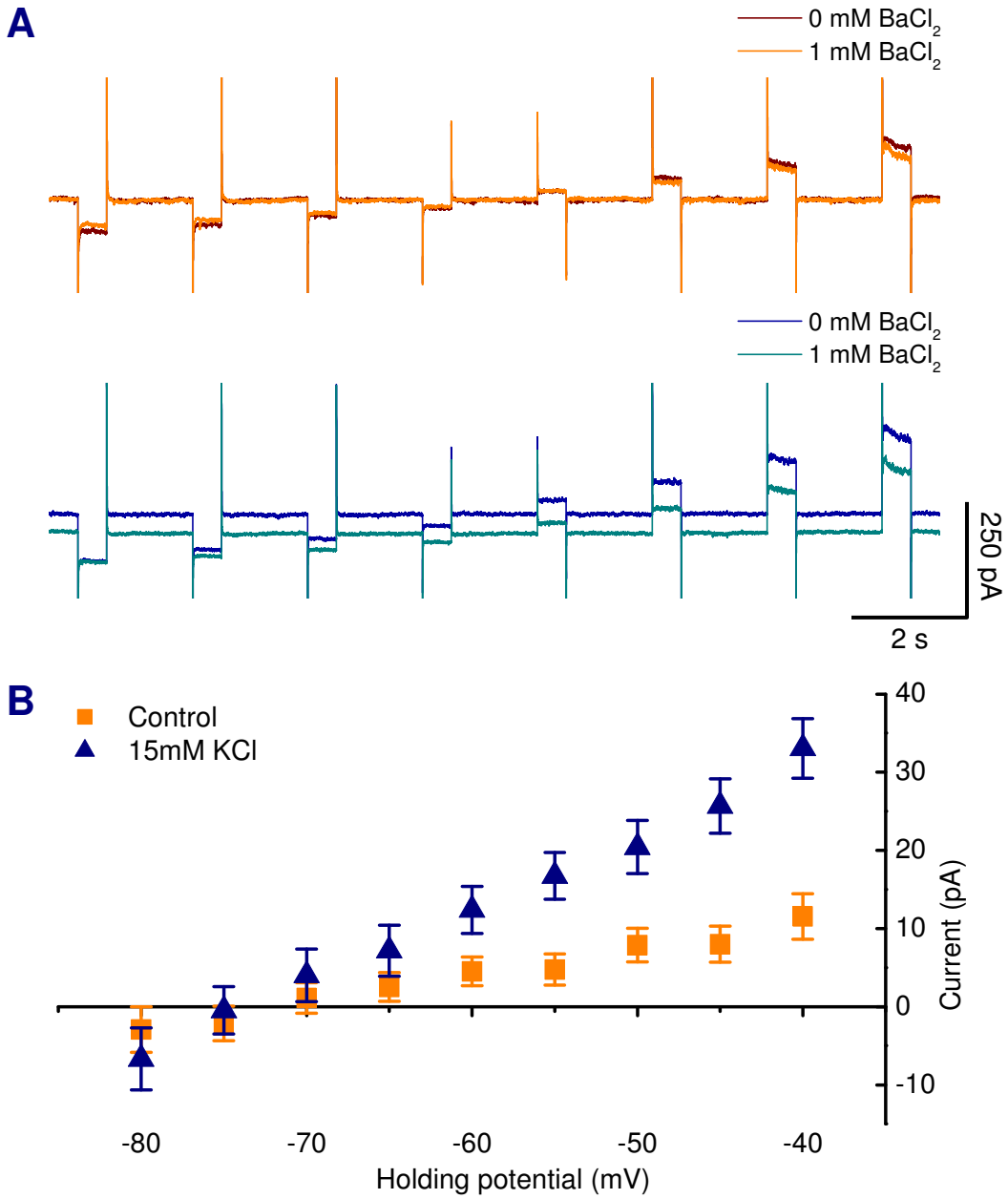

Figure 6.2: Barium–sensitive current

(A) Example current traces in a 10 DIV control cell (top) and a 15 mM KCl-treated cell (bottom), each recorded in the absence and presence of 1 mM $BaCl_2$. Both cells are stimulated in voltage clamp with 500 ms voltage steps in the range –80 to –40 mV, in 5 mV intervals. For illustrative purposes the capacitive transient is truncated in the traces shown. **(B)** Pooled barium-sensitive IV curves for control (n = 11) and KCl-treated cells (n = 11), obtained by subtracting currents recorded in the presence of 1 mM $BaCl_2$ from those recorded in the absence of $BaCl_2$. Mean access resistance values for both groups were not statistically significantly different (control: 29.0 ± 1.2 MΩ, treated: 29.3 ± 1.4 MΩ; p = 0.6, *t*-test).

6.4. Potassium reversal potential and $GABA_B$-receptor activated potassium current

The barium-sensitive component of the leak current should mainly be mediated by potassium channels. The estimated reversal potential of this component was, however, markedly different from the Nernst equilibrium potential calculated for potassium based on the intracellular and extracellular recording solutions (barium component reversal potential is −71.0 ± 4.2 mV, correcting for the liquid junction potential gives a value of −83.4 ± 4.2 mV; the Nernst potential for potassium is −97.1 mV (Methods)). This discrepancy may be due to the signal-to-noise ratio of the relatively low-amplitude barium-sensitive current, so an alternative method of measuring the reversal potential was employed to resolve the issue in treated and control cells.

$GABA_B$ receptors are expressed in hippocampal neurons, particularly CA3 pyramidal cells, and are G-protein-coupled receptors that activate inwardly-rectifying potassium channels in the cell membrane (Gahwiler and Brown 1985; Sodickson and Bean 1996). Using the $GABA_B$-specific agonist, (-)β-chlorophenyl-GABA (baclofen) (Bowery *et al.* 1980), and voltage ramps in the range −120 to −60 mV, the $GABA_B$ receptor-induced current was isolated in both control and treated cells. Recordings were performed in the presence of $CdCl_2$ (200 μM) and TTX (1 μM) to block calcium and sodium currents.

For each cell, the presence of a baclofen-activated current was verified by holding the cell in voltage-clamp at −60 mV and applying the agonist after a control period of 30 seconds. Figure 6.3A shows example traces with clear deflections in the holding current upon baclofen (50 μM) application, indicating that $GABA_B$ receptor-activated currents are indeed expressed in both control and treated cells. The full duration of the induced current was not determined, but found to be in excess of 5 minutes, which is longer than the duration of the voltage ramp experiments.

After verifying the presence of $GABA_B$ receptor-induced current, ten 1 second-long voltage ramps between membrane potentials of −130 and −40 mV were imposed on (n = 9) control cells and (n = 10) treated cells in the presence and absence of baclofen (50 μM). In order to isolate the baclofen-induced potassium current, current

traces that were obtained in the absence of baclofen were subtracted from the current recorded in its presence over the −120 to −60 mV-portion of the recordings, to excluded capacitive current and unwanted voltage-gated currents. The resulting traces, pooled across control and treated cells, are shown in Figure 6.3B.

The slope conductance of the baclofen-induced current is not significantly different between control and treated groups (control: 1.1 ± 0.2 nS; treated 0.9 ± 0.2 nS; p = 0.52, *t*-test). Normalising the conductance estimates to cell capacitance did not affect this result (p = 0.34). The reversal potential of this current is estimated to be −81 ± 2 mV for control cells and −91 ± 3 mV for treated cells. When corrected for the liquid junction potential, these values are −93.3 mV and −103.3 mV, which are both close to the Nernst value (−97.1 mV). Surprisingly, the difference between control and treated cells is statistically significant (p = 0.016, *t*-test), suggesting that the potassium reversal potential may be different between groups despite the fact that internal and external recording solutions are identical for both. This might indicate that dialysis of the cells with internal solution is not complete in these experiments, or that potassium ion transport and buffering is sufficiently altered between conditions to cause a systematic difference in internal concentration, and a detectable difference in reversal potential in spite of the influence of the internal recording solution.

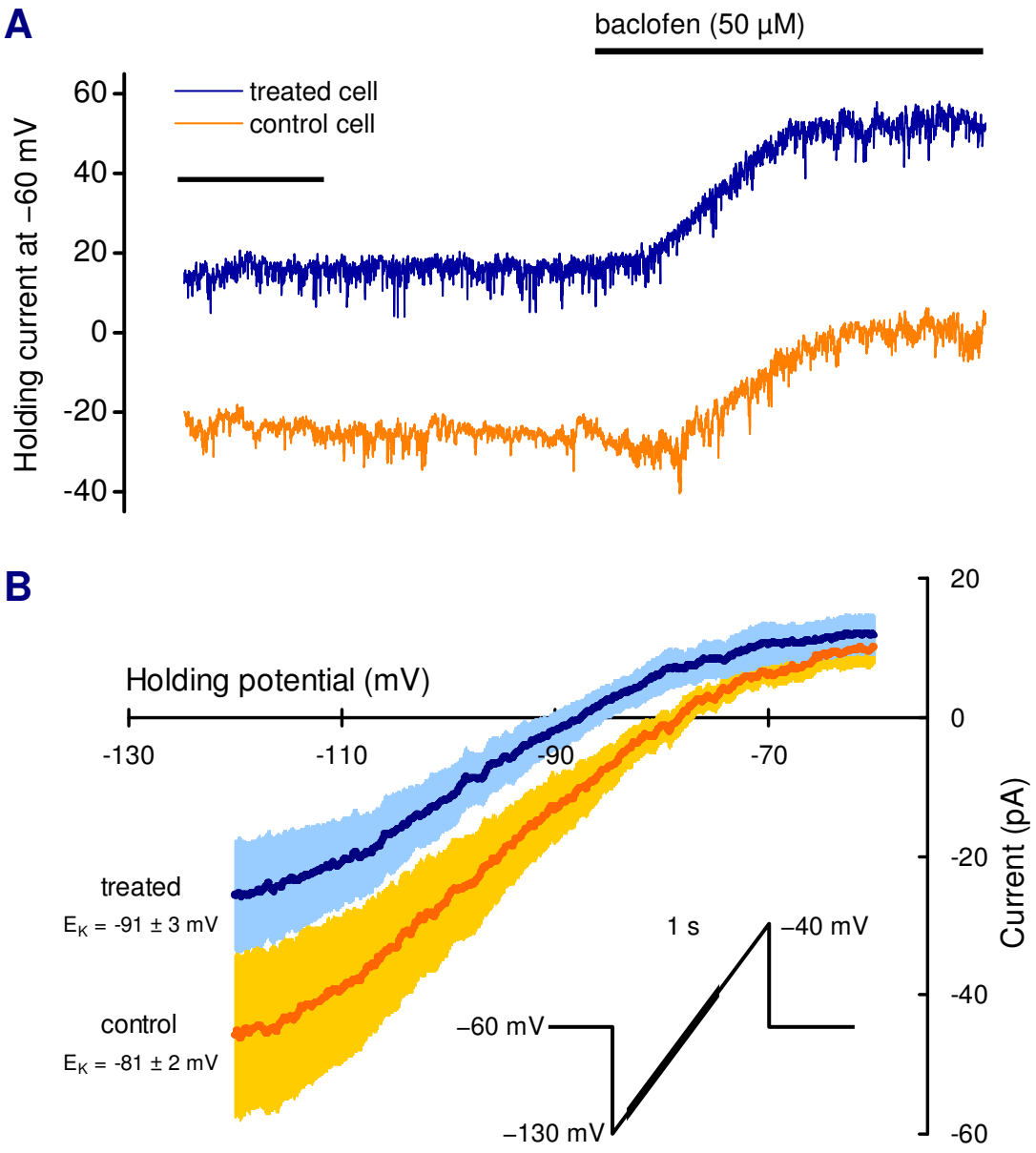

Figure 6.3: Baclofen-induced current

(A) Example voltage-clamp traces of baclofen (50 µM) application in control and treated cells, holding at a potential of –60 mV. **(B)** Mean baclofen-induced current in control (n = 9) and treated (n = 10) cells, averaged over 10 membrane potential sweeps between –120 and –60 mV. The shaded region above and below the traces indicates SEM. **(B, Inset)** Each voltage sweep consists of a 1 s-long voltage ramp from –130 to –40 mV. The subset of potentials for which the current in the presence of baclofen is subtracted from current in its absence, to obtain the baclofen-induced current, is indicated in bold. Mean access resistance values for both groups were not statistically significantly different (control: 29.7 ± 1.9 MΩ, treated: 27.8 ± 2.5 MΩ; $p = 0.5$, *t*-test).

6.5. Sodium currents

Fast action potential generation in neurons is dependent on inward current through voltage-gated sodium channels. Changes in the expression of these channels would therefore have a strong influence on excitability. To examine whether voltage-gated sodium conductances participate in the phenomena characterised here, cells were recorded in voltage-clamp at −80 mV and subjected to a family of voltage steps in the range −60 to +30 mV to invoke sodium currents (Figure 6.4). The intracellular solution used in these experiments was caesium-based (see Methods) to reduce outward current mediated by potassium channels. Synaptic currents were blocked using CPA and voltage-gated calcium currents were blocked with 200 µM $CdCl_2$.

Figure 6.4A shows raw current traces from a control cell. A fast inward current is evident in the traces once a command potential of at least −30 mV is applied. TTX (1 µM) abolishes these currents, establishing their identity as voltage-gated sodium currents (Figure 6.4B). Pointwise subtraction of the TTX traces from the control traces reveals the sodium current in the absence of the capacitive, leak and other voltage-dependent currents that are otherwise present (Figure 6.4C).

As in the previous experiment, control cells (n = 17) were compared with cells grown in 15 mM KCl (n = 15). Example traces from each group are shown in Figure 6.4C. The mean amplitude of evoked sodium current is plotted for each step potential, revealing the activation profile for each group Figure 6.5A. Peak current amplitude is significantly different between groups: −3777 ± 321 pA for control and −1537 ± 190 pA for treated cells, ($p = 2\times10^{-5}$, *t*-test). Apart from this, the two groups have very similar activation profiles with peak evoked current occurring at a command potential of −30 mV in each case. No persistent component to the sodium current was observed in any of the cells recorded.

To control for membrane surface area, and to obtain an estimate of the relative differences in current density between groups, the evoked current amplitudes are normalised to cell capacitance (Figure 6.5B). Upon normalisation, the relative difference in peak amplitude between the groups remains statistically significant ($p = 3.5\times10^{-3}$, *t*-test).

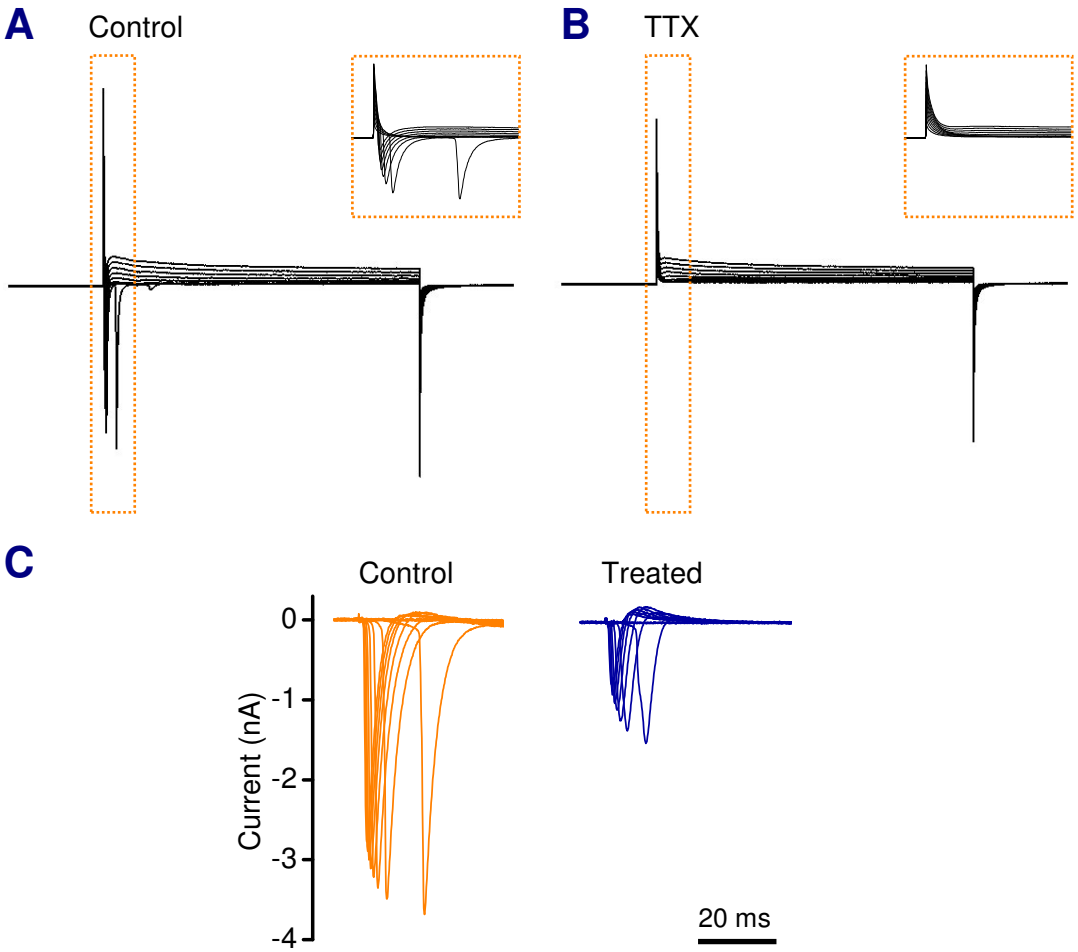

Figure 6.4: Voltage-gated sodium currents

(A) Current traces in a 9 DIV control cell showing evoked currents due to 500 ms voltage steps to potentials in the range –60 to +30 mV from a holding potential of –80 mV. The extracellular recording solution contained 200 µM CdCl2 and CPA and a caesium-based internal solution was used to block potassium channels. **(B)** Current traces from the same cell as in (A), but in the presence of 1 µM tetrodotoxin (TTX). (A, B Insets) Detail of a 75 ms, 8 nA region the recordings showing clear inward currents in (A) that are absent in (B). **(C)** Voltage-gated, TTX-sensitive sodium current traces obtained by subtracting recordings in the presence of TTX from control recordings in a control and treated cell at 11 DIV.

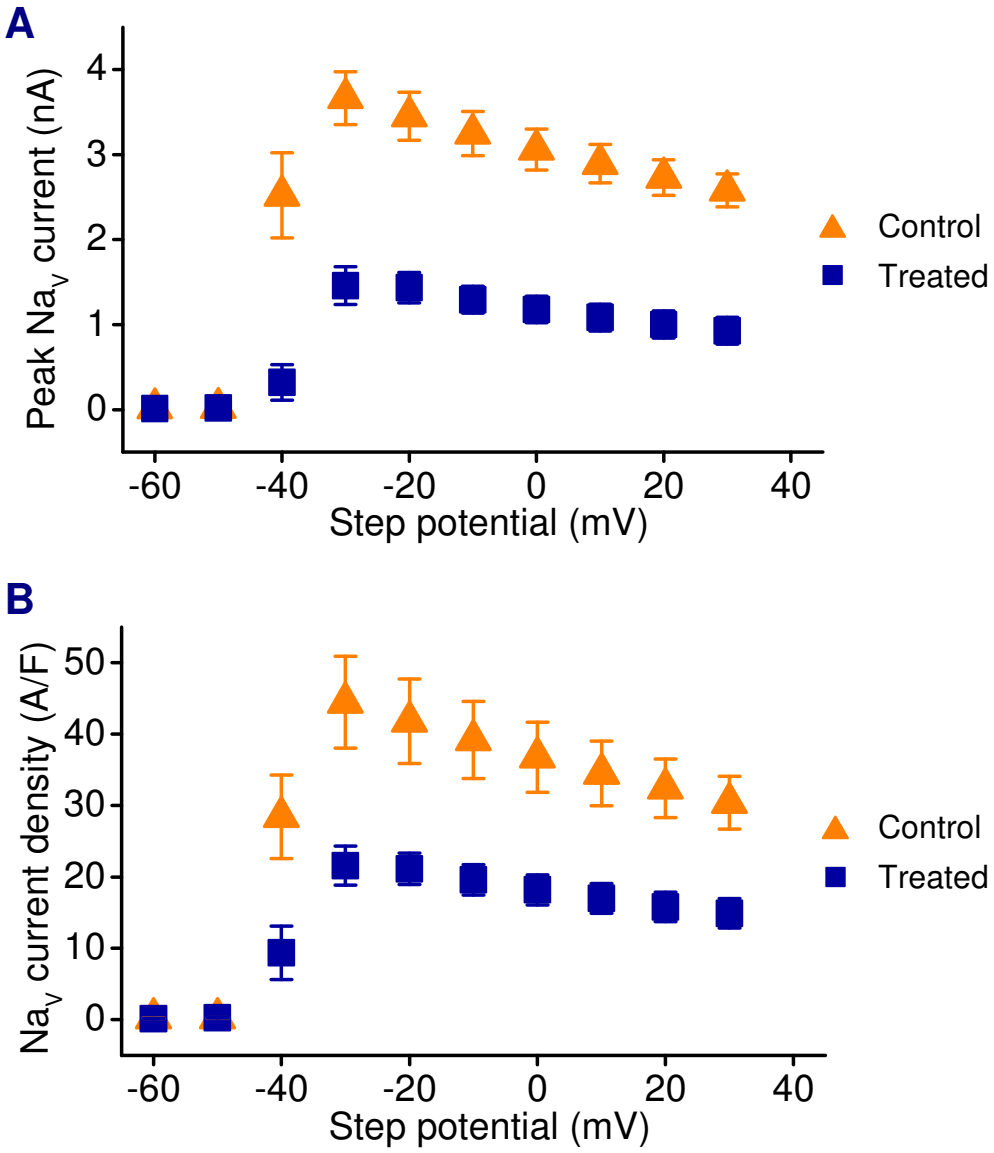

Figure 6.5: Voltage-gated sodium currents

(A) Pooled mean voltage-gated sodium current amplitudes for control (n = 15) and treated cells (n = 17) recorded at 8-11 DIV. Maximum values (at a step potential of –30 mV) are significantly different between conditions: –3777 ± 321 pA for control and –1537 ± 190 pA for treated cells, ($p = 2\times10^{-5}$, *t*-test). **(B)** Sodium current amplitude normalised to cell capacitance for the same cells as in (A). Peak density amplitudes are also significantly different between groups ($p = 3.5\times10^{-3}$, *t*-test). Mean access resistance values for both groups were not statistically significantly different (control: 21.5 ± 1.4 MΩ, treated: 21.7 ± 1.6 MΩ; $p = 0.9$, *t*-test).

6.6. Voltage-gated potassium currents

Voltage-gated potassium channels participate in repolarising the membrane potential during an action potential and, like sodium channels, exert a strong influence on intrinsic excitability. As with sodium currents, voltage-gated potassium currents can be measured using step potentials. There are, however, limitations on the extent to which these currents can be isolated pharmacologically because there is a great diversity in channel subtypes and a dearth of specific and effective antagonists (Coetzee *et al.* 1999).

In particular, leak conductance itself is largely mediated by potassium-permeable channels. Due to the similarity in structure of the pore region, which largely determines ion selectivity, (Hille 2001) leak channel-blocking agents such as barium and caesium also block voltage-gated potassium channels. This means that leak current blockers cannot be used to separate the voltage-gated component from the non-voltage-gated component of the potassium current.

In contrast to sodium currents, therefore, one cannot isolate the entire voltage-gated component of the potassium current by subtracting traces in the presence of a channel antagonist from control traces. Instead, the method employed here is to estimate passive response of the cell to voltage steps, and subtract this response from the traces containing the voltage-gated potassium currents. The procedure for doing this is described in Methods (2.5.2). It is necessary to remove as much of the leak component as possible because we already know that it is substantially altered in treated cells. A measurement of the superposed voltage-gated and passive components of the potassium current would therefore carry a bias due to the difference in leak.

Although the entire voltage-gated component of the potassium current cannot be pharmacologically isolated, two components can be separated directly. Selectivity exists between certain potassium currents that mediate a fast-acting transient component (A-type current) and a slowly-activating, sustained component of the voltage-gated potassium current (delayed-rectifying current). These currents, which may be mediated by more than one channel subtype, are differentially sensitive to millimolar concentrations of 4-aminopyridine (4-AP) and tetraethylammonium (TEA), which preferentially block delayed-rectifying current and the transient, or A-type current, respectively (Nakajima 1966; Thompson 1977; Klee *et al.* 1995; Bekkers 2000; Hille 2001).

Voltage-gated sodium currents, calcium currents and synaptic currents are blocked during all of these experiments using TTX (1 μM), $CdCl_2$ (200 μM) and CPA.

6.6.1. Measuring voltage-gated potassium currents

Prior to applying a stimulation protocol to evoke voltage-gated potassium currents, the passive IV characteristics are estimated for each cell using the voltage step protocol described in Methods (Figure 2.3). Provided access resistance and seal resistance do not change during the course of the experiment, the passive data allows the voltage-gated component of the current to be obtained by subtracting the estimated passive component from the raw current trace. A more succinct way of describing this estimation/subtraction process is 'deconvolution', a term used in linear systems theory and signal processing to describe the process of recovering an original signal from a linearly filtered version. An example of the raw and deconvolved traces is shown in Methods, Figure 2.5. As the other main sources of ionic current (sodium currents, calcium currents and synaptic currents) are blocked, the remaining traces should be composed of voltage-gated potassium currents.

The stimulation protocol used for evoking voltage-gated potassium currents is as follows. Cells are held in voltage-clamp at −80 mV and subjected to 500 ms stimulation pulses at potentials in the range −60 to +40 mV, at a rate of one stimulation every 4s.

Example traces of voltage-gated potassium currents recorded in control and 15 mM KCl-treated cells are shown in Figure 6.6. The raw traces, contaminated with the passive component, are included for comparison. Casual inspection of these traces suggests there is little difference in the voltage-gated potassium currents between the cells. This indeed turns out to be the case when a peak currents are compared for a large sample number in each condition.

Figure 6.7 shows mean voltage-gated potassium current amplitudes for (n= 20) control cells and (n = 26) cells treated with 15 mM KCl, all recorded at 8-11 DIV. An unpaired *t*-test revealed no significant difference in the peak current between conditions ($p = 0.63$; mean peak values were 1684 ± 99 pA and 1760 ± 146 pA for control and treated cells, respectively). When currents are normalised to cell capacitance, to offer a control for cell surface area, the resulting current densities remain statistically indistinguishable between cases. Figure 6.7B shows a plot of the peak current density in the same two groups of cells. Again, a *t*-test revealed no significant difference ($p = 0.46$).

The form of the current as a function of time is remarkably similar between control and treated cells. Mean normalised traces from each group exhibit a fast-rising component which decays to a steady plateau. Outward voltage-gated currents in many neuronal cell types, in particular, Hippocampal neurons, are know to have multiple components that are mediated by numerous potassium channel subtypes (Rudy 1988; Coetzee *et al.* 1999; Hille 2001). The identification of which channel subunits are expressed in different cell types, and the kinetic and pharmacological properties of the functional channels they form is the focus of ongoing research. The following experiments extend the results obtained so far with a basic pharmacological dissection of two distinct types of voltage-gated potassium current that are sensitive to TEA and 4-AP, respectively.

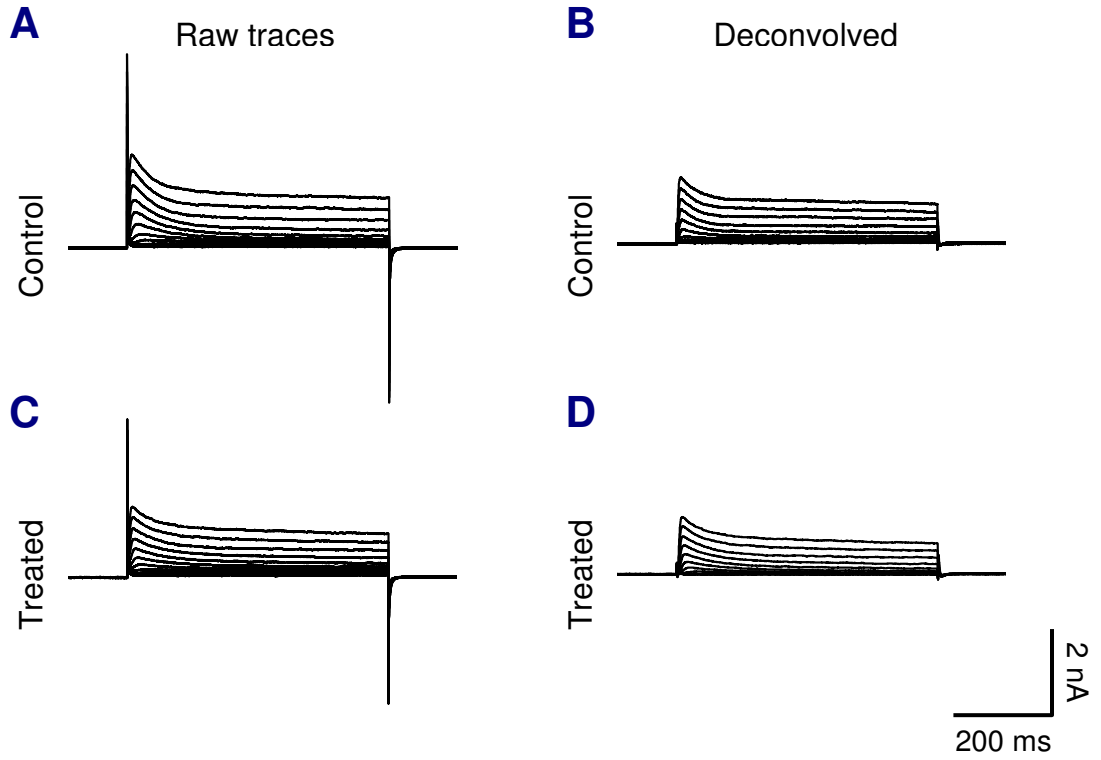

Figure 6.6: Voltage-gated potassium currents

(A) Voltage-clamp traces of evoked currents in the presence of TTX (1 µM), CPA and $CdCl_2$ (200 µM) from a control cell at 10 DIV. **(B)** Current traces from (A) with the capacitive transient and linear leak components removed, as described in Methods, Section 2.5.2. **(C, D)** Example raw and deconvolved traces from a treated cell in the same culture as the control cell, recorded at 10 DIV.

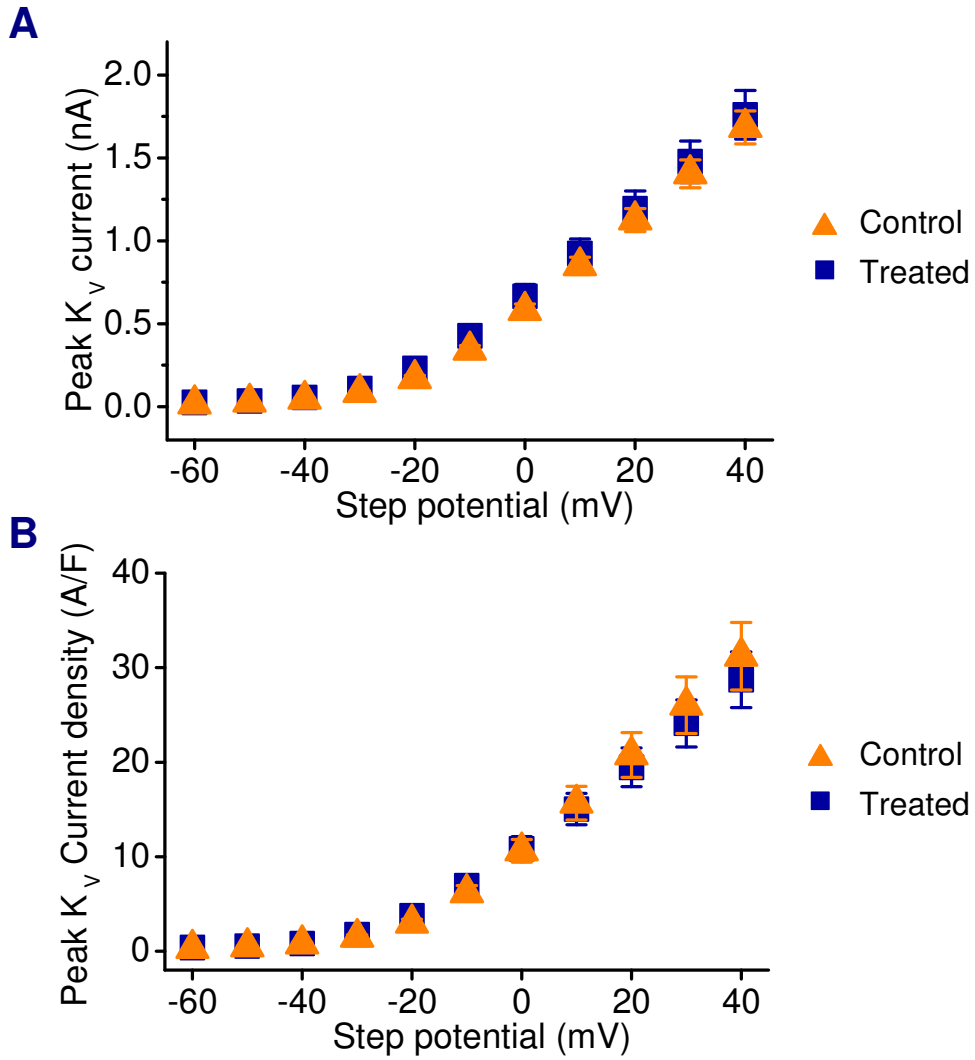

Figure 6.7: Voltage-gated potassium currents

(A) Peak amplitudes of evoked voltage-gated potassium currents in control (n = 20) and treated cells (n = 26) recorded at 8-11 DIV, with linear leak component removed. **(B)** Peak currents normalised to cell capacitance, providing an estimate of current density over the cell membrane surface area. Maximum values for both measures in (A) and (B) were not significantly different under the assumptions of a *t*-test (p = 0.63, p = 0.45, respectively). Mean access resistance values for both groups were not statistically significantly different (control: 25.2 ± 1.6 MΩ, treated: 27.2 ± 1.6 MΩ; p = 0.6, *t*-test).

6.6.2. TEA-sensitive voltage-gated potassium currents

To measure the TEA-sensitive component of the voltage-gated potassium current, control recordings of the total outward current were recorded in each cell in the absence of TEA. Following this, external solution containing 10 mM TEA was applied to the same cells and the evoked responses subtracted from the control recordings to obtain the TEA-sensitive current component. Figure 6.8 shows example current traces for both control and treated cells recorded in the before and after TEA application. The residual traces exhibit a slowly activating outward current which reaches a plateau during the 500 ms voltage step. Plateau amplitudes are comparable between the cells, and the form of the TEA-sensitive current in each is similar in its activation profile.

When compared across a population of cells, the amplitudes of the mean evoked TEA-sensitive currents in control (n = 18) and treated (n = 17) cells are comparable (Figure 6.9). As with total voltage-gated potassium current amplitude, a t-test on the peak amplitudes, whose mean values at +40 mV were 500 ± 60 pA (control) and 530 ± 70 pA (treated), revealed no significant difference (p = 0.72, *t*-test). Normalising the current amplitude to cell capacitance also failed to uncover any difference (p = 0.89, *t*-test, Figure 6.9B).

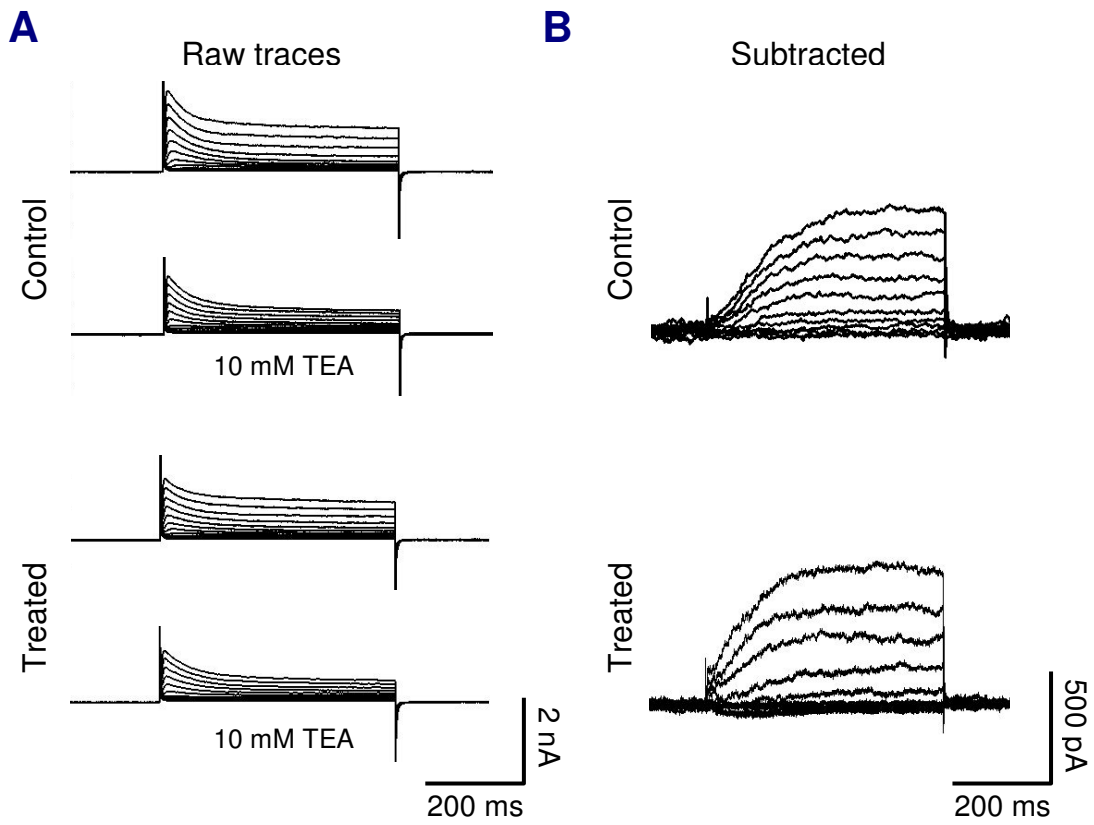

Figure 6.8: TEA-sensitive voltage-gated potassium currents

(A) Example voltage-gated potassium currents recorded at 10 DIV in control and treated cells, in the presence and absence of 10 mM tetraethylammonium chloride (TEA). **(B)** The TEA-sensitive component of the current is obtained by subtracting the traces recorded in the presence of TEA from those recoded in control conditions.

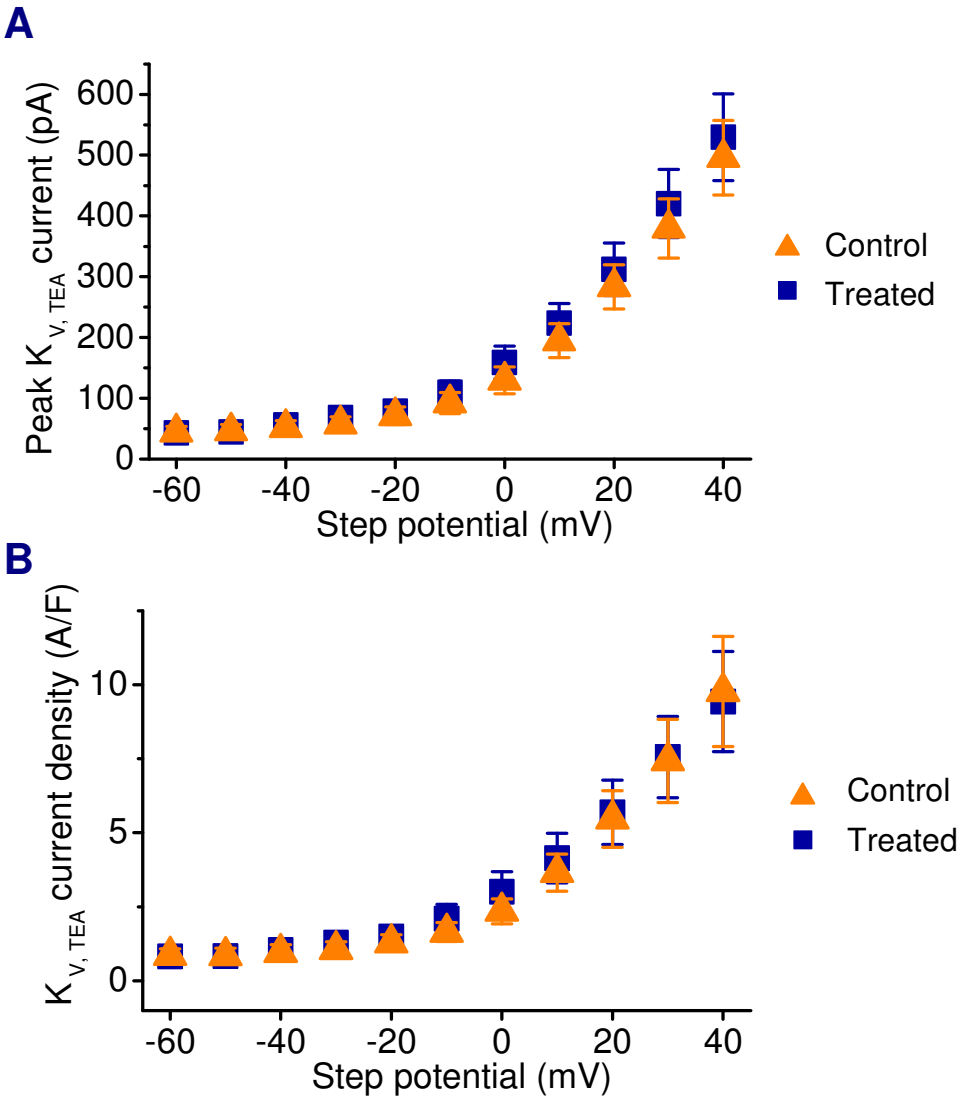

Figure 6.9: TEA-sensitive voltage-gated potassium currents

(A) Peak amplitudes of TEA-sensitive voltage-gated potassium currents in control (n = 14) and treated cells (n = 17) recorded at 8-11 DIV. **(B)** TEA-sensitive current density, estimated by normalising current to cell capacitance. Maximum values for the currents and current density in (A) and (B) were not significantly different between conditions (*t*-test; $p = 0.45$, $p = 0.58$, respectively). Mean access resistance values for both groups were not statistically significantly different (control: 25.0 ± 1.5 MΩ, treated: 26.7 ± 1.6 MΩ; $p = 0.5$, *t*-test).

6.6.3. 4-AP-sensitive voltage-gated potassium currents

Fast-activating transient voltage-gated potassium currents, or A-type currents, are blocked by 4-aminopyridine at millimolar concentrations (Connor and Stevens 1971c; Thompson 1977; Wu and Barish 1992; Klee *et al.* 1995). To find out whether the expression of such currents differs in control and treated cells, I measured the amount of 4-AP-sensitive current in both groups. As with TEA-sensitive current, the 4-AP-sensitive current was obtained by subtracting traces recorded in 1 mM 4-AP from control traces recorded in the absence of 4-AP. Examples of the raw current traces before and after 4-AP application, and the subtracted traces are shown in Figure 6.10.

The mean amplitude of the 4-AP-sensitive current at each step potential was similar for control (n = 17) and treated (n = 20) cells, with peak values of 560 ± 40 pA and 620 ± 70 pA at +40 mV, respectively ($p = 0.44$, *t*-test). This can be seen in the plot in Figure 6.11A. Again, normalising for cell capacitance to obtain current density estimates did not reveal a significant difference between the groups ($p = 0.69$, *t*-test, Figure 6.11B).

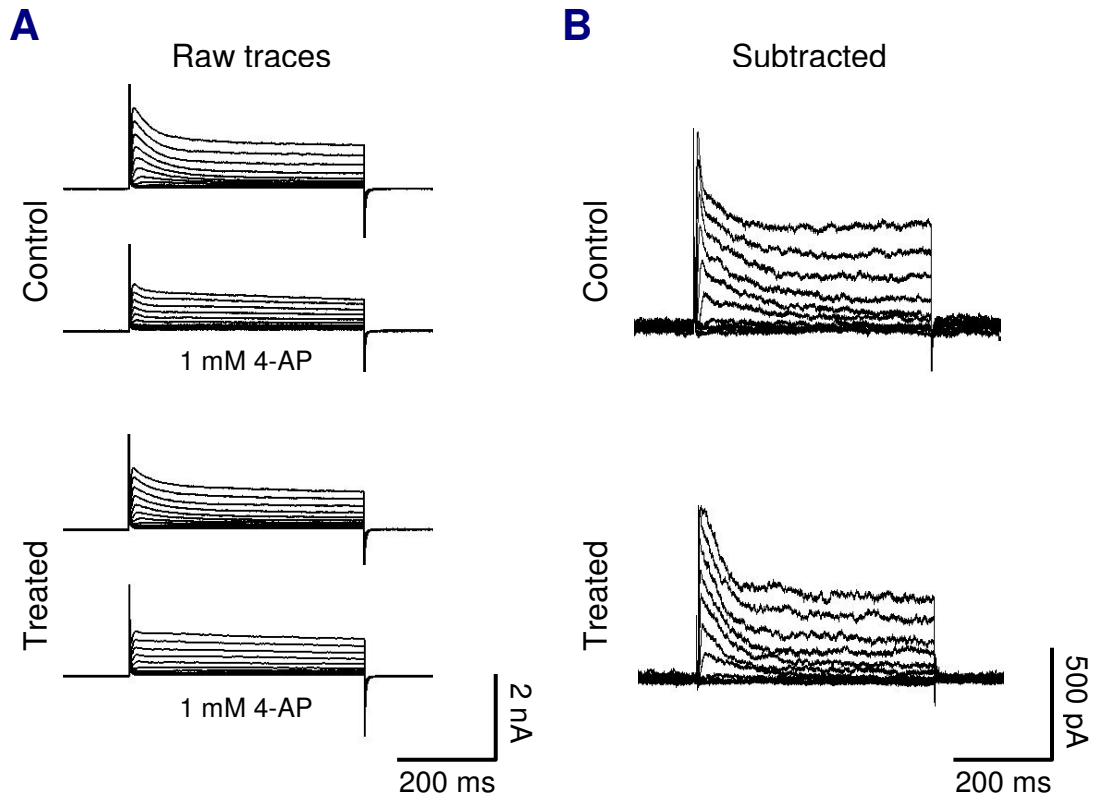

Figure 6.10: 4-AP-sensitive voltage-gated potassium currents

(A) Example voltage-gated potassium currents recorded at 10 DIV in control and treated cells, in the presence and absence of 1 µM 4-aminopyridine (4-AP). **(B)** The 4-AP-sensitive component of the current is obtained by subtracting the traces recorded in the presence of 4-AP from those recoded in control conditions.

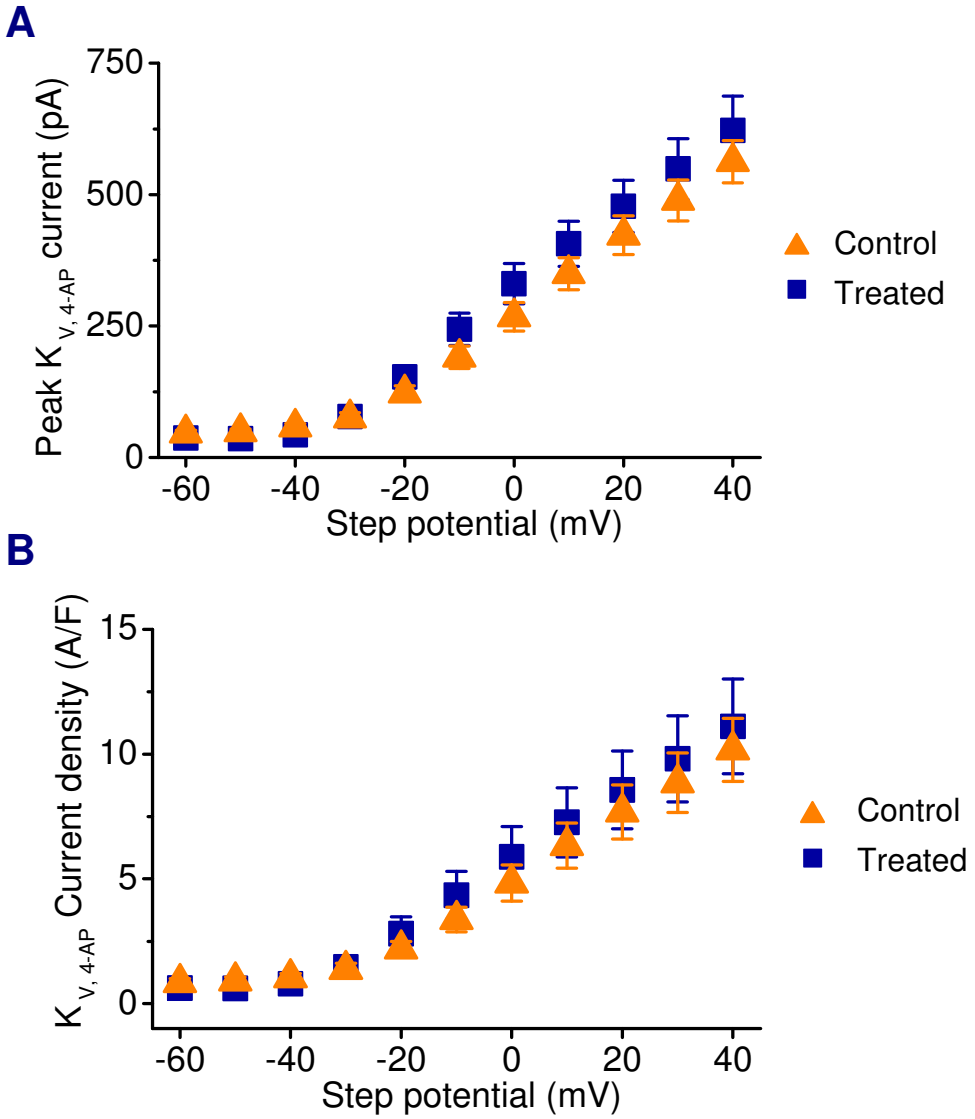

Figure 6.11: 4-AP-sensitive voltage-gated potassium currents

(A) Peak amplitudes of 4-AP-sensitive voltage-gated potassium currents in control (n = 14) and treated cells (n = 19) recorded at 8-11 DIV. **(B)** 4-AP-sensitive currents normalised to cell capacitance, providing an estimate of current density. Maximum values for the currents and current density in (A) and (B) were not significantly different between conditions (*t*-test; $p = 0.57$, $p = 0.75$, respectively). Mean access resistance values for both groups were not statistically significantly different (control: 26.4 ± 1.6 MΩ, treated: 27.3 ± 1.6 MΩ; $p = 0.7$, *t*-test).

6.7. Voltage-gated calcium currents

Depolarisation with 15 mM KCl causes a substantial rise in calcium influx in the control cells (Figure 5.11). Excessive intracellular calcium can interfere with the biochemistry of the cells, and cause cell death above a certain level. If we assume there are homeostatic mechanisms that modify these conductances to cope with depolarising conditions, we would expect a reduction in the amplitude of voltage-gated calcium currents in treated cells. Previous work has documented exactly this type of calcium channel homeostasis in a number of cell types (Delorme and McGee 1986; Liu *et al.* 1994; Li *et al.* 1996). It is therefore important to quantify the expression of voltage-gated calcium conductances in this present work, to see if the results are consistent.

Calcium currents were isolated by exploiting their sensitivity to block by extracellular cadmium. Concentrations of $CdCl_2$ in the micromolar to millimolar range effectively block voltage-gated calcium channels (Kostyuk *et al.* 1977; Hagiwara and Byerly 1981). Calcium currents were therefore defined as the residual inward current obtained by subtracting current traces recorded in the presence of 200 µM $CdCl_2$ from control traces. Both sets of recordings were performed in extracellular solution containing 1 µM TTX and CPA, using a Cs-based internal solution (Methods). Currents were induced by 500 ms voltage steps in the range −60 to +40 mV, from a holding potential of −80 mV.

Figure 6.12 shows example traces from control and treated cells. A transient inward current is evident in the residual traces for both cells. This current is diminished in the treated cell relative to the control, which was the case across the population of treated (n = 18) and control cells (n = 10) in this experiment. Figure 6.13 shows the mean calcium current for both groups, with the values normalised to cell capacitance in Figure 6.13B. Peak values were 550 ± 50 pA and 270 ± 45 pA for control and treated cells, respectively ($p = 9\times10^{-5}$, *t*-test). The difference in the normalised peak values was also statistically significant ($p = 2.6\times10^{-4}$, *t*-test).

Calcium currents are inward and therefore serve to depolarise the membrane potential. Voltage-gated calcium currents are not, however, responsible for fast

action potential generation. In general, action potentials are reliant on sodium and potassium currents. Calcium influx does influence cell excitability in other ways. For instance, the subfamily of calcium-activated potassium channels are important for the spike after-hyperpolarisation (AHP) which directly affects excitability.

Given that a large difference in calcium current density is evident between the groups, it would be negligent to overlook the possibility that calcium currents may exert a detectable influence on the excitability of the cells. This issue was addressed in an experiment which measured FI curves in the presence and absence of 200 µM $CdCl_2$. As can be seen in Figure 6.14, there is no obvious difference in the mean FI curve between conditions. Analysis of the mean current threshold revealed no detectable changes (14.3 ± 4.0 pA for control and 15.9 ± 3.8 pA with 200µM $CdCl_2$, $p = 0.44$, *t*-test), the FI slope, however became steeper when calcium channels were blocked (0.16 ± 0.001 spikes/pA compared to 0.19 ± 0.001 spikes/pA, $p = 3\times10^{-3}$), and the voltage threshold hyperpolarised by 1.5 mV (from −36.7 ± 0.8 mV to −38.3 ± 0.7, $p = 3\times10^{-2}$, *t*-test).

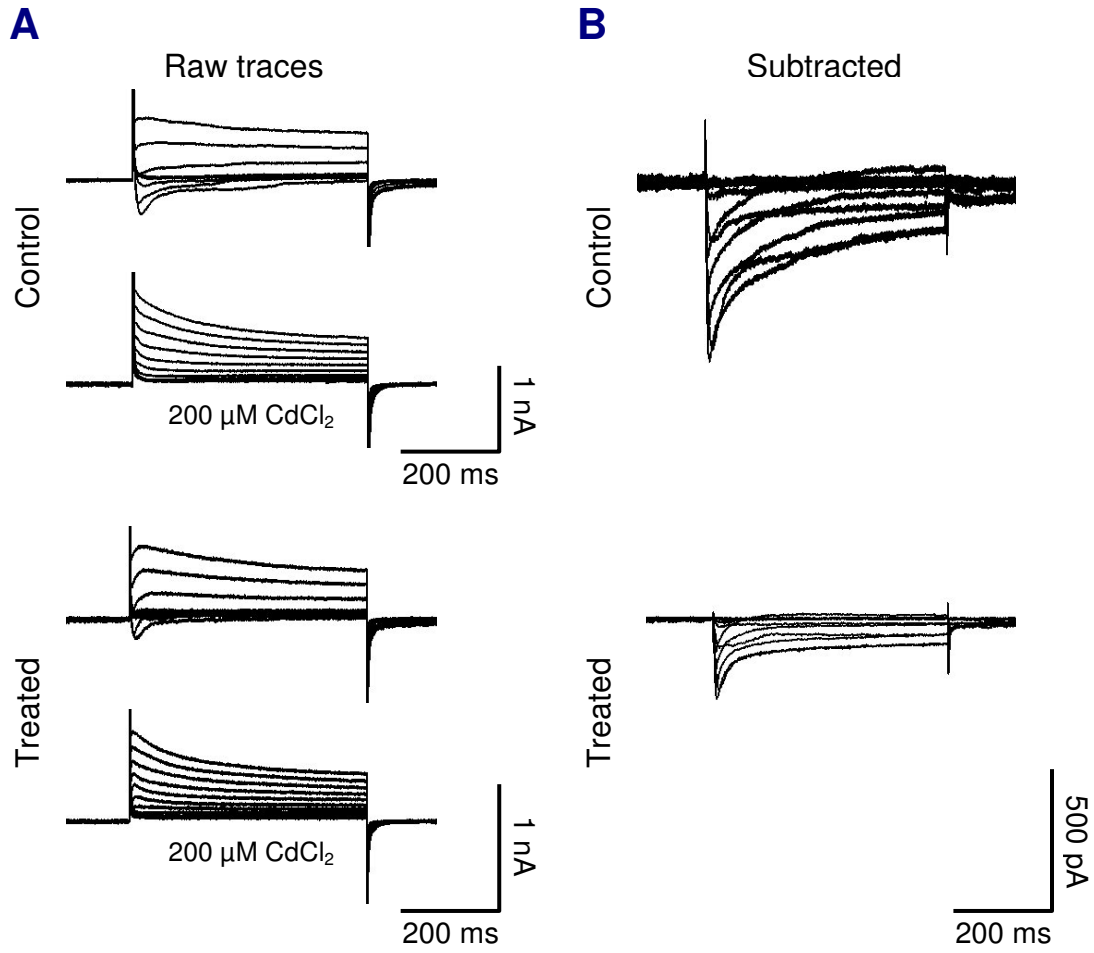

Figure 6.12: Voltage-gated calcium currents

(A) Current traces in a 11 DIV-control and treated cell showing evoked currents due to 500 ms voltage steps to potentials in the range –60 to +40 mV, from a holding potential of –80 mV. The extracellular recording solution contained TTX (1 µM) and CPA and a caesium-based internal solution was used to block potassium channels. Recordings were performed in the presence and absence of $CdCl_2$ (200 µM) **(B)** Cadmium-sensitive voltage-gated calcium currents obtained by subtracting the traces in (A) for each cell.

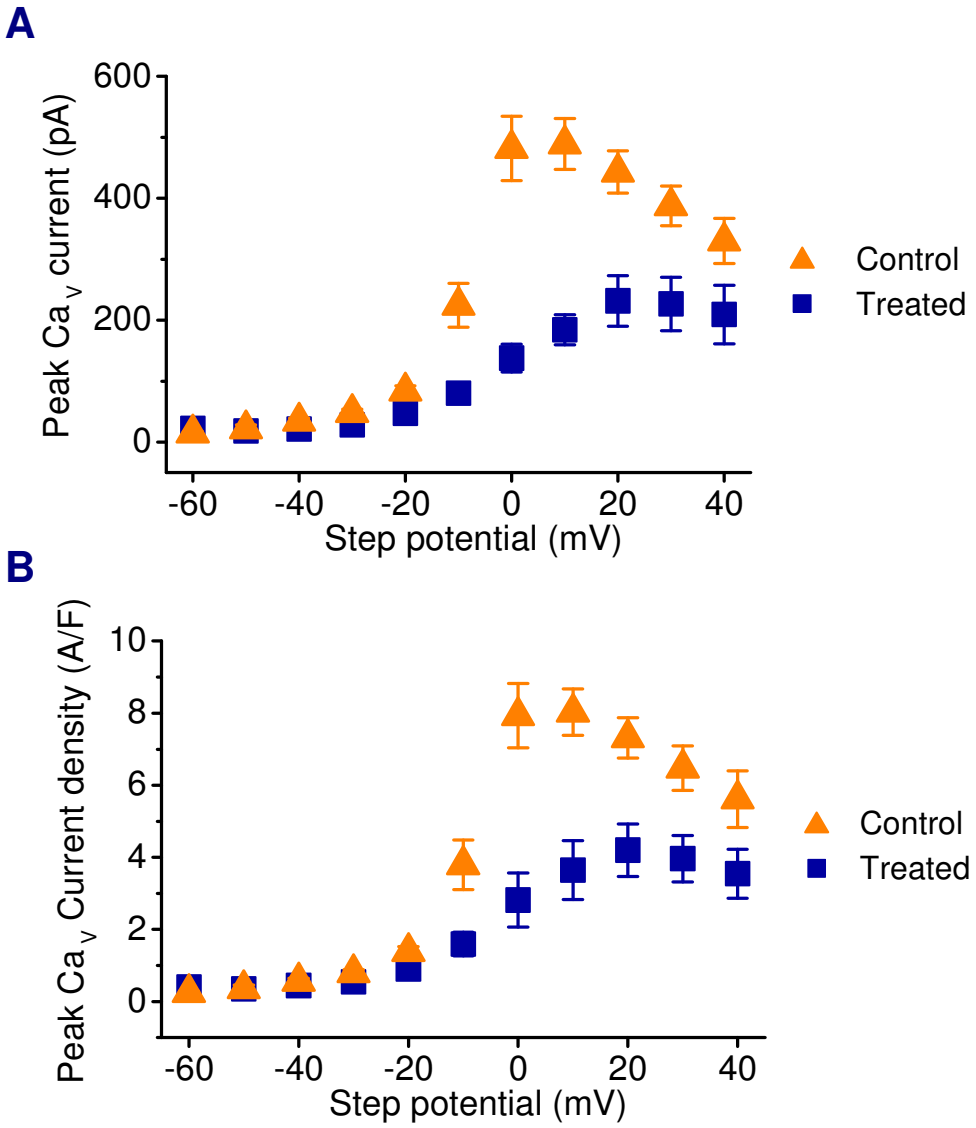

Figure 6.13: Voltage-gated calcium currents

(A) Peak amplitudes of cadmium-sensitive voltage-gated calcium currents in control (n = 10) and treated cells (n = 18) recorded at 8-11 DIV. **(B)** Calcium current amplitudes normalised to cell capacitance, which provides an estimate of current density. Peak amplitudes in (A) and (B) are significantly different for control and treated cells ($p = 9\times10^{-5}$ and $p = 2.6\times10^{-4}$, respectively, *t*-test). Mean access resistance values for both groups were not statistically significantly different (control: 25.5 ± 2.7 MΩ, treated: 27.6 ± 2.3 MΩ; $p = 0.6$, *t*-test).

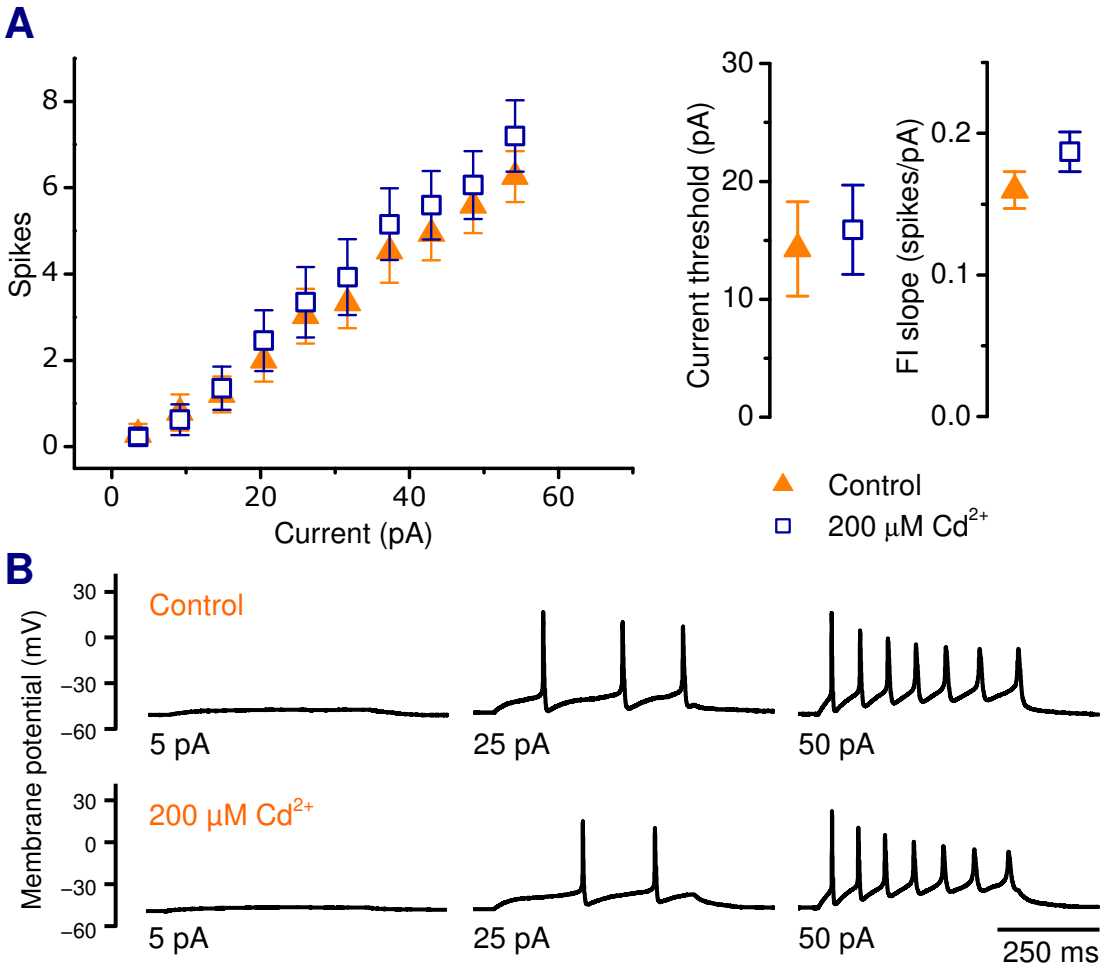

Figure 6.14: Effect of voltage-gated calcium current blockade on excitability

(A) Pooled FI curves for control cells (n = 11) recorded in the absence and presence of 200 µM CdCl2, with mean current threshold (right) and FI curve slope estimates (far right). **(B)** Example current-clamp traces from an FI curve recording before and after the addition of 200 µM CdCl2 to the recording bath.

6.8. Spike shape

Alterations in membrane conductances can influence the action potential waveform (Hodgkin and Huxley 1952d; Connor and Stevens 1971b). It is therefore important to investigate whether any differences exist in the shape of evoked action potential between control and treated cells.

This was examined systematically by evoking action potentials in current-clamp with brief (10 ms) pulses of current. Brief depolarisations were used in conjunction with the access resistance correction routine described in Methods (Section 2.5.3) to ensure the influence of the current injection on the shape of the waveform is minimised. A total of (n = 11) control and (n = 11) treated cells were subjected to stimulation using a current amplitude that reliably elicited spikes in each case. The current threshold, measured using 10 ms pulses for the purposes of this experiment was significantly different between groups: 55.9 ± 7.5 pA (control) and 182.6 ± 29.5 pA (treated cells), $p = 0.002$, *t*-test.

Mean spike shapes for the cells in both conditions are plotted in Figure 6.15. The spike width, defined as the duration of the positive phase of the action potential, was significantly larger in control cells compared to treated cells (control: 2.7 ± 0.2 ms; treated: 1.8 ± 0.1 ms; $p = 2 \times 10^{-4}$, *t*-test). In addition, the magnitude of the after-hyperpolarisation (AHP), was found to be significantly larger in magnitude in treated cells compared to control cells (control: 14.1 ± 1.3 mV; treated: 21.3 ± 1.4 mV; $p = 0.007$, *t*-test). The AHP was defined to be the difference between the minimum value of the membrane potential in the 50 ms window after spiking, and the membrane potential 2.5 ms before the membrane potential exceeds 0 mV.

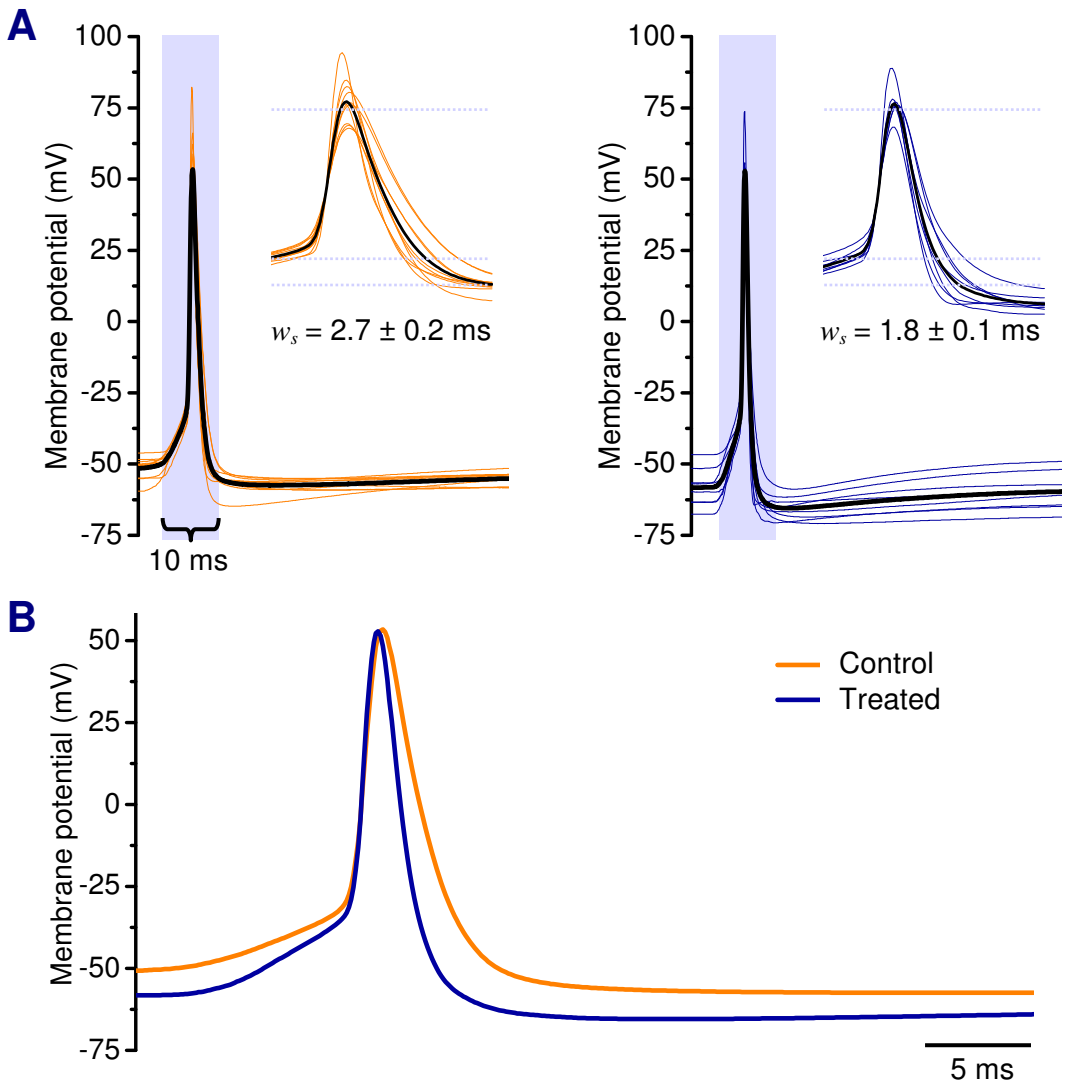

Figure 6.15: Spike shapes

(A) Evoked action potentials recorded in control and treated cells (15 mM KCl) recorded at 8-11 DIV. The black traces are the mean of 11 cells in each case. Individual spike profiles are calculated from the average of 20-40 spikes evoked by a 10 ms current pulse. Averages are computed by horizontally aligning spike waveforms to the zero-crossing point (ZCP) of the rising phase. Insets show detail of the spike profiles inside the gray boxes, with the dotted lines at equal values of membrane potential for comparison. The mean spike width, w_s, is calculated from the duration of the positive part of the spike trace on the voltage axis and was significantly different between groups ($p = 2\times10^{-4}$, *t*-test). **(B)** Mean spike traces, aligned to the ZCP.

6.9. Discussion

Clear differences in the membrane conductance properties are evident between control and treated cells. The effects can be summarised quite simply: chronic depolarisation results in increased leak conductance and decreased amplitudes of evoked voltage-gated sodium and calcium currents. In respect of the results of the previous chapter, the observed changes in excitability that accompany chronic depolarisation are congruent with these alterations in membrane conductance. Enhanced leak serves to increase the amount of current required to reach action potential threshold, while decreases in the amount of inward current due to sodium and calcium conductances clearly reduces the depolarising effect these conductances have on membrane potential when they are active. The details of the results in this chapter will now be discussed in turn.

6.9.1. Passive, subthrehold membrane conductances

Steady current measured in the range of membrane potentials between −80 to −40 mV was taken to represent the linear leak conductance of the cells, and the IV characteristic thus obtained showed an increased slope conductance in treated cells relative to control. In addition, treated cells had a more hyperpolarised reversal potential associated with this conductance (Figure 6.1). Together, these results may account for the changes in resting membrane potential and input resistance that were observed to follow chronic depolarisation in the previous chapter. The extent to which this inference is valid will be addressed in the next chapter, which employs a conductance-based computer model to quantify the effect these conductances have on intrinsic excitability.

In particular, a component of the leak conductance mediated by potassium-permeable channels, isolated here by its sensitivity to barium, was increased by nearly 3–fold in treated cells. Of the non-voltage-gated, or 'leak' potassium channels that are likely to underlie this change, members of the family of two-pore domain channels TASK-1 and TASK-3 (KCNK3, 9) are a possible candidates, as they are sensitive to block by barium in millimolar concentrations (Coetzee *et al.* 1999), although the extent of this sensitivity varies widely across the entire family (Patel and Honore 2001). Inward-recifying (K_{ir}) channels (Nichols and Lopatin 1997) might contribute a small amount

to membrane conductance in the voltage range examined, but as this range (−80 to −40 mV) is more positive than the computed potassium reversal potential (−97 mV), this contribution is likely to be small. In addition, K_{ir} currents are inactivated by the presence of intracellular ATP in millimolar concentrations of (Coetzee *et al.* 1999). Since the concentration of ATP in the internal recording solution is in this range (4 mM), a substantial proportion of K_{ir} channels – if present in the cells – are likely to be inactive.

An increase in leak potassium channel-mediated leak conductance is consistent with the hyperpolarised resting membrane potential of treated cells described in the previous chapter. Specifically, an increase in their expression would enhance the influence of the potassium reversal potential, and, consequently, lead to a shift in resting membrane potential toward this value. In addition, enhanced potassium conductance leads to a shortening of spike-width (Mitterdorfer and Bean 2002), as was observed in the action potential waveforms in the treated cells compared to control (Figure 6.15).

Passive cell properties are not only governed by ion channel expression. In particular, linear input resistance is dependent on axoplasmic resistivity, cell morphology, and membrane conductance (Koch and Segev 1998; Koch 1999). The first two characteristics are not addressed in this project and it is worth commenting on this omission, particularly in light of the fact that input resistance accounts for a large part of the observed phenomena.

Differences in axoplasmic resistivity would be very difficult to measure directly. Such measurements are usually conducted in large cells or cell processes such as in the classical experiments of Cole and Hodgkin (1939) on the squid giant axon. Attempting a similar experiment on hippocampal neurons would be problematic. For example, if one were to patch a cell at the soma with two electrodes, the relevant region of cytoplasm between the electrodes would be heavily dialysed by the internal solution, swamping any contribution due to the endogenous intracellular contents. In any case, it seems unlikely that the total intracellular ionic concentration is different in treated cells because this would have an impact on cytoplasmic osmolarity. Treated cells did not swell or shrink appreciably when placed in external recording

solution, suggesting that there is no major difference in osmotic balance relative to control cells.

It is quite possible that morphological differences account for some of the changes in the passive electrical properties of the cells, and, therefore, their excitability. Several studies have shown that cell growth is strongly influenced by electrical activity (Cohan and Kater 1986; Van Huizen and Romijn 1987; Fields 1998). Chronic depolarisation may therefore cause systematic morphological changes in treated cells.

However, the relationship between cell morphology and electrophysiological characteristics is complex: there is no single, scalar measure (such as volume) which captures all features of a cell's geometry that are relevant to its electrical properties. Indeed, attempts to elucidate this relationship form the basis of entire studies (Rall 1962; Koch *et al.* 1983; van Ooyen *et al.* 2002). Furthermore, despite efforts to record from morphologically similar cells, the cell cultures contain many cell types so it would be difficult to quantify the effects on morphology systematically.

If a reliable marker of a given cell type were used in conjunction with detailed morphological reconstruction, and if relevant measures of cell morphology could be identified, it would be interesting and feasible to pursue this line of enquiry. To do such an experiment properly, one would need to dye-fill individual cells and record from them in each group. This would allow detailed morphological reconstruction and quantification. In addition, this approach would enable electrophysiological properties to be correlated with morphology; at once providing a comprehensive overview of the interplay between depolarisation, excitability and morphology. Interestingly, a recent study of neurons in the deep cerebellar nuclei found that coarse morphology (dendrite length, number of primary dendrites) correlated poorly with electrical properties (Aizenman *et al.* 2003b). This might, in turn, be the result of homeostatic compensation in the distribution of ionic conductances in the cells that were examined.

Despite the issues already raised, it is very unlikely that the apparent changes in conductance are spurious and that morphological changes account for all aspects of

the phenomena observed here. For instance, the resting membrane potential of the cells is consistently different between control and treated groups. This cannot possibly be attributed to cell morphology: resting potential is a function of the relative concentrations of ions inside and outside the cell, and of the density and properties of ion channels and ion pumps in the cell membrane, irrespective of its shape. It would also be difficult to account for differences in the measured amplitudes of sodium currents through morphology alone. Furthermore, if a large and biophysically relevant difference in morphology were present between groups, one would expect a detectable difference in cell capacitance – none was found in any of the experiments in this work.

6.9.2. Sodium currents

Fast voltage-gated sodium currents are responsible for action potential generation, accordingly, the 60% decrease observed in the peak evoked sodium currents in treated cells relative to control values is consistent with the reduced excitability observed in these cells. The kinetics of the currents were not analysed in detail because neurons that have developed processes are difficult to voltage-clamp. Poor voltage control over the duration of the fast, large-amplitude sodium currents introduces error in the voltage-dependent activation profile of evoked currents, and makes detailed analysis of their kinetics problematic. Superficially, the activation profile appears unchanged between the treated and control groups, with the peak current evoked at −30 mV and the half maximum close to −40 mV. Thus it is reasonable to conclude that the main effect chronic depolarisation has on sodium conductances is to elevate their expression in the plasma membrane. As with the observed change in leak conductance, the question of how changes in the amplitude of sodium conductance contribute to excitability is dealt with quantitatively in the next chapter.

The activation profile of the sodium currents in both cell groups (Figure 6.5) also serves to illustrate an important point concerning the accuracy of single-electrode voltage-clamp experiments on neurons. Fitting a straight line to the points above the maximum activation (−30 mV in both cases) predicts that the currents would reverse

at +180 mV in control cells and +140 mV in treated cells[8]. These values are difficult to take seriously given that the predicted reversal potential based on the internal and external sodium concentrations of the recording solutions is +70 mV. A more plausible scenario is that the measurement of the sodium current amplitude suffers from a systematic error at high holding potentials because there is poor voltage control while the channels are open. The combined opening of the sodium and potassium channels would serve to shunt current supplied by the recording electrode and locally clamp the affected region of membrane to some unknown potential.

A possible extension of this study that would allow comparison of the kinetics of sodium currents would be to conduct the experiments with external solution that has a lower sodium concentration. This can be achieved by substituting sodium chloride with choline chloride, for example (Derksen 1965), resulting in lower-amplitude currents that would permit more accurate voltage-clamping. Alternatively, the cell attached-patch method could be used as in (Desai *et al.* 1999b), which would involve stimulating current flow through small patches of cell membrane; or, one could employ the nucleated-patch method, which involves enucleating the cell and maintaining an electrotonically-compact portion of somatic membrane in whole cell configuration (Bekkers 2000).

6.9.3. Potassium currents

It is perhaps surprising that no differences in voltage-gated potassium conductances were found in treated cells (Figure 6.7, Figure 6.11 and Figure 6.9), because the currents mediated by them have a big impact on cell excitability, particularly 4-AP and TEA-sensitive currents (Hille 2001). Also, the depolarisation treatment itself is introduced by raising the extracellular potassium concentration, so one might have anticipated changes in membrane channels that are, themselves, permeable to potassium.

This finding differs with the results from other studies that study regulation of intrinsic properties using alternative systems. Desai *et al*. (1999b) and Aizenman and

[8] A GHK fit would predict an even higher reversal potential because the slope conductance in this case decreases as reversal potential is approached.

Akerman (2003a) report that the mean amplitude of voltage-gated potassium currents is modified in response to chronic TTX-induced changes in excitability in the former study, and to visually-driven excitatory input in the latter.

On the other hand, Brickley *et al* (2001) find that voltage-gated potassium conductances (and other voltage-gated conductances) are robust to changes in tonic inhibition caused by the genetic deletion of a $GABA_A$ receptor subunit in mutant mice. Moreover, Brickley *et al* (2001) report that a change in leak current – mediated by TASK-1 channels – results from this manipulation, a qualitatively similar result to that presented in the current work.

It is interesting that this similarity and differences in the mechanisms that exists despite the major differences that exist between the studies in the basic effect, the protocol, and the preparation. One may speculate that, among studies that examine the homeostatic regulation of membrane conductances, the differences and similarities in results reflect a general mechanism in CNS neurons, whereby voltage-gated potassium, sodium and calcium channel expression is controlled by pathways that are independent of each other.

A more sceptical view is that all studies of this kind reflect limitations in the approach. In the context of the current study and the study of Desai *et al.* (1999b), the pooling measurements of currents in dissociated neuronal cultures – in which it is difficult to exclude heterogeneous cell types – may obscure more nuanced changes in subtypes of membrane conductance. This might also result from the use of pharmacological agents such as 4-AP and TEA, which display a broad action across channel subtypes. However, these issues are not so severe as to throw the basic findings into doubt.

The most obvious criticisms that can be levelled at the validity of the voltage-gated potassium conductance data concerns the attempt to dissociate the total voltage-gated component from the leak by subtracting a linear leak estimate. First, there is a possibility that the current defined as ‘leak’ current contains components that are voltage-gated. If these components were to equate to a substantial proportion of the leak conductance estimate, a bias in the estimate of the residual voltage-gated

currents would result. Secondly, the current-voltage relation for leak current is know to be non-linear. Any membrane conductance that is selectively permeable to a particular ion species follows the Goldman-Hodgkin-Katz (GHK) current equation (Methods, Section 2.5.2). Leak current probably has components attributable to potassium and sodium-selective ion channels, and possibly other ion channels besides these (Hille 2001).

This criticism serves as an important caveat for interpreting the results of the voltage-gated potassium current experiments. It also highlights the difficulties associated with measuring basic electrophysiological properties of neurons. As pointed out in Methods, Section 2.5.2, the use of the GHK equation requires knowledge of membrane permeability and intracellular concentrations of all relevant ions. One might suppose that the known concentrations of the intracellular and extracellular recording solutions provide some of this information, but a calculation of the chloride reversal potential using these concentrations gives a value (−69.2 mV, Methods, Section 2.3.3) that is different from that obtained by measuring $GABA_A$ receptor currents directly (−40 ± 5 mV, or −52.7 mV when corrected for the liquid junction potential Chapter 3, Figure 3.16). Similar discrepancies are found between estimates of the potassium reversal potential from the barium-sensitive current in Figure 6.2 and the theoretical value. Furthermore, the cast of ion channels that contributes to leak is unknown, and potentially variable across both treated and control cell populations; correspondingly, the relative ionic membrane permeability may also differ cell-to-cell.

On the basis of these technical difficulties, and given the known differences in leak conductance between control ant treated cells, it is preferable to subtract an approximation of the leak current from the voltage-gated potassium currents than to ignore it entirely. A linear estimate of the leak component is simple to estimate and implement, and not subject to biases due to ad-hoc estimates of unknown parameters of the GHK equation.

6.9.4. Voltage-gated calcium currents

Chronically depolarised cells exhibited a reduction in the density of voltage-gated

calcium conductance. As with the other conductances that exhibited a change, this raises the question as to whether calcium current regulation accounts for any of the changes in excitability induced by chronic depolarisation, or whether it can be considered to be an epiphenomenon. The case for the latter conclusion will be argued using the available evidence. Before presenting the argument, however, it should be stressed that the two alternatives do not represent a true dichotomy. Calcium currents can and do contribute to excitability (Hagiwara and Byerly 1981; Hille 2001). Aside from providing a source of depolarising current, calcium influx triggers numerous biochemical signalling cascades – some of which directly contribute to the electrical properties of the cell. For example, the family of calcium-activated, voltage-gated potassium channels are modulated by calcium influx. These channels are involved in the spike after-hyperpolarisation (AHP) and are thus key regulators of excitability (Vergara *et al.* 1998). Therefore it would be rash to conclude that the change in voltage-gated calcium currents is an irrelevant result, the question here is whether or not they contribute to the effects observed in this study to any appreciable extent. This issue will be returned to when questions for further work are discussed in the final section of this chapter.

Completely blocking calcium currents did indeed have an effect on the firing characteristics of control cells (Figure 6.14). However, this effect was subtle compared with the changes observed in excitability observed in chronically depolarised cells. Compared to control conditions, FI curves measured in the presence of extracellular cadmium exhibited a slope that was steeper by 17%, with no detectable change in current threshold. In contrast, cells that are depolarised with 15 mM KCl for one week show marked changes in current threshold and have a shallower slope than control cells (Figure 5.7). Furthermore, the change in current threshold is accurately accounted for by the reduction in input resistance and the estimate this provides of the steady current required to raise membrane potential to spiking threshold. Calcium currents have no detectable effect on input resistance, even when completely blocked. Therefore, it can be inferred from these experiments that a ~50% reduction in peak voltage-gated calcium current amplitude is unlikely to underlie the excitability characteristics observed in chronically depolarised cells.

What function, then, does the down-regulation of voltage-gated calcium currents serve? Evidence from other studies is useful in trying to answer this question. Voltage-gated calcium currents have been observed to become down-regulated in response to chronic depolarisation in numerous studies (Delorme and McGee 1986; Franklin *et al.* 1992; Liu *et al.* 1994; Li *et al.* 1996). Calcium homeostasis is critical to many sub-cellular processes: particularly onerous among the effects of calcium influx is the phenomenon of excitotoxic cell death (Schlaepfer and Bunge 1973; Choi 1988; Sattler *et al.* 1998). An excess of free intracellular calcium is capable of inducing apoptosis in neurons, particularly under conditions of high excitatory synaptic activity. Interestingly, a key early paper on this subject concluded that depolarisation-induced calcium influx through L-type calcium channels is implicated in this process (Weiss *et al.* 1990). The relationship between calcium influx and cell survival is complex, however as other studies show that it is crucial for maintaining cell health (Gallo *et al.* 1987; Collins *et al.* 1991; Moulder *et al.* 2003).

6.9.5. Where to look next?

There are many membrane conductances that have been overlooked in this thesis, as well as other biophysically relevant characteristics such as cell morphology. The omission of these lines of enquiry is not an oversight, nor does it tacitly imply that they are irrelevant to the phenomena being studied here. Rather, it is the result of pragmatic thinking and scope: many questions have been raised by the basic observations in Chapter 5, and effort in this chapter has been directed toward addressing a cohesive subset rather than trying to provide a panacea. To ensure the integrity of what has been established and inferred, however, it is necessary to highlight the remaining unknowns and suggest ways in which the study could be extended.

Among the classes of known membrane conductances omitted in this study, some represent subsets of those that were examined, such as leak conductances. Among this family of channels, the TASK and TREK subfamilies of two-pore domain potassium channels are notable candidates for further study because their sensitivity to pH and inhalation anaesthetics enables isolation of current due to these channels (Duprat *et al.* 1997; Buckler *et al.* 2000; Patel and Honore 2001). Moreover, the

barium sensitivity of two pore-domain channels is highly variable (Goldstein *et al.* 2001; Patel and Honore 2001), so the dissection of the leak current carried out here would benefit from further work using more selective pharmacological agents. In addition, these channels, particularly members of the TREK-1 family (Talley *et al.* 2001), are heavily expressed in hippocampal neurons where they have been shown to be important in regulating resting membrane potential.

In addition, the inward-rectifier (K_{ir}) potassium channels are crucial in determining resting membrane potential (Nichols and Lopatin 1997). As pointed out earlier, a significant proportion of these channels will be inactive under the recording conditions in this work. However, it would be interesting to see whether inward-rectifying potassium current is altered by prolonged depolarisation by examining membrane conductances at potentials for which these channels are active, using different intracellular solution if necessary.

Other ion channel families that are important in sub-threshold behaviour include the hyperpolarisation-activated mixed-cation current, I_h. This current is mediated by cyclic nucleotide-activated channels (HCN channels) and thought to underlie the development of 'mature' neuronal integrative characteristics (Bender and Baram 2008). In fact, a direct involvement of I_h in intrinsic excitability regulation has been established in hippocampal neurons on a somewhat shorter timescale (< 1 hour), using, in turn, alpha-latrotoxin and glutamate to enhance excitatory synaptic activity (van Welie *et al.* 2004). Although the work of van Welie *et al.* (2004) employs quite a different approach to inducing excitatory stimulus to the current work, there is a possibility that a similar mechanism involving I_h may also participate in the effects being studied here, particularly at later stages of development *in vitro*.

Conductances mediated by one large family of potassium channels have not been examined at all in this study, namely, the family of calcium-activated potassium channels, or K_{Ca} channels. These channels are important during action potential repolarisation and contribute to the spike after-hyperpolarisation (AHP). An examination of the mean action potential profiles in Figure 6.15 suggests that there is a difference in the AHP between control and treated cells, which would be expected if a large alteration in K_{Ca} channels had occurred following chronic depolarisation.

Furthermore, these channels are important for sustained spiking and therefore have a strong impact on excitability (Vergara *et al.* 1998), an effect that has been found to be modulated in an activity-dependent way (Sourdet *et al.* 2003), making them eminent candidates for further work.

Finally, chloride channels might represent a class of conductances that is relevant to this work. Non-ligand-gated chloride channels have received relatively little attention in electrophysiological studies in neurons. Moreover, they are known to be expressed in hippocampal neurons and are likely to play an important role in regulating resting membrane potential and in maintaining the chloride reversal potential (Jentsch *et al.* 2002; Suzuki *et al.* 2006), especially the hyperpolarisation-activated ClC-2 channel (Sik *et al.* 2000; Haug *et al.* 2003). Given the differences in resting potential that exists between control and treated cells, and the fact that the leak reversal potential differs appreciably from the potassium reversal potential, it is quite possible that differences in chloride channel expression underlie some of the effects reported in this work.

It remains to be established whether the changes in conductances observed in this chapter are due to increases in the number of ion channels in the cell membrane. This could be achieved using methods to quantify the total amount of protein expression for particular subunits of interest, such as sodium channels. It would also be important to quantify the expression level of mRNA associated with the channel genes, to see whether increases in conductance are due to transcription, translation, or both. One potential confounding factor is the issue of subunit expression in astrocytes, which are present in the cultures, and which express mRNA for numerous ion channels, including sodium channels (Schaller *et al.* 1995). The use of microarrays would enable a large-scale screen of candidate mRNAs whose expression level is regulated by depolarisation and, in additions, would help identify other genes involved in the expression of the excitability homeostasis.

Alterations in expression density of ion channels are not the only changes that can impinge on membrane conductance. Post-translation modification of ion channel subunits in-situ is known to modulate ion channel properties and lead to significant changes in activation kinetics and single-channel conductance (Numann *et al.* 1991).

For example, voltage-gated sodium channels, calcium channels and potassium channels (Armstrong 1989; Hoger *et al.* 1991; Li *et al.* 1992), and leak channels (Murbartian *et al.* 2005) can all be modulated by phosphorylation in neurons. The activity of the protein kinases and phosphatises responsible for phosphorylation is, in turn, dynamically regulated by activity, and calcium influx in particular (Braun and Schulman 1995).

Functionally, this kind of modulation has been demonstrated to be triggered by the action of metabotropic glutamate receptors (Carlier *et al.* 2006) and the action of neuromodulators such as dopamine (Chen *et al.* 2007), and, interestingly, is found to depend on calcium influx through L-type voltage-gated channels in the latter case.

Therefore, it is a priority for further work to characterise the conditions under which homeostatic regulation of intrinsic excitability, and regulation of membrane conductances in general, depend on changes in channel density as opposed to changes in channel properties. One may speculate that post-translational modification occurs in the short term, leading to translation and transcription-dependent changes in ion channel expression over longer timescales. Such a process is analogous to so-called early and late-phase LTP as studied in classical preparations such as the CA1-Schaffer collateral pathway of the hippocampus (reviewed in Malenka and Bear 2004). It would be intriguing to test the hypothesis that a similar distinction between the short and long-term mechanisms exists in the regulation of excitability; the system used in this thesis provides an ideal candidate for continuing such work.

Chapter 7. Modelling: do the changes in membrane conductances explain the changes in intrinsic excitability?

7.1. Chapter summary and key findings

1. A single-compartment conductance-based model is fitted to mean conductance data for sodium, potassium and leak conductances obtained from control cells in the previous chapter. The kinetic parameters of the model are set to fit the activation profile of the corresponding currents.

2. Excitable behaviour is observed in the single compartment model. This behaviour, quantified in terms of the FI curve, closely resembles the mean behaviour of control cells.

3. Mean conductance parameters for sodium and leak conductances are altered according to the differences observed between control and treated cells. The resulting model FI curve recapitulates the change in excitability observed in treated cells.

4. Modifying either leak or sodium conductance alone fails to accurately predict the changes in FI curves observed in treated cells.

7.2. Motivation

The last two chapters have, in turn, characterised two aspects of the effects of chronically depolarising neurons. Chapter 5 dealt with changes observed in intrinsic excitability, while Chapter 6 explored the differences in passive and active conductances brought about by sustained depolarisation. Conceptually, the causal structure of the observed effects may be illustrated like this:

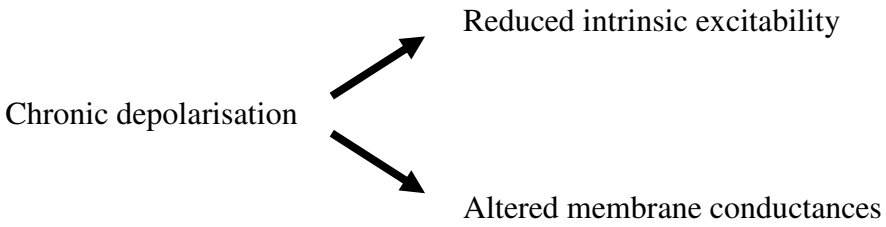

Scientifically, this picture is not particularly interesting because it has little explanatory power; technically, though, this is all that has been achieved so far. In spite of this fact, the subtext for examining the membrane conductances was to provide some account of the underlying causes of the change in intrinsic excitability. What we really want to uncover, then, is the following implication:

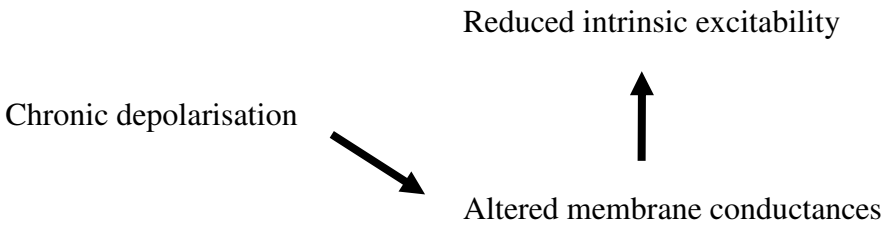

There are several ways to do this in principle. If we could somehow alter the relevant membrane conductances of the cells without chronically depolarising them, and were to observe the same changes in excitability, then evidence for the second causal link would be established. Another route would be to attack the contrapositive statement, in other words, show that preventing a change in intrinsic excitability requires the membrane conductances that have been examined to remain unchanged. Whilst it is difficult to see how an experiment could be designed to probe the latter implication, the former could be addressed using molecular biology techniques to manipulate the expression of ion channels in the cells, perhaps by transfecting cells with mRNA for

leak channels, or interfering with translation of sodium channel subunit expression. This would be technically challenging, however, and it might not be possible to achieve a quantitatively similar conductance profile to that characterised in the chronically depolarised cells. Furthermore, if we assume that the cells are indeed capable of homeostatically regulating their membrane conductances, then an experiment such as this might be confounded by a compensatory response. An easier and arguably more insightful route is to construct a biophysical model of a cell with the known membrane conductance types and densities of control cells. The model can then be used to explore whether a causal link exists between the particular conductance characteristics that were examined, and the intrinsic excitability of the cells.

7.3. Strategy

The explicit goal of this chapter is to parameterise a simplified model of a neuron with the conductance data from Chapter 6, then use the model to examine the relationship between membrane conductances and excitability. An important first step is to construct a model using the conductance data from control cells. If this gives a good approximation of the excitable behaviour of control cells, as captured by the FI curve data, then we can be reasonably confident that the way in which the conductances were classified and measured gives a comprehensive description of the factors underlying excitability.

In addition, an accurate FI curve prediction would engender some confidence that realistic predictions can be made with the model concerning the effect of modifying the conductances. Next, assuming the FI data from control cells can be faithfully reproduced, we can alter the conductance parameters in the control cell model according to the differences observed between the control and treated cell groups in Chapter 6. This allows us to quantify the extent to which the conductance changes account for the alteration in excitability observed experimentally in Chapter 5.

Irrespective of the particular results the model predicts, the process of fitting and analysing the data in this way will tell us two important things: to what extent the conductances examined in the previous chapter govern excitability, and whether the changes observed in these conductances can account for the changes in excitability. In addition, the task ahead will give some insight into whether average conductance data for a population meaningfully represents the characteristics of individual cells – a subtle and important issue that will be addressed in detail in the discussion section of this chapter.

7.4. Choosing an appropriate model

There are many ways of modelling the electrical behaviour of individual neurons and the choice of model typically involves a trade-off between the level of realism that can be achieved with a given model, and the amount of work required to implement the model. In this context 'work' represents several factors, which may be classified as follows:

1. The labour involved in creating the mathematical description of the system. For example, the number of variables and the complexity of the equations in the model.

2. The computational power required to implement the model.

3. The quantity and level of detail of the experimental data required to fit the model parameters.

Factors (1) and (2) are not of concern here because for most approaches, the task of modelling the behaviour of a single neuron with several membrane conductances is neither theoretically demanding, nor computationally expensive. The third factor, however, will need to be considered when constraining the choice of model. Clearly, we do not want an overly simplistic model that we cannot fit to experimental data. On the other hand, we want to make as much use of the data gathered in experiments as possible without overcomplicating the model and resorting to unnecessary guesswork in the process.

What models are available for this task? In order of increasing complexity (and decreasing level of abstraction) the main models of single neurons, and their basic properties, are listed on the following page.

Rate-based models. The input and output of these models is a single real number, usually constrained to a range, which represents 'current' or 'synaptic input', and 'spiking rate', respectively. A single function, usually a sigmoid, describes the response of the model to a given input (Hertz *et al.* 1991).

Integrate-and-fire. In this formalism, membrane potential is typically modelled as the potential difference across a capacitor in series with a resistor (the so-called 'leaky integrate-and-fire' case) – which is equivalent to a single-pole low-pass filter. A threshold value is imposed on the membrane potential such that when the threshold is exceeded, the 'cell' emits a spike, and the membrane potential is reset to some prescribed value. Spikes are therefore discrete events in these models, and do not arise from the dynamics of the equation describing the membrane potential (Koch and Segev 1998).

Reduced state variable models. These use additional state variables besides membrane potential (such as a slowly-varying quantity to model processes like inactivation and calcium dynamics) and can capture phenomena such as rhythmic bursting in addition to having genuine spiking behaviour in their dynamics. They are described as being 'reduced' because they capture important features of conductance based models (described next) but with a reduced number of dynamical variables. The disadvantage of this approach is that the state variables have no direct correspondence with any experimentally measurable quantity. Examples include the Fitzhugh-Nagumo, Morris-Lecar and Izhikevich models (Fitzhugh 1961; Morris and Lecar 1981; Izhikevich 2003).

Conductance-based models. These models originated from Hodgkin and Huxley's seminal study of the squid giant axon (Hodgkin and Huxley 1952d) and are derived from the empirical behaviour of ion-selective voltage-gated conductances in a cell membrane. Ionic reversal potentials for each conductance subtype are included and the gating behaviour is thermodynamically related to membrane potential. This

model is therefore a true biophysical model of an excitable membrane, and all of the parameters correspond to physical quantities that can be determined experimentally.

Stochastic ion channel conductance-based models. Conductance-based models describe ionic conductances as smoothly-varying functions. In reality, the ion channels responsible for these conductances open and close discretely, in a stochastic manner. As single-channel data is now available for many ion channel subtypes it is possible to model the full, stochastic behaviour of a population of individual ion channels in a cell membrane to achieve a level of realism beyond that attainable in conductance-based models. In particular, ion channel noise and random spiking events can occur in these models, whereas ordinary conductance-based models are completely deterministic (Strassberg and Defelice 1993; Schneidman *et al.* 1997; Koch 1999).

Our goal is to relate membrane conductance properties to spiking behaviour, so the first three models in this list are of limited use because they do not explicitly represent membrane conductances. On the other hand, the stochastic ion channel model is clearly too sophisticated: we are using whole-cell current data over a population and are therefore not interested in the effects of individual ion channels, nor do we have single-channel data to fit parameters to. This leaves the conductance-based model as the obvious candidate. However, the details of the implementation need further discussion as there many possible ways to implement such a model.

Conductance-based models can be efficiently simulated using NEURON (Hines and Carnevale 1997), an open-source simulation package that is purposefully designed for detailed single-cell models. NEURON uses the Hodgkin-Huxley formalism for describing ionic conductance kinetics, and the passive electrical behaviour of the cell is approximated using one or more electrically coupled ‘compartments’. This terminology and the theory behind it require further explanation, so the next section will be devoted to a brief review of conductance-based modelling.

7.5. The single-compartment conductance-based model

A cell can be thought of as a boundary between two conducting media, the cytoplasm and the extracellular space. Plasma membrane constitutes the substance of the boundary, and in the absence of ion channels it is an effective electrical insulator. If the resistivity, or, equivalently, the spatial extent of the intracellular and extracellular spaces are ignored, the electrical behaviour of the cell is identical to that of a single capacitor. Taking into account the conductances and reversal potentials due to various ion-selective channels in the membrane introduces a number of resistors in series with EMFs, which are in turn placed in parallel with the membrane capacitance. This circuit is depicted in the schematic in Figure 7.1.

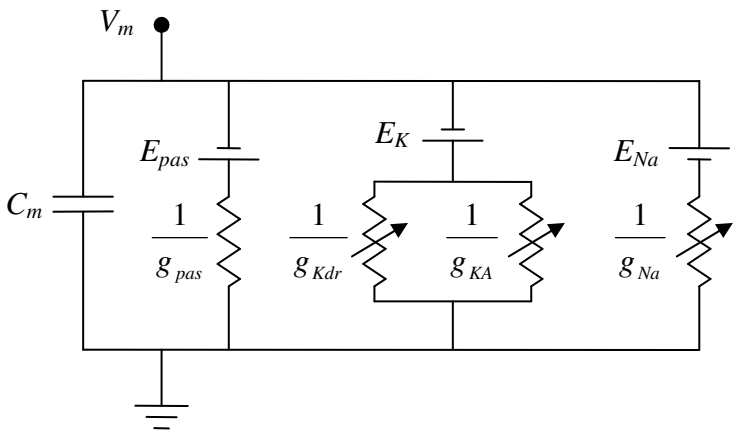

Figure 7.1 A single-compartment conductance-based model

A schematic of the single compartment model. The electrical symbols have their usual meaning and the biophysical parameters are as follows: V_m, membrane potential; C_m, membrane capacitance; E_{pas}, linear IV reversal potential; g_{pas}, linear (passive) IV conductance; E_K, potassium reversal potential; g_{Kdr}, g_{KA}, delayed-rectifier and A-type potassium conductance (both voltage-gated); E_{Na}, sodium reversal potential; g_{Na}, sodium conductance (voltage-gated).

If we were to take the geometry and cytoplasmic resistivity of the cell into account, or indeed any inhomogeneities in the distribution of ionic conductances, we would require more than one compartment to model the cell. Such models are straightforward to construct: each compartment is endowed with trans-membrane conductances as in Figure 7.1, then coupled to neighbouring compartments via a

single resistor representing the cytoplasmic resistance. In this way, a network of compartments can be joined together to take account of the topology of the neuronal processes. The geometry (the physical dimensions of the cell) is dealt with by defining all conductances as conductance densities (conductance per unit area) and assigning a membrane surface area to each compartment.

With the exception of the passive leak conductance, g_{pas}, the conductances in this scheme require relationships to be specified that describe their time-dependence (kinetics) and dependence on membrane potential. This is achieved using the standard Hodgkin-Huxley formalism, and will be exemplified here for a single, hypothetical voltage-dependent membrane conductance for explanatory purposes. The equations and full parameter sets for the actual conductances that will be outlined in subsequent sections and are specified in detail in the appendix.

Consider a voltage-dependent conductance, g_X. The membrane current due to the conductance, I_X, is described by Ohm's law:

$$I_X = g_X(V,t)(V - E_X) \qquad (1.1)$$

Where V is the membrane potential, t is time and E_X the reversal potential associated with X. The voltage- and time-dependence of g_X are made explicit in this equation, but will be omitted from now on. As in Hodgkin and Huxley's original implementation (Hodgkin and Huxley 1952d), Ohm's Law is used to describe the current-voltage relationship instead of the more accurate GHK current equation. This approximation will be used in the modelling work here, and is commonly assumed elsewhere[9].

The functional form of g_X is implicitly defined by solving a system of differential equations that describe the activation and inactivation behaviour of g_X in terms of membrane potential. For illustrative purposes, a single state variable will be used to represent each of these processes. In the original Hodgkin-Huxley model these variables were thought of as describing a population of 'gating particles' that exist in

[9] NEURON uses Ohm's law as standard. The GHK relation can only be implemented by modifying the way NEURON handles membrane currents.

'on' and 'off' states. Denoting the proportion of activation and inactivation particles in the 'on' state by m and h respectively allows us to write the membrane conductance in terms of these proportions:

$$g_X = m^a h^b \bar{g}_X \qquad (1.2)$$

Where $\bar{g}_X$ is the conductance density (maximum conductance) and a and b are integer exponents that are chosen empirically, and may be thought of as the number of independent gating particles associated with each putative ion channel. The proportions, m and n, of particles in 'on' and 'off' states is given by a number between 0 and 1, and assumed to obey thermodynamic laws that describe the state transition of a single particle as a first-order chemical reaction. These reactions and their interpretation as differential equations are as follows:

$$1-m \underset{\beta_m}{\overset{\alpha_m}{\rightleftharpoons}} m \qquad \frac{dm}{dt} = \alpha_m(1-m) - \beta_m m = \frac{m_\infty - m}{\tau_m} \qquad (1.3)$$

$$1-h \underset{\beta_h}{\overset{\alpha_h}{\rightleftharpoons}} h \qquad \frac{dh}{dt} = \alpha_h(1-h) - \beta_h h = \frac{h_\infty - h}{\tau_h} \qquad (1.4)$$

where, $m_\infty = \frac{\alpha_m}{\beta_m + \alpha_m}$, $\tau_m = \frac{1}{\beta_m + \alpha_m}$, $h_\infty = \frac{\alpha_h}{\beta_h + \alpha_h}$, and $\tau_h = \frac{1}{\beta_h + \alpha_h}$

The solutions to equations (1.3) and (1.4) are exponential curves with time-constants τ_m, τ_h and steady-state values m_∞, h_∞ respectively. At each time-step in the simulation, these equations are solved, providing values for m and h, which in turn provides a value for the conductance at that time-step using (1.2).

Crucially, the rate constants of the above reactions, and therefore the steady-state values and time-constants of the gating variables, are voltage-dependent. Data describing this voltage-dependence are found empirically, then fitted to thermodynamic equations that represent the theoretical behaviour of the putative gating particles. The form of these equations is derived from assuming the energy for the forward reaction is supplied by the membrane potential, for example, a rise in

membrane potential may shift the equilibrium of the reaction toward the 'on' state. Hodgkin and Huxley, and subsequently numerous other investigators have fitted empirical conductance data to these equations (for example Connor and Stevens 1971b). This usually requires complete isolation of the conductance type in question and very reliable voltage control of the cell membrane.

Unfortunately, the complete empirical form of the gating kinetics is not accessible from the experimental data available in this study, and would require considerable further work to obtain. However, the necessary data is available from other sources. Particularly useful in this respect are published models of hippocampal neurons that use experimental data from sources which characterised membrane conductances using the same Hodgkin-Huxley formalism as that being implemented here. Migliore *et al.* (1999) provide a comprehensive data set containing the relevant conductance types: fast sodium currents, and A-type and delayed-rectifier-type potassium conductances. In addition, the temperature-dependence of the conductance kinetics is taken account of in these data, so the nominal 20ºC experimental condition can be applied in the model. These three conductances will be included in the single compartment model, along with a linear leak (passive) conductance. Calcium currents, although evident in both control and treated cells, are not included in the model because they were not found to influence excitability markedly when blocked (Chapter 6, Figure 6.14).

	Parameter	Control	Treated	Relative change	Sig.
IV	Slope (nS)	2.30 ± 0.33	4.53 ± 0.38	197 %	*
	E_{rev} (mV)	–49.1 ± 1.9	–56.3 ± 2.2	–7.2 mV	*
Na_V	Peak (pA)	–3777 ± 321	–1537 ± 190	41 %	*
	Peak density (A/F)	47.3 ± 6.6	20.4 ± 2.7	43 %	*
K_V	Total peak (pA)	1684 ± 99	1760 ± 146	104 %	NS
	Total tail (pA)	1135 ± 78	1087 ± 88	96 %	NS
	TEA peak (pA)	428 ± 118	330 ± 49	77 %	NS
	4-AP peak (pA)	733 ± 129	822 ± 85	112 %	NS

Table 7.1: Experimentally measured conductance parameters

Mean peak evoked voltage-gated current amplitudes and linear IV characteristic slope and reversal potential for control and treated cells. Statistically significant differences are denoted by an asterisk in the final column.

7.6. Fitting the model to the data

Ideally, we would fit the model by matching the membrane conductance densities of each conductance type to an experimentally measured value. However, as elaborated upon in the previous chapter, it is hard to accurately measure membrane conductance densities in neurons with extensive processes. Therefore, the approach used here is to construct a single compartment model with the same mean capacitance as the experimental value, then vary the conductance densities to achieve the same peak evoked current over the range of step potentials used experimentally. These experimental data, for control and treated cells, are shown in Table 7.1. For linear leak IV characteristic such a fitting procedure works directly, but for voltage-gated conductances it does not guarantee that the activation profile, as a function of membrane potential, will be the same in the model as in experiments.

To address this issue, evoked currents amplitudes were calculated using the model by subjecting the single compartment to the same family of 500 ms voltage steps as were used in the voltage-gated current experiments of the previous chapter. The peak values for voltage-gated sodium currents, and the peak and tail amplitude of the total

voltage-gated potassium current were fitted to control cell values. Results of this procedure, along with the passive IV fits, are summarised in Table 7.2; the corresponding parameter sets are shown in Table 7.3.

Although it was possible to fit the peak evoked current using the kinetic data of Migliore *et al.* by varying the conductance densities (specified by the $\overline{g}_X$ parameter for conductance *X*), the activation profiles of the evoked currents, as shown in Figure 7.2A, do not fit the control cell data particularly well. To address this, the half-activation parameters of the kinetic equations and several other parameters were modified by hand to achieve a better fit – the details of these modifications are in the appendix. The result of this hand-fitting is shown in Figure 7.2B and will be referred to as 'Model 1'. However, as can be seen in Figure 7.2B, the sodium current profile in this model diverges from control cell data as membrane potential becomes more positive. This could not be remedied by altering the sodium current kinetics, so the sodium reversal potential was instead moved to +170 mV, which is the extrapolated intersection value of the control activation curve with the voltage axis. As discussed in Chapter 6 (Section 6.5), this is unlikely to be a true value of the sodium reversal potential. Rather, it is likely reflect poor voltage control of the region of membrane responsible for conducting the sodium current, such as a axon. Nevertheless, this somewhat artificial fit will be implemented alongside Model 1 as an alternative, called 'Model 2'.

This method of fitting the parameters to the data results in a somewhat 'phenomenological' model of the membrane conductances, but it captures the quantitative aspects that were characterised in experiments. Therefore, any predictions made by the model is completely contingent on the measured conductance data. In addition, provided the spiking behaviour of the control cells is captured by the model, the determination of conductance parameters from differences between control and treated cell data offers a causal link between the effects of chronic depolarisation on conductances and the effects on intrinsic excitability.

We need now to examine whether the control cell spiking behaviour is reproduced by any of the three models. Before proceeding it is worth emphasizing that it is not at all obvious that a faithful prediction will be observed: voltage-clamping a cell 'freezes' the dynamics of the system because the conductances are voltage-gated, and membrane voltage is in turn governed by the state of the conductances. The behaviour of such a dynamical system, even with a handful of variables, is very hard to predict without full knowledge of the parameters of the system, and, as has been made clear throughout this section, we only have limited knowledge of the parameters in this instance.

Current/conductance		Control cells	Model		
			Migliore et al.	Model 1	Model 2
IV	Slope (nS)	2.30 ± 0.33	2.30	2.30	2.30
	E_{rev} (mV)	–49.1 ± 1.9	–49.0	–49.0	–49.0
Na_V	Peak (pA)	–3777 ± 321	–3759	–3737	–3748
	E_{Na} (mV)	?	+55	+55	+170
K_v	Total peak (pA)	1684 ± 99	1691	1634	1634
	Total tail (pA)	1135 ± 78	1150	1103	1103
	E_K (mV)	?	–85	–85	–85

Table 7.2: Fitting conductance and current values

Experimental conductance data from control cells fitted to a single-compartment model. For linear IV characteristic 'Model values' correspond to predictions of the experimental quantity, for example, peak sodium current is measured in the model using the same step potentials as in experiments. 'Model parameters' are the underlying specific conductances and reversal potentials used in the model implementation.

Model conductance parameter		Model		
		Migliore et al.	Model 1	Model 2
$\overline{g}_{pas}$	(S cm^{-2})	2.3×10^{-5}	2.3×10^{-5}	2.3×10^{-5}
E_{pas}	(mV)	–49	–49	–49
$\overline{g}_{Na}$	(S cm^{-2})	1.23×10^{-3}	6.64×10^{-4}	2.75×10^{-4}
E_{Na}	(mV)	+55	+70	+170
$\overline{g}_{Kdr}$	(S cm^{-2})	1.2×10^{-4}	1.3×10^{-4}	1.3×10^{-4}
$\overline{g}_{KA}$	(S cm^{-2})	2.2×10^{-4}	1.7×10^{-4}	1.7×10^{-4}
E_K	(mV)	–85	–85	–85

Table 7.3: Model parameters after fitting

Experimental conductance data from control cells fitted to a single-compartment model. 'Model values' correspond to predictions of the experimental quantity, for example, peak sodium current is measured in the model using the same step potentials as in experiments. 'Model parameters' are the underlying specific conductances and reversal potentials used in the model implementation.

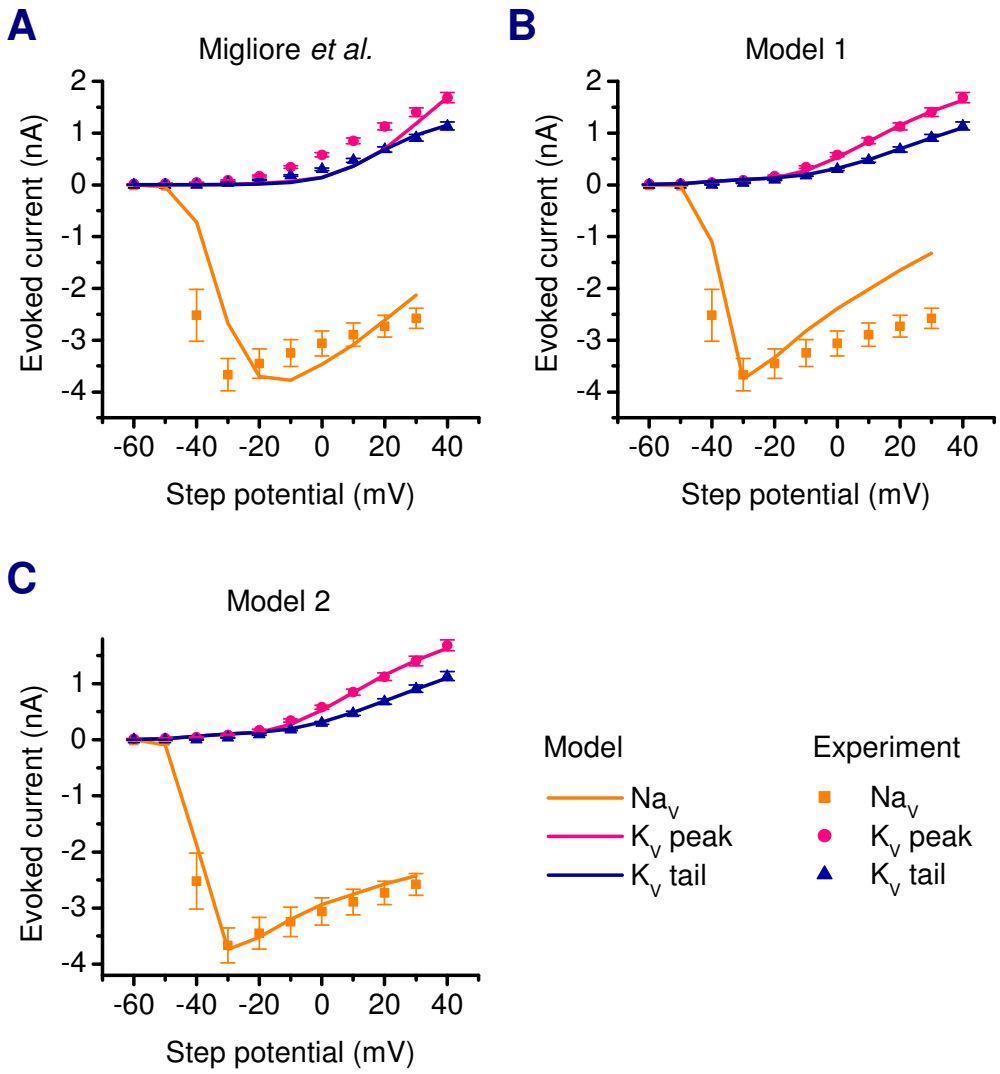

Figure 7.2 Fitting evoked voltage-gated current profiles

Evoked voltage-gated current profiles for sodium (NaV) and peak (KV peak) and tail (KV tail) potassium currents. Potassium currents are the combined contribution of both A-type and delayed rectifier currents in the model. Lines are model fits and symbols are experimental data from control cells. **(A)** A Direct fit of peak current values using the conductance models of Migliore *et al.* without modification. **(B)** Modifying the kinetic equations results in an improved fit. The modified parameters are outlined in the appendix. **(C)** A sodium reversal potential of +170 mV enables a close fit of the sodium current profile that was unattainable by modifying kinetic parameters alone.

7.7. Does the model reproduce the control cell firing properties?

Figure 7.3 compares the result of a 500 ms, 25 pA current injection in a control cell, in a model cell with the kinetic data of Migliore *et al.* and in the two refined models. It is clear from the top right-hand trace that the crude fit of the voltage-clamp data to conductances with the original kinetics left unchanged results in unstable membrane potential dynamics. Before the depolarising current is injected, a spontaneous action potential is fired and the membrane falls into depolarisation block in this particular instantiation of the model. Models 1 and 2, however, produce a train of action potentials that are comparable in number to the control cell, and barely distinguishable from one another in their form.

Evoked currents in Model 1 are compared to control cells in Figure 7.4A (those produced by Model 2 were indistinguishable, apart from the magnitude of the sodium currents, which have already been quantified in Figure 7.2C). The profile of the currents is comparable to control cells. In the case of the potassium current, the total voltage-gated potassium current is compared because it is not known whether the pharmacological definition of the experimental data (into TEA and 4-AP-sensitive currents) corresponds directly to the A-type and delayed-rectifier currents in the model. In addition, Figure 7.4B exhibits the contribution of the voltage-gated sodium and potassium currents to action potential generation in the model. Such data is impossible to obtain experimentally, so these traces are only included for illustrative purposes.

The similarity between both refined models and the control cell data remains apparent in the construction of an FI curve in Figure 7.5B. Apart from slight differences in the number of spikes predicted by the models for large current injections, the forms of the FI curves are qualitatively and quantitatively similar to the mean control cell curve, as summarised in Table 7.4. The current threshold of the control cells is predicted by both models to within 10 pA, and the form of the FI curve, quantified in terms of goodness-of-fit and slope, is quite similar in control cells and in the models (the models' RMS error is approximately ± 1 spike over the entire current range). Furthermore, the fact that the spiking characteristics of Models

1 and 2 show such similarity to one another indicates that varying the sodium reversal potential in the range +70 to +170 mV has little effect on spiking behaviour.

However, there are several important differences between the control cells and the functional models. The current threshold is slightly higher in the model – this may be accounted for in the differences that are evident in the resting membrane potential of the model cells, which are several millivolts more hyperpolarised than control cells (−50.6 ± 1.4 mV for control, −54.4 mV in Model 1 and −54.3 mV in Model 2). Also, the input resistance prediction of the models is smaller than that measured in control cells – a difference that is also likely to increase the current threshold (760 ± 100 MΩ in control cells compared to 540 MΩ in Models 1 and 2).

Although it is probably possible to remedy these differences by altering the activation kinetics of the voltage-gated conductances further, or the reversal potential and slope conductance of the passive IV characteristic, such a move would contradict the spirit of this investigation: we want to examine to what extent the voltage-clamp data, in isolation, is able to explain the current-clamp data using as simple a model as possible. Therefore, we will use Models 1 and 2 as models for control cell behaviour in what follows, without any further modifications. Given the differences that are present, it is unreasonable to expect precise predictions from the model in what follows. Rather, we will concentrate on the relative precision with which several alternative parameter sets fit the excitability profile of treated cells and view the scenario that best accounts for the change as the most likely.

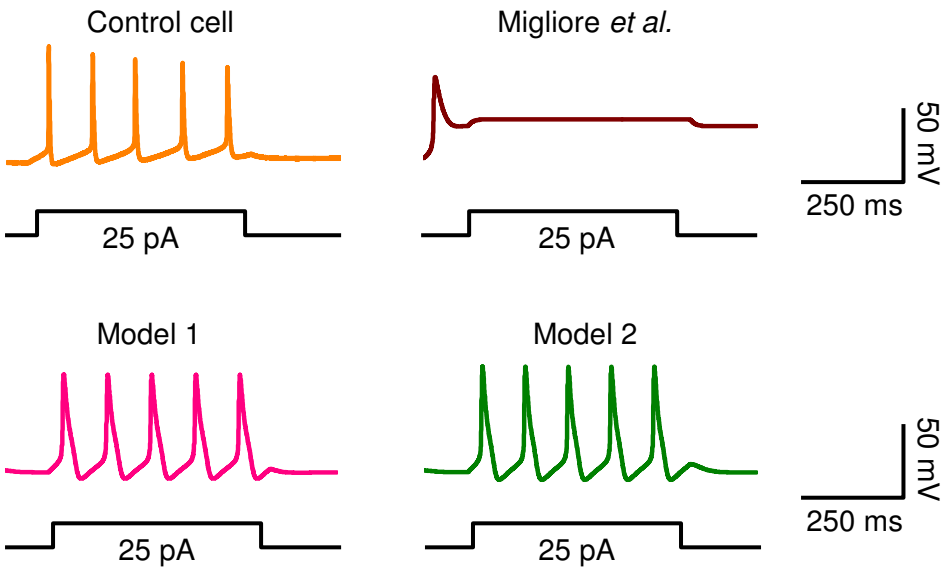

Figure 7.3: Current-clamp behaviour of the model

Example membrane voltage traces showing the result of a 500 ms, 25 pA current pulse in a control cell and in the model with voltage-gated currents fitted to mean control cell values for the three different parameter sets.

Parameter	Control cells	Model 1 prediction	Model 2 prediction
Current threshold (pA)	3.0 ± 1.14	10	9
FI slope (spikes/pA)	0.16 ± 0.01	0.15	0.16
Resting potential (mV)	–50.6 ± 1.4	–54.4	–54.3
Input resistance (MΩ)	760 ± 100	540	540
FI curve RMS error (spikes)		1.28	1.16

Table 7.4: Performance of the control cell models

Predictions of the control cell model compared to experimental control cell data. FI curves were constructed using the model in exactly the same way as in experiments, using 500 ms pulses of depolarising current in the range 5 to 50 pA. The RMS error for the predicted FI curve is calculated with respect to each control data point using the corresponding model value.

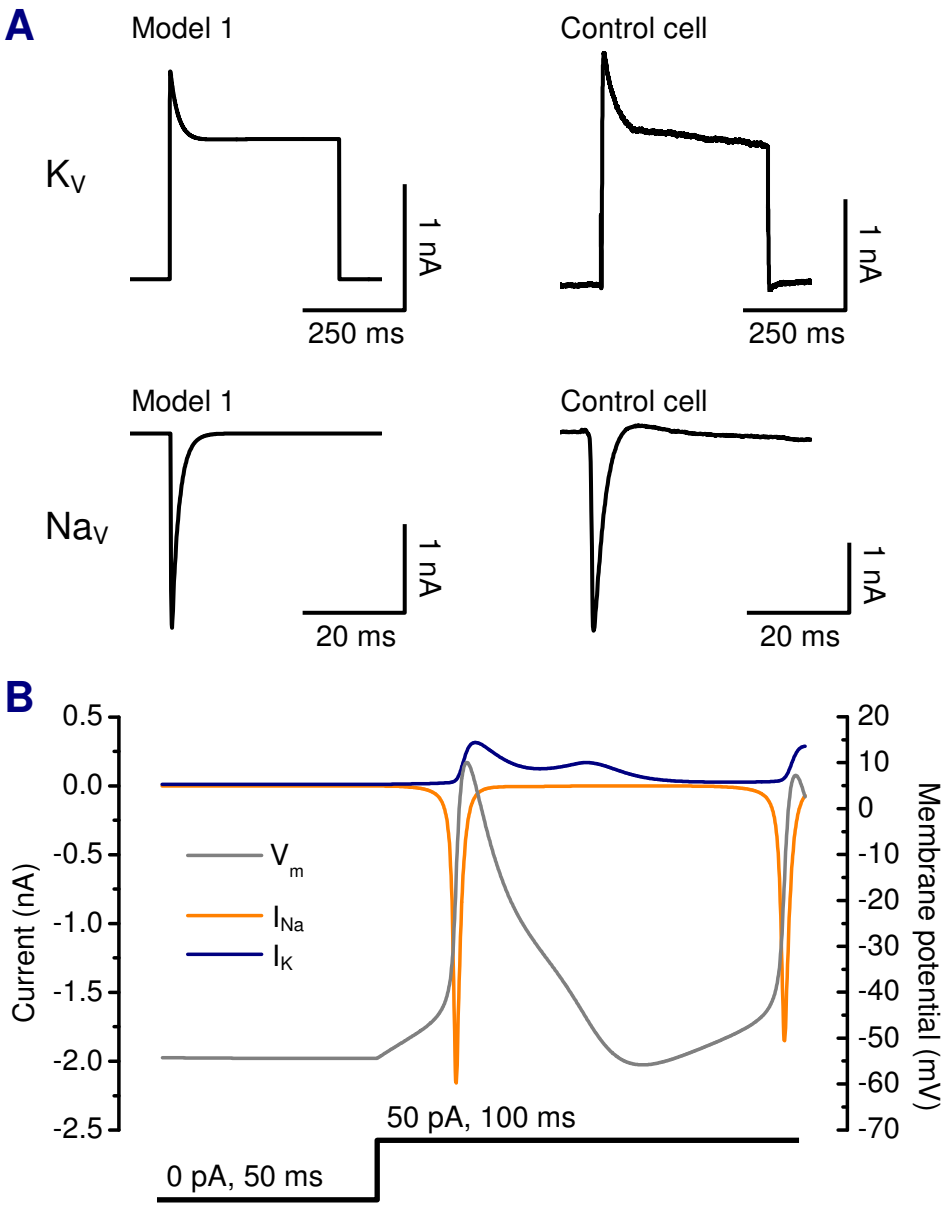

Figure 7.4: Membrane currents and excitable behaviour in the model

(A) Evoked voltage-gated potassium (top) and sodium (bottom) currents in a single-compartment model with 'Model 1' parameter set. To the right are example potassium and sodium currents from a control cell. Sodium currents in both the model and the experiment are the result of a step potential from –80 to 0 mV; potassium currents were evoked using a step potential from –80 to +40 mV. **(B)** A current-clamp recording in the model showing the response of the membrane potential (V_m) to a 50 pA-current step. The underlying sodium (I_{Na}) and potassium (I_K) currents are overlaid for illustrative purposes.

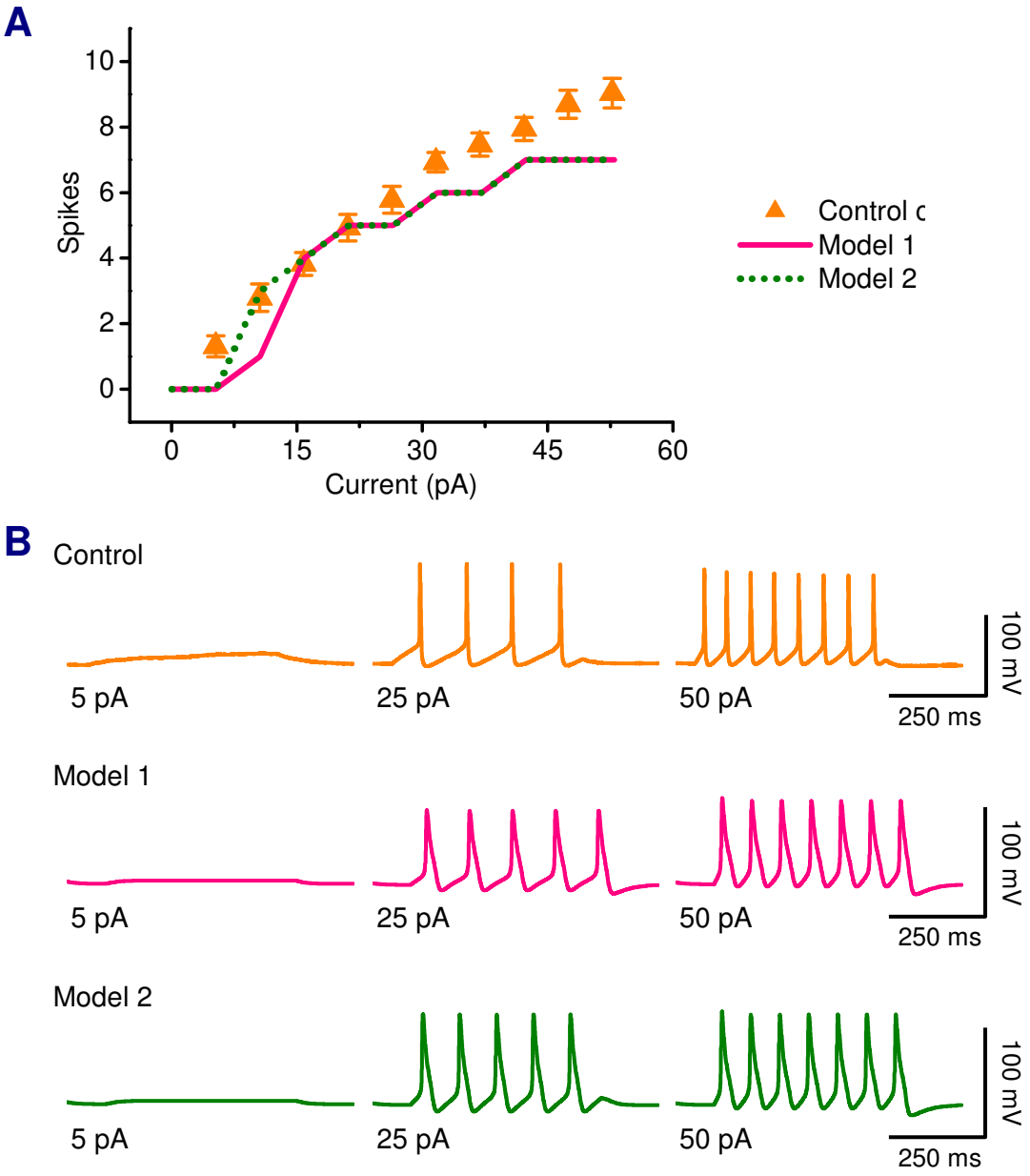

Figure 7.5: Mean control cell FI curve vs. model FI curves

(A) FI data from control cells recorded at 8-11 DIV (symbols) compared to FI curves generated by the single compartment models. **(B)** Example membrane voltage traces showing the result of a 500 ms, 25 pA current pulse in a control cell and in the model with voltage-gated currents fitted to mean control cell values for the three different parameter sets.

7.8. Do conductance changes in the model predict the changes in excitability observed *in vitro*?

Now that the control cell behaviour has been captured in a model to reasonable extent, we are in a position to examine the effect of modifying conductance parameters on spiking behaviour. As the control cell model behaviour is only a modest approximation to that of the population, we shall quantify the quality of prediction in terms of the most prominent changes that were observed to occur in treated cells, in particular the shift in current threshold, and the overall FI curve fit (RMS error).

Table 7.5 shows several model scenarios that will be used to mimic the effect of chronic depolarisation. The 'treated' scenario includes the major changes that were observed to occur in the passive IV characteristic and the sodium currents. Two complementary scenarios, 'A' and 'B', address these changes individually. By comparing the predicted FI curve of the models with each of these scenarios with the treated cell FI curve, we can see whether the conductance changes taken together, or in isolation, provide the best explanation of the observed changes in excitability.

Before examining excitability, it is important to check that the 'treated' parameter set in Table 7.5 gives reasonable predicted values of the peak voltage-gated current and IV characteristic observed in treated cells. Indeed, applying these parameters results in passive IV characteristics and peak evoked current that are comparable to those measured in treated cells (close to being within one standard error in each case, Table 7.6).

As for intrinsic excitability, Figure 7.6 shows the FI curve predictions that result from applying the 'Treated' parameter set to the membrane conductances in Models 1 and 2. Although the precise shape of the FI curve is quite different from the mean treated FI curve, the average slope of the predicted FI curve (calculated by fitting a straight line to the non-zero points) and the current threshold prediction compare favourably to the treated cells. The quantification of this result is presented in Table 7.7 along with input resistance and resting potential predictions. Example current injection traces form a treated cell and the corresponding model traces are compared in Figure 7.6B.

Importantly, the alternative scenarios, A and B, give markedly different predictions of the FI curve in both Models 1 and 2 when compared to the treated cells, and when compared to the 'Treated' model scenario (Figure 7.7). Current threshold in the treated cells was 57.0 ± 6.0 pA, and in Models 1 and 2 the predicted values were +46 and +48 pA, respectively. Although these values differ from the experimental value by more than one standard error, Scenario A (sodium current density at 40% of control values, IV characteristic equal to control) gives values of +20 and +19 pA, whilst Scenario B (sodium current density equal to control, IV characteristic equal to treated cells) predicts a current thresholds of +38 and +34 pA. In addition, the RMS error in the FI curve prediction for both models was higher in Scenarios A and B than in the treated scenario (>3 spikes, compared to 2.46 and 2.36 for Models 1 and 2 in the 'treated' scenario).

Finally, as anticipated, the passive IV characteristic was found to have a greater effect on the input resistance in the models than the sodium conductance density. Both models in the 'treated' scenario, and Scenario B, had input resistances of 270 MΩ (close to the treated cell value of 300 ± 30 pA), whereas Scenario A produced an input resistance of 540 MΩ, a value identical to the control cell models.

Model control value	Scenario values		
	Treated	A	B
$\overline{g}_{pas}$	$\overline{g}_{pas} \times 2$	$\overline{g}_{pas}$	$\overline{g}_{pas} \times 2$
E_{pas}	–56.0 mV	E_{pas}	–56.0 mV
$\overline{g}_{Na}$	$\overline{g}_{Na} \times 0.4$	$\overline{g}_{Na} \times 0.4$	$\overline{g}_{Na}$
$\overline{g}_{Kdr}$	$\overline{g}_{Kdr}$	$\overline{g}_{Kdr}$	$\overline{g}_{Kdr}$
$\overline{g}_{KA}$	$\overline{g}_{KA}$	$\overline{g}_{KA}$	$\overline{g}_{KA}$

Table 7.5: Model parameter sets

Parameter sets for investigating the predicted FI characteristics of the model cell altered subthreshold IV characteristic and sodium conductance. All values are relative to model control cell values. The 'Treated' scenario has equivalent conductances to those measures in experimental treated cells (see Table 7.1). Scenarios A and B address the effect of altering these conductances separately. All parameters not listed in this table are kept constant in each implementation of the model.

Current/conductance		Treated cells	'Treated' scenario	
			Model 1	Model 2
IV	Slope (nS)	4.53 ± 0.38	4.53	4.53
	E_{rev} (mV)	–56.3 ± 2.2	–56.3	–56.3
Na_V	Peak (pA)	–1537 ± 190	–1779	–1386
	E_{Na} (mV)	?	+55	+170
K_v	Total peak (pA)	1760 ± 146	1634	1634
	Total tail (pA)	1087 ± 88	1103	1103
	E_K (mV)	?	–85	–85

Table 7.6: Conductance and current values for the 'Treated' scenario

Experimental conductance data from treated cells compared with the corresponding data in Models 1 and 2 after applying the 'Treated' scenario parameter set.

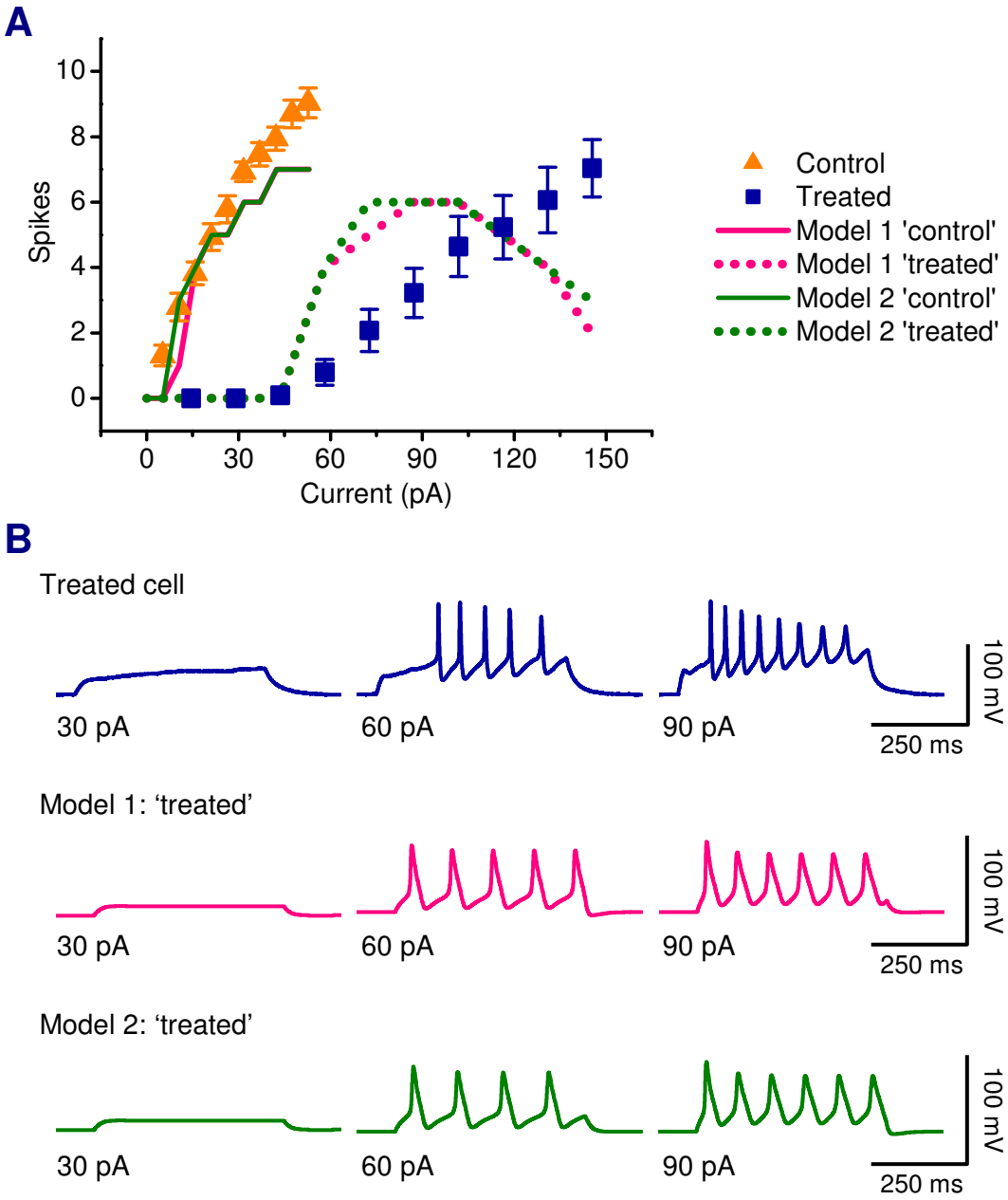

Figure 7.6: Model FI curve predictions

(A) FI curves constructed in the model with control and 'Treated' parameter sets compared to experimental FI curves from control (8-11 DIV) and treated (15 mM KCl, 8-11 DIV) cells. (B) Example current-clamp traces from a treated cell and the model cell counterparts.

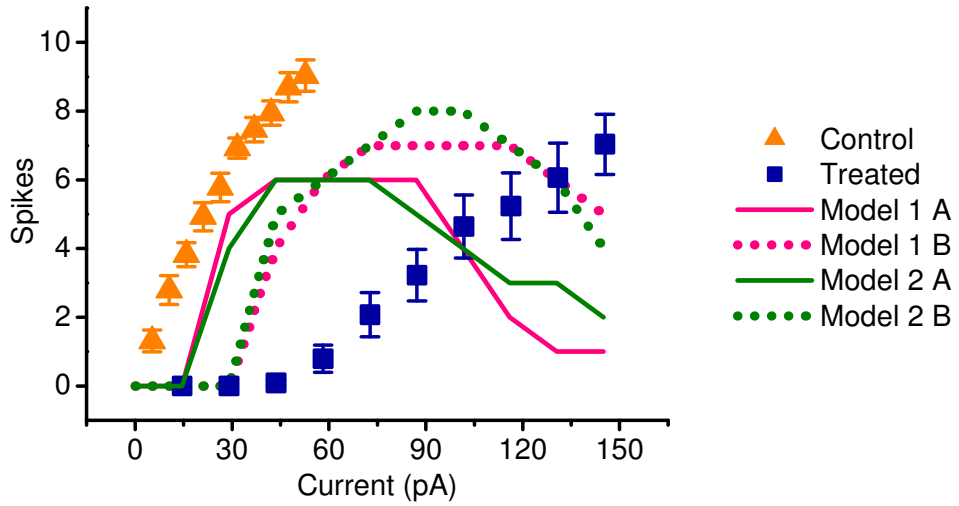

Figure 7.7: FI curve prediction for Scenarios A and B

FI curve model predictions obtained using Scenario A and B parameter sets, compared to control and treated cells.

Parameter	Treated cells	Model (Scenario)					
		(Treated)		(Scenario A)		(Scenario B)	
		1	2	1	2	1	2
Current threshold (pA)	57.0 ± 6.0	46	48	20	19	38	34
FI slope (spikes/pA)	0.07 ± 0.02	0.07	0.10	0.07	0.10	0.07	0.10
Resting potential	–53.0 ± 2.0	–58.1	–58.1	–54.6	–54.6	–58.1	–58.1
Input resistance	300 ± 30	270	270	540	540	270	270
Predicted FI curve RMS error (spikes)		2.46	2.36	4.28	3.70	3.06	3.49

Table 7.7: Model predictions for the treated cell condition

Intrinsic characteristics of treated cells compared with model predictions for all three scenarios defined in Table 7.1 implemented in Models 1 and 2.

7.9. Discussion

In this chapter I have taken a quantitative characterisation of two aspects of the effects chronic depolarisation has on the electrophysiological properties of neurons and attempted to relate them using a model. The basic interpretation of the outcome of this work is that the results are consistent, in the sense that the observed changes in membrane conductances of depolarised cells do indeed predict the observed changes in excitability relative to control cells.

Furthermore, models using a parameter set that represents conductance data from treated cells, with both linear IV characteristic and sodium conductance density altered relative to control cell values, provided the best prediction of the average treated cell FI curve. Models that implemented only one of these differences, embodied in Scenarios A and B, gave far worse predictions overall. This suggests that the changes in both sodium conductance and passive IV characteristic together are required to explain the shift in the FI curve observed in chronically depolarised cells.

There are, however, obvious discrepancies between the model behaviour and the experimental data, and, regardless of the extent to which one considers modelling to be a valid method, it is extremely important to interpret the model predictions with care. Input resistance was markedly lower in the control cell models, compared to the experimental data. This might be due to the presence of additional conductances in the neurons that are not accounted for in the model, or to the approximate nature of the single-compartment assumption, or systematic experimental error (caused, perhaps, by access resistance), or a combination of these factors. Also, resting membrane potentials were consistently different in the models when compared to the experimental values. This can only be put down to discrepancies between the conductance properties of the model compared to the real cells.

It would be straightforward to expand these observations into a piecemeal analysis of the differences and similarities between the models and the data, but such an endeavour is unlikely to be illuminating. Just as it is important to use an appropriate level of detail when parameterising models, it is also important to decide when

comparisons of model predictions with real data are pushing the approximate nature of the model to its limit. For example, it was difficult to arrive at a satisfactory way of defining FI slope in the model. In the case of the control cell models, the FI curves are relatively linear, so a straight line fit to the nonzero data points (as used in experiments) is appropriate. However, the other model scenarios produced highly non-linear FI curves (as can be seen in Figure 7.6 and Figure 7.7). For the sake of consistency, a naïve linear fit was applied to these curves in the same way, but it can hardly be taken to be representative of the precise form of the curve. Issues such as this suggest that highly detailed analysis of the model, and perhaps the experimental data over a population, is somewhat superfluous. The model is useful as a reasoning tool for comparing hypothetical scenarios and discriminating between extremes. Detailed predictions, included for completeness, should be interpreted in this light.

Considering these caveats, it is not unreasonable to question the motivation for applying the modelling approach to this study in the first place. Therefore, I have a duty to provide an answer to questions of this kind. At its best, a model is a concise and quantitative expression of our understanding of observed phenomena. At its worst, a model represents a misleading caricature of the system we are studying. What determines where a given model stands with respect to these two extremes is the applicability of the model to the data available, and the nature of the underlying assumptions made in the model implementation. In respect of the former, a conductance-based model was chosen because FI curves and evoked currents translate directly to quantities that can be identified in the model. Regarding the latter, care has been taken to be explicit about the assumptions being made in this work so far. However, it is useful to summarise the assumptions here:

1. The mean electrical characteristics of a population of cells with complex morphology can be approximated using an equivalent single-compartment.

2. Representative behaviour of a population of neurons can be obtained from a model of a single cell using mean data from that population.

3. The conductances chosen for the model parameterisation are sufficient to dictate the excitable behaviour of any given cell.

Strictly speaking, assumption (1) does not hold in general, but we are somewhat forced to adopt it here. Detailed morphological data were not gathered from the cultured cells, nor was it practical to attempt to measure the distribution of ionic conductances over the cell membrane. Even if these properties were to be measured, an appropriate 'average cell' is troublesome to define (Marder and Goaillard 2006) – although for a purely passive membrane the problem was solved by Wilfred Rall in the form of the 'equivalent cylinder' (Rall 1962). Indeed, part of the motivation for the work in this chapter was to see how good an approximation a single compartment can provide for the excitability data presented in Chapter 5, and this brings us to the second assumption.

It is not necessarily the case that average conductance data represents average spiking behaviour (Foster *et al.* 1993; Beer *et al.* 1999; Golowasch *et al.* 2002; Prinz *et al.* 2004). We can be explicit about the meaning of this assertion: consider the FI curve as a function of input current and all the conductance parameters in the model:

let firing rate, $f(I) = F(I, \theta_1, \ldots, \theta_p)$,

for a given cell, *i*, let $f_i(I) = F(I, \theta_{i,1}, \ldots, \theta_{i,p})$,

where the $\theta_{x,x}$ are conductance parameters. The firing rate function is non-linear in the these parameters, in other words:

$$F(I, a\theta_{i,1} + b_1, \ldots, a\theta_{i,p} + b_p) \quad \neq \quad aF(I, \theta_{i,1}, \ldots, \theta_{i,p}) + \sum_j F(b_j)$$

in general. This can be appreciated by considering the effect that halving the sodium conductance density had on the FI curve in Scenario A: the resulting curve was not equal to a scalar multiple of the control FI curve (compare Figure 7.5 and Figure 7.7). The non-linearity of the FI relation has important implications for calculating averages. By calculating the mean FI curve over a population of *N* cells, we are calculating the following quantity,

$$\overline{F}(I) \quad = \frac{1}{N} \sum_{i=1}^{N} f_i(I).$$

However the FI curve obtained using the mean conductance parameters over the same population is given by:

$$F(I,\overline{\theta}_1,\ldots,\overline{\theta}_p)\text{, where } \overline{\theta}_i = \frac{1}{N}\sum_{j=1}^{N}\theta_{i,j}\ .$$

The non-linearity of F means that these two quantities need not be equal, in other words,

$$\overline{F}(I) \quad \neq \quad F(I,\overline{\theta}_1,\ldots,\overline{\theta}_p)$$

in general. This is illustrated in a concrete example using the model in Figure 7.8. Three different values of the maximal sodium conductance are implemented and FI curves generated in each case Figure 7.8A. If these curves are averaged directly (black curve in Figure 7.8B) the resulting mean FI curve is different from the curve obtained from implementing the arithmetic mean of the three conductances in the model directly (Orange broken line in Figure 7.8B). In this example, the three values are in geometric progression, differing by a factor of 2 in each case. Even when this distribution of values is taken into account by using the geometric mean as the model parameter, the resulting FI curve still differs from the mean curve. Importantly, the current threshold prediction is different in all three cases in Figure 7.8B.

This is why it was important to compare the model predictions to control FI data before manipulating the conductance parameters further. If the model failed to reproduce the mean control FI curve, severe doubts concerning the validity of any further inferences would be raised. The fact that a reasonable prediction of control cell behaviour was achieved suggests that modestly accurate results can be obtained by pooling data, but it is important to understand the quantitative reasons for this. Exploring this problem further in a more general setting would undoubtedly be valuable. However, some insight has been gained into the nature of general problem by applying the modelling approach to specific questions in this study.

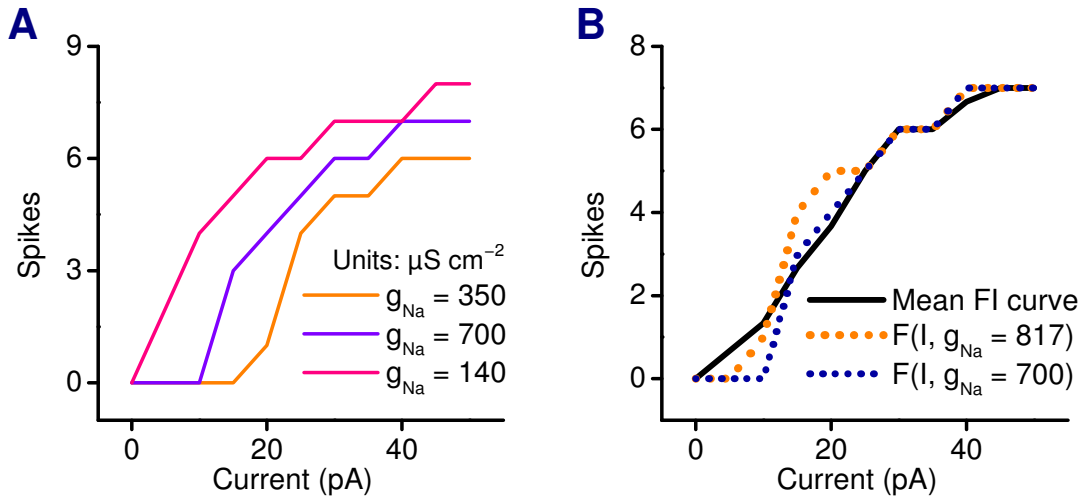

Figure 7.8: An example of the averaging problem

(A) Three values of maximum sodium conductance are implemented independently in the single compartment model (Model 1) and FI curves are constructed using the model. **(B)** Mean FI curve (black trace) and FI curves generated in the model using the arithmetic mean (g_{Na} = 817 μS cm^{-2}) and the geometric mean (g_{Na} = 700 μS cm^{-2})

Indeed, the problem of averaging this kind of data is well known, and interesting in its own right. Relatively recent work (Golowasch *et al.* 2002) gives an explicit example of the failure of averaging in a theoretical setting, by showing that parameter sets for a given spiking behaviour can be convex, so the average value of the parameters lies outside the set, yielding distinct behaviour when implemented. Such work raises questions that go beyond this work, and indeed, beyond electrophysiology. Many biological systems have complex, non-linear behaviour, yet the practice of reporting of results as mean values with standard errors is universal. Of course, our present ignorance of many of the details of biological processes such as cell metabolism means that descriptive statistics of this kind are often all that can measured and interpreted. However, it is probably a good idea to be watchful for situations when averaging makes little sense, and for opportunities to conduct a deeper analysis of quantitative relationships in biology when the appropriate data are available.

Third among the list of assumptions is the claim that the membrane conductances that were measured in Chapter 6 are somehow sufficient to capture the important

aspects of excitability in the cells. The choice of conductances, as indicated in Chapter 6, was not arbitrary, and rested to a large extent on early work in this field, (in particular, Connor and Stevens 1971b). Connor and Stevens' paper is particularly illuminating because they attack the problem of reconstructing spiking behaviour from whole-cell voltage-clamp data in neurons. In particular, the study in question uses very similar conductance types to those used here: a linear leak, voltage-gated sodium and A-type and delayed-rectifier potassium conductances. The level of accuracy achieved in predicting the repetitive firing behaviour using only these conductances is remarkable. Of course, the present study differs from theirs in several important ways: firstly, measurements and predictions were made from a single cell; secondly, the cell in question devoid of processes and therefore easy to voltage-clamp; and thirdly, the cell was from a gastropod and could be maintained at a low temperature where slow ion channel kinetics permit very accurate measurements of the membrane currents.

At this juncture it is worth reiterating the point that there are more membrane conductance types than those that are classified and measured in this study, and a better model of intrinsic excitability can undoubtedly be achieved if additional conductance data were to be gathered and implemented. The practicality of such an endeavour might turn out to be prohibitive, however, if one were to attempt to do this for individual cells. Not only would the range of stimulation protocols require a long and physically detrimental recording to be performed on each cell, but the range of pharmacological agents required to isolate the various conductances might be impractical to administer.

There are more immediate and tractable questions raised in this chapter that could be addressed with further work. For example, a detailed quantitative analysis of the parameter space of conductance based models could be performed using simplified kinetic equations. Parameter space studies exist in the literature (LeMasson *et al.* 1993; Goldman *et al.* 2001), but these use kinetic data that is based on empirical measurements. Simplifying the voltage-dependence of ionic currents, for example, by approximating the underlying activation variable behaviour with single Boltzmann or exponential curves, the size of the total parameter space would be

reduced, and therefore more amenable to systematic analysis.

Another interesting question that could be tackled with a modest amount of modelling work is the issue of averaging intrinsic properties and conductance parameters. Single-compartment models could be assigned conductance parameters at random, from populations with fixed mean and variance. Average FI curves from this population would be straightforward to obtain. This would provide a quantitative picture of how closely population means in conductance parameters space map onto mean FI curves. Indeed, this approach could be applied to the control and treated cell populations in this study, because estimates of the mean and variance of several conductance parameters are readily available.

A final, and somewhat philosophical point remains to be made concerning the motivation for attempting to model the experimental observations. Had the experimental data been offered in the absence of the modelling work, it might have been tempting to present the conductance data as a full explanation for the changes in excitability. It might also have been tempting to surmise that the kind of model constructed here would be trivial to implement, and would offer a trivial contribution to the study – a mere confirmation of our physiological intuition. The work in this chapter shows that this is not so, and therefore affords us the opportunity to appreciate subtleties in the experimental data that are not apparent from the purely experimental perspective.

References

Abbott, L. F. and Nelson, S. B. (2000). *Synaptic plasticity: taming the beast*. Nat Neurosci **3 Suppl**: 1178-83.

Adrian, E. D. and Zotterman, Y. (1926). *The impulses produced by sensory nerve-endings: Part II. The response of a Single End-Organ*. J Physiol **61**(2): 151-71.

Aizenman, C. D., Akerman, C. J., Jensen, K. R. and Cline, H. T. (2003a). *Visually driven regulation of intrinsic neuronal excitability improves stimulus detection in vivo*. Neuron **39**(5): 831-42.

Aizenman, C. D., Huang, E. J. and Linden, D. J. (2003b). *Morphological correlates of intrinsic electrical excitability in neurons of the deep cerebellar nuclei*. J Neurophysiol **89**(4): 1738-47.

Aizenman, C. D. and Linden, D. J. (2000). *Rapid, synaptically driven increases in the intrinsic excitability of cerebellar deep nuclear neurons*. Nat Neurosci **3**(2): 109-11.

Armano, S., Rossi, P., Taglietti, V. and D'Angelo, E. (2000). *Long-term potentiation of intrinsic excitability at the mossy fiber-granule cell synapse of rat cerebellum*. J Neurosci **20**(14): 5208-16.

Armstrong, C. M. and Bezanilla, F. (1973). *Currents related to movement of the gating particles of the sodium channels*. Nature **242**(5398): 459-61.

Armstrong, C. M. and Hille, B. (1998). *Voltage-gated ion channels and electrical excitability*. Neuron **20**(3): 371-80.

Armstrong, D. L. (1989). *Calcium channel regulation by calcineurin, a Ca2+-activated phosphatase in mammalian brain*. Trends Neurosci **12**(3): 117-22.

Ascher, P. and Nowak, L. (1988). *The role of divalent cations in the N-methyl-D-aspartate responses of mouse central neurones in culture*. J Physiol **399**: 247-66.

Banker, G. and Goslin, K. (1998). *Culturing nerve cells*. Cambridge, Mass. ; London, 2nd ed., MIT Press.

Barish, M. E. (1991). *Increases in intracellular calcium ion concentration during depolarization of cultured embryonic Xenopus spinal neurones*. J Physiol **444**: 545-65.

Barish, M. E. (1998). *Intracellular calcium regulation of channel and receptor expression in the plasmalemma: potential sites of sensitivity along the pathways linking transcription, translation, and insertion*. J Neurobiol **37**(1): 146-57.

Barish, M. E. and Mansdorf, N. B. (1991). *Development of intracellular calcium responses to depolarization and to kainate and N-methyl-D-aspartate in cultured mouse hippocampal neurons*. Brain Res Dev Brain Res **63**(1-2): 53-61.

Beer, R. D., Chiel, H. J. and Gallagher, J. C. (1999). *Evolution and analysis of model CPGs for walking: II. General principles and individual variability*. J Comput Neurosci **7**(2): 119-47.

Beggs, J. M. and Plenz, D. (2003). *Neuronal avalanches in neocortical circuits*. J Neurosci **23**(35): 11167-77.

Bekkers, J. M. (2000). *Properties of voltage-gated potassium currents in nucleated patches from large layer 5 cortical pyramidal neurons of the rat*. J Physiol **525 Pt 3**: 593-609.

Bekkers, J. M., Richerson, G. B. and Stevens, C. F. (1990). *Origin of variability in quantal size in cultured hippocampal neurons and hippocampal slices*. Proc Natl Acad Sci U S A **87**(14): 5359-62.

Bekkers, J. M. and Stevens, C. F. (1989). *NMDA and non-NMDA receptors are co-localized at individual excitatory synapses in cultured rat hippocampus*. Nature **341**(6239): 230-3.

Bekkers, J. M. and Stevens, C. F. (1991). *Excitatory and inhibitory autaptic currents in isolated hippocampal neurons maintained in cell culture*. Proc Natl Acad Sci U S A **88**(17): 7834-8.

Bekkers, J. M. and Stevens, C. F. (1993). *NMDA receptors at excitatory synapses in the hippocampus: test of a theory of magnesium block*. Neurosci Lett **156**(1-2): 73-7.

Bekkers, J. M. and Stevens, C. F. (1995). *Quantal analysis of EPSCs recorded from small numbers of synapses in hippocampal cultures*. J Neurophysiol **73**(3): 1145-56.

Bekkers, J. M. and Stevens, C. F. (1996). *Cable properties of cultured hippocampal neurons determined from sucrose-evoked miniature EPSCs*. J Neurophysiol **75**(3): 1250-5.

Ben-Ari, Y. (2002). *Excitatory actions of gaba during development: the nature of the nurture*. Nat Rev Neurosci **3**(9): 728-39.

Ben-Ari, Y., Cherubini, E., Corradetti, R. and Gaiarsa, J. L. (1989). *Giant synaptic potentials in immature rat CA3 hippocampal neurones*. J Physiol **416**: 303-25.

Bender, R. A. and Baram, T. Z. (2008). *HCN channels in developing neuronal networks*. Prog Neurobiol.

Bennett, M. V., Hille, B. and Obara, S. (1970). *Voltage threshold in excitable cells depends on stimulus form*. J Neurophysiol **33**(5): 585-94.

Beurrier, C., Congar, P., Bioulac, B. and Hammond, C. (1999). *Subthalamic nucleus neurons switch from single-spike activity to burst-firing mode*. J Neurosci **19**(2): 599-609.

Bi, G. Q. and Poo, M. M. (1998). *Synaptic modifications in cultured hippocampal neurons: dependence on spike timing, synaptic strength, and postsynaptic cell type*. J Neurosci **18**(24): 10464-72.

Bliss, T. V. and Collingridge, G. L. (1993). *A synaptic model of memory: long-term potentiation in the hippocampus*. Nature **361**(6407): 31-9.

Bowery, N. G., Hill, D. R., Hudson, A. L., Doble, A., Middlemiss, D. N., Shaw, J. and Turnbull, M. (1980). *(-)Baclofen decreases neurotransmitter release in the mammalian CNS by an action at a novel GABA receptor*. Nature **283**(5742): 92-4.

Braun, A. P. and Schulman, H. (1995). *The multifunctional calcium/calmodulin-dependent protein kinase: from form to function*. Annu Rev Physiol **57**: 417-45.

Brette, R., Piwkowska, Z., Monier, C., Rudolph-Lilith, M., Fournier, J., Levy, M., Fregnac, Y., Bal, T. and Destexhe, A. (2008). *High-resolution intracellular*

recordings using a real-time computational model of the electrode. Neuron **59**(3): 379-391.

Brewer, G. J., Torricelli, J. R., Evege, E. K. and Price, P. J. (1993). *Optimized survival of hippocampal neurons in B27-supplemented Neurobasal, a new serum-free medium combination*. J Neurosci Res **35**(5): 567-76.

Brickley, S. G., Revilla, V., Cull-Candy, S. G., Wisden, W. and Farrant, M. (2001). *Adaptive regulation of neuronal excitability by a voltage-independent potassium conductance*. Nature **409**(6816): 88-92.

Buckler, K. J., Williams, B. A. and Honore, E. (2000). *An oxygen-, acid- and anaesthetic-sensitive TASK-like background potassium channel in rat arterial chemoreceptor cells*. J Physiol **525 Pt 1**: 135-42.

Buonomano, D. V. (1999). *Distinct functional types of associative long-term potentiation in neocortical and hippocampal pyramidal neurons*. J Neurosci **19**(16): 6748-54.

Bures, J., Buresova, O. and Krivanek, J. (1984). *The meaning and significance of Leao's spreading depression*. An Acad Bras Cienc **56**(4): 385-400.

Burgess, N., Barry, C. and O'Keefe, J. (2007). *An oscillatory interference model of grid cell firing*. Hippocampus **17**(9): 801-12.

Busch, E., Gyngell, M. L., Eis, M., Hoehn-Berlage, M. and Hossmann, K. A. (1996). *Potassium-induced cortical spreading depressions during focal cerebral ischemia in rats: contribution to lesion growth assessed by diffusion-weighted NMR and biochemical imaging*. J Cereb Blood Flow Metab **16**(6): 1090-9.

Caeser, M., Bonhoeffer, T. and Bolz, J. (1989). *Cellular organization and development of slice cultures from rat visual cortex*. Exp Brain Res **77**(2): 234-44.

Canepari, M., Bove, M., Maeda, E., Cappello, M. and Kawana, A. (1997). *Experimental analysis of neuronal dynamics in cultured cortical networks and transitions between different patterns of activity*. Biol Cybern **77**(2): 153-62.

Carlier, E., Sourdet, V., Boudkkazi, S., Deglise, P., Ankri, N., Fronzaroli-Molinieres, L. and Debanne, D. (2006). *Metabotropic glutamate receptor subtype 1 regulates sodium currents in rat neocortical pyramidal neurons*. J Physiol **577**(Pt 1): 141-54.

Carlisle, H. J., Fink, A. E., Grant, S. G. and O'Dell, T. J. (2008). *Opposing effects of PSD-93 and PSD-95 on long-term potentiation and spike-timing dependent plasticity*. J Physiol.

Castro-Alamancos, M. A. and Connors, B. W. (1997). *Distinct forms of short-term plasticity at excitatory synapses of hippocampus and neocortex*. Proc Natl Acad Sci U S A **94**(8): 4161-6.

Chavez-Noriega, L. E., Halliwell, J. V. and Bliss, T. V. (1990). *A decrease in firing threshold observed after induction of the EPSP-spike (E-S) component of long-term potentiation in rat hippocampal slices*. Exp Brain Res **79**(3): 633-41.

Chen, L., Bohanick, J. D., Nishihara, M., Seamans, J. K. and Yang, C. R. (2007). *Dopamine D1/5 receptor-mediated long-term potentiation of intrinsic excitability in rat prefrontal cortical neurons: Ca2+-dependent intracellular signaling*. J Neurophysiol **97**(3): 2448-64.

Chen, P. E., Johnston, A. R., Mok, M. H., Schoepfer, R. and Wyllie, D. J. (2004). *Influence of a threonine residue in the S2 ligand binding domain in determining agonist potency and deactivation rate of recombinant NR1a/NR2D NMDA receptors*. J Physiol **558**(Pt 1): 45-58.

Choi, D. W. (1988). *Calcium-mediated neurotoxicity: relationship to specific channel types and role in ischemic damage*. Trends Neurosci **11**(10): 465-9.

Coetzee, W. A., Amarillo, Y., Chiu, J., Chow, A., Lau, D., McCormack, T., Moreno, H., Nadal, M. S., Ozaita, A., Pountney, D., Saganich, M., Vega-Saenz de Miera, E. and Rudy, B. (1999). *Molecular diversity of K+ channels*. Ann N Y Acad Sci **868**: 233-85.

Cohan, C. S. and Kater, S. B. (1986). *Suppression of Neurite Elongation and Growth Cone Motility by Electrical-Activity*. Science **232**(4758): 1638-1640.

Cole, K. S. and Curtis, H. J. (1939). *Electric impedance of the squid giant axon during activity*. Journal of General Physiology **22**(5): 649-670.

Cole, K. S. and Hodgkin, A. L. (1939). *Membrane and protoplasm resistance in the squid giant axon*. Journal of General Physiology **22**(5): 671-687.

Collins, F., Schmidt, M. F., Guthrie, P. B. and Kater, S. B. (1991). *Sustained increase in intracellular calcium promotes neuronal survival*. J Neurosci **11**(8): 2582-7.

Connor, J. A. and Stevens, C. F. (1971a). *Inward and delayed outward membrane currents in isolated neural somata under voltage clamp*. J Physiol **213**(1): 1-19.

Connor, J. A. and Stevens, C. F. (1971b). *Prediction of repetitive firing behaviour from voltage clamp data on an isolated neurone soma*. J Physiol **213**(1): 31-53.

Connor, J. A. and Stevens, C. F. (1971c). *Voltage clamp studies of a transient outward membrane current in gastropod neural somata*. J Physiol **213**(1): 21-30.

Connors, B. W. and Gutnick, M. J. (1990). *Intrinsic firing patterns of diverse neocortical neurons*. Trends Neurosci **13**(3): 99-104.

Coulter, D. A., Huguenard, J. R. and Prince, D. A. (1989). *Calcium currents in rat thalamocortical relay neurones: kinetic properties of the transient, low-threshold current*. J Physiol **414**: 587-604.

Cudmore, R. H. and Turrigiano, G. G. (2004). *Long-term potentiation of intrinsic excitability in LV visual cortical neurons*. J Neurophysiol **92**(1): 341-8.

Daoudal, G., Hanada, Y. and Debanne, D. (2002). *Bidirectional plasticity of excitatory postsynaptic potential (EPSP)-spike coupling in CA1 hippocampal pyramidal neurons*. Proc Natl Acad Sci U S A **99**(22): 14512-7.

Darby, I. A. and Hewitson, T. D. (2006). *In situ hybridization protocols*. Totowa, N.J., 3rd ed. / edited by Ian A. Darby, Tim D. Hewitson., Humana Press.

Davis, G. W. (2006). *Homeostatic control of neural activity: from phenomenology to molecular design*. Annu Rev Neurosci **29**: 307-23.

Davis, G. W. and Bezprozvanny, I. (2001). *Maintaining the stability of neural function: a homeostatic hypothesis*. Annu Rev Physiol **63**: 847-69.

Deisseroth, K., Heist, E. K. and Tsien, R. W. (1998). *Translocation of calmodulin to the nucleus supports CREB phosphorylation in hippocampal neurons*. Nature **392**(6672): 198-202.

Delorme, E. M. and McGee, R., Jr. (1986). *Regulation of voltage-dependent Ca2+ channels of neuronal cells by chronic changes in membrane potential*. Brain Res **397**(1): 189-92.

Derksen, H. E. (1965). *Axon membrane voltage fluctuations*. Acta Physiol Pharmacol Neerl **13**(4): 373-466.

Desai, N. S. (2003). *Homeostatic plasticity in the CNS: synaptic and intrinsic forms*. J Physiol Paris **97**(4-6): 391-402.

Desai, N. S., Rutherford, L. C. and Turrigiano, G. G. (1999a). *BDNF regulates the intrinsic excitability of cortical neurons*. Learn Mem **6**(3): 284-91.

Desai, N. S., Rutherford, L. C. and Turrigiano, G. G. (1999b). *Plasticity in the intrinsic excitability of cortical pyramidal neurons*. Nat Neurosci **2**(6): 515-20.

Dickson, C. T., Magistretti, J., Shalinsky, M. H., Fransen, E., Hasselmo, M. E. and Alonso, A. (2000). *Properties and role of I(h) in the pacing of subthreshold oscillations in entorhinal cortex layer II neurons*. J Neurophysiol **83**(5): 2562-79.

Dong, Y., Green, T., Saal, D., Marie, H., Neve, R., Nestler, E. J. and Malenka, R. C. (2006). *CREB modulates excitability of nucleus accumbens neurons*. Nat Neurosci **9**(4): 475-7.

Doyle, D. A., Morais Cabral, J., Pfuetzner, R. A., Kuo, A., Gulbis, J. M., Cohen, S. L., Chait, B. T. and MacKinnon, R. (1998). *The structure of the potassium channel: molecular basis of K+ conduction and selectivity*. Science **280**(5360): 69-77.

Duprat, F., Lesage, F., Fink, M., Reyes, R., Heurteaux, C. and Lazdunski, M. (1997). *TASK, a human background K+ channel to sense external pH variations near physiological pH*. Embo J **16**(17): 5464-71.

Edwards, F. A., Konnerth, A. and Sakmann, B. (1990). *Quantal analysis of inhibitory synaptic transmission in the dentate gyrus of rat hippocampal slices: a patch-clamp study*. J Physiol **430**: 213-49.

Ehrhardt, D. W., Atkinson, E. M. and Long, S. R. (1992). *Depolarization of alfalfa root hair membrane potential by Rhizobium meliloti Nod factors*. Science **256**(5059): 998-1000.

Erreger, K., Dravid, S. M., Banke, T. G., Wyllie, D. J. and Traynelis, S. F. (2005). *Subunit-specific gating controls rat NR1/NR2A and NR1/NR2B NMDA channel kinetics and synaptic signalling profiles*. J Physiol **563**(Pt 2): 345-58.

Fatt, P. and Katz, B. (1953). *The electrical properties of crustacean muscle fibres*. J Physiol **120**(1-2): 171-204.

Fields, R. D. (1998). *Effects of ion channel activity on development of dorsal root ganglion neurons*. Journal of Neurobiology **37**(1): 158-170.

FitzHugh, R. (1955). *Mathematical models of threshold phenomena in the nerve membrane.* Bulletin of Mathematical Biology **17**(4): 257-278.

Fitzhugh, R. (1960). *Thresholds and plateaus in the Hodgkin-Huxley nerve equations*. J Gen Physiol **43**: 867-96.

Fitzhugh, R. (1961). *Impulses and Physiological States in Theoretical Models of Nerve Membrane*. Biophysical Journal **1**(6): 445-&.

Foster, W. R., Ungar, L. H. and Schwaber, J. S. (1993). *Significance of conductances in Hodgkin-Huxley models*. J Neurophysiol **70**(6): 2502-18.

Franklin, J. L., Fickbohm, D. J. and Willard, A. L. (1992). *Long-term regulation of neuronal calcium currents by prolonged changes of membrane potential*. J Neurosci **12**(5): 1726-35.

Gahwiler, B. H. and Brown, D. A. (1985). *GABAB-receptor-activated K+ current in voltage-clamped CA3 pyramidal cells in hippocampal cultures*. Proc Natl Acad Sci U S A **82**(5): 1558-62.

Gallo, V., Kingsbury, A., Balazs, R. and Jorgensen, O. S. (1987). *The role of depolarization in the survival and differentiation of cerebellar granule cells in culture*. J. Neurosci. **7**(7): 2203-2213.

Ganguly, K., Kiss, L. and Poo, M. (2000). *Enhancement of presynaptic neuronal excitability by correlated presynaptic and postsynaptic spiking*. Nat Neurosci **3**(10): 1018-26.

Ghosh, A., Ginty, D. D., Bading, H. and Greenberg, M. E. (1994). *Calcium regulation of gene expression in neuronal cells*. J Neurobiol **25**(3): 294-303.

Glynn, I. M. (2002). *A hundred years of sodium pumping*. Annu Rev Physiol **64**: 1-18.

Goldman, M. S., Golowasch, J., Marder, E. and Abbott, L. F. (2001). *Global structure, robustness, and modulation of neuronal models*. J Neurosci **21**(14): 5229-38.

Goldstein, S. A., Bockenhauer, D., O'Kelly, I. and Zilberberg, N. (2001). *Potassium leak channels and the KCNK family of two-P-domain subunits*. Nat Rev Neurosci **2**(3): 175-84.

Golowasch, J., Abbott, L. F. and Marder, E. (1999a). *Activity-dependent regulation of potassium currents in an identified neuron of the stomatogastric ganglion of the crab Cancer borealis*. J Neurosci **19**(20): RC33.

Golowasch, J., Buchholtz, F., Epstein, I. R. and Marder, E. (1992). *Contribution of Individual Ionic Currents to Activity of a Model Stomatogastric Ganglion Neuron*. Journal of Neurophysiology **67**(2): 341-349.

Golowasch, J., Casey, M., Abbott, L. F. and Marder, E. (1999b). *Network stability from activity-dependent regulation of neuronal conductances*. Neural Comput **11**(5): 1079-96.

Golowasch, J., Goldman, M. S., Abbott, L. F. and Marder, E. (2002). *Failure of averaging in the construction of a conductance-based neuron model*. J Neurophysiol **87**(2): 1129-31.

Hafting, T., Fyhn, M., Molden, S., Moser, M. B. and Moser, E. I. (2005). *Microstructure of a spatial map in the entorhinal cortex*. Nature **436**(7052): 801-6.

Hagiwara, S. and Byerly, L. (1981). *Calcium channel*. Annu Rev Neurosci **4**: 69-125.

Harlow, E. and Lane, D. (1999). *Using antibodies : a laboratory manual*. Cold Spring Harbour, Cold Spring Harbour Laboratory Press.

Haug, K., Warnstedt, M., Alekov, A. K., Sander, T., Ramirez, A., Poser, B., Maljevic, S., Hebeisen, S., Kubisch, C., Rebstock, J., Horvath, S., Hallmann, K., Dullinger, J. S., Rau, B., Haverkamp, F., Beyenburg, S., Schulz, H., Janz, D., Giese, B., Muller-Newen, G., Propping, P., Elger, C. E., Fahlke, C., Lerche, H. and Heils, A. (2003). *Mutations in CLCN2 encoding a voltage-gated chloride channel are associated with idiopathic generalized epilepsies*. Nat Genet **33**(4): 527-32.

Hertz, J. A., Krogh, A. and Palmer, R. G. (1991). *Introduction to the theory of neural computation*. Reading, Mass. ; Wokingham, Addison-Wesley.

Hille, B. (2001). *Ion channels of excitable membranes*. Sunderland, Mass. ; [Great Britain], 3rd ed., Sinauer.

Hille, B., Armstrong, C. M. and MacKinnon, R. (1999). *Ion channels: from idea to reality*. Nat Med **5**(10): 1105-9.

Hines, M. L. and Carnevale, N. T. (1997). *The NEURON simulation environment*. Neural Comput **9**(6): 1179-209.

Hodgkin, A. L. (1948). *The local electric changes associated with repetitive action in a non-medullated axon*. J Physiol **107**(2): 165-81.

Hodgkin, A. L. and Huxley, A. F. (1939). *Action potentials recorded from inside a nerve fibre*. Nature **144**: 710-711.

Hodgkin, A. L. and Huxley, A. F. (1952a). *The components of membrane conductance in the giant axon of Loligo*. J Physiol **116**(4): 473-96.

Hodgkin, A. L. and Huxley, A. F. (1952b). *Currents carried by sodium and potassium ions through the membrane of the giant axon of Loligo*. J Physiol **116**(4): 449-72.

Hodgkin, A. L. and Huxley, A. F. (1952c). *The dual effect of membrane potential on sodium conductance in the giant axon of Loligo*. J Physiol **116**(4): 497-506.

Hodgkin, A. L. and Huxley, A. F. (1952d). *A quantitative description of membrane current and its application to conduction and excitation in nerve*. J Physiol **117**(4): 500-44.

Hodgkin, A. L., Huxley, A. F. and Katz, B. (1952). *Measurement of current-voltage relations in the membrane of the giant axon of Loligo*. J Physiol **116**(4): 424-48.

Hodgkin, A. L. and Katz, B. (1949). *The effect of sodium ions on the electrical activity of the giant axon of the squid*. J Physiol **108**(1): 37-77.

Hoger, J. H., Walter, A. E., Vance, D., Yu, L., Lester, H. A. and Davidson, N. (1991). *Modulation of a cloned mouse brain potassium channel*. Neuron **6**(2): 227-36.

Huxley, A. (2002). *From overshoot to voltage clamp*. Trends Neurosci **25**(11): 553-8.

Ivenshitz, M. and Segal, M. (2006). *Simultaneous NMDA-dependent long-term potentiation of EPSCs and long-term depression of IPSCs in cultured rat hippocampal neurons*. J Neurosci **26**(4): 1199-210.

Iverson, L. E., Tanouye, M. A., Lester, H. A., Davidson, N. and Rudy, B. (1988). *A-type potassium channels expressed from Shaker locus cDNA*. Proc Natl Acad Sci U S A **85**(15): 5723-7.

Izhikevich, E. M. (2000). *Neural excitability, spiking and bursting*. International Journal of Bifurcation and Chaos **10**(6): 1171-1266.

Izhikevich, E. M. (2003). *Simple model of spiking neurons*. Ieee Transactions on Neural Networks **14**(6): 1569-1572.

Jackson, L. B. (1989). *Digital filters and signal processing*, Second edition, Kluwer.

Jahr, C. E. and Stevens, C. F. (1990). *Voltage dependence of NMDA-activated macroscopic conductances predicted by single-channel kinetics*. J Neurosci **10**(9): 3178-82.

Jan, L. Y. and Jan, Y. N. (1997). *Cloned potassium channels from eukaryotes and prokaryotes*. Annu Rev Neurosci **20**: 91-123.

Jentsch, T. J., Stein, V., Weinreich, F. and Zdebik, A. A. (2002). *Molecular structure and physiological function of chloride channels*. Physiol Rev **82**(2): 503-68.

Jimbo, Y. and Robinson, H. P. (2000). *Propagation of spontaneous synchronized activity in cortical slice cultures recorded by planar electrode arrays*. Bioelectrochemistry **51**(2): 107-15.

Johnston, D., Magee, J. C., Colbert, C. M. and Christie, B. R. (1996). *Active Properties of Neuronal Dendrites*. Annual Review of Neuroscience **19**(1): 165-186.

Kamioka, H., Maeda, E., Jimbo, Y., Robinson, H. P. and Kawana, A. (1996). *Spontaneous periodic synchronized bursting during formation of mature patterns of connections in cortical cultures*. Neurosci Lett **206**(2-3): 109-12.

Kandel, E. R. (1989). *Genes, nerve cells, and the remembrance of things past*. J Neuropsychiatry Clin Neurosci **1**(2): 103-25.

Kandel, E. R., Schwartz, J. H. and Jessell, T. M. (2000). *Principles of neural science*. New York ; London, 4th ed., McGraw-Hill, Health Professions Division.

Kao, J. P., Harootunian, A. T. and Tsien, R. Y. (1989). *Photochemically generated cytosolic calcium pulses and their detection by fluo-3*. J Biol Chem **264**(14): 8179-84.

Kawaguchi, Y. (1993). *Groupings of nonpyramidal and pyramidal cells with specific physiological and morphological characteristics in rat frontal cortex*. J Neurophysiol **69**(2): 416-31.

Kawaguchi, Y. (1995). *Physiological subgroups of nonpyramidal cells with specific morphological characteristics in layer II/III of rat frontal cortex*. J Neurosci **15**(4): 2638-55.

Kilman, V., van Rossum, M. C. and Turrigiano, G. G. (2002). *Activity deprivation reduces miniature IPSC amplitude by decreasing the number of postsynaptic GABA(A) receptors clustered at neocortical synapses*. J Neurosci **22**(4): 1328-37.

Kirkwood, A., Dudek, S. M., Gold, J. T., Aizenman, C. D. and Bear, M. F. (1993). *Common forms of synaptic plasticity in the hippocampus and neocortex in vitro*. Science **260**(5113): 1518-21.

Klee, R., Ficker, E. and Heinemann, U. (1995). *Comparison of voltage-dependent potassium currents in rat pyramidal neurons acutely isolated from hippocampal regions CA1 and CA3*. J Neurophysiol **74**(5): 1982-95.

Koch, C. (1999). *Biophysics of computation : information processing in single neurons*. New York ; Oxford, Oxford University Press.

Koch, C., Poggio, T. and Torre, V. (1983). *Non-Linear Interactions in a Dendritic Tree - Localization, Timing, and Role in Information-Processing*. Proceedings of the National Academy of Sciences of the United States of America-Biological Sciences **80**(9): 2799-2802.

Koch, C. and Segev, I. (1998). *Methods in neuronal modeling : from ions to networks*. Cambridge, Mass. ; London, 2nd ed., MIT Press.

Kofuji, P. and Newman, E. A. (2004). *Potassium buffering in the central nervous system*. Neuroscience **129**(4): 1045-56.

Kostyuk, P. G., Krishtal, O. A. and Shakhovalov, Y. A. (1977). *Separation of sodium and calcium currents in the somatic membrane of mollusc neurones*. J Physiol **270**(3): 545-68.

Kuehl-Kovarik, M. C., Pouliot, W. A., Halterman, G. L., Handa, R. J., Dudek, F. E. and Partin, K. M. (2002). *Episodic bursting activity and response to excitatory amino acids in acutely dissociated gonadotropin-releasing hormone neurons genetically targeted with green fluorescent protein*. J Neurosci **22**(6): 2313-22.

Lasher, R. S. and Zagon, I. S. (1972). *The effect of potassium on neuronal differentiation in cultures of dissociated newborn rat cerebellum*. Brain Res **41**(2): 482-8.

LeMasson, G., Marder, E. and Abbott, L. F. (1993). *Activity-dependent regulation of conductances in model neurons*. Science **259**(5103): 1915-7.

Leslie, K. R., Nelson, S. B. and Turrigiano, G. G. (2001). *Postsynaptic depolarization scales quantal amplitude in cortical pyramidal neurons*. J Neurosci **21**(19): RC170.

Li, C. Y., Lu, J. T., Wu, C. P., Duan, S. M. and Poo, M. M. (2004). *Bidirectional modification of presynaptic neuronal excitability accompanying spike timing-dependent synaptic plasticity*. Neuron **41**(2): 257-68.

Li, M., Jia, M., Fields, R. D. and Nelson, P. G. (1996). *Modulation of calcium currents by electrical activity*. J Neurophysiol **76**(4): 2595-607.

Li, M., West, J. W., Lai, Y., Scheuer, T. and Catterall, W. A. (1992). *Functional modulation of brain sodium channels by cAMP-dependent phosphorylation*. Neuron **8**(6): 1151-9.

Liu, J., Bangalore, R., Rutledge, A. and Triggle, D. J. (1994). *Modulation of L-type Ca2+ channels in clonal rat pituitary cells by membrane depolarization*. Mol Pharmacol **45**(6): 1198-206.

Liu, Z., Golowasch, J., Marder, E. and Abbott, L. F. (1998). *A model neuron with activity-dependent conductances regulated by multiple calcium sensors*. J Neurosci **18**(7): 2309-20.

Llinas, R. and Jahnsen, H. (1982). *Electrophysiology of mammalian thalamic neurones in vitro*. Nature **297**(5865): 406-8.

Llinas, R. R. (1988). *The intrinsic electrophysiological properties of mammalian neurons: insights into central nervous system function*. Science **242**(4886): 1654-64.

Lucas, K. (1905). *On the gradation of activity in a skeletal muscle-fibre*. J Physiol **33**(2): 125-37.

Magee, J., Hoffman, D., Colbert, C. and Johnston, D. (1998). *Electrical and calcium signaling in dendrites of hippocampal pyramidal neurons*. Annu Rev Physiol **60**: 327-46.

Malenka, R. C. and Bear, M. F. (2004). *LTP and LTD: an embarrassment of riches*. Neuron **44**(1): 5-21.

Malenka, R. C. and Nicoll, R. A. (1999). *Long-term potentiation--a decade of progress?* Science **285**(5435): 1870-4.

Marder, E., Abbott, L. F., Buchholtz, F., Epstein, I. R., Golowasch, J., Hooper, S. L. and Kepler, T. B. (1993). *Physiological Insights from Cellular and Network Models of the Stomatogastric Nervous-System of Lobsters and Crabs*. American Zoologist **33**(1): 29-39.

Marder, E. and Bucher, D. (2007). *Understanding circuit dynamics using the stomatogastric nervous system of lobsters and crabs*. Annual Review of Physiology **69**: 291-316.

Marder, E. and Goaillard, J. M. (2006). *Variability, compensation and homeostasis in neuron and network function*. Nat Rev Neurosci **7**(7): 563-74.

Markram, H., Lubke, J., Frotscher, M. and Sakmann, B. (1997). *Regulation of synaptic efficacy by coincidence of postsynaptic APs and EPSPs*. Science **275**(5297): 213-5.

Marquardt, D. W. (1963). *An Algorithm for Least-Squares Estimation of Nonlinear Parameters*. Journal of the Society for Industrial and Applied Mathematics **11**(2): 431-441.

Martin, S. J., Grimwood, P. D. and Morris, R. G. (2000). *Synaptic plasticity and memory: an evaluation of the hypothesis*. Annu Rev Neurosci **23**: 649-711.

Martina, M., Schultz, J. H., Ehmke, H., Monyer, H. and Jonas, P. (1998). *Functional and molecular differences between voltage-gated K+ channels of fast-spiking interneurons and pyramidal neurons of rat hippocampus*. J Neurosci **18**(20): 8111-25.

Mayer, M. L. and Westbrook, G. L. (1987). *Permeation and block of N-methyl-D-aspartic acid receptor channels by divalent cations in mouse cultured central neurones*. J Physiol **394**: 501-27.

McBain, C. and Dingledine, R. (1992). *Dual-component miniature excitatory synaptic currents in rat hippocampal CA3 pyramidal neurons*. J Neurophysiol **68**(1): 16-27.

McBain, C. J. and Fisahn, A. (2001). *Interneurons unbound*. Nat Rev Neurosci **2**(1): 11-23.

McCormick, D. A. and Huguenard, J. R. (1992). *A model of the electrophysiological properties of thalamocortical relay neurons*. J Neurophysiol **68**(4): 1384-400.

McCulloh, D. H., Lynn, J. W. and Chambers, E. L. (1987). *Membrane depolarization facilitates sperm entry, large fertilization cone formation, and prolonged current responses in sea urchin oocytes*. Dev Biol **124**(1): 177-90.

Mee, C. J., Pym, E. C., Moffat, K. G. and Baines, R. A. (2004). *Regulation of neuronal excitability through pumilio-dependent control of a sodium channel gene*. J Neurosci **24**(40): 8695-703.

Meisler, M. H., Kearney, J., Ottman, R. and Escayg, A. (2001). *Identification of epilepsy genes in human and mouse*. Annu Rev Genet **35**: 567-88.

Meisler, M. H., Sprunger, L. K., Plummer, N. W., Escayg, A. and Jones, J. M. (1997). *Ion channel mutations in mouse models of inherited neurological disease*. Ann Med **29**(6): 569-74.

Mermelstein, P. G., Bito, H., Deisseroth, K. and Tsien, R. W. (2000). *Critical dependence of cAMP response element-binding protein phosphorylation on L-type calcium channels supports a selective response to EPSPs in preference to action potentials*. J Neurosci **20**(1): 266-73.

Migliore, M., Hoffman, D. A., Magee, J. C. and Johnston, D. (1999). *Role of an A-type K+ conductance in the back-propagation of action potentials in the dendrites of hippocampal pyramidal neurons*. J Comput Neurosci **7**(1): 5-15.

Mikami, A., Imoto, K., Tanabe, T., Niidome, T., Mori, Y., Takeshima, H., Narumiya, S. and Numa, S. (1989). *Primary structure and functional expression of the cardiac dihydropyridine-sensitive calcium channel*. Nature **340**(6230): 230-3.

Mishina, M., Kurosaki, T., Tobimatsu, T., Morimoto, Y., Noda, M., Yamamoto, T., Terao, M., Lindstrom, J., Takahashi, T., Kuno, M. and et al. (1984).

Expression of functional acetylcholine receptor from cloned cDNAs. Nature **307**(5952): 604-8.

Misonou, H., Menegola, M., Mohapatra, D. P., Guy, L. K., Park, K. S. and Trimmer, J. S. (2006). *Bidirectional activity-dependent regulation of neuronal ion channel phosphorylation*. J Neurosci **26**(52): 13505-14.

Misonou, H., Mohapatra, D. P., Park, E. W., Leung, V., Zhen, D., Misonou, K., Anderson, A. E. and Trimmer, J. S. (2004). *Regulation of ion channel localization and phosphorylation by neuronal activity*. Nat Neurosci **7**(7): 711-8.

Mitterdorfer, J. and Bean, B. P. (2002). *Potassium currents during the action potential of hippocampal CA3 neurons*. J Neurosci **22**(23): 10106-15.

Morris, C. and Lecar, H. (1981). *Voltage Oscillations in the Barnacle Giant Muscle-Fiber*. Biophysical Journal **35**(1): 193-213.

Moulder, K. L., Cormier, R. J., Shute, A. A., Zorumski, C. F. and Mennerick, S. (2003). *Homeostatic effects of depolarization on Ca2+ influx, synaptic signaling, and survival*. J Neurosci **23**(5): 1825-31.

Moyer, J. R., Jr., Thompson, L. T. and Disterhoft, J. F. (1996). *Trace eyeblink conditioning increases CA1 excitability in a transient and learning-specific manner*. J Neurosci **16**(17): 5536-46.

Mulley, J. C., Scheffer, I. E., Petrou, S. and Berkovic, S. F. (2003). *Channelopathies as a genetic cause of epilepsy*. Curr Opin Neurol **16**(2): 171-6.

Murbartian, J., Lei, Q., Sando, J. J. and Bayliss, D. A. (2005). *Sequential phosphorylation mediates receptor- and kinase-induced inhibition of TREK-1 background potassium channels*. J Biol Chem **280**(34): 30175-84.

Nakajima, S. (1966). *Analysis of K inactivation and TEA action in the supramedullary cells of puffer*. J Gen Physiol **49**(4): 629-40.

Neher, E. (1992). Correction for Liquid Junction Potentials in Patch Clamp Experiments. *Methods in Enzymology*, Academic Press. **207:** 123-131.

Neher, E. and Sakmann, B. (1976). *Single-channel currents recorded from membrane of denervated frog muscle fibres*. Nature **260**(5554): 799-802.

Nernst (1888). *Zur kinetik der in lösung befindlichen körper: Theorie der diffusion.* Z. Chem. Phys.: 613–637.

Nichols, C. G. and Lopatin, A. N. (1997). *Inward rectifier potassium channels*. Annu Rev Physiol **59**: 171-91.

Nilius, B. (2003). *Pflugers Archiv and the advent of modern electrophysiology - From the first action potential to patch clamp*. Pflugers Archiv-European Journal of Physiology **447**(3): 267-271.

Noda, M., Ikeda, T., Suzuki, H., Takeshima, H., Takahashi, T., Kuno, M. and Numa, S. (1986). *Expression of functional sodium channels from cloned cDNA*. Nature **322**(6082): 826-8.

Noda, M., Shimizu, S., Tanabe, T., Takai, T., Kayano, T., Ikeda, T., Takahashi, H., Nakayama, H., Kanaoka, Y., Minamino, N. and et al. (1984). *Primary structure of Electrophorus electricus sodium channel deduced from cDNA sequence*. Nature **312**(5990): 121-7.

Noda, M., Takahashi, H., Tanabe, T., Toyosato, M., Furutani, Y., Hirose, T., Asai, M., Inayama, S., Miyata, T. and Numa, S. (1982). *Primary structure of alpha-subunit precursor of Torpedo californica acetylcholine receptor deduced from cDNA sequence*. Nature **299**(5886): 793-7.

Numann, R., Catterall, W. A. and Scheuer, T. (1991). *Functional modulation of brain sodium channels by protein kinase C phosphorylation*. Science **254**(5028): 115-8.

Nusser, Z., Cull-Candy, S. and Farrant, M. (1997). *Differences in synaptic GABA(A) receptor number underlie variation in GABA mini amplitude*. Neuron **19**(3): 697-709.

Offord, J. and Catterall, W. A. (1989). *Electrical activity, cAMP, and cytosolic calcium regulate mRNA encoding sodium channel alpha subunits in rat muscle cells*. Neuron **2**(5): 1447-52.

Ogden, D. (1994). *Microelectrode techniques : the Plymouth Workshop handbook*. Cambridge, 2nd ed., Company of Biologists.

Papazian, D. M., Schwarz, T. L., Tempel, B. L., Jan, Y. N. and Jan, L. Y. (1987). *Cloning of genomic and complementary DNA from Shaker, a putative potassium channel gene from Drosophila*. Science **237**(4816): 749-53.

Patel, A. J. and Honore, E. (2001). *Properties and modulation of mammalian 2P domain K+ channels*. Trends Neurosci **24**(6): 339-46.

Peacock, J. H. (1979). *Electrophysiology of dissociated hippocampal cultures from fetal mice*. Brain Res **169**(2): 247-60.

Picciotto, M. R. and Wickman, K. (1998). *Using knockout and transgenic mice to study neurophysiology and behavior*. Physiol Rev **78**(4): 1131-63.

Piccolino, M. (1997). *Luigi Galvani and animal electricity: two centuries after the foundation of electrophysiology*. Trends Neurosci **20**(10): 443-8.

Piccolino, M. (1998). *Animal electricity and the birth of electrophysiology: the legacy of Luigi Galvani*. Brain Res Bull **46**(5): 381-407.

Platoshyn, O., Golovina, V. A., Bailey, C. L., Limsuwan, A., Krick, S., Juhaszova, M., Seiden, J. E., Rubin, L. J. and Yuan, J. X. (2000). *Sustained membrane depolarization and pulmonary artery smooth muscle cell proliferation*. Am J Physiol Cell Physiol **279**(5): C1540-9.

Prinz, A. A., Bucher, D. and Marder, E. (2004). *Similar network activity from disparate circuit parameters*. Nat Neurosci **7**(12): 1345-52.

Rae, J., Cooper, K., Gates, P. and Watsky, M. (1991). *Low access resistance perforated patch recordings using amphotericin B*. J Neurosci Methods **37**(1): 15-26.

Rall, W. (1962). *Theory of physiological properties of dendrites*. Ann N Y Acad Sci **96**: 1071-92.

Rall, W. and Rinzel, J. (1973). *Branch Input Resistance and Steady Attenuation for Input to One Branch of a Dendritic Neuron Model*. Biophysical Journal **13**(7): 648-688.

Ramakers, G. J., Corner, M. A. and Habets, A. M. (1990). *Development in the absence of spontaneous bioelectric activity results in increased stereotyped burst firing in cultures of dissociated cerebral cortex*. Exp Brain Res **79**(1): 157-66.

Richards, K. S., Simon, D. J., Pulver, S. R., Beltz, B. S. and Marder, E. (2003). *Serotonin in the developing stomatogastric system of the lobster, Homarus americanus*. Journal of Neurobiology **54**(2): 380-392.

Rieke, F. (1997). *Spikes : exploring the neural code*. Cambridge, Mass. ; London, MIT Press.

Ringer, S. and Buxton, D. W. (1885). *Concerning the Action of small quantities of Calcium, Sodium, and Potassium Salts upon the Vitality and Function of Contractile Tissue and the Cuticular Cells of Fishes*. J Physiol **6**(4-5): 154-161.

Ringer, S. and Buxton, D. W. (1887). *Concerning the Action of Calcium, Potassium, and Sodium Salts upon the Eel's Heart and upon the Skeletal Muscles of the Frog*. J Physiol **8**(1): 15-19.

Rolfe, D. F. and Brown, G. C. (1997). *Cellular energy utilization and molecular origin of standard metabolic rate in mammals*. Physiol Rev **77**(3): 731-58.

Rudy, B. (1988). *Diversity and ubiquity of K channels*. Neuroscience **25**(3): 729-49.

Salkoff, L. and Wyman, R. (1981). *Genetic modification of potassium channels in Drosophila Shaker mutants*. Nature **293**(5829): 228-30.

Sattler, R., Charlton, M. P., Hafner, M. and Tymianski, M. (1998). *Distinct influx pathways, not calcium load, determine neuronal vulnerability to calcium neurotoxicity*. J Neurochem **71**(6): 2349-64.

Schaller, K. L., Krzemien, D. M., Yarowsky, P. J., Krueger, B. K. and Caldwell, J. H. (1995). *A novel, abundant sodium channel expressed in neurons and glia*. J Neurosci **15**(5 Pt 1): 3231-42.

Schlaepfer, W. W. and Bunge, R. P. (1973). *Effects of calcium ion concentration on the degeneration of amputated axons in tissue culture*. J Cell Biol **59**(2 Pt 1): 456-70.

Schneider, M. F. and Chandler, W. K. (1973). *Voltage dependent charge movement of skeletal muscle: a possible step in excitation-contraction coupling*. Nature **242**(5395): 244-6.

Schneidman, E., Freedman, B. and Segev, I. (1997). *Ion channel stochasticity may be a critical factor in determining the reliability of spike timing*. Neuroscience Letters: S43-S44.

Seeburg, D. P. and Sheng, M. (2008). *Activity-induced Polo-like kinase 2 is required for homeostatic plasticity of hippocampal neurons during epileptiform activity*. J Neurosci **28**(26): 6583-91.

Seyfarth, E. A. (2006). *Julius Bernstein (1839-1917): pioneer neurobiologist and biophysicist*. Biological Cybernetics **94**(1): 2-8.

Sherman, S. M. (2001). *Tonic and burst firing: dual modes of thalamocortical relay*. Trends Neurosci **24**(2): 122-6.

Shouval, H. Z., Bear, M. F. and Cooper, L. N. (2002). *A unified model of NMDA receptor-dependent bidirectional synaptic plasticity*. Proc Natl Acad Sci U S A **99**(16): 10831-6.

Siegel, M., Marder, E. and Abbott, L. F. (1994). *Activity-dependent current distributions in model neurons*. Proc Natl Acad Sci U S A **91**(24): 11308-12.

Sik, A., Smith, R. L. and Freund, T. F. (2000). *Distribution of chloride channel-2-immunoreactive neuronal and astrocytic processes in the hippocampus*. Neuroscience **101**(1): 51-65.

Sjostrom, P. J., Turrigiano, G. G. and Nelson, S. B. (2001). *Rate, timing, and cooperativity jointly determine cortical synaptic plasticity*. Neuron **32**(6): 1149-64.

Sodickson, D. L. and Bean, B. P. (1996). *GABAB receptor-activated inwardly rectifying potassium current in dissociated hippocampal CA3 neurons*. J Neurosci **16**(20): 6374-85.

Solomon, P. R., Vander Schaaf, E. R., Thompson, R. F. and Weisz, D. J. (1986). *Hippocampus and trace conditioning of the rabbit's classically conditioned nictitating membrane response*. Behav Neurosci **100**(5): 729-44.

Somjen, G. G. (2001). *Mechanisms of spreading depression and hypoxic spreading depression-like depolarization*. Physiol Rev **81**(3): 1065-96.

Sourdet, V., Russier, M., Daoudal, G., Ankri, N. and Debanne, D. (2003). *Long-term enhancement of neuronal excitability and temporal fidelity mediated by metabotropic glutamate receptor subtype 5*. J Neurosci **23**(32): 10238-48.

Spitzer, N. C. (1991). *A developmental handshake: neuronal control of ionic currents and their control of neuronal differentiation*. J Neurobiol **22**(7): 659-73.

Spruston, N. and Johnston, D. (1992). *Perforated patch-clamp analysis of the passive membrane properties of three classes of hippocampal neurons*. J Neurophysiol **67**(3): 508-29.

Stemmler, M. and Koch, C. (1999). *How voltage-dependent conductances can adapt to maximize the information encoded by neuronal firing rate*. Nat Neurosci **2**(6): 521-7.

Strassberg, A. F. and Defelice, L. J. (1993). *Limitations of the Hodgkin-Huxley Formalism - Effects of Single-Channel Kinetics on Transmembrane Voltage Dynamics*. Neural Computation **5**(6): 843-855.

Suzuki, M., Morita, T. and Iwamoto, T. (2006). *Diversity of Cl(-) channels*. Cell Mol Life Sci **63**(1): 12-24.

Swensen, A. M. and Bean, B. P. (2005). *Robustness of burst firing in dissociated purkinje neurons with acute or long-term reductions in sodium conductance*. J Neurosci **25**(14): 3509-20.

Talley, E. M., Solorzano, G., Lei, Q., Kim, D. and Bayliss, D. A. (2001). *Cns distribution of members of the two-pore-domain (KCNK) potassium channel family*. J Neurosci **21**(19): 7491-505.

Tanabe, T., Takeshima, H., Mikami, A., Flockerzi, V., Takahashi, H., Kangawa, K., Kojima, M., Matsuo, H., Hirose, T. and Numa, S. (1987). *Primary structure of the receptor for calcium channel blockers from skeletal muscle*. Nature **328**(6128): 313-8.

Tateno, T., Harsch, A. and Robinson, H. P. (2004). *Threshold firing frequency-current relationships of neurons in rat somatosensory cortex: type 1 and type 2 dynamics*. J Neurophysiol **92**(4): 2283-94.

Tempel, B. L., Papazian, D. M., Schwarz, T. L., Jan, Y. N. and Jan, L. Y. (1987). *Sequence of a probable potassium channel component encoded at Shaker locus of Drosophila*. Science **237**(4816): 770-5.

Thompson, R. F. (1986). *The neurobiology of learning and memory*. Science **233**(4767): 941-7.

Thompson, S. H. (1977). *Three pharmacologically distinct potassium channels in molluscan neurones*. J Physiol **265**(2): 465-88.

Triesch, J. (2005). *A gradient rule for the plasticity of a neuron's intrinsic excitability*. Artificial Neural Networks: Biological Inspirations - Icann 2005, Pt 1, Proceedings **3696**: 65-70.

Tsien, R. W., Lipscombe, D., Madison, D. V., Bley, K. R. and Fox, A. P. (1988). *Multiple types of neuronal calcium channels and their selective modulation*. Trends Neurosci **11**(10): 431-8.

Turrigiano, G. (2007). *Homeostatic signaling: the positive side of negative feedback*. Curr Opin Neurobiol **17**(3): 318-24.

Turrigiano, G., Abbott, L. F. and Marder, E. (1994). *Activity-dependent changes in the intrinsic properties of cultured neurons*. Science **264**(5161): 974-7.

Turrigiano, G., LeMasson, G. and Marder, E. (1995). *Selective regulation of current densities underlies spontaneous changes in the activity of cultured neurons*. J Neurosci **15**(5 Pt 1): 3640-52.

Turrigiano, G. G. (1999). *Homeostatic plasticity in neuronal networks: the more things change, the more they stay the same*. Trends Neurosci **22**(5): 221-7.

Turrigiano, G. G., Leslie, K. R., Desai, N. S., Rutherford, L. C. and Nelson, S. B. (1998). *Activity-dependent scaling of quantal amplitude in neocortical neurons*. Nature **391**(6670): 892-6.

Turrigiano, G. G. and Marder, E. (1993). *Modulation of Identified Stomatogastric Ganglion Neurons in Primary-Cell Culture*. Journal of Neurophysiology **69**(6): 1993-2002.

Turrigiano, G. G. and Nelson, S. B. (2000). *Hebb and homeostasis in neuronal plasticity*. Curr Opin Neurobiol **10**(3): 358-64.

Turrigiano, G. G. and Nelson, S. B. (2004). *Homeostatic plasticity in the developing nervous system*. Nat Rev Neurosci **5**(2): 97-107.

Van Huizen, F. and Romijn, H. J. (1987). *Tetrodotoxin enhances initial neurite outgrowth from fetal rat cerebral cortex cells in vitro*. Brain Res **408**(1-2): 271-4.

van Ooyen, A., Duijnhouwer, J., Remme, M. W. H. and van Pelt, J. (2002). *The effect of dendritic topology on firing patterns in model neurons*. Network-Computation in Neural Systems **13**(3): 311-325.

van Welie, I., van Hooft, J. A. and Wadman, W. J. (2004). *Homeostatic scaling of neuronal excitability by synaptic modulation of somatic hyperpolarization-activated Ih channels*. Proc Natl Acad Sci U S A **101**(14): 5123-8.

van Welie, I., van Hooft, J. A. and Wadman, W. J. (2006). *Background activity regulates excitability of rat hippocampal CA1 pyramidal neurons by adaptation of a K+ conductance*. J Neurophysiol **95**(3): 2007-12.

Vergara, C., Latorre, R., Marrion, N. V. and Adelman, J. P. (1998). *Calcium-activated potassium channels*. Curr Opin Neurobiol **8**(3): 321-9.

Verkhratsky, A., Krishtal, O. A. and Petersen, O. H. (2006). *From Galvani to patch clamp: the development of electrophysiology*. Pflugers Archiv-European Journal of Physiology **453**(3): 233-247.

Walker, W. C. (1937). *Animal electricity before Galvani*. Annals of Science **2**(1): 84 - 113.

Wang, H. X., Gerkin, R. C., Nauen, D. W. and Bi, G. Q. (2005). *Coactivation and timing-dependent integration of synaptic potentiation and depression*. Nat Neurosci **8**(2): 187-93.

Weimann, J. M., Meyrand, P. and Marder, E. (1991). *Neurons That Form Multiple Pattern Generators - Identification and Multiple Activity Patterns of Gastric Pyloric Neurons in the Crab Stomatogastric System*. Journal of Neurophysiology **65**(1): 111-122.

Weiss, J. H., Hartley, D. M., Koh, J. and Choi, D. W. (1990). *The calcium channel blocker nifedipine attenuates slow excitatory amino acid neurotoxicity*. Science **247**(4949): 1474-1477.

West, A. E., Chen, W. G., Dalva, M. B., Dolmetsch, R. E., Kornhauser, J. M., Shaywitz, A. J., Takasu, M. A., Tao, X. and Greenberg, M. E. (2001). *Calcium regulation of neuronal gene expression*. Proc Natl Acad Sci U S A **98**(20): 11024-31.

Wilcox, K. S., Buchhalter, J. and Dichter, M. A. (1994). *Properties of inhibitory and excitatory synapses between hippocampal neurons in very low density cultures*. Synapse **18**(2): 128-51.

Wittenberg, G. M. and Wang, S. S. (2006). *Malleability of spike-timing-dependent plasticity at the CA3-CA1 synapse*. J Neurosci **26**(24): 6610-7.

Witter, M. P. and Moser, E. I. (2006). *Spatial representation and the architecture of the entorhinal cortex*. Trends Neurosci **29**(12): 671-8.

Wu, R. L. and Barish, M. E. (1992). *Two pharmacologically and kinetically distinct transient potassium currents in cultured embryonic mouse hippocampal neurons*. J Neurosci **12**(6): 2235-46.

Xu, J., Kang, N., Jiang, L., Nedergaard, M. and Kang, J. (2005). *Activity-dependent long-term potentiation of intrinsic excitability in hippocampal CA1 pyramidal neurons*. J Neurosci **25**(7): 1750-60.

Zhang, L. I. and Poo, M. M. (2001). *Electrical activity and development of neural circuits*. Nat Neurosci **4 Suppl**: 1207-14.

Zhang, W. and Linden, D. J. (2003). *The other side of the engram: experience-driven changes in neuronal intrinsic excitability*. Nat Rev Neurosci **4**(11): 885-900.

Appendix: state equations and parameters for the single compartment model

The equations and parameter values are taken from the model published Migliore *et al.* (1999) and made available in ModelDB (http://senselab.med.yale.edu/modeldb). onductance mechanisms are implemented in NEURON using NMODL (Hines & Carnevale 1997).

Notes

All symbols have the meanings defined in Chapter 7. Temperature, T = 20 ºC throughout. Membrane potential is denoted by v. Parameter units are included in parenthesis, 'N. D.' denotes dimensionless parameters. Primed variables ($'$) indicate derivatives with respect to time. Parameters that differ in the model from the values used by Migliore *et al.* (1999) are written in red.

Sodium conductance

State equations

$$
\begin{aligned}
I_{Na} &= \bar{g}_{Na} m^3 h (v - E_{Na}) \\
m' &= (m_\infty - m)/\tau_m \\
h' &= (h_\infty - h)/\tau_h \\
m_\infty &= \alpha_m/(\alpha_m + \beta_m) \\
\tau_m &= 1/q_t(\alpha_m + \beta_m) \\
\alpha_m &= R_a (v - t_{ha})/\left(1 - \exp(-(v - t_{ha})/q_a)\right) \\
\beta_m &= R_b (v - t_{ha})/\left(\exp((v - t_{ha})/q_a) - 1\right) \\
h_\infty &= 1/\left(1 + \exp((v - t_{h\infty})/q_\infty)\right) \\
\tau_h &= 1/q_t(\alpha_h + \beta_h) \\
\alpha_h &= R_d (v - t_{hi1})/\left(1 - \exp(-(v - t_{hi1})/q_d)\right) \\
\beta_h &= R_g (v - t_{hi2})/\left(\exp((v - t_{hi2})/q_g) - 1\right) \\
q_t &= q_{10}^{((T-24)/10)}
\end{aligned}
$$

If ($\tau_m < m_{min}$) then $\tau_m = m_{min}$; If ($\tau_h < h_{min}$) then $\tau_h = h_{min}$.

Sodium conductance parameters:

Parameter name (units)		Parameter value	
		Migliore et al (1998)	Model 1 & 2
R_a	(ms^{-1})	0.4	0.4
R_b	(ms^{-1})	0.124	0.124
t_{ha}	(mV)	–30	–35
q_a	(mV)	7.2	5
$t_{h\infty}$	(mV)	–50	–50
q_∞	(mV)	4	4
R_d	(ms^{-1})	0.03	0.03
R_g	(ms^{-1})	0.01	0.01
t_{hi1}	(mV)	–25	–25
t_{hi2}	(mV)	–45	–45
q_d	(mV)	1.5	1.5
q_g	(mV)	1.5	1.5
q_{10}	N. D.	2	2
m_{min}	(ms)	0.02	0.02
h_{min}	(ms)	0.5	0.5

Sodium conductance parameters (*continued*)

A-type potassium conductance

State equations

$$
\begin{aligned}
I_{Ka} &= \bar{g}_{Ka}\, pl\,(v - E_K) \\
p' &= (p_\infty - p)/\tau_p \\
l' &= (l_\infty - l)/\tau_l \\
p_\infty &= 1/(\alpha_p + 1) \\
\tau_p &= \beta_p / q_t a_{0p} (\alpha_p + 1) \\
\alpha_p &= \exp(t_{ka}\zeta(v - v_{hp})) \\
\beta_p &= \exp(t_{ka}\zeta g_{mp}(v - v_{hp})) \\
\zeta &= \zeta_p + p_w / \left(1 + \exp((v - t_q)/q_q)\right) \\
l_\infty &= 1/(\alpha_l + 1) \\
\tau_l &= t_l (v - v_{hl1})/q_{t1}
\end{aligned}
$$

$$\alpha_l = \exp(t_{ka}\zeta(v - v_{hl}))$$
$$t_{ka} = 1\times10^{-3}\cdot 9.648\times10^{-4}/(8.315\times(273.16+T))$$
$$q_t = q_{10}^{((T-24)/10)}$$

If ($\tau_p < p_{min}$) then $\tau_p = p_{min}$; If ($\tau_l < l_{min}$) then $\tau_l = l_{min}$.

A-type potassium conductance parameters

		Parameter value	
Parameter name (units)		Migliore et al (1998)	Model 1 & 2
a_{0p}	(ms^{-1})	0.05	0.05
v_{hp}	(mV)	11	−10
g_{mp}	N. D.	0.55	0.55
ζ_p	N. D.	−1.5	−1.5
p_w	N. D.	−1	−1
t_q	(mV)	−40	−40
q_q	(mV)	5	5
t_l	(mV^{-1})	0.26	0.26
v_{hl1}	(mV)	−56	−45
v_{hl}	(mV)	−50	−50
q_{t1}	(ms^{-1})	1	1
q_{10}	N. D.	5	5
p_{min}	(ms)	0.1	0.1
l_{min}	(ms)	2	2

Delayed-rectifier potassium conductance

State equations

$$I_{Kdr} = \bar{g}_{Kdr} n (v - E_K)$$
$$n' = (n_\infty - n)/\tau_n$$
$$n_\infty = 1/(\alpha_n + 1)$$
$$\tau_n = \beta_n/q_t a_{0n}(\alpha_n + 1)$$
$$\alpha_n = \exp(t_{ka}\zeta_n(v - v_{hn}))$$
$$\beta_n = \exp(t_{ka}\zeta_n g_{mn}(v - v_{hn}))$$

$$t_{ka} = 1\times10^{-3}\cdot 9.648\times10^{-4}/(8.315\times(273.16+T))$$

$$q_t = q_{10}^{((T-24)/10)}$$

If ($\tau_n < n_{min}$) then $\tau_n = n_{min}$.

Delayed-rectifier potassium conductance parameters

		Parameter value	
Parameter name (units)		Migliore et al (1998)	Model 1 & 2
a_{0n}	(ms^{-1})	0.02	0.01
v_{hn}	(mV)	13	10
g_{mn}	N. D.	0.7	0.7
ζ_n	N. D.	−3	−1.5
q_{10}	N. D.	1	1
n_{min}	(ms)	2	2